50272-101

REPORT DOCUMENTATION PAGE	1. REPORT NO. NSF/ENG-88047	2.	3. PB91-210880

4. Title and Subtitle
Liquefaction Potential of Sand Deposits Under Low Levels of Excitation

5. Report Date
August 1988

6.

7. Author(s)
D.P. Carter and H. Bolton Seed

8. Performing Organization Rept. No.
UCB/EERC-88/11

9. Performing Organization Name and Address
Earthquake Engineering Research Center
University of California, Berkeley
1301 S 46th St.
Richmond, CA 94804

10. Project/Task/Work Unit No.

11. Contract(C) or Grant(G) No.
(C)
(G) CEE-8411912

12. Sponsoring Organization Name and Address
National Science Foundation
1800 G. St. NW
Washington, DC 20550

13. Type of Report & Period Covered

14.

15. Supplementary Notes

16. Abstract (Limit: 200 words)

Many researchers currently believe that liquefaction will not occur unless the peak ground surface accelerations generated at a site exceed some value between about 0.05g and 0.10g. This investigation attempted to determine the minimum levels of ground shaking capable of causing liquefaction both from seismic and non-seismic sources of vibration such as blasting, dynamic compaction, pile driving, construction equipment, and road and rail traffic. It now seems probable that levels of shaking significantly less than the value above are not only capable of causing liquefaction but have caused liquefaction in the past.

17. Document Analysis a. Descriptors

blasting
compaction
frequency
liquefaction
shear strain
shear stress
sloping sites
vibrations

b. Identifiers/Open-Ended Terms

c. COSATI Field/Group

18. Availability Statement:	19. Security Class (This Report)	21. No. of Pages
Release Unlimited	unclassified	335
	20. Security Class (This Page) unclassified	22. Price

(See ANSI-Z39.18) See Instructions on Reverse

OPTIONAL FORM 272 (4-77)
(Formerly NTIS-35)
Department of Commerce

PB91-210880

REPORT NO.
UCB/EERC-88/11
AUGUST 1988

EARTHQUAKE ENGINEERING RESEARCH CENTER

LIQUEFACTION POTENTIAL OF SAND DEPOSITS UNDER LOW LEVELS OF EXCITATION

by

DAVID P. CARTER
H. BOLTON SEED

A report on research sponsored by
the National Science Foundation

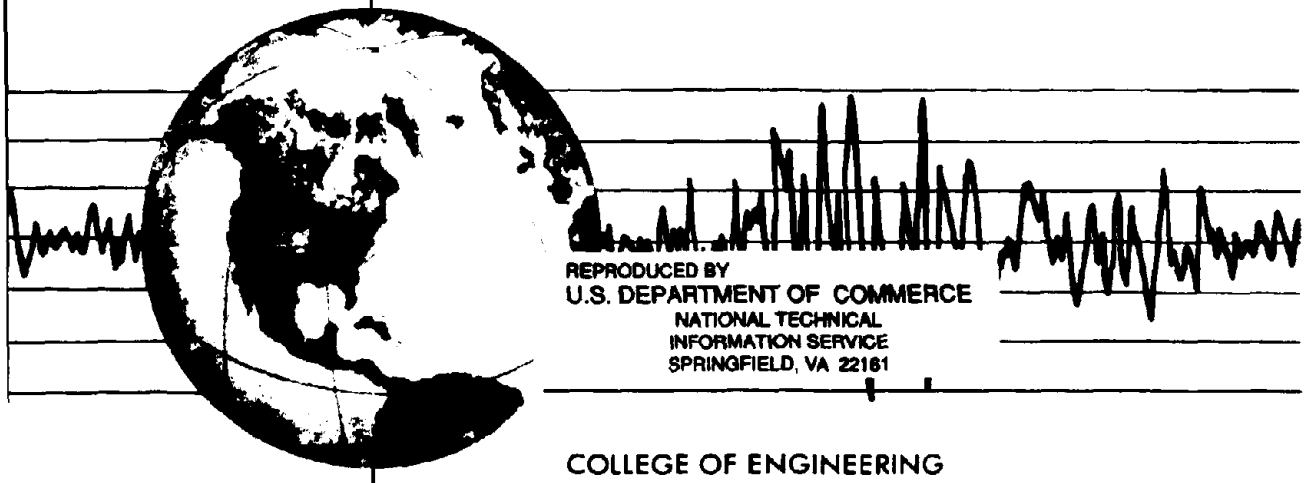

COLLEGE OF ENGINEERING

UNIVERSITY OF CALIFORNIA AT BERKELEY

For sale by the National Technical Information Service, National Bureau of Standards, U.S. Department of Commerce, Springfield, Virginia 22151

See back of report for up to date listing of EERC reports.

EARTHQUAKE ENGINEERING RESEARCH CENTER

LIQUEFACTION POTENTIAL OF SAND DEPOSITS UNDER LOW LEVELS OF EXCITATION

by

David P. Carter

and

H. Bolton Seed

Report No. UCB/EERC-88/11

August 1988

A report on research sponsored by
the National Science Foundation

College of Engineering
Department of Civil Engineering
University of California
Berkeley, California

ACKNOWLEDGEMENTS

This research was made possible through the support provided by the National Science Foundation, under Grant no. CEE-8411912. This support is gratefully acknowledged. The authors also express appreciation to the many colleagues and friends who also contributed to the studies described in the report.

TABLE OF CONTENTS

LIST OF FIGURES

LIST OF TABLES

CHAPTER 1

Introduction

1.1. Introduction

Over the last two and a half decades, a significant amount of research has been conducted in the field of soil liquefaction. This research has led to the development of several techniques which can now be used to make reasonable assessments of the liquefaction potentials of sand sites under most levels of earthquake shaking. One aspect of the problem which is still under debate however, is the minimum level of shaking required to liquefy a deposit.

Many researchers currently believe that liquefaction will not occur unless the peak ground surface accelerations generated at a site exceed some value between about 0.05g and 0.10g. This range is based on relationships between Intensity, say as measured on the Modified Mercalli Scale, and observed field performance. In addition, it appears to be supported, at least for level sites, by experimental data such as laboratory-determined values of threshold strain.

However, while such a range might seem appropriate, it also seems probable that levels of shaking significantly less than this value have caused liquefaction in the past. For example, Fuller (1912) reports that a sand island near Vicksburg, Mississippi disappeared during the 1811 New Madrid earthquake (approximately magnitude 8.2). This island was located at a distance of about 460 kms (300 miles) from the epicentral

region and presumably failed as a result of soil liquefaction. The above observation is significant because the ground surface accelerations generated at this distance are expected to be about 0.03g (based on the attenuation relationships referred to in Section 2.2), thereby suggesting that the minimum level of shaking may actually be about one-half to one-third of the higher values referred to above.

Further support for the lower level is provided by the observation that even non-seismic sources of vibration are reported to be capable of causing liquefaction. For example, Broms (1978) states that the stability of slopes is affected by "a temporary increase in pore water pressure in the bottom layers from e.g. vibrations caused by pile driving, heavy traffic, etc." Such an observation is important because the ground vibrations generated by non-seismic sources are of a very low level compared with the shaking generated be even small (magnitude 5) earthquakes.

In fact, over the last 40 years alone, non-seismic sources appear to have caused a number of large-scale liquefaction failures (Szerdy, 1985), some involving up to 4 million cubic yards of soil. Seven slides which seem to have been clearly associated with the liquefaction of sands, are listed in Table 1.1. The causes of these failures are reported to include quarry blasting, blasting for removal of trees, vibrations associated with pile driving, and those associated with the passage of trains.

Thus, it indeed seems probable that levels of ground shaking significantly less than 0.05g may well be capable of inducing liquefaction, and while this suggestion appears to be in conflict with the levels based on the Modified Mercalli Intensity scale, it may not be inconsistent with the levels determined from experimental results. For

Table 1.1 : Landslides Induced by Sources of Low Level Vibrations

Case No.	Location and Date	Soil Type	Slide Area	Volume	Vibration Source
1.	Toulnustouc River, Canada May 23, 1962	Very stiff, sensitive clay with silt and sand seams	3200′ × 800′	3×10^6 cu. yds.	Light blasting to remove trees (Conlon, 1966).
2.	Froland, Sweden June 5, 1978	Sensitive clay with silt and sand seams	600′ × 400′	5×10^5 cu. yds.	Blasting in quarry about 80 meters from slide area (Bjurstrom and Broms, 1973).
3.	Surte, Sweden Sept. 29, 1950	Sensitive clay with sand seams and lenses	2000′ × 1200′	4×10^6 cu. yds.	Pile driving in slide area. Train had just left area (Jacobsen, 1952).
4.	Save River, Sweden Aug. 6, 1966	Sensitive clay with silt and sand seams	400′ × 160′	7×10^4 cu. yds.	Slide occurred about 4 hrs. after driving 60 timber piles in slide area (Broms and Bennemark, 1967).
5.	Guntorp, Sweden April 13, 1953	Sensitive clay with silt and sand seams	240′ × 200′	3×10^4 cu. yds.	Slide occurred just after passage of train on upper end of slide area (Fellenius, 1955).
6.	Cajon Pass, Calif. March 6, 1978	Uncompacted clean sand embankment	100′ × 120′	1×10^4 cu. yds.	Train on slide mass at time of failure.
7.	San Joaquin River Delta, California	Sand embankment saturated at base.			Train on slide mass at time of failure.

example, the higher accelerations were computed for level deposits subjected to zero initial shear stress, and recent experimental evidence has shown that as the magnitudes of the initial shear stress/normal stress ratios imposed upon a sand are increased, the liquefaction resistance of loose sands is significantly reduced (Szerdy, 1985, Vaid and Chern, 1983, Castro et al., 1982, and Yoshimi and Oh-Oka, 1975). Since the magnitudes of the initial shear stress/normal stress ratios are a function of both the slope of the site, and the artesian pressure conditions, certain deposits may well be predicted to liquefy under much lower levels of shaking.

The ability of certain non-seismic sources to induce liquefaction has been noted for many years. In fact, engineers have used techniques such as blasting and dynamic compaction to densify sand deposits by causing liquefaction. Another source which might also be capable of causing liquefaction is trains. This belief is based on the fact that trains are associated with several of the failures listed in Table 1.1, and that they are commonly regarded as a significant source of ground vibration. It therefore seemed appropriate to try to determine the levels of shaking generated by this source, and hence determine whether train-induced ground vibrations might have caused any of the failures referred to above.

1.2. Scope

This study was performed in four parts:

1) A literature survey which was undertaken to both determine the levels of ground shaking generated by various non-seismic sources of vibration, and to relate these levels to observed field performance.

2) Measurements were made of train-induced ground vibration amplitudes in the field, since it appeared that the levels reported in the literature were somewhat inconsistent with the common perception that trains are a significant source of ground vibration.

3) Analytical studies were performed to predict the levels of cyclic shear stress and shear strain, likely to be induced within a site by trains, and hence attempt to determine whether trains might be capable of causing liquefaction.

4) Analytical studies which were also performed to examine the effects of both artesian pore pressures and initial static shear stresses on the minimum level of shaking required to cause liquefaction at a site.

1.3. Outline

To assist the reader, a brief outline of the material covered in each chapter is presented below.

The characteristics of the ground motions that are generated by the following non-seismic sources of ground vibration are presented in Chapter 2: blasting, dynamic compaction, pile driving, construction equipment, and road and rail traffic. This information is presented along with a brief discussion on the maximum distances at which different magnitude earthquakes have caused liquefaction. Chapter 3 presents a summary of the methods that may be used to evaluate the liquefaction potential of sand sites subjected to ground shaking. The relative advantages and disadvantages of the two approaches, the shear strain and the shear stress approach, are discussed.

The characteristics of the train-induced ground vibration records that were obtained during this investigation are presented in Chapter 4. This is followed by an evaluation of their liquefaction potential (in Chapter 5), and their possible relevance in two of the liquefaction failures that have been associated with trains (and are listed in Table 1.1).

The effects of both artesian pore pressures and initial static shear stresses on the minimum level of earthquake shaking required to cause liquefaction at a site is investigated in Chapter 6. Conclusions are presented in the final chapter along with recommendations for further study.

CHAPTER 2

Sources of Low Level Excitation and Their Liquefaction Potential

2.1. Introduction

Most engineers associate large-scale liquefaction with ground vibrations generated by earthquakes. However as discussed in Chapter 1 non-seismic sources of ground vibration also appear to be capable of causing liquefaction failures of a similar magnitude. This lack of awareness can possibly be attributed to the fact that earthquakes themselves are large dramatic events and that non-seismic ground vibrations appear to have caused a much smaller number of large-scale failures. This is not meant to imply that non-seismic sources of vibration cause fewer liquefaction failures since in reality they cause a large number of these types of failures. Rather that most liquefaction failures associated with non-seismic sources of vibration result in small ground settlements close to the source.

The differences between the general extent of failures associated with each source of vibration (seismic or non-seismic) can probably be attributed to differences in the characteristics of the ground vibrations produced by each source. One of the principal differences is in the amount of energy that is imparted to the soil since ground vibrations produced by even a moderate earthquake, contain much larger amounts of energy than ground vibrations generated by non-seismic sources. Another major difference is in the frequency contents of these motions. The ground vibrations that are generated

by earthquakes are altered as they propagate vertically up through a site. Since motions with frequencies close to the natural period of the site are amplified, the predominant period of the surface motion is often close to the natural period of the site which typically ranges from 1/4 to 2 seconds (1/2 to 4 Hz). In contrast, non-seismic sources tend to produce transient ground vibrations with much higher predominant frequencies, even though these frequencies also appear to depend on the soil type at the site. Predominant frequencies for different soils have been presented by a number of researchers such as Wiss (1967) and Martin (1980) whose values are listed in Table 2.1. Dalmatov et al (1968) further report that ground motions with a predominant frequency of 24 Hz were recorded at a site consisting of 24m of loam (glacial in origin) which was overlain by 2.0m of rubbish. These motions were produced by impact pile driving.

When energy is imparted to a soil mass, most of the energy is transmitted as some combination of compression waves (P waves), shear waves (S waves) and Rayleigh waves. However the proportion of energy that is carried by each wave type is

Table 2.1 : Predominant Frequencies for Different Soils

Material	Predominant Frequencies after Martin (1980)	Predominant Frequencies after Wiss (1967)
peat	5 - 10 Hz	
loose alluvial fill		5 - 10 Hz
silt	10Hz	
clay	20 - 30 Hz	15 - 25 Hz
sand		30 - 40 Hz

unknown. In 1955, Miller and Pursey (1955) examined the case of a uniformly distributed circular energy source, oscillating vertically on the surface of an ideal, homogeneous, isotropic, elastic half space and they concluded from this analysis that approximately two-thirds of the energy that was imparted to the soil was transmitted as Rayleigh waves. As a result of their findings, most researchers now believe that surface sources of vibration predominantly generate Rayleigh waves. Researchers such as Dalmatov et al (1968) and Lo (1976) have confirmed Miller and Pursey's findings by measuring attenuation rates in the field.

The attenuation rates of P waves, S waves, and Rayleigh waves can be determined approximately by elastic theory. Such an analysis shows that both compression waves and shear waves which are collectively known as body waves, attenuate at a significantly faster rate than Rayleigh waves. For example, body waves traveling within an elastic half-space radiate outwards from the source on a spherical front and therefore the amplitude of this motion attenuates at a rate which is proportional to d^{-1}, (where d is defined as the distance from the energy source). At the surface of an elastic half-space, the amplitudes of body waves attenuate at an even faster rate proportional to d^{-2}. In contrast, Rayleigh waves which radiate from the source on a conical front, attenuate at a rate which is proportional to $d^{-\frac{1}{2}}$. Rayleigh waves with real wave numbers, K, are characterized by the fact that all points on a vertical plane move in phase with each other.

The ground vibrations that are produced by non-seismic sources can further be classified as one of three types of vibration (after Wiss, 1981):

1) Transient or impact ground vibrations which are typically generated by activities such as blasting, impact pile driving and demolition, where there is sufficient time between each impact for vibrations to attenuate significantly,

2) steady-state or continuous vibrations which are generated by pieces of equipment such as vibratory pile drivers, large pumps and compressors, and

3) pseudo-steady-state vibrations which are typically produced by equipment such as jackhammers, pavement breakers, trucks, bulldozers, cranes and scrapers. These vibrations are either random in nature or generated by surface impacts which occur at a short enough interval so that the induced vibrations approach steady-state conditions.

These three types of vibration are illustrated in Figure 2.1.

Before vibration levels for the various sources are presented it should also be pointed out that the magnitude of non-seismic ground vibrations is usually assessed by measuring peak particle velocities at the ground surface. This measure was probably chosen because early researchers were primarily interested in the effects of ground vibrations on structures and it was concluded that levels of structural damage could best be correlated with peak ground surface velocities measured adjacent to the structure (Edwards and Northwood (1960), Northwood et al (1963) and Nicholls et al

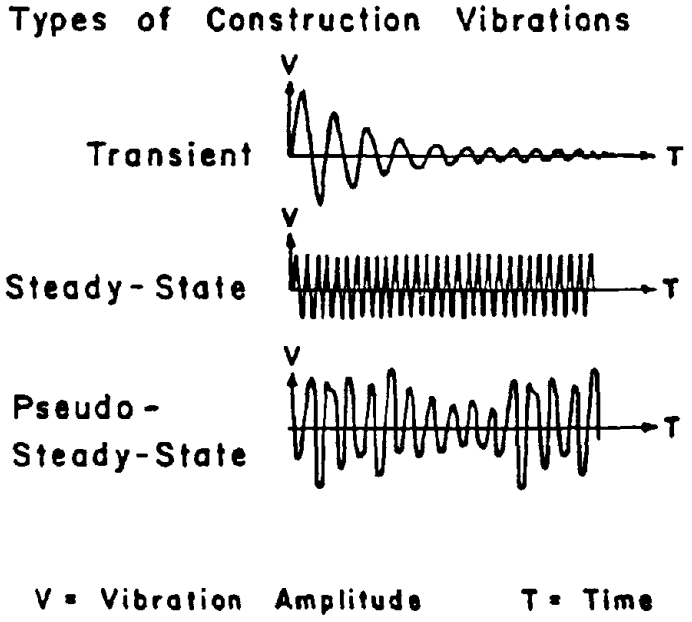

FIG 2.1 THREE TYPES OF NON-SEISMIC GROUND VIBRATIONS (from Wiss, 1981).

(1971)). Other researchers subsequently found that peak particle velocity could also be closely related to ground settlements and to levels of human awareness. For example Dalmatov et al (1968) report that peak particle velocity is closely related to ground settlements associated with pile driving, and Wiss (1974) states that human awareness to vibrations is closely related to the peak particle velocity. It should also be noted however, that levels of building damage, human awareness, and ground settlements have also been related to peak ground accelerations and peak ground displacements.

This chapter presents a summary of the characteristics of ground vibrations that are generated by such non-seismic sources as blasting, dynamic compaction, pile driving, construction equipment, road traffic and rail traffic. No attempt was made to investigate the characteristics of ground vibrations produced by machinery or by the demolition of buildings. A brief discussion of earthquake-induced liquefaction is also presented in order to provide an indication of the lowest levels of acceleration at which liquefaction is known to have occurred during these events.

2.2. Liquefaction Potential of Earthquakes

The maximum distance at which liquefaction can occur from the zone of faulting has been studied by a number of investigators including Kuribayashi and Tatsuoka (1975) who developed a plot of the maximum distance of liquefaction, R, versus earthquake magnitude. The distance, R, was defined by these authors as being the distance from the epicenter of an earthquake to the most distant occurrence of liquefaction. While it is commonly accepted that the level of shaking at a site is more closely

related to the shortest distance from the surface expression of rupture than to the epicentral distance, rupture surface determinations were only made for a few of the earthquakes reported by Kuribayashi and Tatsuoka (Davis and Berrill, 1983). Therefore the amount of data that could be shown on a plot of earthquake magnitude versus closest distance to the causative fault would be insufficient to produce an acceptable upper bound for R. The data points presented in the Kuribayashi and Tatsuoka plot represent Japanese sites which liquefied during the last century. Approximately 100 sites were noted to have liquefied during more than 44 earthquakes.

Several authors have subsequently added points to Kuribayashi and Tatsuoka's original plot. These authors include Youd (1977) who provided points from 13 non-Japanese earthquakes, Davis and Berrill (1983) who provided 5 points from earthquakes recorded in several countries, and Tokimatsu and Seed (1984) who provided the additional 7 points listed in Table 2.2. A complete plot showing all of this data is presented in Figure 2.2.

Since post-earthquake reconnaissance studies such as the study conducted by Youd (1977) appear to show that earthquakes below a magnitude of about 5 are incapable of inducing liquefaction, the upper bound curve in Figure 2.2 drops off sharply for earthquake magnitudes less than about $5\frac{1}{4}$ and is shown dashed in this region. Youd investigated several magnitude 4 to 5 earthquakes which occurred in areas containing potentially liquefiable sediments, and was unable to find any evidence of liquefaction. The limiting earthquake magnitude suggested by this figure is approxi-

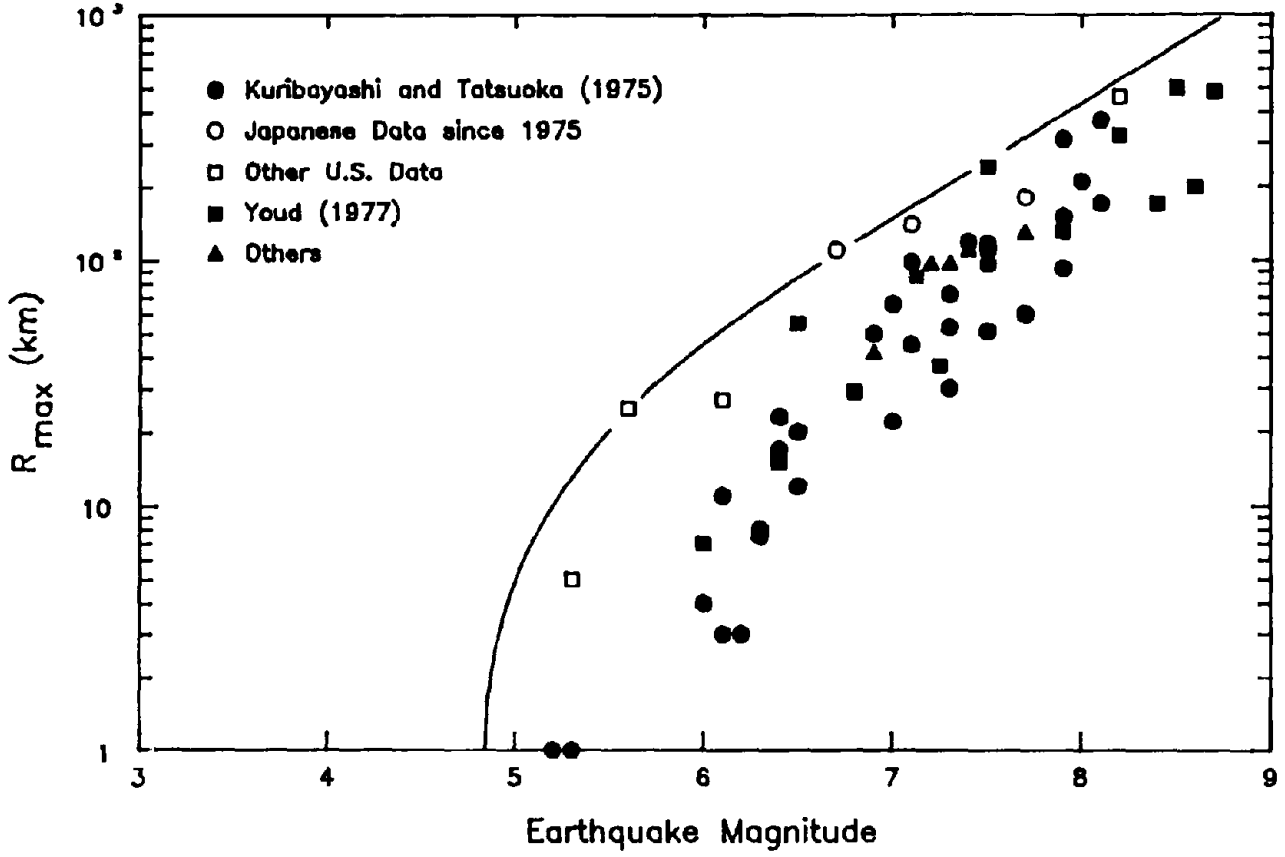

FIG 2.2 MAXIMUM DISTANCE OF LIQUEFACTION FROM THE ZONE OF FAULTING (based on data from Tokimatsu and Seed, 1984).

Table 2.2 : Case Histories of Maximum Distance to Liquefaction versus Earthquake Magnitude

Year	Earthquake	Magnitude	Epicentral Distance (km)
1811	New Madrid EQ (Fuller, 1912)	8.2	460
1966	Parkfield EQ (Ross, 1968)	5.6	25
1981	Mammoth Lakes EQ (LADWP, 1981)	6.1	27
1957	San Francisco EQ (Ross, 1968)	5.3	5
1978	Miyagiken-oki EQ (Tohno and Yasuda, 1981)	6.7	110
1983	Nihonkai-chubu EQ (Tohno et al, 1983)	7.7	180
1983	6/21/83 EQ (Tohno et al, 1983)	7.1	140

mately equal to $4\frac{3}{4}$ and is only slightly smaller than the cutoff of M = 5 suggested by Youd.

With the aid of both the upper bound curve shown in Figure 2.2 and available attenuation relationships between maximum ground acceleration, earthquake magnitude and epicentral distance, it is possible to estimate the minimum ground accelerations for which liquefaction has been induced by earthquake shaking. The values of ground acceleration shown adjacent to the curve in Figure 2.3 were obtained by averaging the results of attenuation relationships presented by Orphal and Lahoud (1974), McGuire (1977), Donovan and Bornstein (1978), Iwasaki et al (1978a), McGuire (1978), Cornell et al (1979), Battis (1981) and Hasegawa et al (1981). It may be noted from this

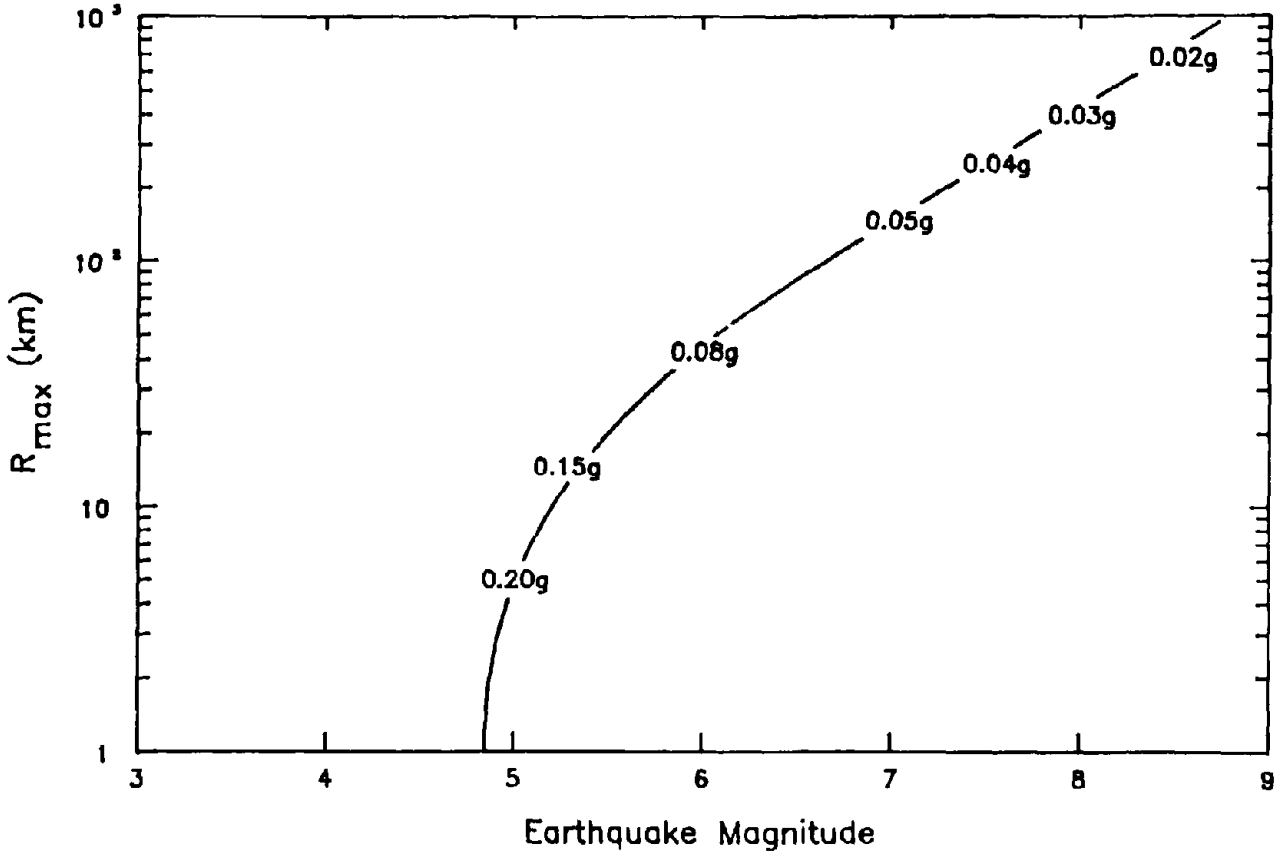

FIG 2.3 MINIMUM LEVEL OF SURFACE SHAKING ESTIMATED FROM FIELD PERFORMANCE DATA IN FIG. 2.2.

figure that ground vibrations generated by magnitude 8 earthquakes are predicted to be capable of liquefying sands when their ground surface accelerations exceed a value of about 0.02g. This level of shaking is significantly smaller than 0.05 - 0.10g, which is commonly perceived to be the minimum level of shaking required to induce liquefaction.

2.3. Ground Vibrations Produced by Blasting

The ground vibrations that are generated by blasting are known to be capable of liquefying saturated sands. In fact engineers have used this capability to densify deep deposits of loose saturated sand by detonating charges within these layers. Ground vibrations produced by the blast liquefy the sand which increases in density as the pore pressures dissipate. This ability to liquefy sands has also been used by Russian engineers as a means of evaluating the liquefaction potential of sand sites.

The characteristics of ground vibrations that are produced by blasting have been extensively studied by numerous researchers. However despite this effort, researchers are still unable to predict the intensity of shaking with a high degree of accuracy, primarily because of the large number of factors which influence the ground vibration magnitudes. It is the influence of these factors which include the weight of charge per delay, the delay timing, the geological conditions, the type of explosive and the geometry of the blast that helps to explain the large amount of scatter in any plot of peak particle velocity versus some scaled distance term.

The high degree of uncertainty that is associated with predicting blast-induced ground vibration levels is a direct consequence of the large amount of scatter evident in the recorded data. This scatter is clearly illustrated in a plot developed by Dowding (1985), who plotted values of peak particle velocity against scaled distance for over 2500 construction, quarry, and surface coal mine blasts. Dowding attempted to reduce the scatter in this plot by making separate plots for construction blasts, quarry blasts and surface coal mine blasts; however replotting the data in this fashion did not significantly reduce the scatter. These three plots which are reproduced in Figure 2.4 show that peak particle velocity still varies by as much as two orders of magnitude for any single value of scaled distance.

It is because of this scatter that most empirical formulae which predict ground vibration magnitudes represent specific levels of exceedence as illustrated by the lines shown in Figure 2.4. The line labeled 50 is the least squares, best fit line for the data, while the other two lines are bounds below which lie 84% and 95% of the data points. Most researchers state that in the absence of site specific measurements, 95 percentile relationships should be used to predict peak particle velocities at any given site.

The velocity amplitudes of blast-induced ground vibrations are most commonly expressed as a function of either square root scaled distance, $\frac{d}{\sqrt{w}}$ or cube root scaled distance, $\frac{d}{w^{1/3}}$, where d is defined as the distance from the source and w is the weight of explosive detonated per delay. Both of these terms were derived from the more general non-dimensionalized term $\frac{w}{\rho c^2 d^3}$. Dowding (1985) states that both ρ

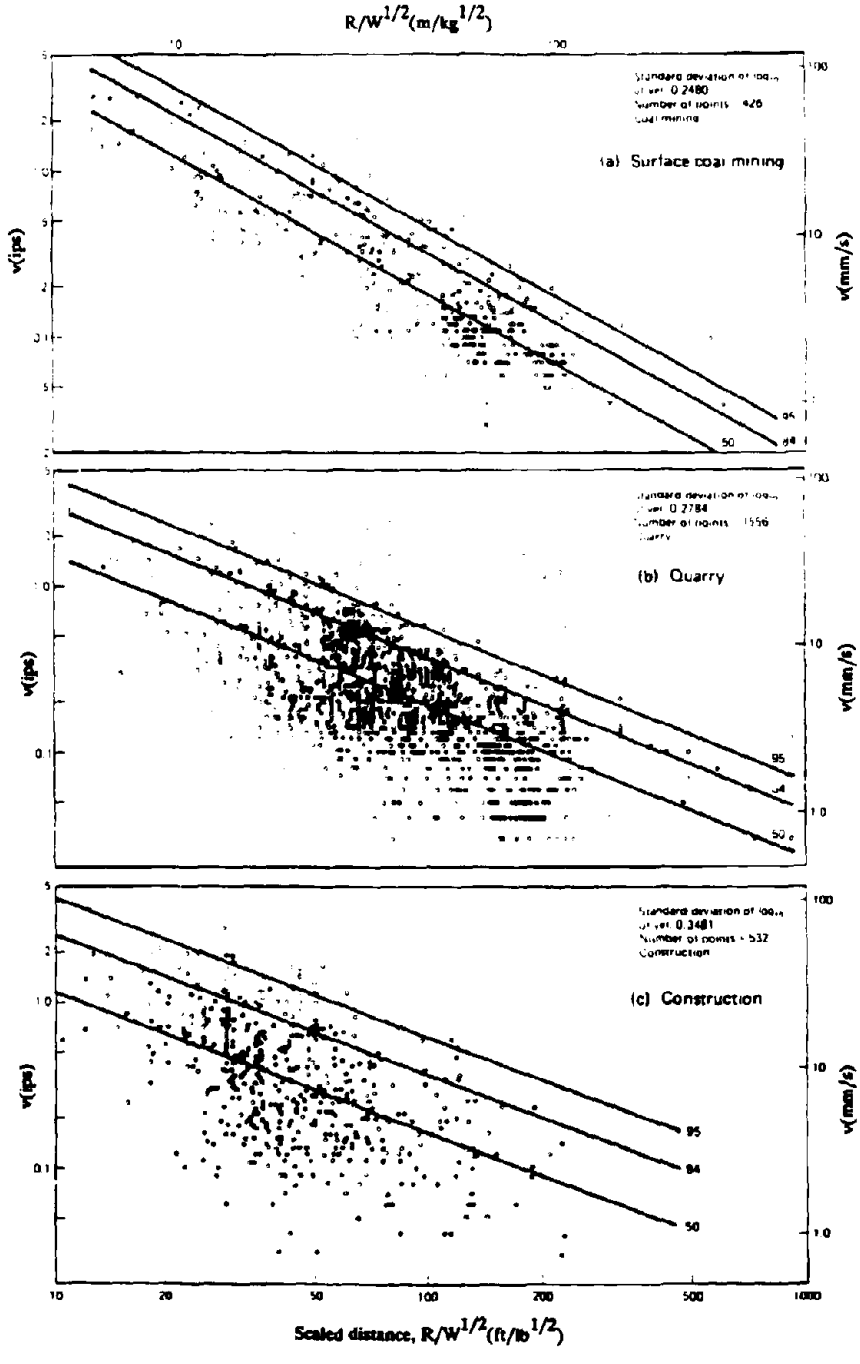

FIG 2.4 PEAK PARTICLE VELOCITY AS A FUNCTION OF SCALED DISTANCE FOR CONSTRUCTION, QUARRY, AND SURFACE COAL MINE BLASTS (from Dowding, 1985).

(the density of the rock mass) and c (the seismic velocity of rock) were subsequently neglected because these parameters are not observed to vary significantly for different rocks. However the seismic velocity may vary from one rock to another by a factor of two, and changes in seismic velocity of this magnitude would appear to significantly affect the value of the non-dimensionalized term.

Several of the attenuation relationships which predict vibration levels as a function of cube root scaled distance are presented in Figure 2.5. The solid line shown in this figure was proposed by Ambraseys and Hendron (1968), who developed their relationship from measurements of ground vibrations at a wide range of sites. The ground vibrations at these sites were produced by blasts in which the weight of charge per delay varied from 14 to 14,500 kg (30 to 32,000 lbs). Ambraseys and Hendron's relationship implies that ground vibrations decay at a rate proportional to $d^{-2.8}$ near to the source, and at a rate proportional to $d^{-1.6}$ for scaled distances greater than 10; these rates of decay are similar to the rates of decay associated with body waves (refer to Section 2.2).

Three of the most commonly used square root relationships are shown in Figure 2.6. Curves A and B in this figure represent upper and lower bounds for peak particle velocities produced by conventional blasts and Oriard (1971) states that the upper bound curve, curve B, should be used to predict peak particle velocities in the absence of a site-specific survey. Since blasts with unusual confinement tend to produce ground vibrations of greater magnitude than conventional blasts, curve C should be used to predict vibration levels produced by these types of blasts. Two examples of

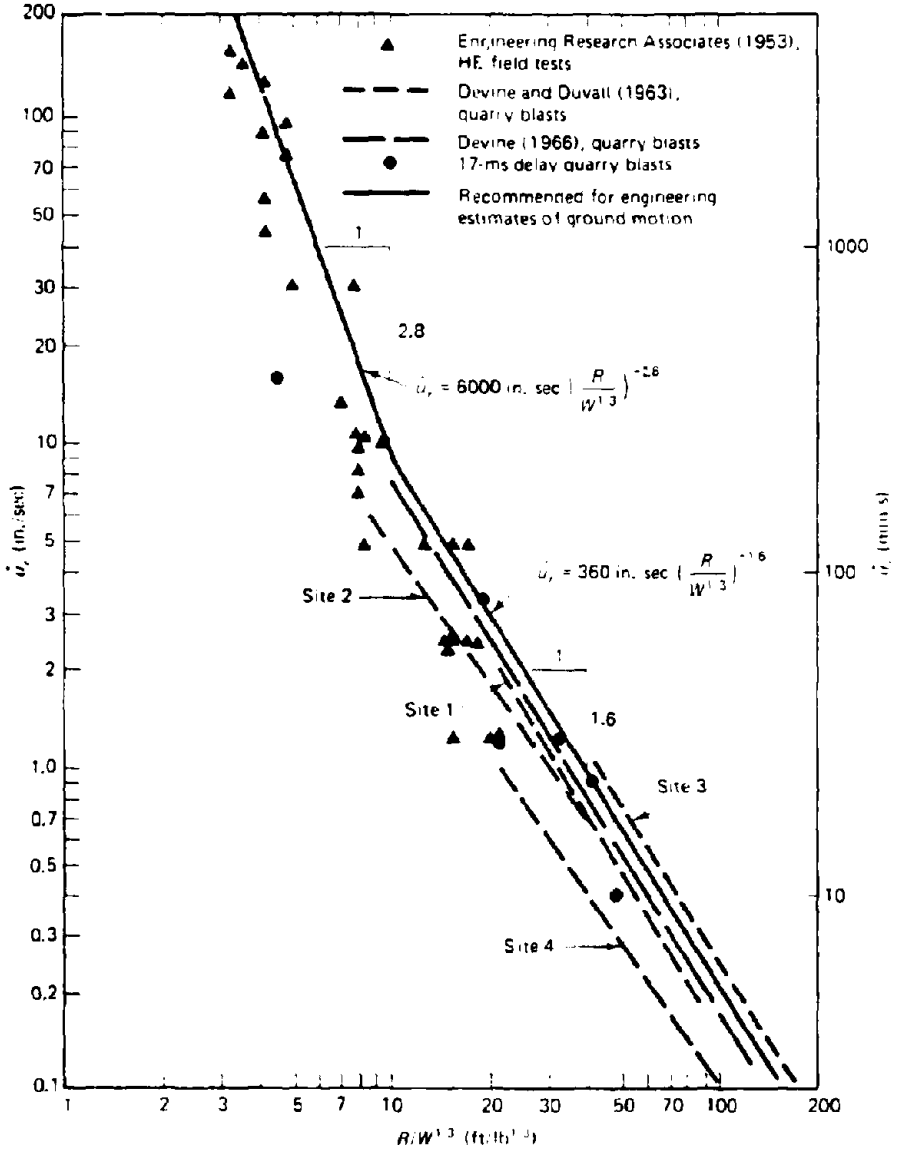

FIG 2.5 MAXIMUM RADIAL PARTICLE VELOCITY AS A FUNCTION OF CUBE ROOT SCALED DISTANCE (from Ambraseys and Hendron, 1968).

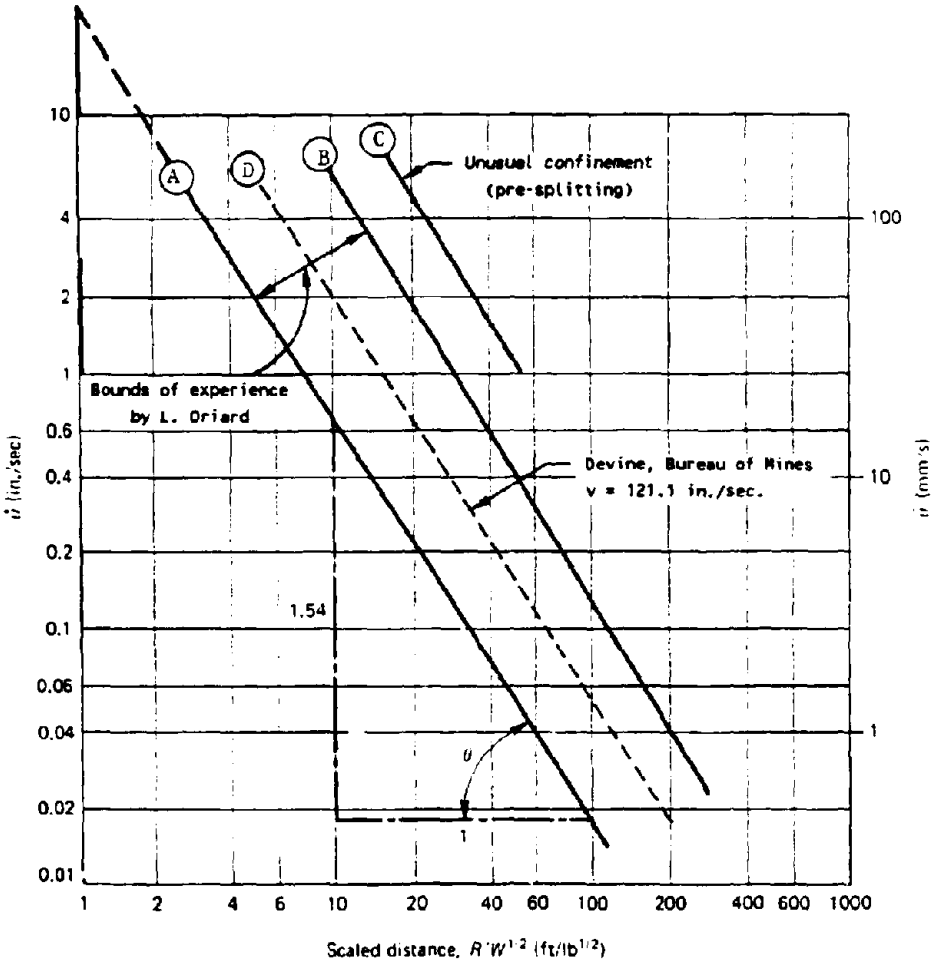

FIG 2.6 MAXIMUM PARTICLE VELOCITY AS A FUNCTION OF SQUARE ROOT SCALED DISTANCE (after Hendron, 1977, and Dowding, 1985).

blasts with unusual confinement are blasts produced by the simultaneous detonation of holes along a presplit line or blasts produced by detonation of the first holes in the cut round of a tunnel. Curves A, B and C are based on Oriard's personal experience with ground vibration amplitudes while Line D is the line of best fit suggested by Devine (1966). Curves A and B imply that peak particle velocities vary by approximately one order of magnitude for any value of scaled distance. Hendron (1977) states that a scatter of this magnitude is typical for data obtained from down-hole blasting.

It is worth noting that the peak particle velocities predicted by square root scaling relationships are approximately the same as those predicted by cube root scaling relationships, a point which is amply illustrated by Dowding (1985), who compared the peak particle velocities predicted by Oriard's (1971) relationship and Ambraseys and Hendron's (1968) relationship. Dowding found that the velocities predicted by these two relationships were not significantly different within a range of 6m to 31m (20 ft to 100 ft) from the blast. At distances greater than 31m from the source however, the square root relationship suggested by Oriard was observed to be more conservative while the cube root relationship was more conservative at distances closer than 6m from the source.

Time history traces depicting the three perpendicular components of a typical blast-induced ground vibration are shown in Figure 2.7. This ground vibration was produced by a blast in a surface coal mine. Component L (the longitudinal component) depicts the motion along a horizontal radius from the blast, component V depicts the vertical component, and component T depicts the transverse component which

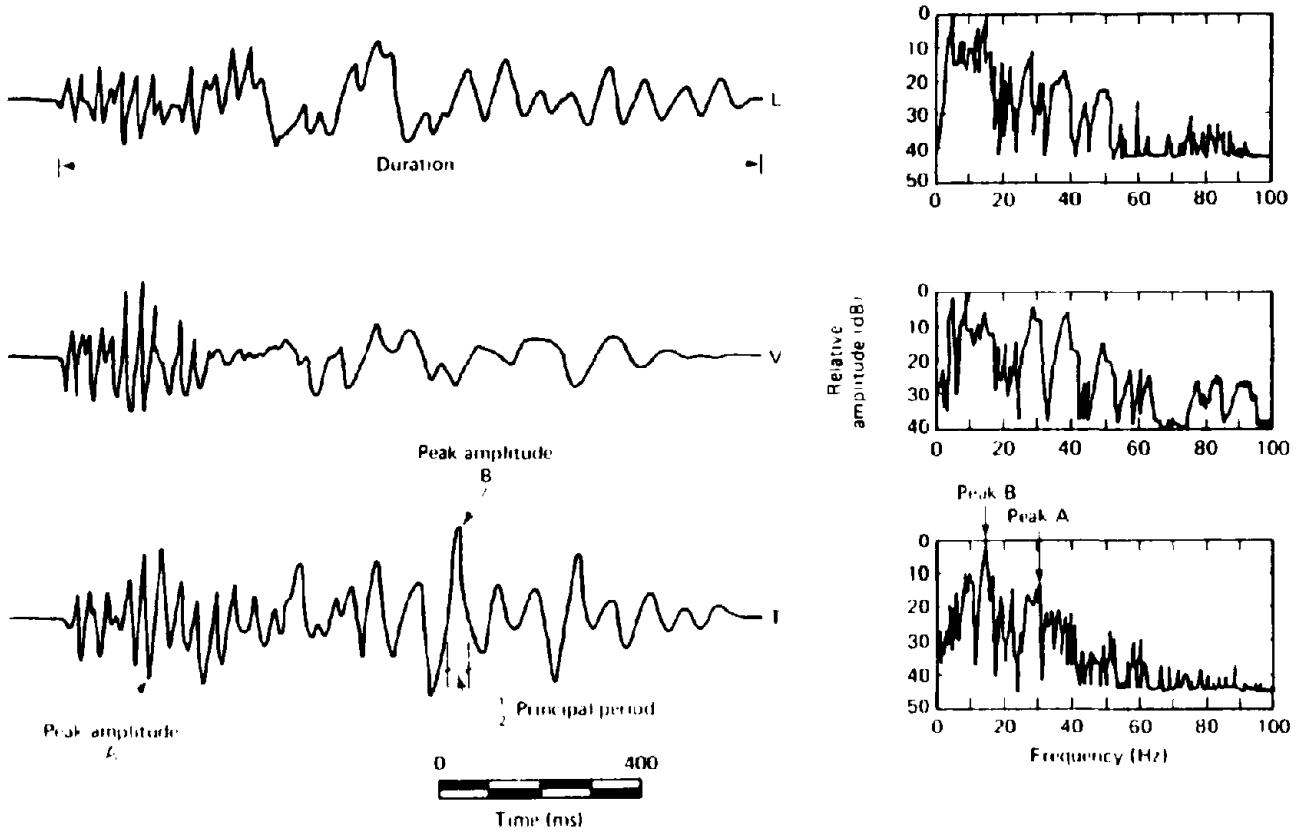

FIG 2.7 TYPICAL COAL MINE BLAST VIBRATION TIME HISTORIES (from Stagg et al, 1980).

is perpendicular to the longitudinal component. Fourier amplitude spectra indicating the relative amplitudes of different frequency peaks for these motions are shown on the right of this figure.

The dominant frequencies of blast-induced ground vibrations are noted to vary over a range of 0.5 to 200 Hz (Cording et al, 1975). However this range is misleading since individual types of blasting tend to produce a more limited range of frequencies as shown in Figure 2.8 (after Siskind, 1980). The bar graphs for surface coal mine blasting, quarry blasting and construction blasting that are presented in this figure suggest the following ranges of predominant frequency:

Surface coal mine blasting	:	5 to 25 Hz
Quarry blasting	:	10 to 35 Hz
Construction blasting	:	15 to 60 Hz

The frequency content of ground vibrations is also dependent on the distance from the source and the medium through which the motions propagate.

One recent development in the field of blast vibration prediction is the development of techniques to predict response spectra for ground motions produced by blasting. The development of these techniques is important because the dynamic response of a structure is dependent upon both the magnitude of the ground vibrations and their frequency content. Components of ground motions with frequencies close to the natural frequency of the structure will be amplified. One of the first techniques for developing response spectra for blast-induced vibrations was proposed by Dowding (1971), and a detailed description of this procedure is provided by Dowding (1985).

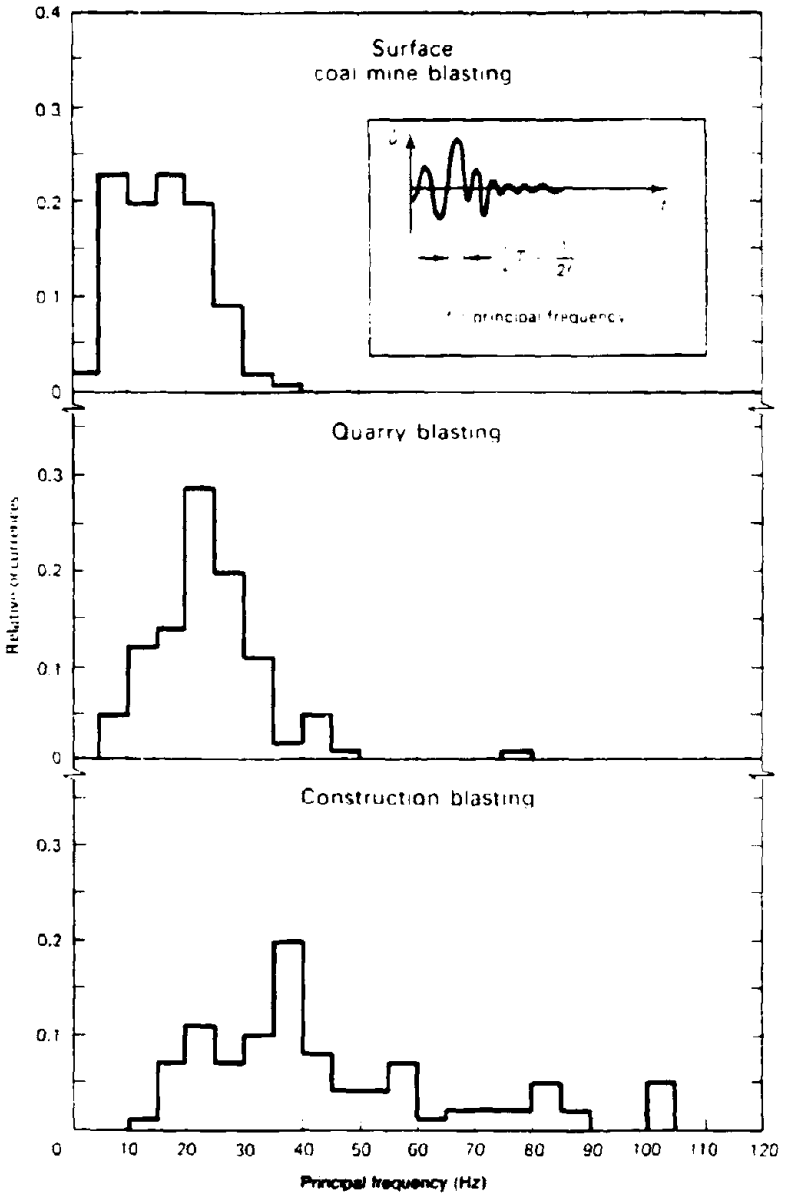

FIG 2.8 PREDOMINANT FREQUENCY HISTOGRAMS AT STRUCTURES OF CONCERN (after Siskind et al, 1980).

Other procedures for developing response spectra for ground vibrations produced by blasting have been presented by Medearis (1977) and Naik (1979)

Despite the fact that the characteristics of ground vibrations produced by blasting have been studied extensively, it is concluded that researchers are still unable to predict the magnitude of blast-induced vibrations with any reasonable degree of accuracy. Accurate prediction is thwarted by the large number of factors which influence the intensity of shaking and it is these factors that are responsible for the wide ranges in values of typical blast parameters, presented in Table 2.3 (after Cording et al, 1975). Since these values are associated with normal blasting operations for tunneling, surface mining and construction activities, Dowding (1985) states that the ranges presented in this table should be extended to higher values for special cases such as close-in blasting. Unfortunately data is not available for vibration levels close to the source because most monitoring equipment is unable to withstand this extreme environment.

Table 2.3 : Typical Range for Blast Parameters (after Cording et al, 1975)

Parameter	Range
displacement	10^{-4} - 10 mm
velocity	10^{-3} - 10^{-1} *mm/sec*
acceleration	10^{-3} - 10 g
pulse duration	0.5 - 2 secs
wavelength	3 to 1500m
frequency	0.5 to 200 Hz
strain	3×10^{-6} to 5×10^{-2}

Because peak particle velocity is observed to vary by as much as 2 orders of magnitude for any value of scaled distance, the best way to determine ground vibration characteristics is to conduct a site specific survey. Ground vibration levels measured at the site can be extrapolated to greater distances by expressing these levels as a function of either square root scaled distance or cube root scaled distance. In the absence of such a survey however, vibration levels should be predicted by using formulae which represent 95 percentile upper bound curves for previously recorded data; these levels should be revised once blasting has commenced. Figure 2.9 which shows velocity attenuation curves for blasts involving 10 kg (22 lbs), 100 kg and 1000 kg of charge per delay, is included to provide the reader with a feel for the amplitudes of typical blast-induced ground vibrations. These curves are based on the upper bound curve (curve B in Figure 2.6) proposed by Oriard (1971).

2.4. Ground Vibrations Produced by Dynamic Compaction

Even though dynamic compaction has been used to compact soils for centuries, it was not until 1970 that Louis Menard formally promoted this technique as a means of attaining significant levels of ground improvement. The technique of dynamic compaction involves dropping weights from significant heights onto the ground surface; most weights vary in size from 5 to 20 tonnes (5.5 to 22 tons), and drop heights typically range from 10 to 25m (30 to 85 ft); however they may be as high as 40m. The degree of densification that can be attained and the depth of significant improvement, are dependent upon the soil profile and the impact energy of the weight.

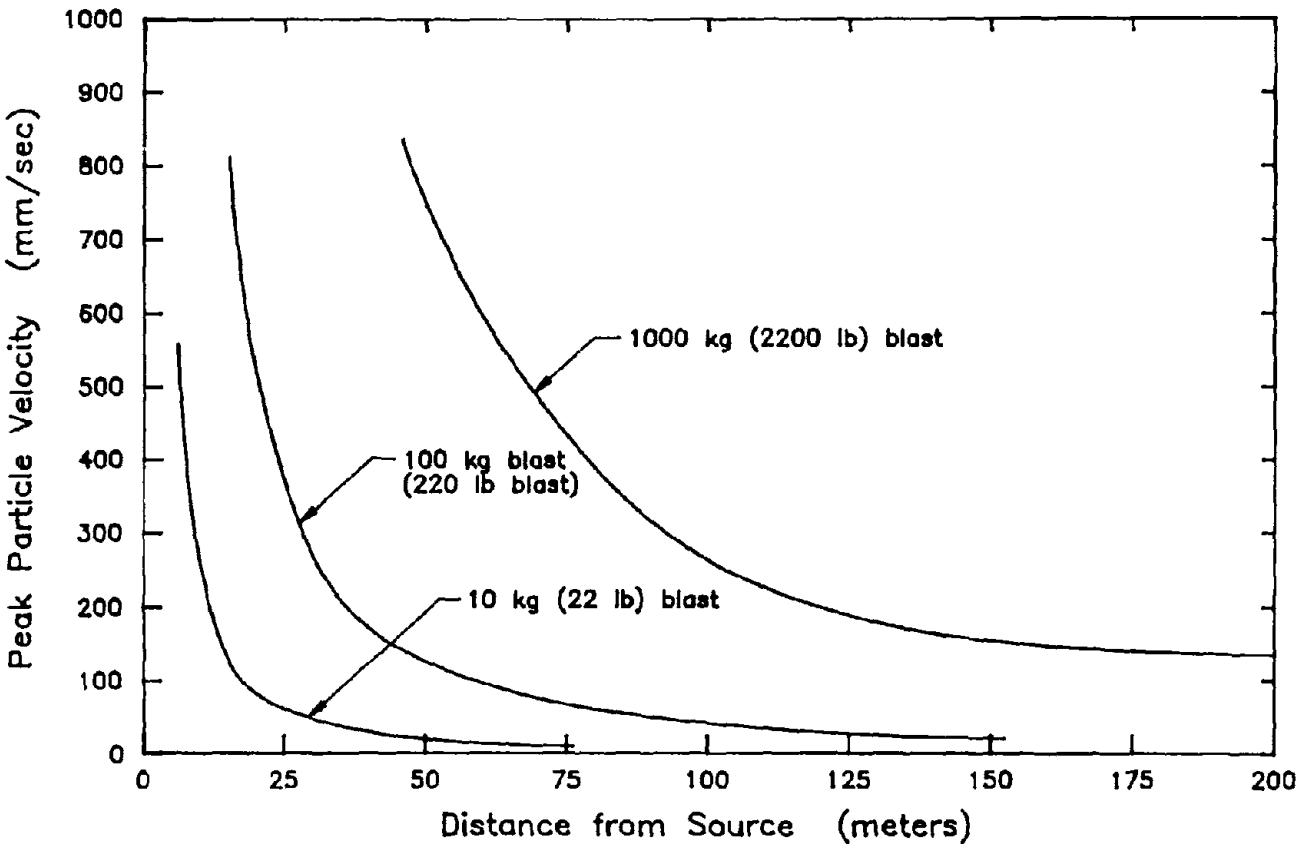

FIG 2.9 PEAK PARTICLE VELOCITIES AS A FUNCTION OF DISTANCE FOR BLASTS INVOLVING 10 kg, 100 kg, AND 1000 kg OF CHARGE PER DELAY, BASED ON THE SQUARE ROOT ATTENUATION RELATIONSHIP PROPOSED BY ORIARD (1971).

Dynamic compaction is particularly effective as a method for compacting loose saturated cohesionless soils, principally because the ground vibrations generated by the impact of a weight on the ground surface, are capable of liquefying these types of soils. This capacity to liquefy saturated cohesionless soils is noted by Mitchell (1981) and a specific example is cited by Lukas (1980). In addition Charles et al (1981) who measured the pore pressure response in a piezometer located directly beneath a pounder, observed that the pore pressure rose over a period of half a second. This observation is significant since the duration of significant shaking produced by a single impact typically lasts for about half a second.

Numerous researchers have proposed empirical relationships which predict ground vibration levels produced by dynamic compaction; the simplest of these express peak particle velocity as a function of distance. Relationships of this latter type have been proposed by both Leonards et al (1980) and Mayne (1985) who compiled a plot of peak particle velocity versus distance for ground vibration levels recorded at twelve dynamic compaction sites. Equations 2.1 and 2.2 represent upper bounds for the data.

$$PPV\ (mm/sec) = \left[\frac{153}{d(m)}\right]^{1.7} \qquad 2.1$$

$$PPV\ (ips) = \left[\frac{75}{d(ft)}\right]^{1.7} \qquad 2.2$$

where PPV = peak particle velocity
and d = distance to point of impact

The data presented in Mayne's plot indicates that peak particle velocities varied by more than one order of magnitude for any given distance, a scatter that is typical of such plots. This scatter may be partially attributed to the observation that the size of weights being dropped at these sites varied from 3.1 to 40.5 tonnes (3.4 to 45 tons), and that the drop heights varied from 1.5 to 30.5 meters (5 to 100 ft). The soils at most of the twelve sites were granular fill.

The majority of empirical relationships which predict ground vibration levels produced by dynamic compaction express peak particle velocity as a function of some scaled distance term involving the potential energy of the falling mass. Relationships of this type have been proposed by Mayne, Jones and Dumas (1984), Lukas (1984), Gambin (1984) and Mayne (1985) who plot peak particle velocity as a function of $\frac{\sqrt{E_o}}{d}$, where E_o is the potential energy of the falling weight and d is the distance from the point of impact. The plot compiled by Mayne, Jones and Dumas presents field data from some 14 sites which included deposits of silty sands, sandy fills, sandy clays rubble, coal spoil and debris fill. They concluded from their plot that a safe upper limit for preliminary estimates of peak particle velocity is provided by the equation:

$$PPV\ (mm/sec) \leq 70 \left[\frac{\sqrt{W \cdot H}}{d}\right]^{1.4} \qquad 2.3$$

where W = mass of weight (tonnes),
H = height of drop (meters), and
d = distance from impact (meters)

A typical plot of peak particle velocity versus scaled distance is shown in Figure 2.10 (from Mayne, 1985). The data shown in this plot was recorded at 12 compaction sites and is bounded by the equations:

$$PPV\ (mm/sec) = 92 \left[\frac{\sqrt{W \cdot H}}{d}\right]^{1.7} \qquad 2.4$$

where W is measured in tonnes, and
d, and H are measured in meters

$$PPV\ (in/sec) = 8 \left[\frac{\sqrt{W \cdot H}}{d}\right]^{1.7} \qquad 2.5$$

where W is measured in tons, and
d, and H are measured in feet

Since the peak particle velocities shown in Figure 2.10 vary by almost one order of magnitude for any given value of scaled distance, it may be concluded that neither the relationships derived from plots of PPV versus scaled distance nor those derived from plots of PPV versus distance are able to predict the amplitude of dynamic compaction-induced ground vibrations with a high degree of accuracy. A similar degree of scatter

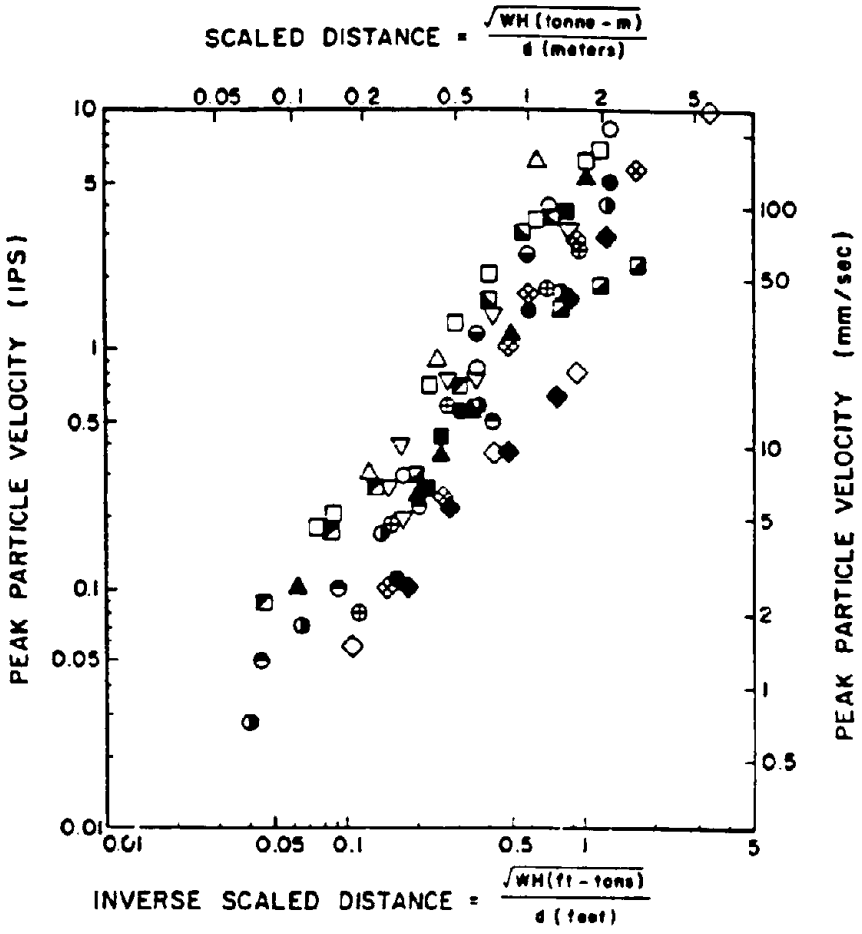

FIG 2.10 PARTICLE VELOCITY AS A FUNCTION OF INVERSE SCALED DISTANCE FOR DYNAMIC COMPACTION (from Mayne, 1985).

was also evident in Mayne, Jones and Dumas's (1984) plot of PPV versus scaled distance.

The best relationship for predicting peak particle velocity appears to be that proposed by Mayne (1985) who observed that the scatter in ground vibration levels was greatly reduced by plotting the data as normalized particle velocity against a normalized distance term. Mayne normalized the peak particle velocities by dividing them by the theoretical velocity of the free falling weight on impact, while the distance from the point of impact was normalized against the radius of the weight, r_o. Replotting the data in Figure 2.10 in this form lead to the greatly reduced scatter shown in Figure 2.11. This small degree of scatter is particularly encouraging considering the wide range of weights and drop heights involved; however Mayne cautions that it may be fortuitous. The best representative line through the data in Figure 2.11 (after Mayne, 1985) is expressed by the equation:

$$\frac{PPV}{\sqrt{2 \cdot g \cdot H}} = 0.2 \left[\frac{d}{r_0}\right]^{-1.7} \qquad 2.6$$

where d and r_0, and PPV and $\sqrt{2 \cdot g \cdot H}$ are in consistent units.

This apparent dependence of peak particle velocity on the dimensions of the falling weight was also observed by Menard (no date) who notes: "the amplitude of the vibrations is only slightly influenced by the height of fall of the pounder but increases noticeably with the area of impact." However since in reality, the equivalent radii of most dynamic compaction weights only range from 0.6 to 1.1m (2 to 3.5 ft), scatter is

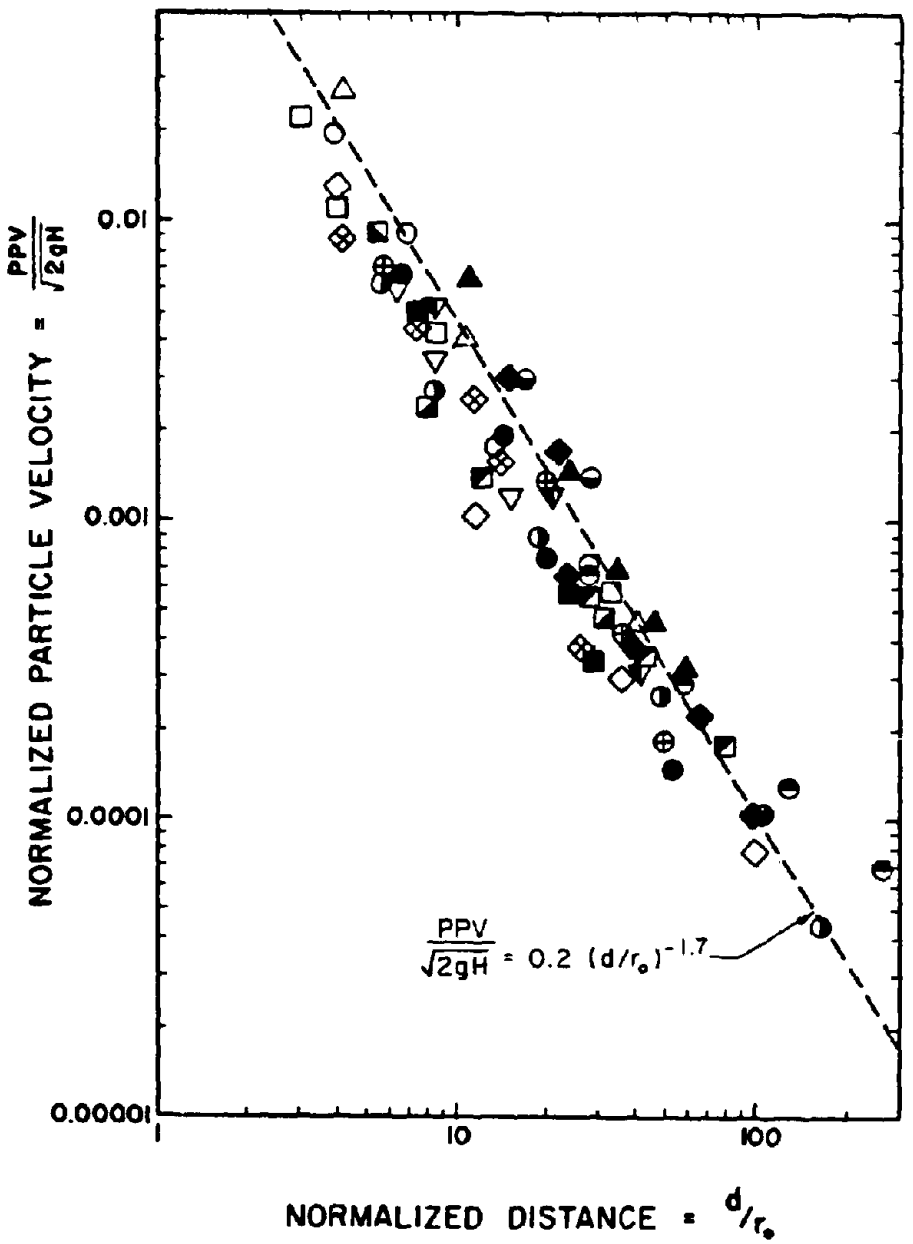

FIG 2.11 OBSERVED ATTENUATION OF NORMALIZED PARTICLE VELOCITY WITH NORMALIZED DISTANCE FOR DYNAMIC COMPACTION. (from Mayne, 1985).

also likely to be small in plots of normalized peak particle velocity versus distance.

A typical recording of a near field dynamic compaction-induced ground motion is shown in Figure 2.12. This trace which was produced by the impact of a 5.9 tonne (6.5 ton) weight falling from a height of 12 meters (40 ft), was recorded by a seismograph located on a footing at a distance of 3.5 meters from the point of impact. As is typical of these ground motions the longitudinal component of the ground motion shown in Figure 2.12 is dominant and the transverse component is very small. Published ground vibration records also appear to show that each impact typically produces 2 to 3 cycles of significant shaking near to the source and that this number of cycles tends to increase as the waves propagate away from the source due to wave dispersion. Menard (no date) states that a typical compaction-induced ground vibration consists of 3 to 6 cycles of almost constant amplitude.

Both Mitchell (1981) and Mayne (1985) suggest that the predominant frequencies of ground vibrations produced by dynamic compaction range from about 2 to 20 Hz. Menard however proposes a more limited range of 2 to 12 Hz and further states that predominant frequencies of 3 to 4 Hz are most common. Values of predominant frequency reported by other investigators include the following:

Leonards et al. (1980)	:	Loose fine to medium sand	6 - 8 Hz
Lukas (1984)	:	Rubble fill	10 - 20 Hz

Because the predominant frequencies of dynamic compaction-induced ground vibrations are typically much smaller than the predominant frequencies of ground vibrations

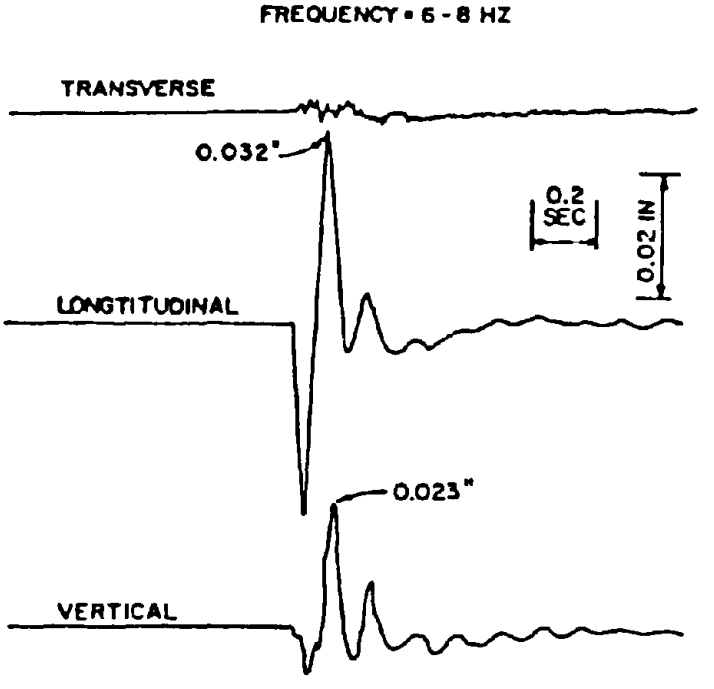

FIG 2.12 TYPICAL NEAR-FIELD DYNAMIC COMPACTION-INDUCED GROUND MOTION (from Leonards et al, 1980).

produced by other non-seismic sources and the natural frequencies of many residential structures lie within the same range, ground vibrations generated by dynamic compaction are potentially more damaging than those generated by other non-seismic sources. The relatively low predominant frequencies are attributed to the large strains induced in the soil by the impact of the falling weight; Hansbo (1977, 1978) states that the shear modulus associated with such large strains is about one tenth of the low strain shear modulus.

One factor of major interest in the use of dynamic compaction is the depth of significant ground improvement which is primarily a function of the impact energy imparted by the falling weight. Three formulae which predict this depth are listed in Equations 2.7, 2.8 and 2.9. Menard and Broise (1975) suggest that the maximum depth of influence can be calculated using:

$$D = \sqrt{W \cdot H} \qquad 2.7$$

where D = maximum depth of influence (meters),
W = mass of falling weight (tonnes), and
H = height of drop (meters)

Leonards et al (1980), who plotted the results from seven sites, found that the line of best fit through their data was given by Equation 2.8:

$$D = 0.5 \sqrt{W \cdot H} \qquad 2.8$$

The third relationship which was proposed by Lukas (1980) is as follows:

$$D = (0.65 - 0.80)\sqrt{W \cdot H} \qquad 2.9$$

These different results may be partially attributed to the fact that the depth of significant ground improvement is a matter of subjective judgement. As Mitchell (1981) points out, this depth depends upon both the method of measurement and the engineer's definition of what constitutes significant ground improvement. Two factors which also influence the maximum depth of improvement are the efficiency of the weight-dropping system and the nature of the soil profile at the site. For example Leonards et al (1980) report that clay seams within a site greatly reduced the efficiency of dynamic compaction.

All of of the formulae that have been presented thus far are based on field performance data; however it should also be pointed out that several researchers such as Scott and Pearce (1975), Mayne, Jones and Boudra (1983), Mayne, Jones and Fedosick (1982) and Wallays (1983) have developed formulae based on numerical models. Most of these formulae predict the impact stresses generated by a weight colliding with the ground surface; however several also predict stress attenuation from the point of contact. Mayne and Jones (1983) reviewed formulae of this type and concluded that elastic theory provided a reasonable prediction of stress attenuation in granular soils, even though only those relationships proposed by Wallays had been compared with the results of full scale tests. Since acceptable predictions were made in four out of the five case studies that Wallays examined, Wallays concluded that his formulae

provided an acceptable means of forecasting the performance of dynamic compaction and particularly the maximum depth of influence. Wallays also proposed formulae which predict the likely magnitudes of settlements at the surface and those at any depth within the site. Theoretical formulae for predicting the depth of influence, peak particle velocities and properties of the compacted soil such as effective stress friction angle, soil modulus, undrained shear strength, and overconsolidation ratio, have been presented by Mayne, Jones and Fedosick (1982).

In summary, it may be stated that most formulae which predict the level of ground vibrations produced by dynamic compaction express these levels as a function of either distance or some scaled distance term and since plots of peak particle velocity versus either distance or scaled distance indicate that measured values of peak particle velocity typically range over at least one order of magnitude for any given value of either distance, most of these formulae predict upper bound vibration levels. The formula which appears to provide the most accurate prediction of ground vibration levels is Equation 2.6, which was developed by Mayne (1985). Mayne discovered that by plotting normalized ground vibration levels against a normalized distance term the scatter in his data was greatly reduced although he cautions that such a limited scatter may be fortuitous.

In order to compare the levels of ground vibration that are likely to be generated by the various different non-seismic sources, Equation 2.6 has been used to produce velocity attenuation curves for two hypothetical dynamic compaction operations. These curves which are shown in Figure 2.13 are believed to depict upper bound

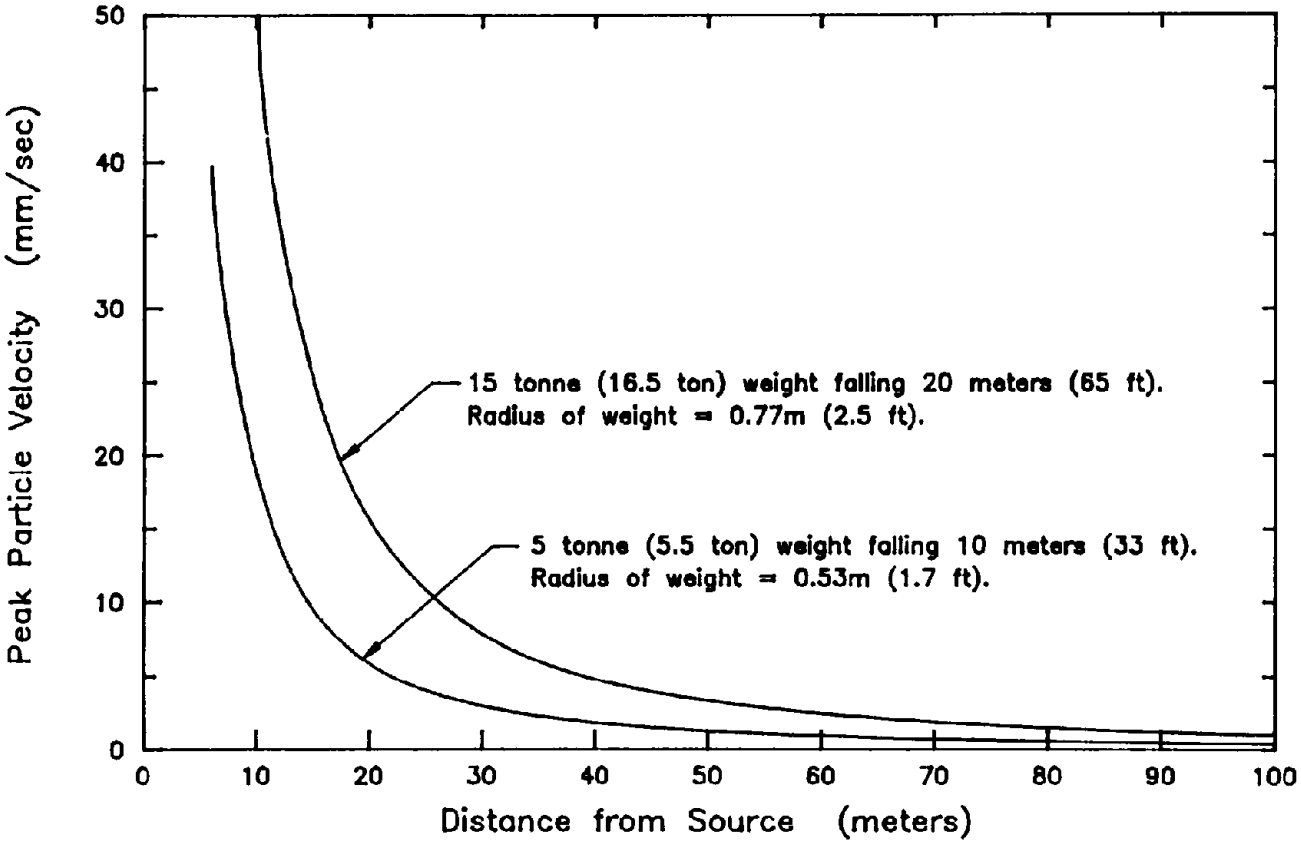

FIG 2.13 PEAK PARTICLE VELOCITY AS A FUNCTION OF DISTANCE FOR TWO HYPOTHETICAL DYNAMIC COMPACTION OPERATIONS, BASED ON THE RELATIONSHIP PROPOSED BY MAYNE (1985).

vibration levels for a 5 tonne weight falling from a height of 10m and a 15 tonne weight falling from a height of 20m and were calculated assuming a radius of 0.53m for the 5 tonne weight and a radius of 0.77m for the 15 tonne weight.

Over the last two decades dynamic compaction has become an accepted technique for compacting large areas of loose fills economically. This technique is particularly effective in compacting saturated cohesionless materials because the high levels of ground vibration that are produced by dynamic compaction are able to liquefy these materials. However, while such high levels of vibration are advantageous when trying to liquefy a soil they are also detrimental since these levels of vibration are capable of damaging structures. Dynamic compaction-induced ground vibrations are particularly damaging because they contain low predominant frequencies that are close to the natural frequencies of structures; therefore caution is required in using dynamic compaction in urban areas. Thompson and Herbert (1978) report a case history where ground vibrations produced by dynamic compaction were successfully arrested by digging 3m deep trenches at a distance of 10m from a bridge abutment. As a result vibrations in the abutment were reduced in amplitude by 95%.

2.5. Ground Vibrations Produced by Impact Pile Driving and Dynamic Pile Driving

Pile driving operations at sites containing saturated loose to medium-dense sands commonly cause significant ground settlements which often appear to be associated with some degree of liquefaction of the sand. This observation is supported by Lacy

and Gould (1985) who state that "in vulnerable sands the effect of pile driving is sometimes similar to that of a limited liquefaction in which materials are reported to have gone "quick"". Lacy and Gould further note that even marginally contractive sands may be liquefied by hard driving.

The settlements that are caused by pile driving are typically small in magnitude and are usually of little consequence. However in some cases, these settlements have had serious consequences and have led to the demolition of buildings located close to pile driving operations. Tschebotarioff (1973) describes a case history where H piles were being driven into a saturated medium-dense sand using both impact pile drivers and vibratory pile drivers. The wall of a six story building adjacent to the site had been underpinned in an attempt to prevent damage and the top of the wall was maintained to within 25 mm (1 inch) of its original position throughout the driving. Unfortunately, settlements occurred at distances well beyond the underpinned wall and as a result of these settlements two buildings, a 6 story building adjacent to the site and a neighboring 16-story building, had to be demolished.

Case histories involving ground settlements associated with pile driving have been reported by Lynch (1960), Dalmatov et al (1968), Tschebotarioff (1973), Heckman and Hagerty (1978), Clough and Chameau (1980), Lacy and Gould (1985) and Picornell and del Monte (1985) and several of these are presented in Table 2.4 (after Lacy and Gould, 1985). It is interesting to note that liquefaction is cited as the cause of most of the failures listed in this table. For example, Lacy and Gould state that settlement of the street in case b was probably caused by an increase in pore pressures due to pile

Table 2.4 : Possible Liquefaction Failures Induced by Pile Driving (after Lacy and Gould, 1985)

Case Desig.	Location	Description of Operation	Distance to Measurement	Velocity	D_R of Sand	Settlement
A	Foley Square, New York City	80ft long, 14HP73 piles at 3ft centers.	20 ft. 20 ft. 20 ft.	0.19 in/s 0.14 in/s 0.19 in/s	42-49% 53-57%	Building at 20ft settled 3" (destroyed). 1ft settlement between piles.
B	Lower Manhattan, New York City	60ft long, 18" dia. open pipe. Close spacing.			40-60%	Sheetpile wall displaced 2ft at top, causing street to settle 1.5ft.
C	West Brooklyn, New York City	100-150ft long, 14HP73 piles. 40 driven.	5-30 ft.	0.1 in/s on building	30-50% 40-60%	Structure settled 3" as piles were driven. Piling operation stopped.
D	South Brooklyn, New York City	80-150ft long, 10.75" closed-end pipe piles.	10-80 ft.	0.1 in/s to 0.9 in/s	40%	Structure on 30ft long timber piles settled 3". 220 piles driven.
E	Lower Connecticut River	80ft long, 12HP53 piles. 160 piles at 3ft centers.			40%	Pier foundation underwater. 2.75ft settlement between piles.

driving. These increased pore pressures are believed to have reduced the passive resistance of berms inside the excavation, thus permitting the walls of the unbraced cofferdam to move inward.

It is evident from the large number of pile driving-induced failures that are reported in the literature, that pile driving operations cause a significant amount of distress within the ground. Two possible reasons for this are as follows:

1) Most pile driving contracts produce a large number of cycles of ground vibration. Crockett (1979) notes that driving 10 piles to a depth of 10 meters is likely to produce approximately 10,000 cycles of ground vibration. In contrast, a site near a quarry will probably only be subjected to several hundred cycles of vibration over a period of several years.

2) Most of the pile driving energy that is transferred to the soil, is transferred through the base of the pile. Lacy and Gould (1985) report a case history where surface vibration levels generated by pile driving were similar in magnitude to those produced by vehicular traffic on streets adjacent to a site. However despite this fact, no settlements were observed as a result of the vehicular traffic prior to the commencement of pile driving. Lacy and Gould conclude that the ground vibrations produced by pile driving caused more distress because most of the energy was imparted at depth. Ground vibrations produced by vehicles are confined to the surface layers.

Despite the fact that ground vibrations generated by pile driving have been studied in detail, very few, if any, of the numerous empirical relationships that have been

developed are able to predict ground vibration levels with a high degree of accuracy. This particularly applies to the simplest of these relationships which are derived from plots of peak particle velocity versus distance. Plots of this type, such as those developed by Luna (1967), Dalmatov et al (1968), Attewell and Farmer (1973), Lo (1976), Heckman and Hagerty (1978), Mallard and Barstow (1979) and Theissen and Wood (1982), commonly show that values of peak particle velocity vary by almost 2 orders of magnitude for any given distance. Such a scatter is shown in the Skipp (1984) plot presented in Figure 2.14 and may be partially attributed to pile drivers of varying capacities.

Several relationships attempted to account for the effect of different capacity drivers, by expressing peak particle velocity as a function of scaled distance terms, which incorporate the energy imparted by a pile driver. Unfortunately plotting the data in this manner does not appear to significantly reduce the scatter. The scaled distance term which is most commonly used is $\frac{\sqrt{E}}{d}$, where E is the input energy provided by the pile driver, and d is the distance from the pile and plots of peak particle velocity versus $\frac{\sqrt{E}}{d}$ have been presented by Wiss (1967), Attewell and Farmer (1973) and Mallard and Barstow (1979). Attewell and Farmer's plot which is based on data from five sites where the soils ranged from coarse sand to laminated clays is shown in Figure 2.15. The least squares line of best fit through the data in this figure and an upper bound line for the same data, are described by Equations 2.10 and 2.11, respectively:

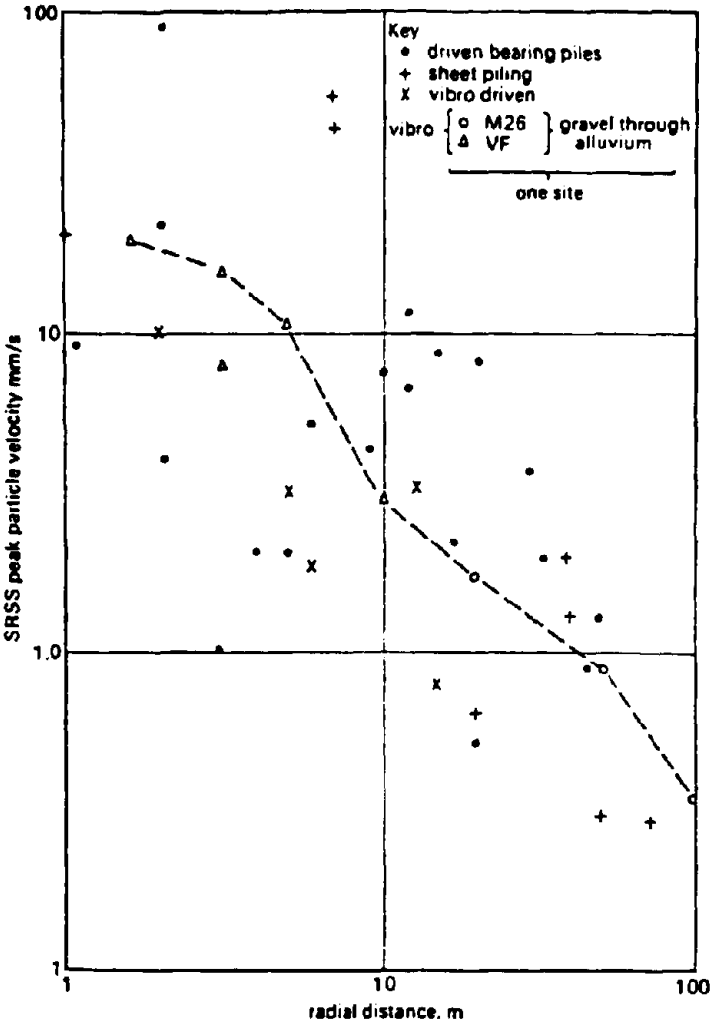

FIG 2.14 GROUND VIBRATION FROM A VARIETY OF PILE DRIVING OPERATIONS (from Skipp, 1984).

$$V = 0.76 \left[\frac{\sqrt{E}}{d}\right]^{0.87} \qquad 2.10$$

$$V = 1.5 \frac{\sqrt{E}}{d} \qquad 2.11$$

where E = input energy (joules),
d = distance from pile (meters), and
V = particle velocity (mm/sec)

Because of the scatter that is evident in such a plot, Attewell and Farmer recommend the use of upper bound values determined by Equation 2.11 to predict ground vibrations levels produced by pile driving. However they also acknowledge that the use of the coefficient 1.5 in this equation is probably conservative, since vibration levels measured at 4 of the 5 sites for which data are presented are bounded by the equation:

$$V = 0.75 \frac{\sqrt{E}}{d} \qquad 2.12$$

The ground vibration data plotting above this line were produced by driving sheet piles through a stiff silty clay which was underlain by a firm laminated clay.

As previously noted, the scatter in plots of vibration amplitude versus scaled distance (approximately equal to $1\frac{1}{2}$ orders of magnitude in Figure 2.15) does not appear to be significantly less than the scatter in plots of peak particle velocity versus distance. Researchers have attributed this remaining scatter to factors such as soil properties, type of hammer, size and type of pile, and the efficiency of the pile driving system.

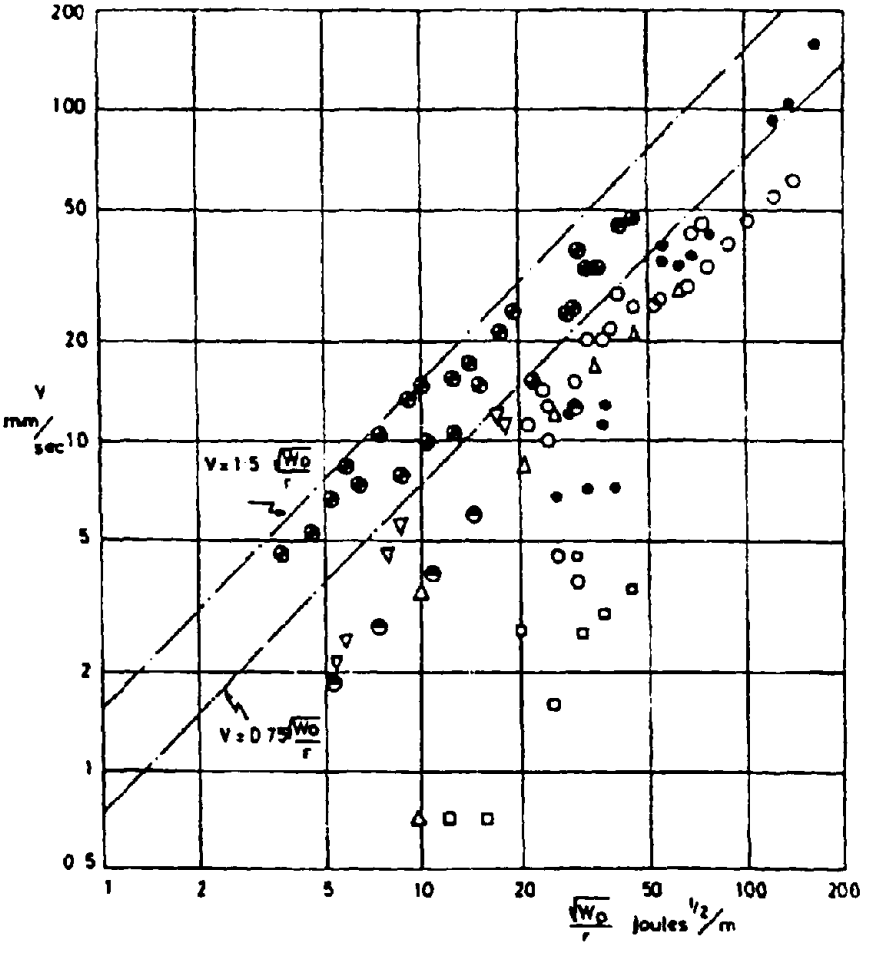

FIG 2.15 PARTICLE VELOCITY ATTENUATION WITH DISTANCE FOR SEVERAL PILE DRIVING OPERATIONS (from Attewell et al. 1973).

Other formulae which predict peak particle velocity as a function of scaled distance are presented in Equations 2.13, 2.14 and 2.15. Equation 2.13 which was developed by Mallard and Barstow defines the line of best fit through their data.

$$V = 32.36 \left[\frac{\sqrt{E}}{d}\right]^{1.6} \qquad 2.13$$

where E is the input energy in kNm,
d is the distance from the pile in meters, and
V is the particle velocity in mm/sec

Equations 2.14 and 2.15 which were developed by Heckman and Hagerty (1978) are based on levels of ground vibrations generated by driving piles into a silty loam using an impact hammer.

$$For\ 305\ mm\ (12'')\ H\ piles: \quad V = 0.98\ \frac{\sqrt{E}}{d} \qquad 2.14$$

$$For\ 350\ mm\ (14'')\ H\ piles: \quad V = 0.52\ \frac{\sqrt{E}}{d} \qquad 2.15$$

where E is the input energy in joules,
d is the distance from the pile in meters, and
V is the particle velocity in mm/sec

Because the ground vibration levels recorded by Heckman and Hagerty appeared to be significantly influenced by the impedance of the pile being driven, these authors developed a third relationship which expresses peak particle velocities as a function of both pile impedance and scaled distance: This formula is described by the equation:

$$V = K \frac{\sqrt{E}}{d} \qquad 2.16$$

where K is a function of the pile impedance and is dependent on the units of E and d.

The impedance of a pile which is a measure of the maximum force that can be transmitted along a pile. is defined by Peck, Hanson and Thornburn (1974) as being equal to the pile area multiplied by the pile density and the sonic velocity of the pile. Heckman and Hagerty's plot of K versus pile impedance is presented in Figure 2.16.

It appears from the limited scatter shown in this figure that Equation 2.16 is likely to predict peak particle velocities more accurately than the other relationships currently available. However, even so, the results obtained from this equation are still only approximate. This is due to the large number of remaining factors such as the position of the water table, the composition of the soil profile, the advent of hard driving and possible resonance effects that also influence ground vibration levels but are not taken into account. The effect of one such factor is illustrated in Figure 2.16. Point 1 which lies significantly above the curve proposed by Heckman and Hagerty, was recorded on the surface of a rubble fill through which piles were being driven. Heckman and Hagerty state that the position of this point is due the influence of the hard layer on transmitting vibrations. In soft soils, most of the impact energy goes into advancing the pile, while in stiff soils most of the energy is transmitted out into the soil mass as waves. A plot indicating a direct relationship between peak particle velocities and SPT blow counts was presented by these authors and is shown in Figure 2.17.

	PILE TYPE	HAMMER ENERGY
Case 1	Pipe piles driven with a mandrel (45 ft long, 14 in. dia.)	30,000 ft-lbs (40,700 joules)
Case 2	12 HP 53 Piles (2* - 14 HP 102)	24,400 ft-lbs (33,000 joules)
Case 5	Pipe piles, 14 inch diameter 3/8 inch-thick wall	16,000 ft-lbs (21,600 joules)
Case 6	12 HP 53	30,000 ft-lbs (40,700 joules)
Case 7	14 HP 114 (measurement in an excavation)	87,000 ft-lbs (118,000 joules)
Case 8	600 mm diameter hollow-core concrete piles	44,000 ft-lbs (60,000 joules)
Case 9	Sheet piles, various sizes	18,000-45,000 ft-lbs (24,200-60,700 joules)
Case 10	H-piles, various sizes	6,700-27,000 ft-lbs (9,100-36,500 joules)

RANGES OF PILE IMPEDANCE

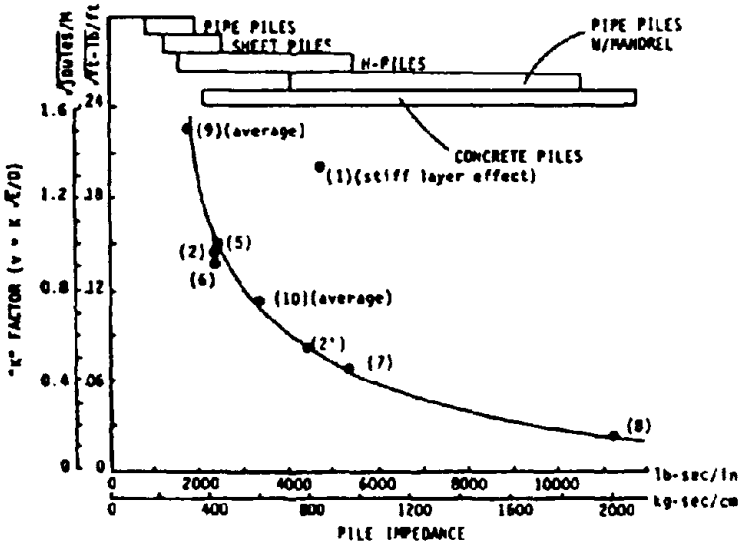

FIG 2.16 INFLUENCE OF PILE IMPEDENCE ON PEAK PARTICLE VELOCITY (from Heckman and Hagerty, 1978).

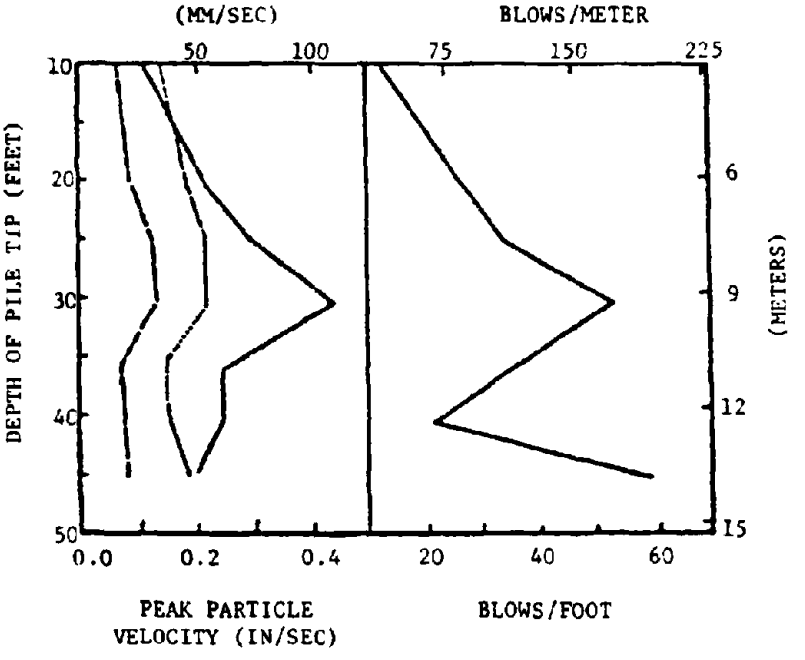

FIG 2.17 PEAK PARTICLE VELOCITY AND DRIVING RESISTANCE VALUES AS A FUNCTION OF PILE PENETRATION (from Heckman and Hagerty, 1978).

The fact that very few researchers have attempted to develop theoretical formulae which predict the magnitude of ground vibrations induced by pile driving can probably be attributed to the complicated nature of the wave field that is generated by driving a pile. A schematic illustration of this wave field is presented in Figure 2.18 (from Martin, 1980). When a hammer impacts on the top of a pile, a body wave is generated in the pile. This body wave travels down the pile to its base where some of the energy is transmitted into the soil as P waves and S waves before being reflected back up the pile. As the wave propagates down the pile energy is lost through skin friction along the side of the pile, although Attewell and Farmer (1973) believe that most of the impact energy is transmitted through to the pile base. Attewell and Farmer further suggest that the relative energy contents of the transmitted and reflected waves can be estimated from Zoeppitz's equations (presented by Richart et al, 1970), use of which is based on the assumption that both the pile and the soil remain elastic. If these equations are used, the approximate ratio of transmitted energy to reflected energy is estimated to be 2 to 1 at a steel-soil interface.

The shear waves that are produced at the base of the pile radiate outwards from their source and those S waves arriving at the surface at some critical distance from the pile, approximately equal to the depth of the pile tip, create a headwave. Both of these waves interact with the low amplitude conical expanding shear waves generated as a result of skin friction between the pile and the soil, to form a very complex surface motion. Attewell and Farmer report that true Rayleigh wave motions are only likely to develop at greater distances from the pile.

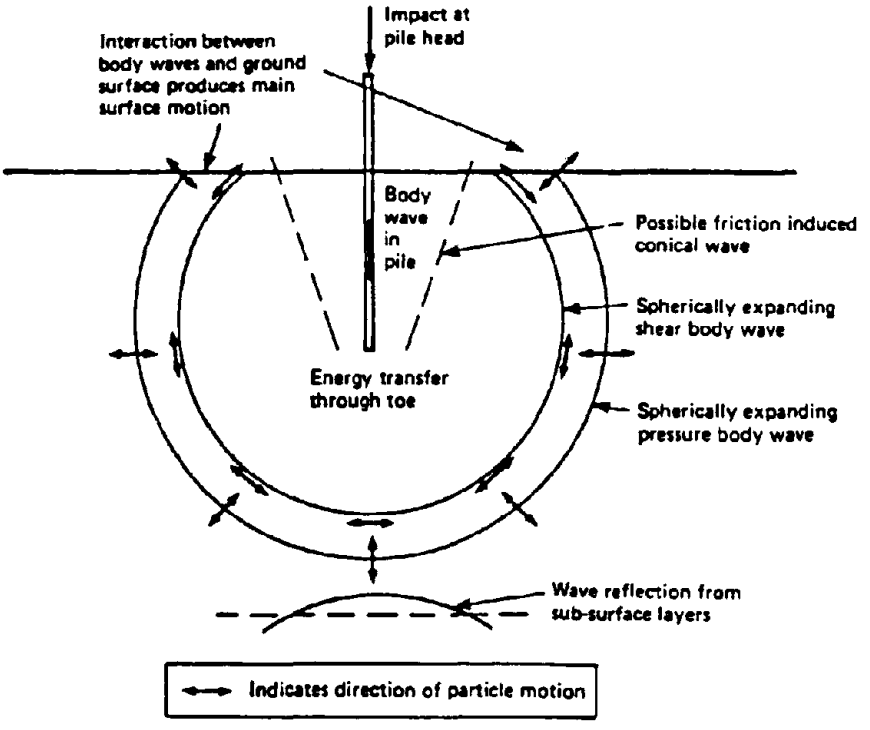

FIG 2.18 WAVE COMPONENTS NEAR TO A DRIVEN PILE (from Martin, 1980).

Due to the complex nature of this wave field the exact amount of energy that is associated with each wave form is unknown. Many researchers contend that at least in the near-field region, the surface motions generated during pile driving primarily consist of body waves. This contention is often based on the observation that the peak particle velocities generated by pile driving attenuate at a rate proportional to about d^{-1} (for example, Attewell and Farmer, 1973), a rate which is the same as the attenuation rate for body waves propagating within an ideal elastic half-space. Along the surface of such a half-space, these waves attenuate at a rate proportional to d^{-2}. Other evidence which may suggest that pile driving-induced ground vibrations primarily consist of body waves is presented by Mallard and Barstow (1979) who report a case history where the amplitudes of the horizontal components of ground vibrations (produced by pile driving) were observed to increase in magnitude with the advent of hard driving. They state that the amplitudes of the horizontal surface motions are not expected to increase if these motions are comprised of "pure surface waves". Mallard and Barstow attributed this phenomena to two possible causes:

1) the arrival of shear waves generated at the base of the pile, and

2) the prebored pile starting to whip horizontally.

However while much of the evidence appears to support the contention of body waves, some of this evidence appears to be inconclusive. For example, Attewell and Farmer (1973) who present plots of the motions at points on the ground surface at varying distances away from the pile, state that these vibrations are not wholly typical of surface R wave transmissions. This may be true but nonetheless it is also somewhat surprising

since the motions at these points are shown to be retrograde, and the dominant Rayleigh wave mode of vibration is also likely to be retrograde. Further, for most natural deposits, numerous Rayleigh waves are generated with significantly different mode shapes and therefore it would seem hard to determine what a typical Rayleigh motion should look like. The conclusion by Attewell and Farmer that most of the energy is transmitted as body waves may also be in partial conflict with the line of best fit drawn through their data. For example, this line indicates that pile driving-induced ground vibrations attenuate at a rate proportional to $d^{-0.897}$ and even in the near-field region, the amplitudes of body waves might be expected to attenuate at a rate significantly faster than $d^{-1.0}$ due to material damping.

Two authors who conclude that Rayleigh waves transmit most of the pile driving energy that is imparted to a soil are Dalmatov et al (1968) and Lo (1976). Lo's belief is based on the observation that he was able to adequately predict the attenuation of ground vibrations by using the following equation which was established for Rayleigh waves:

$$A = A_1 \cdot \sqrt{\frac{d_1}{d}} \cdot e^{-\alpha(d-d_1)} \qquad 2.17$$

where A, A_1 are the amplitudes of particle velocity measured at distances r and r_1 respectively,
d, d_1 are distances from the source, and
α = coefficient of attenuation

Several values of α are listed in Table 2.5 and a more complete listing for different soils is provided by Barkan (1962).

Table 2.5 : Values of α Proposed by Different Investigators

Reference	Soil Type	α (m^{-1})
Lo (1976)	soft-medium saturated silts sands and gravels	0.04 - 0.06 0.12
Barkan (1962)	average value	0.05
Attewell and Farmer (1975)		0.03 - 0.12
Richart Hall and Woods (1971)		0.02 - 0.14

The likelihood that liquefaction will occur during pile driving is most commonly assessed by measuring the magnitude of peak particle velocities at the ground surface. Crockett (1979) states that vibrations with amplitudes less than 0.3 mm/sec (0.1 inches/sec) have caused undesirable levels of soil compaction in some piling contracts. However it appears that these are extreme cases and a peak particle velocity of 2.5 mm/sec (0.1 inches/sec) might be a more appropriate minimum level of surface vibration. Table 2.4 presented earlier, lists several case histories where significant surface settlements were associated with peak particle velocities of 2.5 mm/sec and Lacy and Gould (1985) state that pile driving-induced ground vibrations with peak particle velocities at the ground surface as low as 2.5 to 5.1 mm/sec (0.1 to 0.2 inches/sec) appear to cause significant ground settlement. As a rough comparison, Crandell (1949) reports that pile driving-induced ground vibrations were not observed to damage structures unless their peak particle velocities exceeded 85 mm/sec (3.3 inches/sec). Thus it may be concluded that levels of ground vibration well below the levels required to

damage structures are capable of inducing significant ground settlements.

The probability that liquefaction will be induced by pile driving is also a function of the type of pile driver, its operating frequency, the hammer energy, the size of the job, the soil type and the position of the water table. For example, the overall size of a piling contract can determine whether settlements are likely to be insignificant or potentially damaging. Lacy and Gould (1985) cite a case history where neighboring structures started to settle after the first 100 piles had been driven, and continued to settle at a steady rate during driving of the next 120 piles. Particle velocities at the ground surface ranged from 2.5 to 23 mm/sec (0.1 to 0.9 inches/sec). A dewatering system was subsequently installed and no further settlements were observed during the driving of an additional 250 piles, leading Lacy and Gould to surmise that the dewatering system mitigated the effects of pore pressure buildup.

The soils that are most likely to settle during pile driving are loose to medium dry or dense sands, and particularly those with relative densities less than about 55%. In addition, the gradation curves for these sands commonly lie within the range for sands that are susceptible to liquefaction during earthquakes (refer to Figure 2.19). The gradation curves presented in this figure are the curves for those sands that were thought to have liquefied in case histories reported by Lacy and Gould (1985). Curves A, B, D and E in Figure 2.19 are the gradation curves for those sands that liquefied in cases A, B, D and E in Table 2.4.

It is worth noting that several investigators including Clough and Chameau (1980) and Dalmatov et al (1968) have shown that the magnitude of ground settlements is

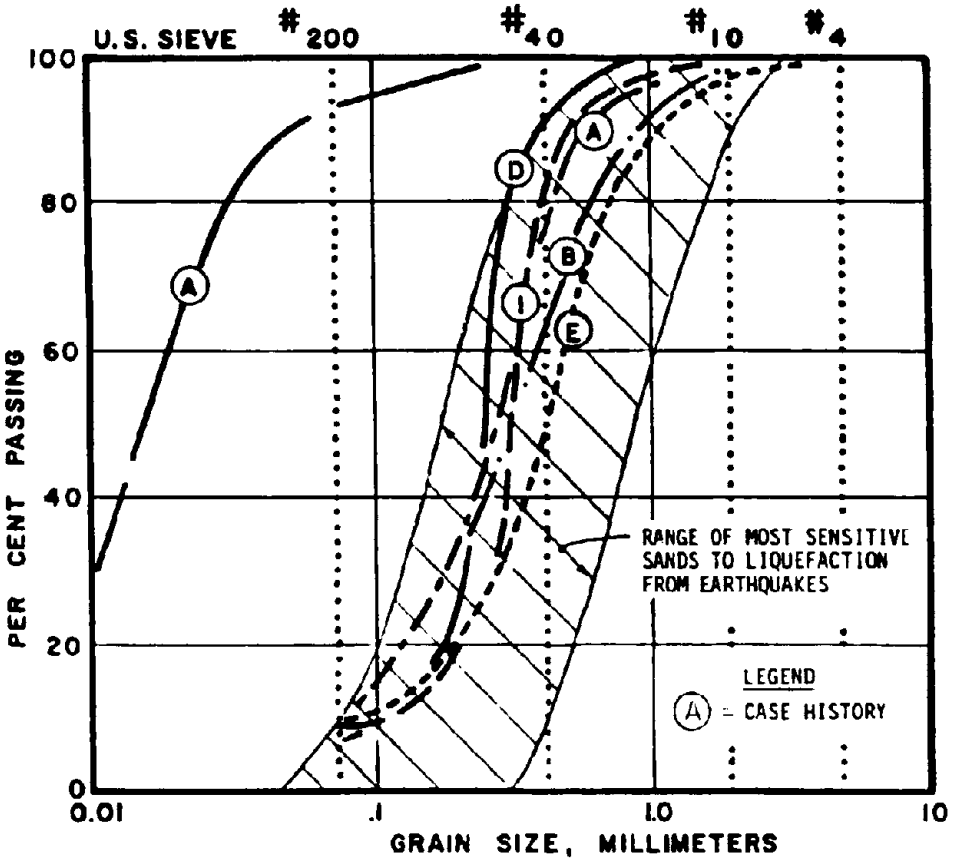

FIG 2.19 GRADATION CURVES FOR SANDS THAT ARE REPORTED TO HAVE LIQUEFIED DURING PILE DRIVING (from Lacy and Gould, 1985).

also closely related to peak ground surface accelerations. Dalmatov et al analyzed the results of two case histories where piles were driven by an impact hammer. The first of these involved driving sheet piles into a saturated silty sand with a relative density of 50% while the second case history involved driving cast iron pipe piles into a 22 meter thick layer of loam (lacustrine-glacial and glacial in origin) which was overlain by 2 meters of building waste (described as consisting of vegetable ground, broken bricks, etc). Dalmatov et al noted that no settlements occurred at either site unless the surface vibration levels exceeded a certain critical acceleration. The critical acceleration for the sand site was 98 mm/sec^2 (0.01g) while the critical acceleration level at the second site was 500 mm/sec^2 (0.05g). Dalmatov et al were also able to predict theoretically the magnitude of the recorded settlements by using general equations developed for calculating foundation settlements under the action of static loads. Dalmatov et al achieved this by using moduli (determined by Kovalevsky, 1965) which represented the total deformation of soils subjected to dynamic loads.

The effects of driving sheet piles with a vibratory hammer were monitored by Clough and Chameau (1980) during construction of the San Francisco sewer outfall system. Field data showed that permanent vertical strains in the soil did not exceed 0.3% in areas where the ground surface accelerations were less than 0.1g. Clough and Chameau not only concluded that there was an excellent correlation between permanent strains and surface accelerations, but that these settlements could have been predicted from plots of vertical strain versus applied acceleration, using data developed by Silver and Seed (1971). Silver and Seed's curves were based on the response of a

dry sand (D_R = 40%) subjected to 10 cycles of loading at a frequency of 10 Hz. In performing their calculations, Clough and Chameau assumed that all of the settlement occurred within lenses of medium-dense (D_R = 50 - 60%) and loose (D_R = 30 - 40%) sand that were present in the soil profile.

The form of ground vibrations generated by driving piles is dependent upon the type of pile driver. For example, impact pile drivers which impart a single blow to the top of the pile at a frequency within the range 0.5 to 6 Hz, typically produce ground vibrations that are transient in nature. As a rough guideline, most single acting impact hammers operate at frequencies around 1 Hz, while most double acting impact hammers operate at frequencies of around 2.5 Hz. Records which illustrate the nature of ground vibrations generated by these types of hammers have been presented by Luna (1967), Wiss (1967), Attewell and Farmer (1973), Lo (1976), Mallard and Barstow (1979) and Martin (1980). These records not only show that the vibrations produced by impact pile drivers are transient in nature but that they contain predominant frequencies which appear to depend on the soil at the site (as discussed in Section 2.1). It is also observed that each blow of the pile driver appears to generate 1 to 2 significant cycles of ground motion at distances close to the pile. Ground motions that have been recorded at distances of 100 meters from a pile appear to contain 2 to 6 significant cycles of loading. One of the records presented by Martin (1980) is shown in Figure 2.20.

In contrast, ground vibrations produced by vibratory pile drivers are continuous in nature and contain predominant frequencies that are the same as the operating

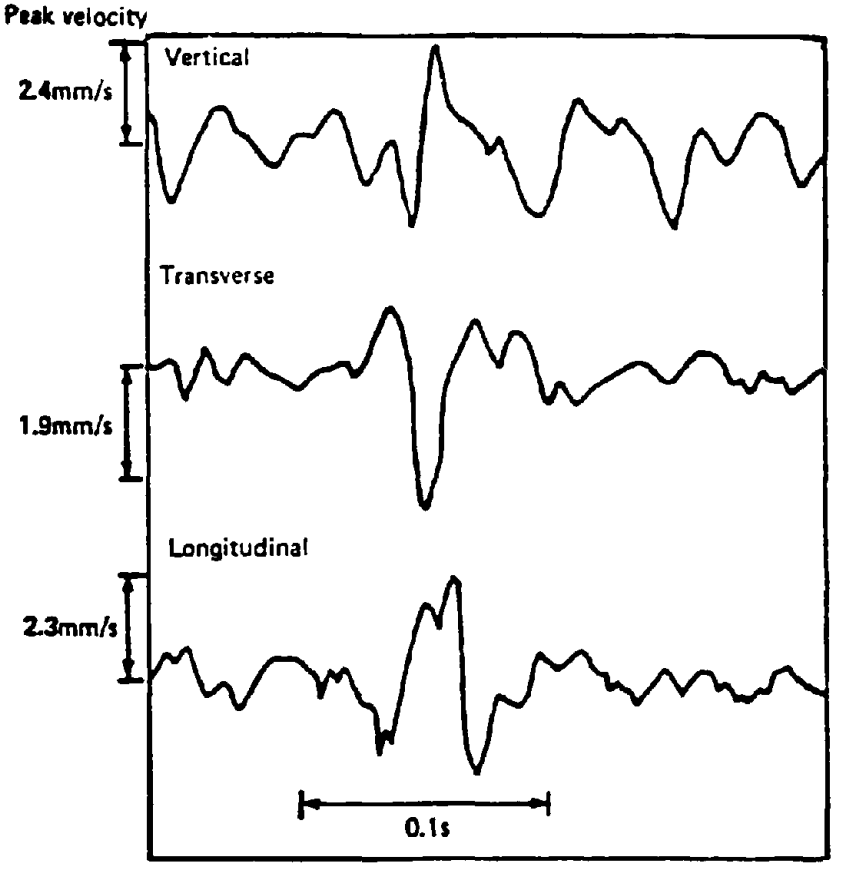

FIG 2.20 GROUND VIBRATIONS GENERATED BY A 2.5 TONNE DROP HAMMER DRIVING 356mm DIAMETER CASED PILES INTO CLAY AT 4 METERS DEPTH - MEASUREMENTS AT 15m FROM PILE (from Martin, 1980).

frequency of the pile driver; most vibratory pile drivers operate at frequencies between 10 and 40 Hz; however some drivers, often referred to as sonic pile drivers, operate at frequencies up to 135 Hz. Records of ground vibrations generated by vibratory pile drivers also show these drivers typically produce vibrations that are significantly smaller in amplitude than the vibrations produced by a comparable impact pile driver. This observation is reiterated by Wiss (1967) who further states that the ground vibrations produced by sonic pile driving are usually one order of magnitude less than those produced by impact pile driving; however vibration amplitudes vary continuously and may reach half the magnitude of those produced by a comparable impact hammer. The fact that these vibration levels may become extreme when a vibratory pile driver is operated at frequencies at or near the predominant frequency of a soil deposit is noted by both Heckman and Hagerty (1978) and Tschebotarioff (1973) who reports that ground vibrations increased sharply as the operating frequency of the pile driver approached 30 Hz and then reduced rapidly as the operating frequency climbed above this level. Because sonic pile drivers operate at frequencies that are above the natural frequency of the soil, significant levels of shaking are generated whenever the operation of these drivers is interrupted; therefore such interruptions are undesirable.

Resonance can also occur when several pile drivers are operating at the same site; Lacy and Gould report a case history where two pile drivers were operating at the same site and peak particle velocities increased by a factor of 4 when the hammers became synchronous.

Despite the fact that ground vibrations produced by vibratory pile driving are usually smal. r in amplitude than vibrations produced by impact pile driving they are potentially more hazardous. This is primarily due to two factors: (1) the possibility of resonance, and (2) the larger number of cycles of ground motion that are produced by vibratory pile drivers. Wiss (1967) allows for these two effects by suggesting that allowable vibration levels for continuous vibrations should be one-half to one-fifth of those permissible for transient vibrations.

In summary, it appears tha. he best means of predicting ground vibration levels is to conduct a site-specific study prior to the start of operations, a belief which is shared by all researchers including Heckman and Hagerty (1978) who emphasize that field experimentation and measurements will always be the most meaningful and practical method for determining vibration levels. In the absence of such a survey, ground vibration levels can probably be most accurately predicted by using Equation 2.16, which takes into account the effect of pile impedence. It should be remembered however that these results are only approximate due to the large number of factors that influence pile driving-induced ground vibrations. It is these factors that are responsible for peak particle velocities varying over $1\frac{1}{2}$ orders of magnitude for any value of $\frac{\sqrt{E}}{d}$.

The curves shown in Figure 2.21 are believed to depict upper bound velocity attenuation curves for ground vibrations produced by a typical vibratory pile driver, a 40 kNm (30,000 ft-lb) impact pile driver and a 75 kNm (55,000 ft-lb) impact pile driver.

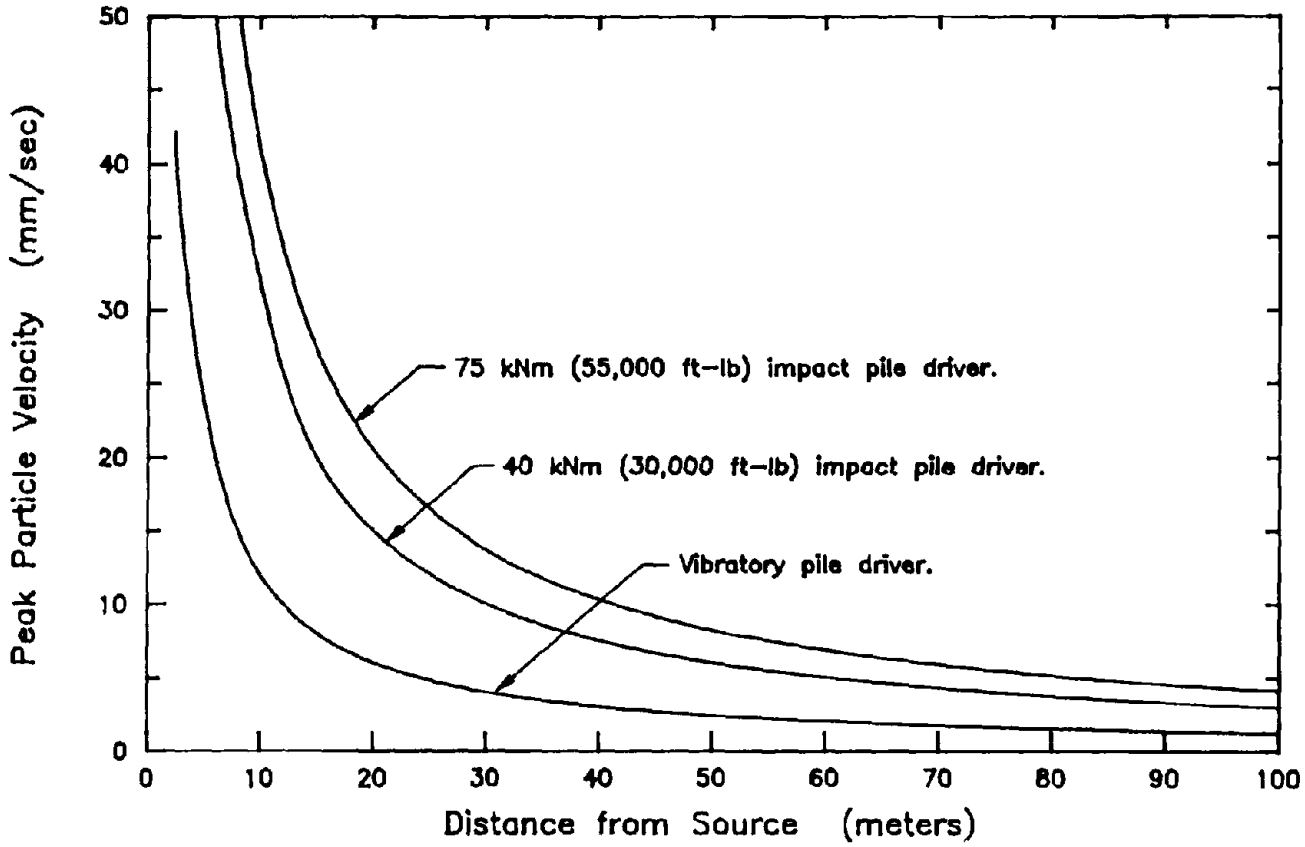

FIG 2.21 PEAK PARTICLE VELOCITY AS A FUNCTION OF DISTANCE FOR TWO HYPOTHETICAL IMPACT PILE DRIVING OPERATIONS, BASED ON THE RELATIONSHIP PROPOSED FOR 500mm DIAMETER PIPE PILES BY HECKMAN AND HAGERTY (1978), AND FOR A HYPOTHETICAL VIBRATORY PILE DRIVING OPERATION.

The maximum distance at which significant ground settlements can occur during pile driving is a function of both the soil type and the level of shaking that is generated during driving and each site must be evaluated separately. It appears that levels of shaking less than 2.5 mm/sec are unlikely to be associated with significant settlements in most cases. It should also be noted that rules of thumb such as those provided by Luna (1967) who states that Energy Ratios become negligible at distances equal to the pile length in sands and 2 to 3 times the pile length in clays, are generally unconservative since these rules were developed to prevent structural damage and the level of surface ground vibrations associated with significant ground settlements may be as low as one-tenth of the level of shaking required to cause structural damage. Crockett (1979) reports that in some cases surface vibrations as low as 0.3 mm/sec have been associated with significant settlements, a value which is one-hundredth of the level required to produce structural damage.

The magnitude of ground vibrations generated by pile driving can be significantly reduced by reducing the capacity of the pile driver. However, such an action may not reduce the detrimental effects of pile driving since a smaller driver will take longer to drive each pile and thus will increase the number of cycles of ground shaking. In addition, a smaller pile driver may not be able to drive the pile to reach its desired capacity.

2.6. Ground Vibrations Produced by Construction Equipment

A paper written by Wiss (1981) is one of the few references that provide information on the characteristics of ground vibrations generated by construction equipment. In this paper, Wiss presents a plot of peak particle velocity versus distance for various non-seismic sources of ground vibrations. This plot is reproduced in Figure 2.22. The lines shown on this figure represent approximate levels of peak particle velocity and provide a good indication of the relative intensities of ground vibrations produced by the various sources. The data used to prepare Figure 2.22 were obtained by measuring ground vibration levels during actual construction operations (Wiss, 1974).

The velocity attenuation relationships presented in Wiss's figure imply that the vibration levels produced by pieces of construction equipment (other than pavement breakers) are relatively insignificant. This observation is particularly true at sites where piles are being driven since the levels of ground vibration generated by pile driving are approximately one order of magnitude larger than those produced by trucks, large bulldozers, and the drilling of caissons; and since construction sources of vibration typically produce far fewer cycles of loading at lower amplitudes of vibration than vibratory pile drivers, it is unlikely that they will be capable of causing liquefaction, except in the immediate vicinity of the equipment. This belief is reinforced by the fact that no case histories describing settlements induced by construction equipment have been found in the literature.

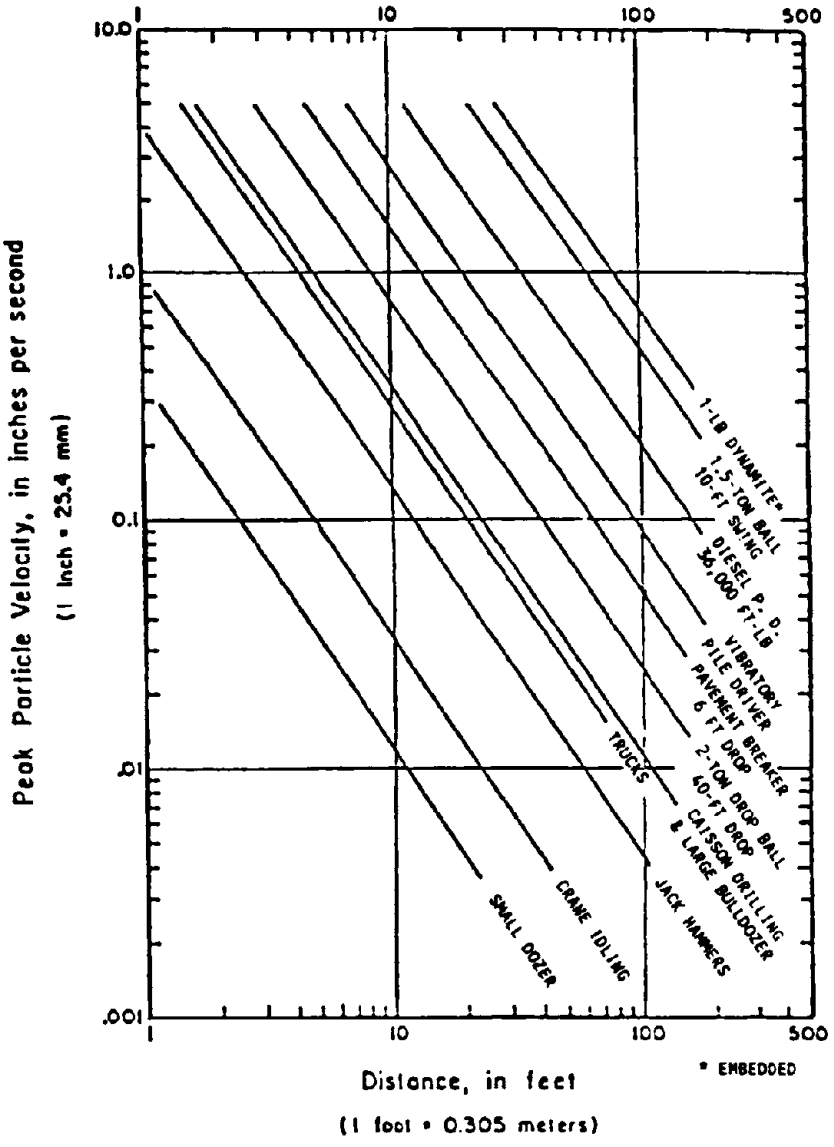

FIG 2.22 RELATIVE INTENSITIES OF CONSTRUCTION OPERATIONS (from Wiss, 1981).

Information on the amplitude of ground vibrations generated by pieces of construction equipment such as Cat D8 and D9 bulldozers, Cat Earthmovers, Euclid Earthmovers and a Pavement Breaker is also provided by Ames et al (1976). It is worth noting that only the ground vibrations that were generated by a pavement breaker exceeded the attenuation curve for large bulldozers shown in Figure 2.22.

The maximum ground vibrations reported by Ames et al were produced by an EMSCO Pavement Breaker which generated peak particle velocities of 73 mm/sec (2.88 inches/sec) and 7 mm/sec (0.275 inches/sec) at distances of 10 ft and 38 ft respectively. These peak particle velocities are noted to lie slightly above the attenuation curve for pavement breakers shown in Figure 2.22 and imply an attenuation rate that is consistent with the rate of attenuation in Wiss's plot. Since ground vibrations generated by pavement breakers are similar in amplitude to those generated during vibratory pile driving (refer to Figure 2.22), it seems likely that these vibrations are capable of causing significant ground settlements. However any such settlements are anticipated to be smaller in magnitude than the settlements induced by vibratory pile drivers due to the significantly smaller number of cycles of ground shaking that are likely to be involved.

Only one case history has been located where ground settlements were attributed to vibrations generated by a pavement breaker, and this involved a 6 ft thick layer of glacial till that was dry to a depth of 3 feet settling approximately one inch beneath a house. For reference, peak particle velocities of 25 mm/sec (1 inch/sec) were measured adjacent to the house which was located 9 meters from the compactor.

2.7. Ground Vibrations Produced by Road Traffic

The amplitudes of ground vibrations generated by road traffic appear to be small in comparison to vibrations produced by other non-seismic sources such as pile driving, dynamic compaction or blasting. This observation is based on data presented by numerous researchers including Ames et al (1976), who compiled a plot of ground vibration data for a wide variety of vehicular equipment, highway structures and ground conditions. For example, the maximum particle velocity reported by Ames et al is approximately equal to 1.4 mm/sec (0.056 inches/sec), a value recorded at a distance of 17 feet from a fully-loaded fill haul truck, traveling over San Francisco Bay Fill. In comparison, Figure 2.22 indicates that peak particle velocities of about 50 mm/sec (2.0 inches/sec) may be generated at a distance of 20 ft from a 49 kNm (36,000 ft-lb) diesel impact pile driver. The vibration levels that are reported by Ames et al are consistent with ground vibration levels provided by Nicholls et al (1971), Brown (1971), Tynan (1973) and Whiffin and Leonard (1971) who report that the amplitude of normal running vibrations produced by cars varied from 0.06 to 0.25 mm/sec. Whiffin and Leonard further report that the amplitude of vibrations associated with irregularities in the pavement (such as manhole covers, expansion joints, differential settlements, and potholes) may vary from 0.69 to 1.47 mm/sec.

The levels of ground vibration that are produced by road traffic are primarily a function of vehicle weight, vehicle speed and surface roughness while other factors such as the resonant frequencies of a vehicle's suspension systems, different foundation materials, the position of the water table and different road structures influence

vibration levels to a lesser extent. The effect of vehicle weight and surface roughness on vibration amplitude is clearly shown in the results of experiments reported by Whiffin and Leonard. These experiments which involved driving trucks of different weights over planks of varying thickness, at a range of speeds, showed that peak ground surface velocities of up to 5 mm/sec (0.2 inches/sec) could be developed by driving the trucks over 20 mm high planks and led Whiffin and Leonard to conclude that both the size of the irregularity and the weight of the vehicle had a pronounced effect on ground vibration levels. The same conclusions were also drawn from experiments conducted by Frydenlund (no date), and Rudder (1978) who observed that ground vibration levels increased by approximately 40% for each doubling of gross vehicle weight.

Whiffin and Leonard also examined the effect of vehicle speed on vibration amplitude and concluded that vehicle speed had only a minor influence on ground vibration levels. However, this conclusion is inconsistent with observations made by other investigators such as Rudder who noted that doubling a vehicle's speed appeared to increase the induced ground vibration levels by 40 to 100%. In addition, other data presented by Lande (1974) show an almost linear increase in peak particle velocity with increasing speeds for vibration levels recorded within a pavement. Thus it may be concluded that vehicle speed does have a pronounced effect on ground vibration amplitudes. Since these speed effects appear to be dependent upon surface roughness (Rudder 1978), any relationship between vehicle speed and ground vibration levels must be considered on a site specific basis.

Traffic-induced ground vibration data from 5 sites where the soils ranged from loose to medium-dense sands to stiff clays are summarized in a recent study reported by Barneich (1985) and presented in Figure 2.23. These data which were recorded at distances of 3 to 6m (10 to 20 ft) from the passing traffic are plotted versus frequency for different types of vehicles and different values of surface roughness where surface roughness, R, is defined by Barneich as being the maximum height of an irregularity divided by the square root of the distance between irregularities. Barneich found that cars traveling over very rough roadways were observed to generate maximum particle velocities of about 0.4 mm/sec (0.015 inches/sec), values that are both consistent with the levels of vibration presented earlier by Ames et al and similar in magnitude to the levels generated by buses and trucks traveling over smooth roadways (refer to Figure 2.23). However, the maximum amplitudes of ground vibrations produced by trucks and buses are approximately six times larger than the highest levels reported by Ames et al. Figure 2.23 shows that trucks and buses are capable of generating ground vibrations with velocities as large as 8.9 mm/sec (0.35 inches/sec).

Barneich also examined the effect of vehicle speed and vehicle weight on ground vibration levels and concluded that peak particle velocities increased linearly with both of these parameters, results which confirm the findings of Whiffin and Leonard (1971), Lande (1974) and Rudder (1978).

As mentioned in Section 2.1, the belief that road traffic-induced ground vibrations consist predominantly of Rayleigh waves, is largely based on a theoretical analysis presented by Miller and Pursey (1955). It should be noted however, that some ground

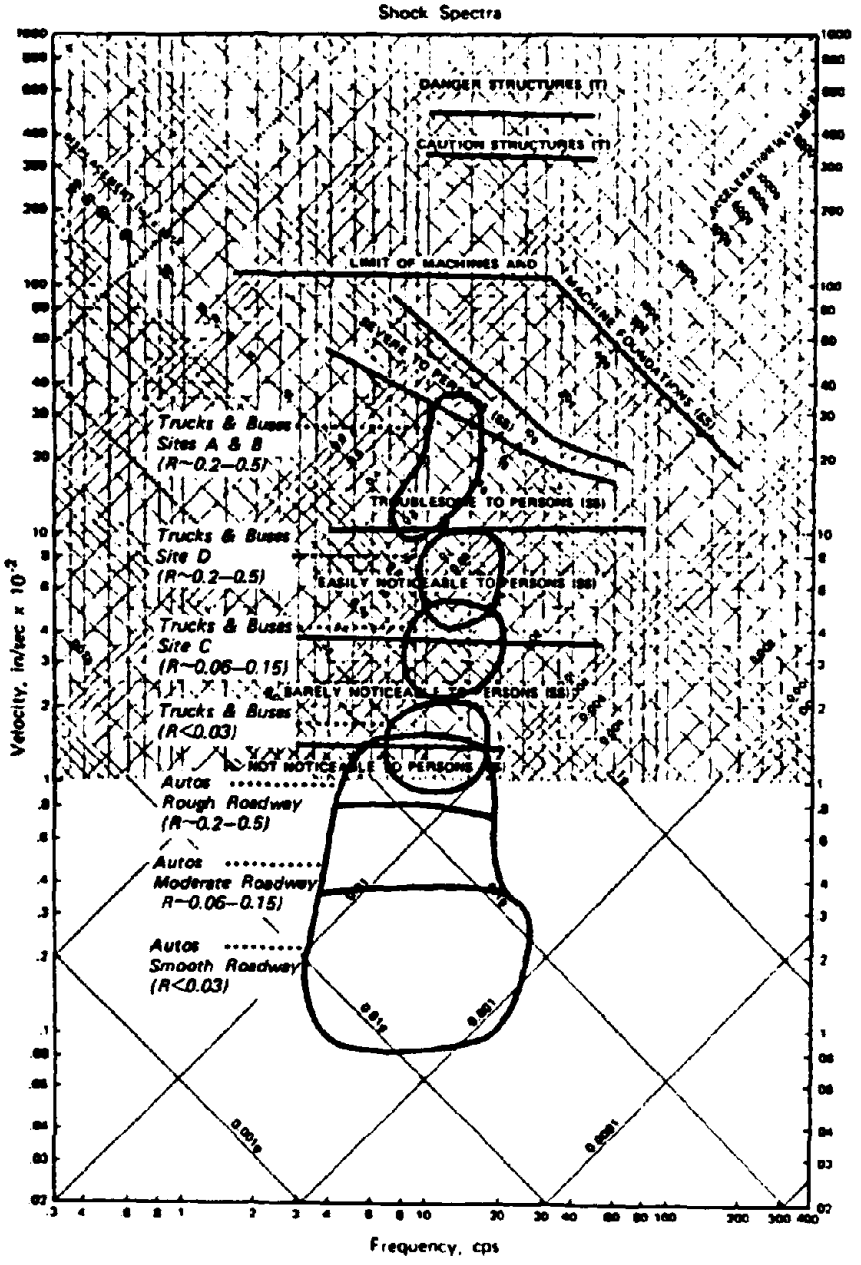

FIG 2.23 SUMMARY OF CURB SIDE GROUND VIBRATION LEVELS FOR AUTOS, TRUCKS, AND BUSES (from Barneich, 1985).

vibration measurements appear to contradict this belief. For example, Whiffin and Leonard report that the magnitude of horizontal motions tends to be negligible in comparison to the magnitude of vertical motions. This observation is significant since the horizontal and vertical components of Rayleigh waves should be similar in magnitude. However it is also inconsistent with the results of Fydenlund's (no date) experiments which indicate a much smaller difference in magnitude between these two components. Frydenlund reports that it was difficult to distinguish between the 3 components at distances near to the source and while the vertical components of vibration were typically 5 times larger than the transverse components they were only twice as large as the longitudinal vibrations for measurements made at a distance of 20 m from the road.

The predominant frequencies of most traffic-induced ground vibrations lie within the range of 3 to 30 Hz. This range is suggested by both Rudder (1978) and Barneich (1985), who further conclude that the peak response usually occurs within the range of 5 to 20 Hz. A larger range of 1 to 45 Hz is proposed by Whiffin and Leonard (1971). The frequency content of ground vibrations adjacent to the road is probably governed to a large extent by the characteristics of the tire/suspension systems of the different vehicles. The resonant frequencies of these systems for typical highway vehicles (after Chilton et al, 1975) are approximately 1.5 Hz for body oscillations, 10 Hz for rear axle oscillations and 12 Hz for front axle oscillations. At distances farther away from the source the predominant frequency of the soil deposit appears to dominate.

Judging by the vibration amplitudes reported in the literature most traffic-induced ground vibrations are too small to be capable of liquefying saturated sands in the

majority of cases. However this is not true in all cases since fully laden trucks traveling at high speeds over very rough roads are capable of generating peak particle velocities up to 8.9 mm/sec (0.35 inches/sec), a value which exceeds the level of 2.5 mm/sec which has been associated with significant ground settlements caused by pile driving. It should be pointed out that the magnitudes of such traffic induced settlements are anticipated to be significantly less than those produced by pile driving vibrations of a similar amplitude because most of the energy that is imparted to the soil during pile driving is imparted at depth, whereas ground motions produced by road traffic are confined to the surface layers. Lacy and Gould (1985) cite a case history where vehicular traffic on streets adjacent to a site produced ground vibrations of a similar magnitude to pile driving-induced vibrations; nonetheless they attributed the observed ground settlements to ground vibrations produced by pile driving. Both sources of vibration will produce a very large number of cycles of ground shaking.

The conclusion that traffic-induced ground vibrations are unlikely to liquefy sands is also supported by the fact that only a small number of case histories have been presented where road traffic is cited as a cause of significant ground settlements. The most significant of these case histories is provided by Terzaghi and Peck (1967) who report that in Munich, where most buildings rest on 20 feet of dense sand and gravel overlying rock, truck traffic of increasing intensity caused settlements of such magnitude that several streets had to be entirely closed to trucking. Terzaghi and Peck further report that new buildings adjoining old main highways in Holland commonly tilt away from the highway. This tilt is attributed to traffic vibrations having

compacted the soil beneath and adjacent to the highway, whereas the sand supporting the rear part of the building was still in its original condition. The detrimental effects of traffic-induced ground vibrations are also referred to by Crockett (1966) who claims that settlement of the foundations of certain ancient buildings can be attributed to the accumulated effect of traffic over several centuries. However Whiffin and Leonard (1971) state that Crockett's claim is very difficult to prove because of the many other possible reasons for subsidence.

Since the low levels of vibration that are reported in the literature are consistent with the small number of published references describing settlements caused by this source, it seems reasonable to conclude that the papers referenced in this section provide a good indication of the range of vibrations that can be expected.

2.8. Ground Vibrations Produced by Train Traffic

The magnitude of train-induced ground vibrations is a complex function of a variety of factors including axle weight, suspension design, train speed, ground conditions and track features such as rail joints, sleeper pitch and long wavelength corrugations. The influence of factors such as axle weight and suspension design is evidenced by the fact that vibration levels produced by individual trains may significantly exceed the levels produced by an average train passing over the same piece of track. This fact was borne out in an English survey (conducted by Walker and Field and reported by Griffin and Stanworth, 1985) which found that Electric Multiple Units (E.M.U.) were more likely to cause complaints concerning vibration levels than Diesel Multiple

Units. Griffin and Stanworth concluded that this was probably due to the higher unsprung mass of the traction motors in the Electric Multiple Units. The survey also found that wagons with wedge loaded friction damped suspensions carrying bulk cargo at 25 tons per axle were particularly likely to cause complaints, a statement which infers that these types of wagons generated higher levels of vibration than the levels produced by either average wagons or by Electric Multiple Units.

The effect of train speed on vibration levels is summarized by Dawn (1983), who reports ground vibration levels measured at a distance of 25 m (82 ft) from a passing train. The train, which consisted of 4 axle, 100 ton cars, was repeatedly run over a section of test track at speeds ranging from 23 and 88 km/h. The results of this study which are presented in Figure 2.24. show that ground response peaked when the train was traveling at a critical speed of 24.7 km/h, a speed which is believed to occur "when the sleeper passage frequency coincided with the resonant frequency of the total vehicle on the track." Since the peak ground surface velocities presented in Figure 2.24 are expressed in units of decibels, dB, it is useful to point out that a 3 dB increase is approximately equal to increasing the peak particle velocity by 40%. This figure also shows that the amplitude of ground vibrations generated by trains increases only slightly with increasing train speed for trains traveling at speeds greater than 30 km/h, thus implying that reducing the train speed is unlikely to significantly reduce the magnitude of ground vibrations. It is worth pointing out that if the train speed is decreased until it is near to the critical speed then ground vibration levels may significantly increase.

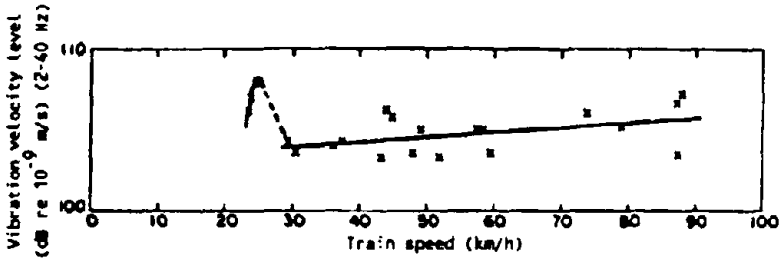

FIG 2.24 VIBRATION VELOCITY LEVEL AS A FUNCTION OF TRAIN SPEED - MEASUREMENTS MADE AT A DISTANCE OF 25 METERS FROM THE TRACKS (from Dawn, 1983).

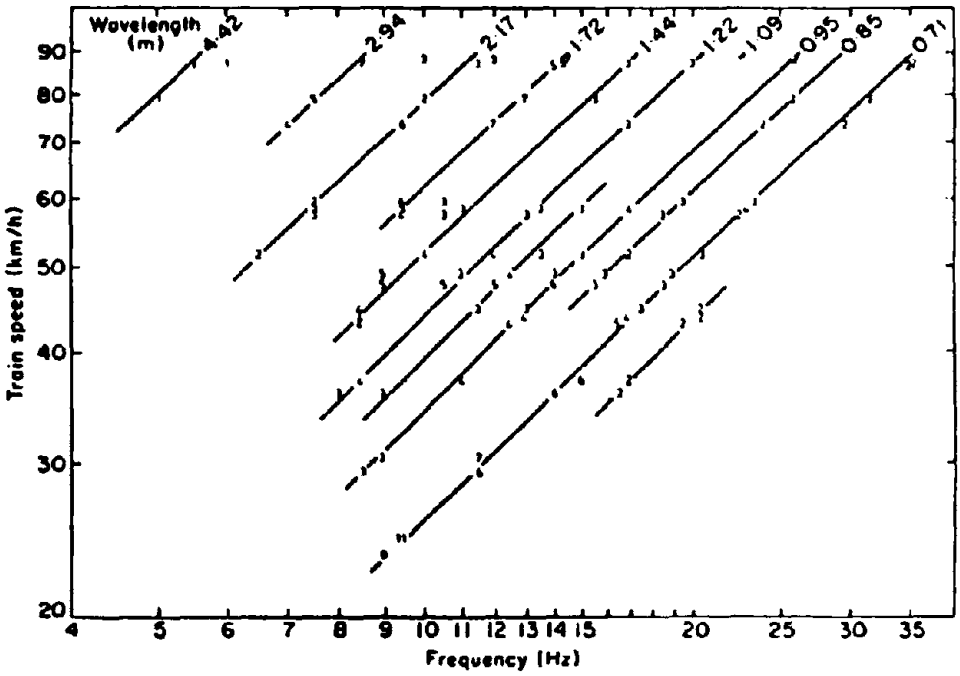

FIG 2.25 FREQUENCY OF SPECTRAL PEAKS IN GROUND SURFACE VERTICAL VIBRATION. NUMBERS PLOTTED ARE NEAREST INTEGER VALUES OF RMS ACCELERATION ($ms^{-2} \times 10^3$) (from Dawn, 1983).

Ground vibration levels are also influenced by the foundation material; for example larger amplitude vibrations appear to be generated in soft ground than in hard ground. Some researchers have attempted to quantify these effects by using survey techniques to determine the elastic properties of the ground. However as yet researchers are still unable to relate measured vibration levels to specific ground properties (Griffin and Stanworth, 1985).

The dominant frequencies of train-induced ground vibrations are functions of both train speed and the wavelengths of various repeating features such as vehicle length, sleeper spacing, rail length, and wheel circumference. This primary dependence is clearly demonstrated by the results of experiments conducted by Dawn (1983) and is shown in Figure 2.25. The speed-dependent peaks that are plotted in this figure are linked by lines of constant slope, and the wavelength quoted against each line is defined by Dawn as the distance traveled by the train for one cycle of oscillation. As mentioned previously, these wavelengths correspond to the wavelengths of various repeating features, such as sleeper or tie spacing, which is approximately equal to 0.71 m. It is this wavelength that "tunes in" to give a maximum response at a speed of 24.7 km/h and a frequency of 9.7 Hz, which is thought to be the resonant frequency of the total vehicle weight on the track. The resonant frequency is primarily a function of the unsprung mass of the train and the stiffness of the ballast. Other measurements which indicate dominant frequencies corresponding to wavelengths of 0.7 m, 1.78 m, 2.48 m and 6.1 m have been reported by Dawn and Stanworth (1979). The peaks at 1.78 m and 2.48 m are caused by long wavelength correlations in the rail, and 6.1

meters is equal to half the engine length and one-third of the rail length; every time the train advances 6.1 m a set of bogies will pass over a rail joint.

The predominant frequencies of most train-induced ground vibrations lie within the range of 10 to 60 Hz. This range is proposed by both Griffin and Stanworth and Dawn and Stanworth who further report that most of the energy in the soil is propagated by motions with frequencies in the range of 10 to 20 Hz. Ground vibrations analyzed by Rickley et al (1981) contain peaks at frequencies of around 40 Hz.

Measurement of vibrations induced within the rails has shown that significant vibrations are also generated by sources such as uneven rail joints and wheel flats. However these vibrations primarily affect the life of the rail. When a wheel impinges on an uneven rail joint, two forces are produced as shown in Figure 2.26. The existence of these forces which are commonly denoted as P_1 and P_2 was confirmed in experiments conducted by Jenkins et al (1974). The P_1 force which is the largest of these forces may be as large as $2\frac{1}{2}$ times the axle weight (Ahlbeck, 1986) and is unlikely to be transmitted to the ballast since the frequency of this force varies from 1000 to 2000 Hz. However, the P_2 forces which are unlikely to exceed the axle weight in amplitude are readily transmitted to the ballast since they oscillate at frequencies between 20 and 100 Hz. Wheel flats also produce significant vertical impact loads. Impact loads of 400 kN (90 kips) have been recorded beneath static wheel loads of only 111 kN (25 kips).

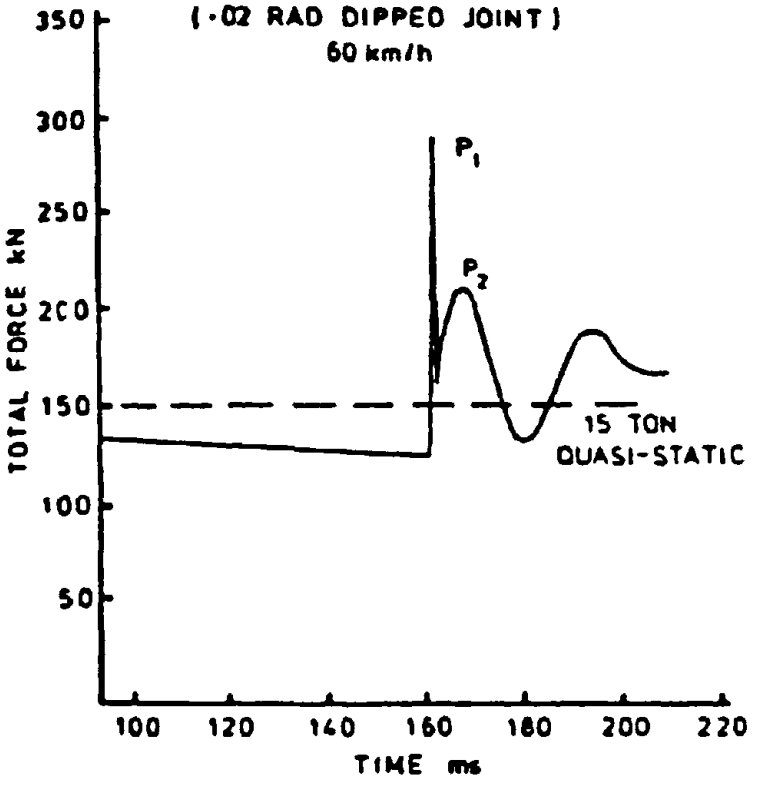

FIG 2.26 EXAMPLE OF WHEEL/RAIL FORCE VARIATION AT DIPPED JOINT (from Frederick and Round, 1985).

In summary it may be stated that while most people believe that trains are a source of significant ground vibrations, this belief is inconsistent with the relatively low levels of vibration that are reported in the literature. For example, the largest peak particle velocity reported by Ames et al (1976) is equal to 3.9 mm/sec (0.153 inches/sec). This velocity which was recorded at a distance of 2 m from a diesel locomotive is smaller in amplitude than peak particle velocities induced by small pieces of construction equipment such as jackhammers, operating at the same distance. What makes the low levels of vibration that are reported by Ames et al. even more surprising is that their data were compiled from measurements made at 3 sites in response to complaints about vibration levels. It would appear therefore that either people's perception of the magnitude of train-induced ground vibrations is wrong or vibration levels reported by Ames et al significantly underestimate the levels of vibrations generated by trains. The latter premise is more likely to be true for two reasons. Firstly, vibration levels that have been recorded at large distances from trains imply that vibration levels close to the train should exceed 4 mm/sec; and secondly, train-induced ground vibrations appear to have induced several large scale liquefaction failures.

Ames et al. report that ground vibrations recorded at a distance of 30m from a passing train contained a peak particle velocity of about 1.4 mm/sec (0.055 inches/sec). If the amplitude of these ground vibrations is assumed to attenuate at the same rate as those of an ideal Rayleigh wave, then this value implies a peak particle velocity of approximately 5.7 mm/sec at a distance of 2 m from the tracks. In reality, this

assumption is probably conservative and vibration amplitudes should attenuate at some rate between that for an ideal Rayleigh wave and that for a body wave at the ground surface, or possibly at an even higher rate. If the ground vibrations are thus assumed to attenuate at the same rate as an ideal undamped body wave, then the vibration level at a distance of 2 m the train is calculated to be about 23 mm/sec (0.92 inches/sec). Both of these values are significantly higher than the maximum level of 3.9 mm/sec reported by Ames et al.

The other reason for believing that reported amplitudes of vibration are too low is that train-induced ground vibrations of these magnitudes are unlikely to be capable of liquefying a soil. This observation is important since some investigators believe that ground vibrations generated by trains have caused large-scale liquefaction failures, several of which are reported in Table 1.1. Two of these failures occurred in 1980 and involved railroad embankments which failed while trains were traveling over them; these embankments were principally constructed from sand and water was ponded on one side of both embankments at the time of failure. Since in both cases the lead engines passed safely over the embankments and came to rest on the far side of the failed section, it is believed that their failure was possibly induced by ground vibrations generated by the first or second locomotives. The railroad companies suffered significant economic losses as a result of these failures. Another case history involving a levee failure in Holland has been learned of, where the failure was attributed to liquefaction caused by train-induced ground vibrations. Unfortunately no reference was provided for this failure. Terzaghi and Peck (1967) report that a railway

embankment which rested on a fairly dense sand settled approximately 360 mm (14 inches) during 40 years of operation.

In view of the conflicting evidence concerning the amplitudes of train-induced vibrations, it seems desirable to collect further data on this subject. The results of supplementary studies conducted at four sites are presented in Chapter 4.

2.9. Acceptable Levels of Ground Vibration

2.9.1. Introduction

Construction operations in urban areas are sometimes limited by the ground vibration magnitudes that they are allowed to generate at a site. These levels might be set in order to prevent structural damage or to minimize the disruption to neighbors, and because the levels of vibration that are perceptible to people are much less than the levels of vibration that are required to cause structural damage, human response may well govern construction operations. This is particularly true when noise accompanies vibrations since humans are much more sensitive to vibrations associated with noise.

The number of complaints that are made against construction operations can be greatly reduced by good public relations. This involves informing neighbors of both the expected levels of vibration and the proposed activities, prior to the commencement of operations. In addition, surveys should be made of all houses in the vicinity in order to ascertain how much damage, if any, is caused by the vibrations and whether any of the neighboring buildings house vibration-sensitive equipment such as

machine tools, test gear, precision instruments and computers. It is worth noting that ground vibrations generated by driving piles are large enough to halt the production from certain types of machinery such as precision milling machines, jig barers and profiling millers.

This section attempts to summarize the effects of ground vibrations on both humans and structures.

2.9.2. Response of Humans to Vibrations

One of the first comprehensive studies into the response of humans to steady-state vibrations was conducted by Reiher and Meister (1931) who examined the responses of a group of healthy young people to steady-state vibrations which varied both in amplitude and in frequency. These investigators classified the reactions of their subjects as one of six levels of perception (imperceptible, just perceptible, easily noticeable, annoying, unpleasant, and painful) which are still in use; in fact, O'Neill (1971) states that "no more comprehensive study has since been conducted" to the best of his knowledge. Because Reiher and Meister expressed their levels of perception as a function of displacement amplitudes and most researchers currently prefer to express levels of vibration in terms of peak particle velocities, Wiss (1974) replotted these relationships as a function of particle velocity and frequency. This plot which is presented in Figure 2.27 indicates that the response of humans to peak particle velocity is independent of frequency at low levels of vibration. Goldman (1948) also compiled the results of a study on human response to steady-state vibrations.

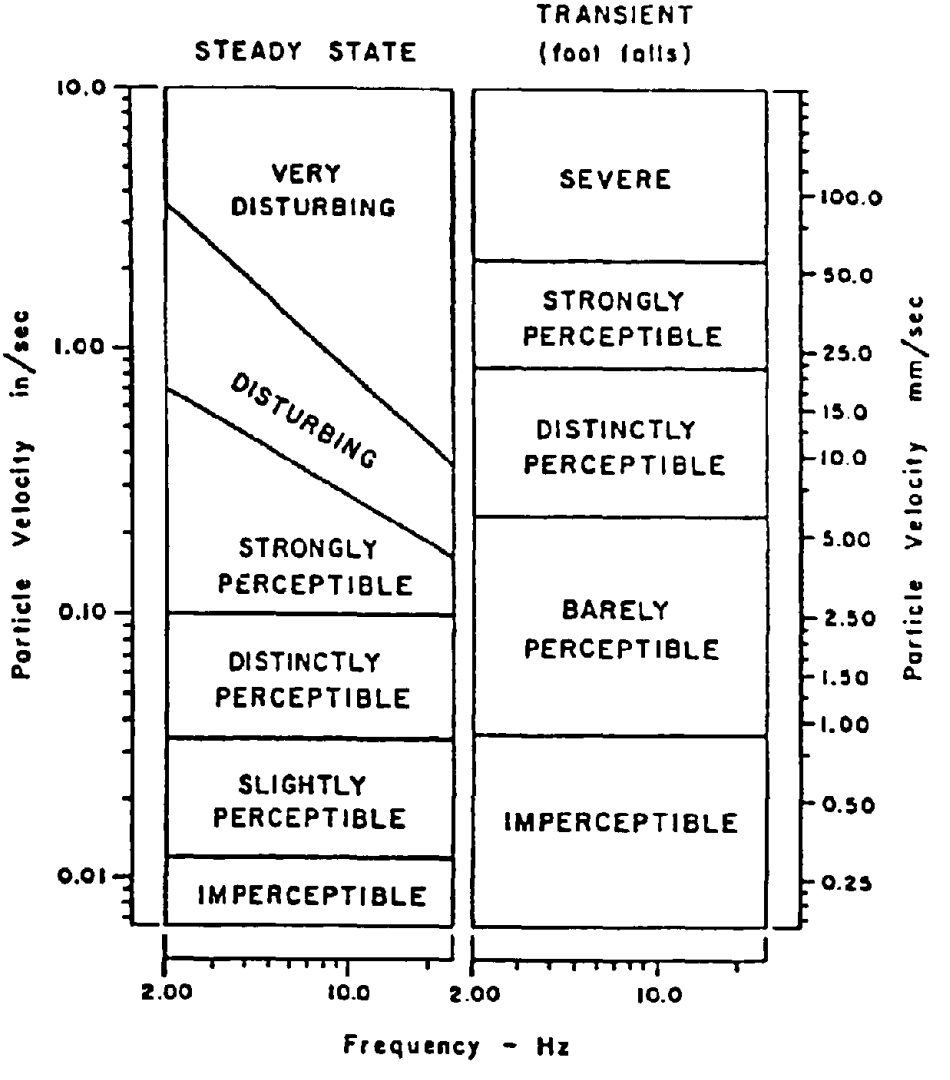

FIG 2.27 COMPARISON OF HUMAN RESPONSE TO STEADY STATE AND TRANSIENT VIBRATIONS (from Wiss, 1981).

The response of humans to transient vibrations has also been studied and corresponding levels of perception have been proposed by Crandell (1949), Rathbone (1963), Bollinger (1970), and Wiss and Parmelee (1974) who proposed the criteria shown in Figure 2.27. The results of these studies show that humans appear to be less sensitive to transient vibrations than to steady-state vibrations.

Research conducted by Hendron has shown that humans appear to be much more sensitive to ground vibrations when they are accompanied by sound. Hendron (1977) states that "all rules for predicting response appear to fall apart when sound effects accompany the motion and the motion is of short duration", primarily because the average person is believed to be incapable of isolating the characteristics of ground motions from their accompanying sound effects. Hendron summarizes this as follows: "Simply stated he (the average person) thinks the building was subject to strong shaking because he heard the sounds of vibrations in parts of the structure." A plot suggesting levels of perception for transient vibrations accompanied by sound (after Hendron, 1977) indicates that humans appear to be somewhat more sensitive to transient vibrations accompanied by sound than to steady state vibrations.

It is important to realize that the levels of perception that are presented in Figure 2.27 are merely subjective assessments, and that people exhibit a wide range of sensitivity when they are making subjective judgments. This range in sensitivity is graphically illustrated by Wiss and Parmelee (1974), who asked their subjects to determine levels of ground displacement that the subjects considered to be "distinctly perceptible." Wiss and Parmelee then plotted these levels of ground displacement as a function

of frequency. The ground vibrations that were judged to be "distinctly perceptible" ranged over one order of magnitude, leading the investigators to concluded that the human body is an excellent detector of vibrations but a poor measuring device.

People's feelings, attitudes and even work performance can be affected by exposure to ground vibrations. In addition, different people may like, dislike or be indifferent to a given level of vibration, depending on their background. Chilton, Friesz and Chen (1975) suggest that these psychological effects may be caused by a direct response to the vibrations or by emotional experiences and associations. Research also appears to show that long term exposure to vibrations may be very fatiguing. Chilton et al quote Goldman and van Gierke (1961) as stating that continuous exposure to vibrations at levels only slightly above the level of human perception leads to irritation and fatigue.

It is interesting to note that certain frequencies seem to excite resonances in specific organs and organ groups of the human body. Chilton et al quote resonant frequencies of 3 to 5 Hz for the thorax abdomen system, 2 to 3 Hz for the shoulder and head, 20 to 30 Hz for the head alone and 2 to 12 Hz for the whole body. These resonant frequencies are dependent upon the position and muscle tension of the body.

2.9.3. Damage Criteria for Structures

Numerous authors have presented papers outlining damage criteria for structures, most of which were developed by observing the response of buildings to blast-induced ground vibrations. These criteria also tend to focus on the behavior of residential

structures, probably because most of the complaints that arise from construction-induced ground vibrations are made by the owners of residential structures.

One of the first researchers to present damage criteria for structures was Crandell (1949) who expressed damage levels as a function of Energy Ratio as defined by the equation:

$$E.R. = \frac{a^2}{f^2} \qquad 2.18$$

where a = peak acceleration (ft/sec^2)
and f = frequency (Hz)

This comprehensive study investigated the effects of blasting on over 1000 residences, including residential homes, 2 story businesses, schools and churches and reached the following conclusions:

1) Structures of average workmanship and good materials would not be damaged by ground vibrations with Energy Ratios less than 3. This level of vibration was conditional on the fact that the buildings were not overstressed.

2) Ground vibrations with Energy Ratios between 3 and 6 were capable of opening up old cracks and causing the spalling of loose veneers in structures in poor condition or structures that were overstressed.

3) Structures subjected to ground vibrations with Energy Ratios greater than six, could be seriously damaged. Serious damage was defined as the

development of new cracks or actual cracking of foundations and walls in extreme cases.

Since Energy Ratio is defined as a function of both frequency and peak ground surface acceleration, values of Energy Ratio can be converted to values of peak particle velocity by assuming that the ground motions consisted of a sinusoidal wave of any single frequency; while this is obviously a simplifying assumption it provides some idea of vibration levels for comparison purposes. Energy ratios of 3 and 6 are thus equivalent to particle velocities of 85 mm/sec (3.3 inches/sec) and 120 mm/sec (4.7 inches/sec) respectively, implying that the levels associated with Crandell's damage criteria are similar in magnitude to the vibration levels subsequently proposed by other authors.

The damage criteria proposed by Nicholls, Johnson and Duvall (1971) for the U.S. Bureau of Mines, Edwards and Northwood (1958), and Langefors et al (1958)are compared in Figure 2.28 (after Wiss, 1981) and while these three sets of criteria indicate that damage is only likely to occur if vibration levels exceed 100 mm/sec (4.0 inches/sec), both Nicholls et al and Edwards et al suggest that a peak particle velocity of 50 mm/sec (2.0 inches/sec) should be used as a safe upper limit for allowable vibrations.

The criteria that are presented in Figure 2.28, associate similar levels of structural damage with similar levels of ground vibration, an observation which is interesting because these three sets of criteria were produced by different authors, from data compiled in three different countries. Remarkable similarities between criteria developed

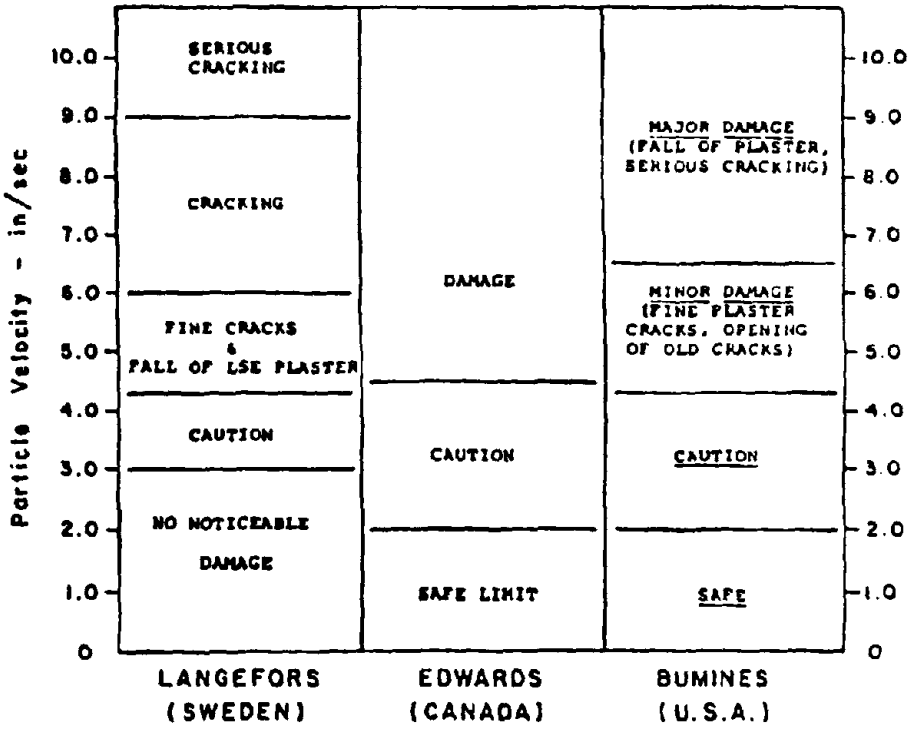

FIG 2.28 COMPARISON OF DAMAGE CRITERIA FOR RESIDENTIAL-TYPE STRUCTURES (from Wiss, 1981).

by different investigators is also reported by Duvall and Fogelson (1962) who statistically analyzed the vibration measurements and damage criteria presented by Edwards and Northwood (1960), Langefors et al (1958) and Thoenen and Windes (1942) and like the studies summarized in Figure 2.28, these three studies were also developed from observations of the response of buildings in three different countries, over different time periods. The analyses performed by Duvall and Fogelson showed that there was a 50% probability that structures would suffer major damage such as serious cracking and the fall of plaster when they were subjected to ground vibrations with peak particle velocities equal to 190 mm/sec (7.6 inches/sec). In addition, the probability of structures suffering minor damage when subjected to ground motions with peak particle velocities equal to 140 mm/sec (5.4 inches/sec) was calculated to be slightly less than 50%. Minor damage is associated with the production of fine plaster cracks and the opening of old cracks.

Other criteria which define damage levels of vibration have been proposed by Chae (1978) and Koch (1953) who defines 6 levels of damage as a function of displacement amplitude and frequency. After comparing his damage criteria with the levels of human perception quoted by Reiher and Meister, Koch concluded that damage could be expected when the levels of vibration became annoying to humans.

Criteria proposed by Chae (1978) are presented in Table 2.6 and it may be seen that they suggest the same vibration limits for sound structures as those proposed by Nicholls et al (presented in Figure 2.28). Chae's criteria classify buildings into one of four categories and propose a different damage level vibration for each category.

Table 2.6 : Damage Criteria Recommended by Chae (1978)

Class	Peak particle velocity, in inches per second	Peak particle velocity, in millimeters per second
I[a]	4	100
II[b]	2	50
III[c]	1	25
IV[d]	0.5	12

[a] Structures of substantial construction.
[b] Relatively new residential structures in sound condition.
[c] Relatively old residential structure in poor condition.
[d] Old residential structures in very poor condition.
Note: If structure is subjected to repeated blasting, or if blasting is done without instrumentation, lower category by one.

It might appear from the high degree of similarity between criteria developed by different investigators that the damage potential of all sources of non-seismically induced ground vibrations can be assessed with a reasonable degree of accuracy. However this is unlikely considering the fact that all of the criteria presented thus far are based on the observed response of structures to blast-induced ground vibrations. Since such vibrations are transient in nature and typically generate only a small number of cycles of significant shaking, it is unlikely that the aforementioned criteria can be used to make a reasonable prediction of the degree of damage that is likely to be caused by sources which generate many more cycles of loading such as pile driving and freeway traffic. Ground vibrations that are smaller in magnitude but act for many more cycles may be significantly more damaging than a smaller number of larger amplitude vibrations. Unfortunately, far fewer criteria have been developed for

sources of ground vibrations which produce large numbers of cycles of significant ground shaking.

One set of criteria which associates levels of human reaction and structural response with the magnitude of vibrations produced by road traffic is presented by Whiffin and Leonard (1971). These criteria not only suggest that peak particle velocities of 10 to 15 mm/sec (.39 to .59 inches/sec) will cause architectural damage and possibly some minor structural damage. but that peak particle velocities as low as 5 mm/sec (0.20 inches/sec) may be large enough to cause "architectural damage to houses with plastered walls and ceilings". In contrast, blast-induced ground vibrations are not predicted to cause architectural damage until the peak particle velocities exceed 100 mm/sec (4 inches/sec).

Crockett (1979) has proposed a comprehensive method for assessing the damage potential of ground vibrations generated by pile driving. This method attempts to account for both the number of cycles of significant shaking that are associated with different size piling contracts and other factors such as the type and age of a building, specific construction details and the soil type. Crockett incorporated the number of cycles of significant shaking since this parameter may vary greatly with the size of the project and damage increases with an increase in this number of cycles; small piling contracts typically generate ten thousand cycles of shaking while large piling contracts may produce more than one million cycles. An importance factor is also introduced which rates buildings on a scale of one to ten. Light industrial buildings are given a rating of one, while sensitive historic buildings are given a rating of ten. Crockett's method is not presented in detail in this document.

The acceptable vibration levels that are proposed in the Swiss Vibration Standard, SN 640312, entitled "Effects of Vibrations on Structures." are summarized in Table 2.7. This standard which is based on measurements recorded in Switzerland since the 1960's proposes separate criteria for buildings subjected to blast-induced ground vibrations and to ground vibrations produced by machines and road traffic. These buildings are further separated into four categories based on structural type. It may be noted from Table 2.7 that the damage criteria proposed for blast-induced vibrations are more conservative than the criteria presented in Figure 2.28, principally because the Swiss values were set so as to minimize damage as much as possible. Studer and Suesstrunk (1981) state that the aim of SN 640312 is to set allowable vibration levels below which light damage to buildings is improbable and damage to the basic support structure of a building is excluded. Light damage is associated with the formation of cracks, the falling away of plaster and the breakage of windows that are improperly fixed.

It is interesting to note that of all the criteria presented in this section only the Swiss Standard provides different vibration levels for ground motions with different frequency contents. This is somewhat surprising since it is universally acknowledged that a building's response to ground vibrations is significantly influenced by the ratio of the natural frequency of the structure to the predominant frequency of the input vibrations. Since structural response is greatest when this ratio is equal to one, permissible vibration levels should be lower for sources of vibration which generate motions

Table 2.7 : Swiss Vibration Standard, SN 640312

Building class	Vibration source	Range of frequency, in hertz	Peak particle velocity, in millimeters per second	Peak particle velocity, in inches per second
I[a]	Machines, traffic	10 - 30	12	0.5
		30 - 60	12 - 18	0.5 - 0.7
	Blasting	10 - 60	30	1.2
		60 - 90	30 - 40	1.2 - 1.6
II[b]	Machines, traffic	10 - 30	8	0.3
		30 - 60	8 - 12	0.3 - 0.5
	Blasting	10 - 60	18	0.7
		60 - 90	18 - 25	0.7 - 1.0
III[c]	Machines, traffic	10 - 30	5	0.2
		30 - 60	5 - 8	0.2 - 0.3
	Blasting	10 - 60	12	0.5
		60 - 90	12 - 18	0.5 - 0.7
IV[d]	Machines, traffic	10 - 30	3	0.12
		30 - 60	3 - 5	.12 - 0.2
	Blasting	10 - 60	8	0.3
		60 - 90	8 - 12	0.3 - 0.5

[a] Buildings in steel or reinforced concrete, like factories, retaining walls, bridges, steel towers, open channels; underground chambers and tunnels with and without concrete alignment.

[b] Buildings with foundation walls and floors in concrete, walls in concrete or masonry; stone masonry retaining walls; underground chambers and tunnels with masonry alignments; conduits in loose material.

[c] Buildings as mentioned previously but with wooden ceilings and walls in masonry.

[d] Construction very sensitive to vibrations; objects of historic interest.

with frequencies that are close to the natural frequency of the structure. One way to account for the effect of frequency is to predict levels of building response by using response spectra for these ground motions. Dowding (1985), Medearis (1977) and Naik (1979) have all proposed techniques for predicting the response spectra of ground vibrations generated by blasting.

Damage criteria have also been proposed for tunnels. For example, Langefors and Kihlstrom (1963) state that a peak particle velocity of 300 mm/sec (12 inches/sec) is the minimum level of shaking required to induce the "fall of rock in unlined tunnels" and Hendron (1977) states that particle velocities in excess of 600 mm/sec (24 inches/sec) are required to form new cracks in rock. A more detailed summary of the damage limits for tunnels is provided by Hendron (1977).

Having reported that published criteria for underground utilities such as tile or concrete drainpipes, sewer and water mains and pipelines are not available, Wiss (1981) goes on to state that he is not aware of any cases where ground motions with peak particle velocities less than 75 mm/sec (3 inches/sec) have damaged pipes or mains, and that high pressure pipelines have withstood peak particle velocities of 250 to 500 mm/sec (10 to 20 inches/sec) without experiencing any distress. Dynamic strain gauge measurements were made to assess the conditions of the pipes.

A problem which is commonly encountered during construction operations is the detrimental effect of ground vibrations on green concrete, a problem that often arises on building sites where piles are being driven at the same time that concrete is being placed. Wiss (1981) believes that cured concrete can safely withstand vibrations up to

125 mm/sec (5 inches/sec), while Atkins and Dixon (1979) propose a safe level of 100 mm/sec (4 inches/sec). It is suggested by these authors that the permissible vibration level at times earlier than 28 days can be determined by linearly relating it to the percentage of total strength (defined as 28 day strength) that has been developed by the concrete.

A collection of bar graphs which compare damage criteria proposed by a large number of authors has been presented by Theissen and Wood (1982) and is presented in Appendix B.

CHAPTER 3

Summary of Theoretical Liquefaction Evaluation Procedures

3.1. Shear Stress Approach

3.1.1. Discussion

The liquefaction potentials of sand sites subjected to ground shaking can be evaluated by following either one of two basic approaches: the shear stress approach or the shear strain approach. The shear stress approach, which is the most commonly used of the two approaches, evaluates liquefaction potential by comparing the levels of cyclic shear stress predicted to be induced within a soil deposit (by the ground vibrations) with the levels required to cause liquefaction.

Reasonable estimates for the magnitudes the stresses that are generated by earthquakes can probably be obtained by performing ground response analyses. In such analyses rock motions are applied to the base of a deposit and equivalent-linear programs such as the computer program SHAKE (or more complex non-linear computer programs) are used to propagate these motions up through the site. Alternatively, the site response may be determined approximately by following some simplified procedure such as that proposed Seed and Idriss (1971). This procedure replaces the irregular earthquake-induced shear stress time history with a sinusoidal motion comprised of an equivalent number of cycles of loading at a constant level of cyclic

shear stress (as defined by Equation 3.1). Typical equivalent numbers of uniform stress cycles for earthquakes of several different magnitudes are listed in Table 3.1.

The average uniform stress associated with this ideal motion may be calculated from the equation:

$$\tau_{av} = 0.65 \cdot \frac{\gamma h}{g} \cdot a_{max} \cdot r_d \qquad 3.1$$

where τ_{av} = average shear stress,
γ = density of the soil,
h = depth of layer being considered,
a_{max} = maximum ground surface acceleration and
r_d = stress reduction factor

The maximum ground surface acceleration, a_{max}, can be obtained from attenuation curves which express the maximum surface acceleration as a function of soil type, earthquake magnitude and distance; a plot of r_d versus depth is also presented by the authors of the method.

However while accepted procedures exist for computing the amplitudes of earthquake-induced cyclic shear stresses (with a reasonable degree of accuracy), no such procedures exist for determining the levels of cyclic shear stress likely to be induced by non-seismic sources of vibration. This lack of acceptable methods can probably be attributed to the following factors: the more complex nature of the wave-fields produced by most non-seismic sources, and the relatively small amount of research that has been conducted in the field of non-seismically-induced soil liquefaction. It should be pointed out that simplified procedures such as the approach

described above cannot be used to predict these levels, primarily because such motions typically contain significantly higher predominant frequencies than most earthquake-induced ground vibrations. As a result, non-seismic motions induce much lower levels of cyclic shear stress and strain for the same levels of surface shaking. In addition, these motions are usually confined to the surface layers and do not propagate up through the site from depth, as is the case with earthquake shaking.

The procedure that was used to estimate the magnitudes of the cyclic shear stresses induced by trains is outlined in Chapter 5. It is important to realize that the limitations discussed above are not unique to the shear stress approach but are also encountered when following the shear strain approach, since both procedures require prediction of the levels of shaking within the site.

The other step in the shear stress approach involves the prediction of the levels of cyclic shear stress that are required to liquefy a sand in-situ. One way of estimating these stresses is to sample the soil in the field and then subject these samples to laboratory tests which simulate the effects of earthquake shaking. However while such a procedure may seem appropriate, it also has several disadvantages, the most important being that sampling causes significant disturbance effects on the soil. For example, experience has shown that sampling not only tends to densify loose sands and loosen dense sands, but that it also affects the degree of cementation between particles and the structure of the sand.

A feel for the amount by which the density of a sand may be changed, can be obtained from the following case history. Seed, Singh, Chan and Vilela (1982) report

that a dense sand with an in-situ density of 1810 kg/m^3 (113 lb/ft^3) was sampled by taking block samples and by using a piston sampler. The resulting densities of the sand specimens extracted from the block samples were found to be about 1680 kg/m^3 (105 lb/ft^3) while the densities of the samples extracted by piston sampling were even less (about 1630 kg/m^3, 102 lb/ft^3), thus showing that sampling may significantly alter the density of a sand. Changes in relative density of these magnitudes have been shown to have a large effect on the liquefaction resistance of sand (Seed, 1979).

Obviously, such changes in relative density may be overcome by recompacting the sand to its in-situ density. However this approach is also undesirable since cementation is destroyed in the process and it is very unlikely that the soil structure produced in the laboratory will be the same as the soil structure present in the field. Seed (1979) reports that the presence of aging or cementation can increase the liquefaction resistance of a sand by more than 50% and that different compaction techniques may cause a sands resistance to change by as much ± 50%.

It should be noted at this point that while undisturbed samples can be obtained by freezing the soil in the field (before sampling) and then keeping the sample frozen until it is installed in the testing apparatus, this technique is very expensive and further, questions would still arise with regards to the ability of the testing equipment to model in-situ loadings exactly.

It has therefore been suggested that the levels of cyclic shear stress required to liquefy sands in-situ can be determined most accurately by using field performance plots of cyclic stress ratio versus standard penetration resistance to correlate

liquefaction resistance with the penetration resistance measured at the site. This approach not only circumvents the problems associated with sample disturbance but it also avoids any questions about the similarity between field loading conditions and those imposed by laboratory testing equipment. Correlation of field performance data with in-situ property measurements was first employed by Japanese engineers who used measurements of standard penetration resistance to differentiate between liquefiable and non-liquefiable deposits in the Niigata Earthquake.

Investigators such as Seed (1979) have developed the use of standard penetration resistance as an index for assessing the liquefaction resistance of a sand based on two observations: (1) that the main factors influencing the liquefaction resistance of a sand, also influence the penetration resistance in a generally similar manner and (2) that there appears to be a close correlation between field performance and penetration resistance. While other soil characteristics such as shear wave velocity, electrical properties or cone penetration resistance might also correlate well with liquefaction resistance, insufficient data exists to enable reliable correlations to be established between these properties and liquefaction resistance. In contrast, standard penetration resistance values are available for numerous sites that have been subjected to earthquake shaking.

Recent plots of soil liquefaction resistance versus Standardized Penetration Resistance, $(N_1)_{60}$, where Standardized Penetration Resistance is defined as the penetration resistance that a soil would exhibit if the soil was subjected to an overburden pressure of 1 ksc (1 tsf) and 60% of the potential hammer energy was transmitted to the drill string, are shown in Figures 3.1 and 3.2 (after Seed, Tokimatsu, Harder and Chung,

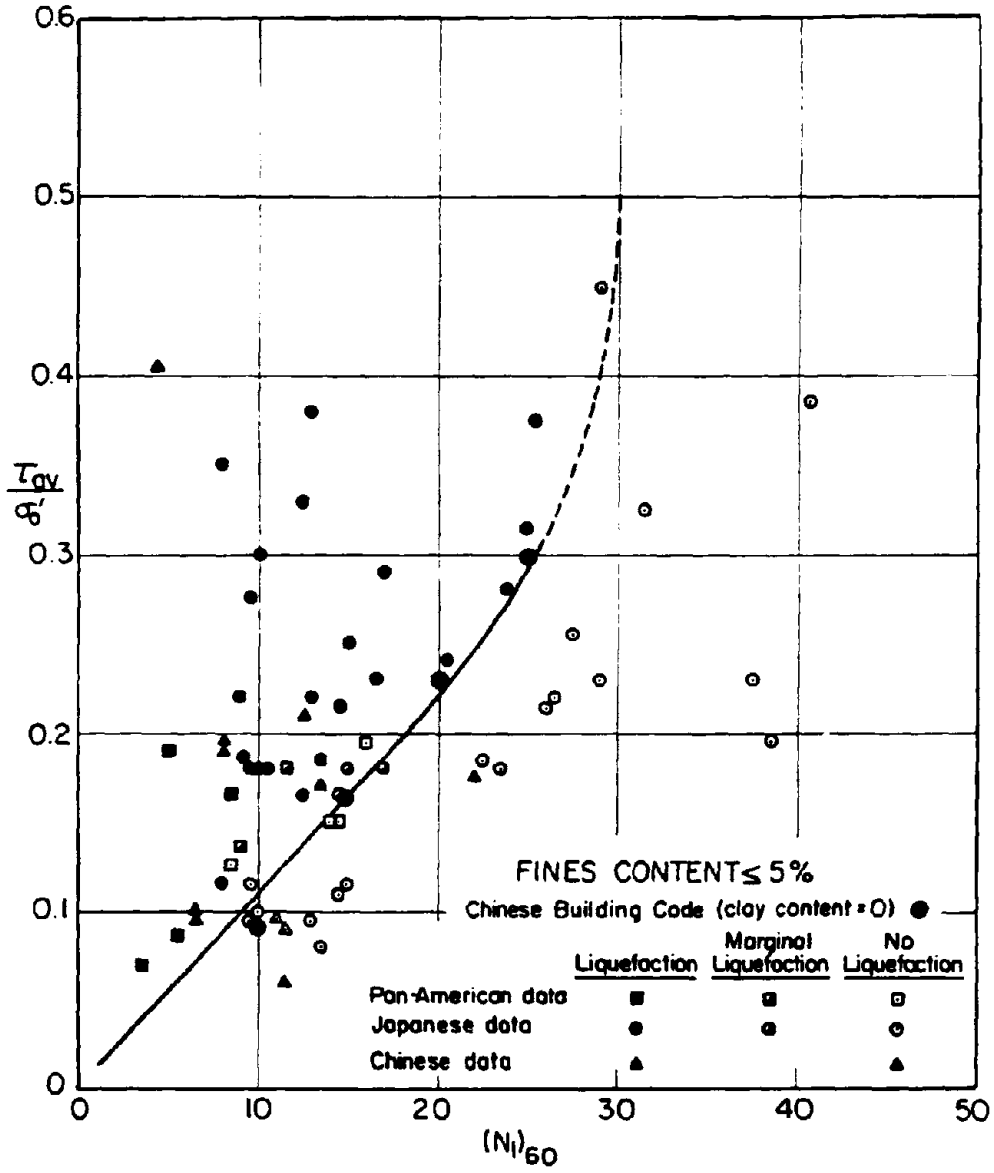

FIG 3.1 RELATIONSHIP BETWEEN STRESS RATIOS CAUSING LIQUEFACTION AND $(N_1)_{60}$ VALUES FOR CLEAN SANDS FOR M = 7-1/2 EARTHQUAKES (from Seed et al., 1984).

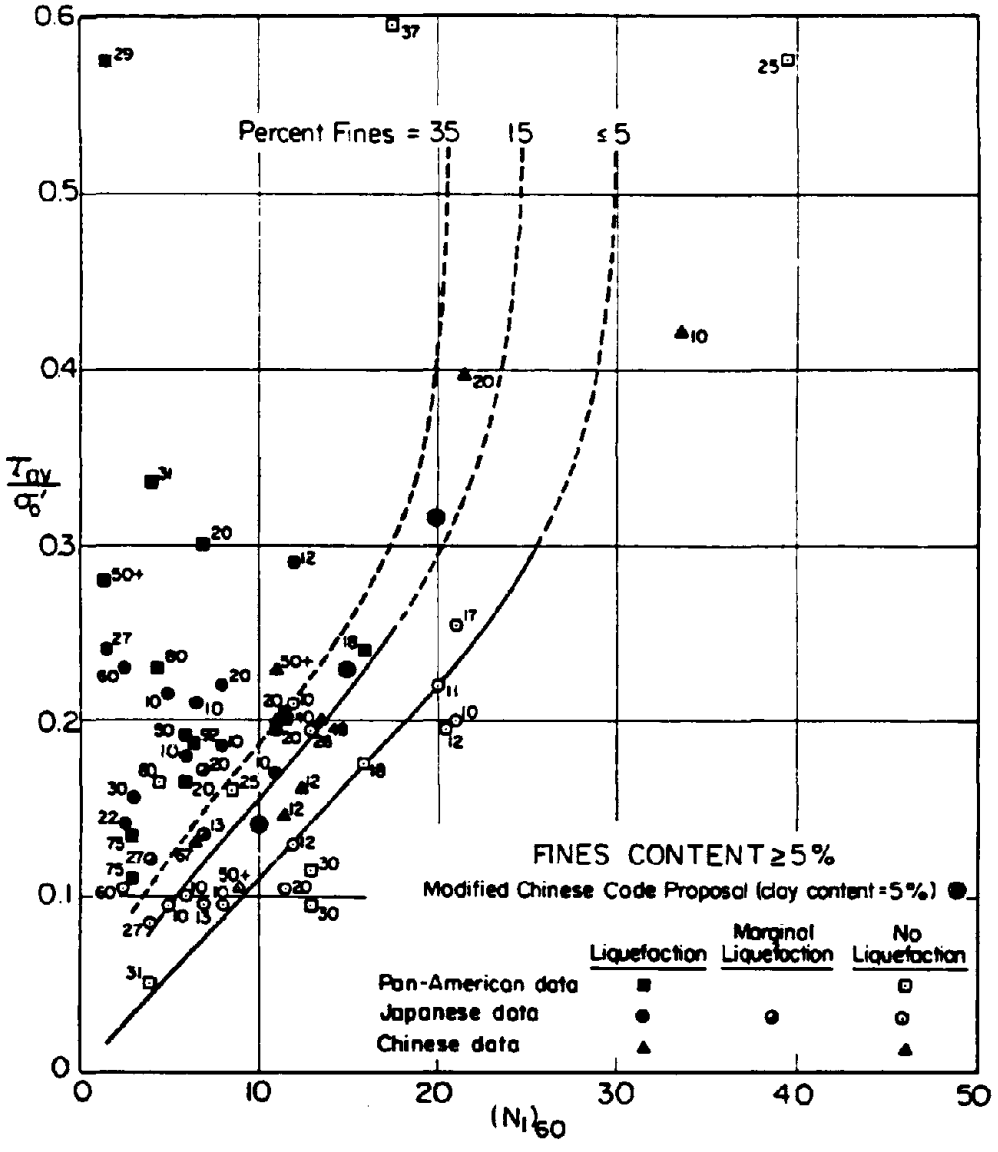

FIG 3.2 RELATIONSHIP BETWEEN STRESS RATIOS CAUSING LIQUEFACTION AND $(N_1)_{60}$ VALUES FOR SILTY SANDS FOR M = 7-1/2 EARTHQUAKES (from Seed et al., 1984).

1984). Most of the data presented in these figures were obtained from North and South American, Japanese and Chinese sites that were shaken by magnitude 7.5 earthquakes. The remaining data which pertains to magnitude 6.7, 6.6, 6.3, 6.1, 5.6, and 5.3 earthquakes were adjusted to represent magnitude 7.5 earthquakes by applying the correction factors proposed by Seed et al (1983) (see Table 3.1). All of the field data and their corrected values are listed in tables presented by Seed et al (1984). It should be pointed out that the values of cyclic stress ratio shown in Figures 3.1 and 3.2 were calculated using Equation 3.1 and that these values apply to overburden pressures typically less than about 1 ksc (1 tsf).

The boundary lines shown in Figures 3.1 and 3.2 define approximate lower bounds for sites that did not liquefy when they were shaken by magnitude 7.5 earthquakes and as such, they appear to provide a reliable basis for assessing the in-situ

Table 3.1 : Correction factors for the Influence of Earthquake Magnitude on Liquefaction Resistance (after Seed et al., 1983)

Earthquake Magnitude, M.	No. of Representative cycles at $0.65\tau_{max}$	$\frac{\left[\frac{\tau_{av}}{\sigma_o'}\right]_l \text{ for } M=M}{\left[\frac{\tau_{av}}{\sigma_o'}\right]_l \text{ for } M=7.5}$
8.5	26	0.89
7.5	15	1.0
6.75	10	1.13
6	5 - 6	1.32
5.25	2 - 3	1.50

liquefaction resistance of sands subjected to ground shaking produced by earthquakes of this magnitude. These curves can be modified to represent earthquakes of other magnitudes (or even ground vibrations generated by non-seismic sources) by using laboratory-developed curves of required cyclic stress ratio versus the number of cycles to liquefaction, to account for the different numbers of representative cycles of loading generated by each event. This number of cycles is defined as being the number of cycles of shaking at a constant stress level that will theoretically impose the same amount of distress on a soil as the irregular earthquake record.

After statistically analyzing numerous earthquake records, Seed et al (1975) concluded that magnitude 7.5 earthquakes typically produce about 15 representative cycles of loading at a constant cyclic shear stress level of $0.65\tau_{max}$. Thus, the levels of cyclic stress ratio required to liquefy a sand in-situ (in almost any number of cycles) can be estimated by multiplying the cyclic stress ratio determined from Figure 3.1 by the appropriate correction factor. This factor is equal to the cyclic stress ratio required to cause liquefaction in n cycles, divided by the cyclic stress ratio required to cause liquefaction in 15 cycles, where n is the number of cycles of representative shaking that is produced by the source being studied. It should be noted that the lower bound lines shown in Figures 3.1 and 3.2 vary with the fines content of the sand.

Figures which relate applied cyclic shear stress to the number of cycles of loading required to induce initial liquefaction have been presented by numerous authors, including De Alba et al (1976). The De Alba et al relationships were developed from the results of large-scale cyclic simple shear tests on Monterey sand. Since the cyclic

loading applied in such tests is thought to resemble in-situ loadings more closely than the loading applied in other laboratory tests, it is believed that these relationships provide the best representation of in-situ behavior. The original curves which were developed for relative densities of 90%, 82%, 68%, and 54%, were normalized (by dividing the values of required cyclic shear stress by the shear stress that caused liquefaction in one cycle) and then averaged to produce the single curve shown in Figure 3.3 (after Seed and Idriss, 1982).

As shown in this figure, the relationship derived from De Alba et al's research extends over the range of 1 to 100 cycles and while this range is suitable for evaluating the liquefaction potential of earthquake-induced vibrations, it is too small for analyzing many non-seismically-induced ground vibrations. Therefore a second curve which extends to larger numbers of cycles of loading was derived from the results of tests presented by Szerdy (1985). This latter curve was obtained as described above by dividing the values of required cyclic stress ratio by the cyclic stress ratio required to cause failure in one cycle. These normalized curves were subsequently averaged to produce the single relationship shown in Figure 3.3. It is worth noting that even though Szerdy subjected some samples to more than 10,000 cycles of loading, the relationship derived from Szerdy's data is only shown to extend over the range of 10 to 1000 cycles because most of his data fell within the more limited range.

Szerdy's curves were developed from the results of cyclic triaxial tests performed on samples of Sacramento River Fine sand. These samples were compacted to a range of relative densities, and subjected to different values of confining stress and initial

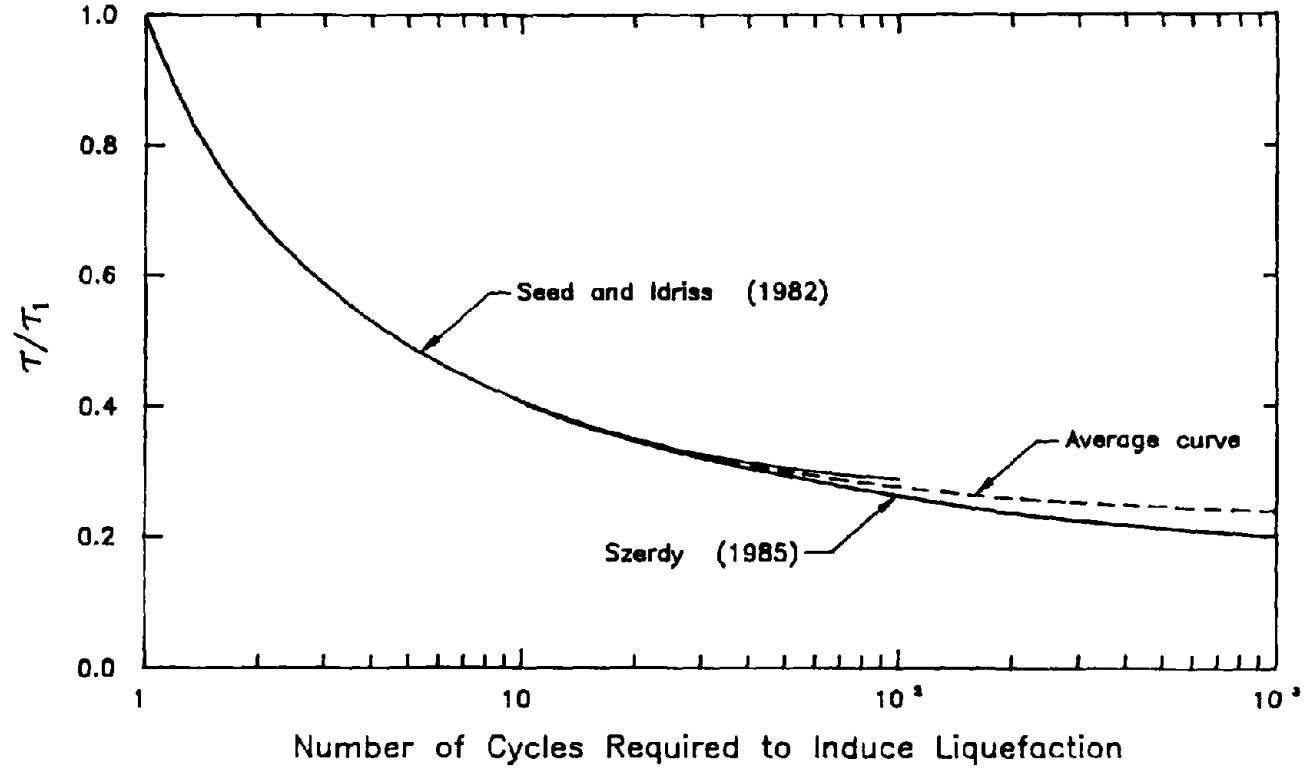

FIG 3.3 REPRESENTATIVE RELATIONSHIP BETWEEN τ/τ_1 AND THE NUMBER OF CYCLES REQUIRED TO CAUSE LIQUEFACTION IN A SAND.

shear stress/normal stress ratio. It is interesting to note that changes in relative density, confining pressure and the initial shear stress/normal stress ratio did not appear to significantly affect the shape of the normalized curve.

The average curve shown in Figure 3.3. is believed to provide a realistic representation of in-situ behavior, even though Szerdy's data were obtained from cyclic triaxial tests, because at large numbers of cycles of loading there appears to be little difference of loading between the relationships developed from cyclic simple shear tests and those developed from cyclic triaxial tests. De Alba et al (1976) who report the results of both cyclic triaxial tests and cyclic simple shear tests found that the relationships developed from the two types of tests are essentially the same for more than about 10 cycles.

In addition to the number of cycles of loading, the cyclic stress ratio required to liquefy a sand, is also a function of both the initial shear stress/normal stress ratio and the applied confining pressure. The effect of confining pressure can be taken into account by applying the K_σ factor. This factor is defined as being equal to the cyclic stress ratio required to liquefy a sand subjected to any given confining pressure, divided by the cyclic stress ratio required to liquefy the same sand in the same number of cycles when subjected to a confining pressure of 1 ksc (1 tsf); values of K_σ can be obtained from Figure 3.4. The plot shown in this figure was developed from a figure produced by Harder (1988) who plotted data for 18 different sands.

Because the ground motions that are generated by most non-seismic sources are confined to the surface layers, and most of the data presented in Harder's plot pertains

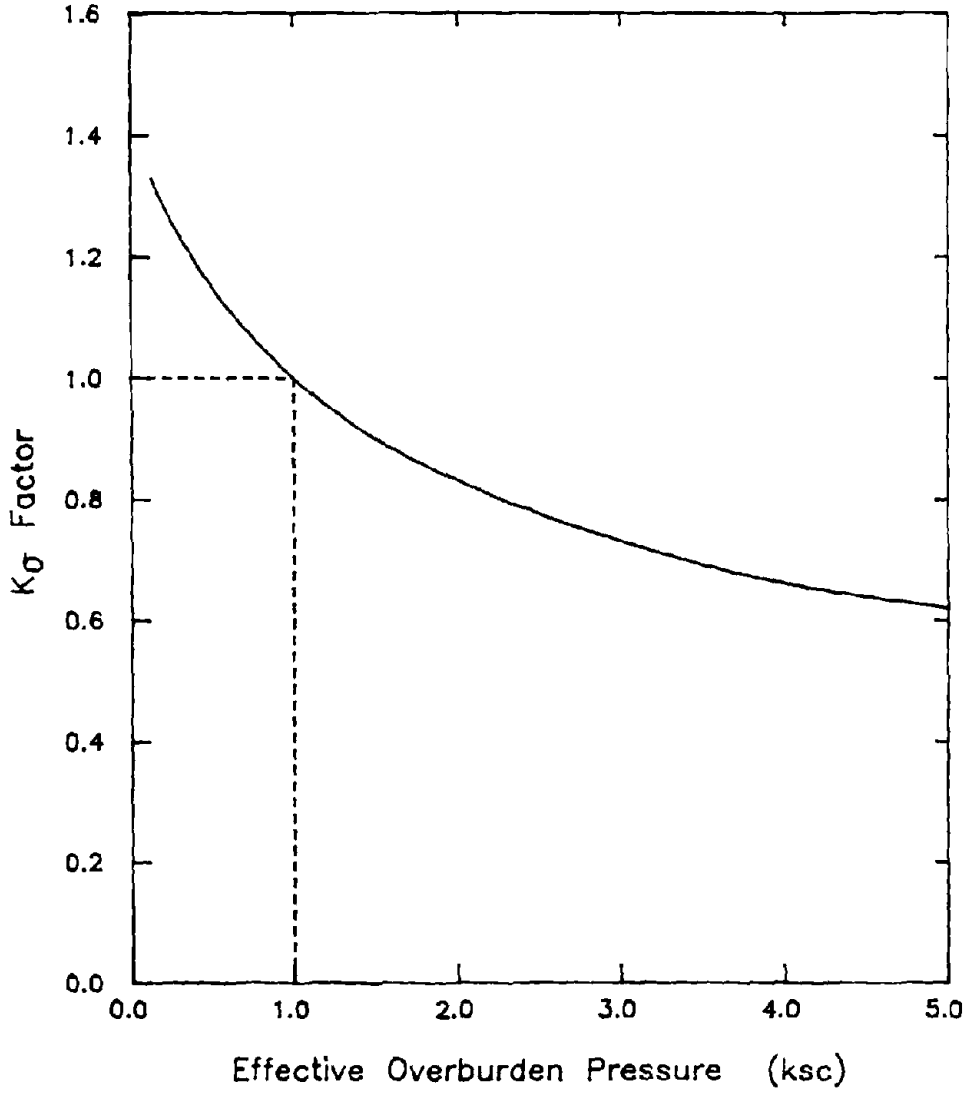

FIG 3.4 RELATIONSHIP BETWEEN THE K_σ FACTOR AND EFFECTIVE OVERBURDEN PRESSURE (after Harder, 1988).

to confining pressures in excess of 1 ksc, this plot was amended by adding points in the low confining stress range. These new data points are based on the results of cyclic triaxial tests performed on samples of sand which were subjected to confining pressures of 0.5 ksc, 1.0 ksc and 2.0 ksc (reported by Szerdy, 1985). A line of best fit was then drawn through through the amended plot and it is this line that is shown in Figure 3.4.

Several researchers have also examined the influence of initial static shear stresses on liquefaction resistance (including Vaid and Chern (1983), Szerdy (1985) and Castro et al. (1982)) and these studies have shown that the effect of such stresses is dependent upon the relative density of the sand. For example, the applied cyclic stress ratio that is required to liquefy loose sands appears to decrease significantly as the initial static shear stress/normal stress ratio is increased. The converse is true for medium-dense and dense sands. The plot shown in Figure 3.5 (after Szerdy, 1985) illustrates the influence of initial shear stresses on the liquefaction resistance of loose saturated sands.

It should be pointed out that two of the curves from Szerdy's original plot were revised before they were replotted in Figure 3.5. These two curves are the relationships developed by Szerdy(1985) and Vaid and Chern (1983), both of which are derived from the results of cyclic triaxial tests. Based on the premise that the cyclic stress ratios required to liquefy sands in-situ can be determined approximately by multiplying those ratios determined from cyclic triaxial tests, by a correction factor, Szerdy multiplied the cyclic stress ratios associated with zero initial shear stress by a factor of 0.57 (after Seed, 1979). However the cyclic stress ratios that were associated with

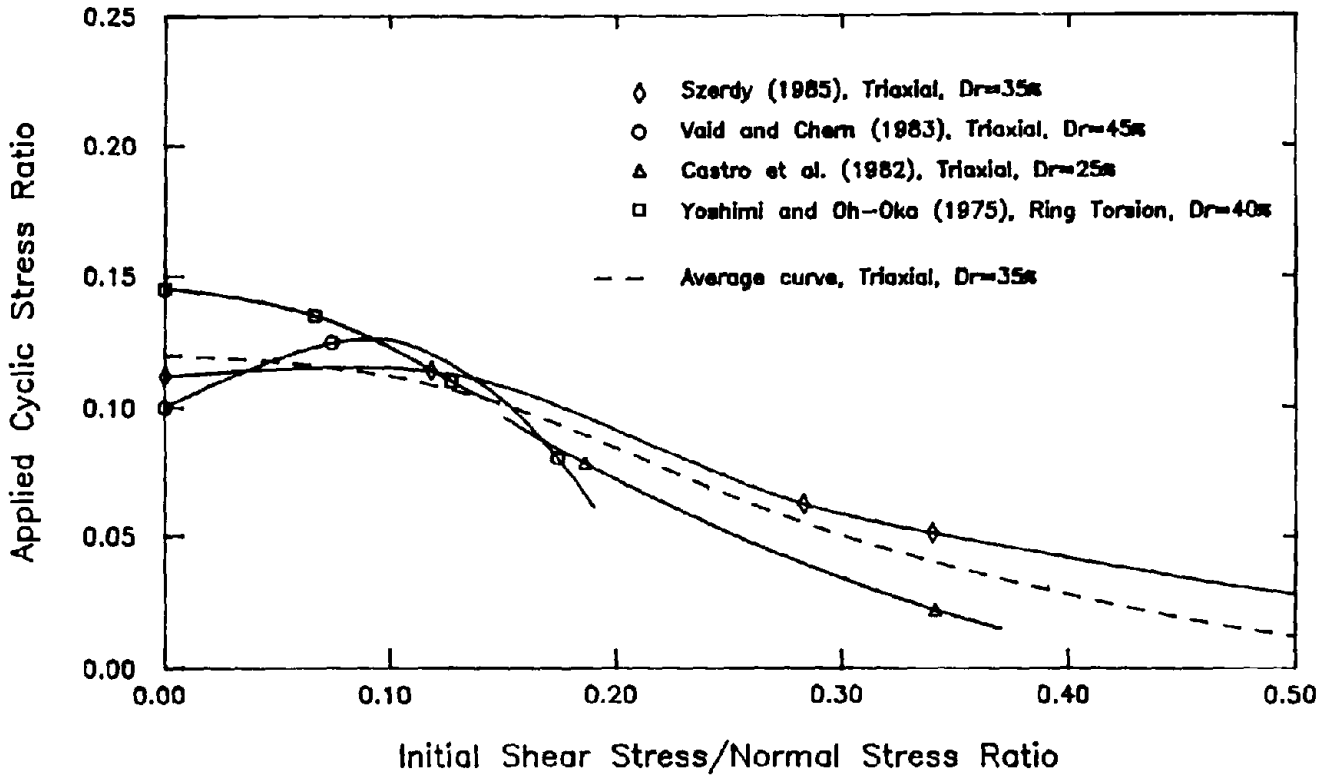

FIG 3.5 APPLIED CYCLIC STRESS RATIO VERSUS INITIAL SHEAR STRESS/NORMAL STRESS RATIO FOR FAILURE IN 10 CYCLES IN LOOSE SAND SAMPLES (after Szerdy, 1985).

higher values of initial shear stress/normal stress ratio were not reduced, thus leading to the seemingly erroneous prediction that slightly sloping ground might be almost twice as stable as level ground. Since such an approach appears to be inconsistent, both Szerdy's and Vaid and Chern's uncorrected curves are plotted in Figure 3.5. The decision to plot the uncorrected curves is further supported by the observation that these curves are more similar in shape to the curve determined by Yoshimi and Oh-Oka which is based on the results of ring torsion tests. The loading applied in ring torsion tests models in-situ cyclic loading more closely than the loading applied in cyclic triaxial tests.

The average curve shown in Figure 3.5 is believed to provide a reasonable representation of the effect of initial static stresses on the liquefaction resistance of a 35% relative density, saturated sand.

3.1.2. Advantages and Disadvantages of the Shear Stress Approach

The primary reason for using a shear stress approach to evaluate the liquefaction resistance of a site is that the amplitudes of the cyclic shear stresses induced within a site are closely related the magnitude of the ground surface accelerations. This observation is particularly apt when analyzing soil behavior under earthquake shaking conditions since accepted methods now exist for making a reasonable prediction of surface accelerations and relating these values to levels of cyclic shear stress. In contrast, the cyclic shear strains that are induced as a result of ground shaking are a function of both the ground surface accelerations and the shear modulus of the soil. Since the

shear modulus changes as pore pressures are generated, the amplitudes of the induced cyclic shear strains cannot be evaluated as accurately as the amplitudes of the induced cyclic shear stresses.

The liquefaction resistance of a soil can probably be determined most accurately by relating the standard penetration resistance of the soil to known field performance data. Such an approach circumvents the inaccuracies that are inherent with sampling sands and testing them in a laboratory. The use of standard penetration resistance as an index for evaluating field performance is supported by the observation that there appears to be a close correlation between field performance and standard penetration resistance. Furthermore, changes in soil characteristics which influence liquefaction resistance also influence the standard penetration resistance in a generally similar manner.

Use of the shear stress approach is supported by the large number of stress-controlled laboratory tests that have been performed on sands. The results of these tests provide researchers with a good understanding of the factors which influence the liquefaction resistance of soils and enable plots of field performance versus standard penetration resistance to be extrapolated to account for a large variation in the number of cycles of loading. This is particularly important when evaluating the liquefaction potential of non-seismic sources of vibration since such sources typically generate many more cycles of loading than even large magnitude earthquakes. For example, a single pile driving operation may produce over one million cycles of loading.

Another factor which is probably significant when analyzing the liquefaction potential of non-seismically-induced ground vibrations is the ability of the shear stress approach to account for the presence of initial static shear stresses. Such an ability is perceived to be important for the following reason: all of the large-scale liquefaction failures that are listed in Table 1.1 occurred on sloping ground, therefore the sands that failed were probably subjected to initial static shear stresses, and recent experimental evidence has shown that the liquefaction resistance of loose sands is reduced significantly as magnitudes of the initial static shear stress/normal stress ratios imposed upon these sands are increased. Since many of these sites may well have contained artesian pressure conditions, and the presence of these pressures tends to increase the magnitudes of the high initial shear stress/normal stress ratios present within the slope, it may be that non-seismic sources of ground vibration are only capable of liquefying sands that are subjected to such initial shear stress/normal stress ratios.

In the light of the above appraisal, it seems reasonable to conclude that the shear stress approach provides a good basic technique for assessing the liquefaction potential of sand sites being shaken by non-seismic sources of ground vibration. However, this approach does have one major limitation for this purpose; that is, the difficulty of taking into account the difference between the frequency content of most non-seismically-induced ground vibrations and the loading frequency at which cyclic triaxial tests are generally performed. As discussed in Chapter 2, the predominant frequencies of most non-seismically induced ground motions vary from 10 to 30 Hz and most triaxial tests are performed at a much lower frequency of 1 to 2 Hz.

Wong (1971) examined the effect of frequency at low frequencies by comparing the results of tests performed at 1/60 Hz (1 cycle/minute) and 0.33 Hz and observed that increasing the loading frequency by a factor of 20 reduced the cyclic stress ratio required to cause liquefaction by about 10%. It does not seem reasonable to conclude however, that further increasing the testing frequency from 1 to 20 Hz would decrease the liquefaction resistance by a similar amount. In fact, logic would seem to suggest that this cyclic stress ratio might begin to increase at high frequencies rather than continuing to decrease. Such a belief is based on the premise that the pore pressure buildup in sands is primarily related to cyclic shear strain and not cyclic shear stress, and at high frequencies of loading, the cyclic shear strains induced within the soil are likely to be less than those induced at low frequencies (by the same level of applied cyclic shear stress) because inertial effects may well become significant. Simply stated, if a shear stress does not act in one direction for a sufficiently long period of time, the soil does not have enough time to reach a strain in equilibrium with the applied cyclic shear stress before the direction of loading is reversed. Therefore the strains that are induced in the soil are no longer directly related to the levels of applied cyclic shear stress. Since no laboratory tests results have been found where soils have been tested at frequencies of loading in excess of 10 Hz, this supposition has not been substantiated and thus it remains an open question with regard to the applicability of the shear stress approach.

3.2. Shear Strain Approach

3.2.1. Discussion

The liquefaction potential of ground vibrations may also be evaluated by using the shear strain approach. This approach is based on the premise that cyclic shear strain is the fundamental parameter governing both the settlement of dry sands, and pore pressure buildup in saturated sands, during cyclic loading. Laboratory test data showing this strong dependence (on cyclic shear strain) has existed for many years, although it is only recently that the shear strain approach has been formally advocated as a liquefaction evaluation technique. The shear strain approach is currently the subject of extensive research.

Dobry, Yokel and Ladd (1981b) suggest that the cyclic shear strains that are induced by earthquakes may be determined approximately by using the following equation which was derived from Equation 3.1:

$$\gamma_e = \frac{\tau_e}{G} = 0.65 \cdot \frac{a_{max}}{g} \cdot \frac{\gamma \cdot h \cdot r_d}{G_{max} \cdot \left[\frac{G}{G_{max}}\right]_{\gamma_e}} \qquad 3.2$$

where γ_e = equivalent uniform strain,
G = equivalent shear modulus of the soil,
G_{max} = maximum, small strain shear modulus and
$\left[\frac{G}{G_{max}}\right]$ = modulus reduction coefficient

As with the earlier equation, Equation 3.2 replaces the irregular shear strain time history produced by an earthquake, by an equivalent uniform cyclic shear strain, γ_e which is assumed to act for an equivalent number of cycles of loading, n_γ. While this number of cycles (n_γ) is related to the number of representative cycles of shear stress loading, the two values are not the same and no references have been found where values of n_γ are related to earthquake magnitude.

Since Equation 3.2 is derived from the simplified formula proposed by Seed and Idriss, and this latter formula is believed to provide an acceptable means of modeling the actual site response, it might seem reasonable to conclude that Equation 3.2 is capable of predicting the levels of cyclic shear strain with a similar degree of accuracy. However this is not the case, primarily because for any given value of γ_e, the ratio $(G / G_{max})_{\gamma_e}$ changes during the earthquake due to changes in pore pressures within the soil, and the rate of pore pressure buildup in soils during earthquakes cannot be determined accurately. Accurate prediction of the levels of induced cyclic shear strain is further limited by the accuracy with which G_{max} can be determined, since γ_e is shown to be heavily dependent upon the shear modulus of the sand. Values of G_{max} can be measured directly by employing in-situ geophysical techniques such as the cross-hole method; however, such tests are very sensitive and different operators may determine significantly different values of G_{max} for the same site.

The shear strain approach evaluates liquefaction resistance by performing strain-controlled laboratory tests on sand samples taken from the site. However unlike the shear stress approach where laboratory test results are significantly influenced by

sample disturbance, in this case such a procedure appears to be acceptable. Experiments such as those reported by Vucetic and Dobry (1987) have shown that sample disturbance has only a minor influence on the rate of pore pressure buildup in strain-controlled tests. These investigators report the results of strain-controlled tests performed on two Imperial Valley, California, silty sands which liquefied during an earthquake in 1981. The results of these tests showed pore pressures to build up at the same rate in "intact" samples as they did in completely reconstituted samples.

The effect of soil structure alone, has been studied by both Park and Silver (1975) and Dobry and Ladd (1980). The latter investigators plotted values of induced pore pressure ratio versus cyclic shear strain for sands compacted by dry vibration and wet rodding (see Figure 3.6) and found that the pore pressure ratios differed by less than about 10% after 10 cycles of loading. The data presented in the Dobry and Ladd plot was computed from the results of strain-controlled laboratory tests reported by Park and Silver (1975) and Dobry and Ladd (1980).

The buildup of pore pressure during cyclic strain-controlled tests has been examined by a number of researchers and plots depicting this pore pressure buildup have been presented by Vucetic and Dobry (1987), Dyvik et al (1984), Thomas and Dobry (1984), Dobry, Ladd, Yokel, Chung and Powell (1982) and Dobry et al. (1981b). The plots shown in Figures 3.7, 3.8 and 3.9 (from Dobry et al., 1982) depict the influence of relative density, confining pressure and number of cycles of loading respectively, on the amount of pore pressure buildup. These curves were developed from the results of twelve undrained strain-controlled cyclic triaxial tests performed on samples of

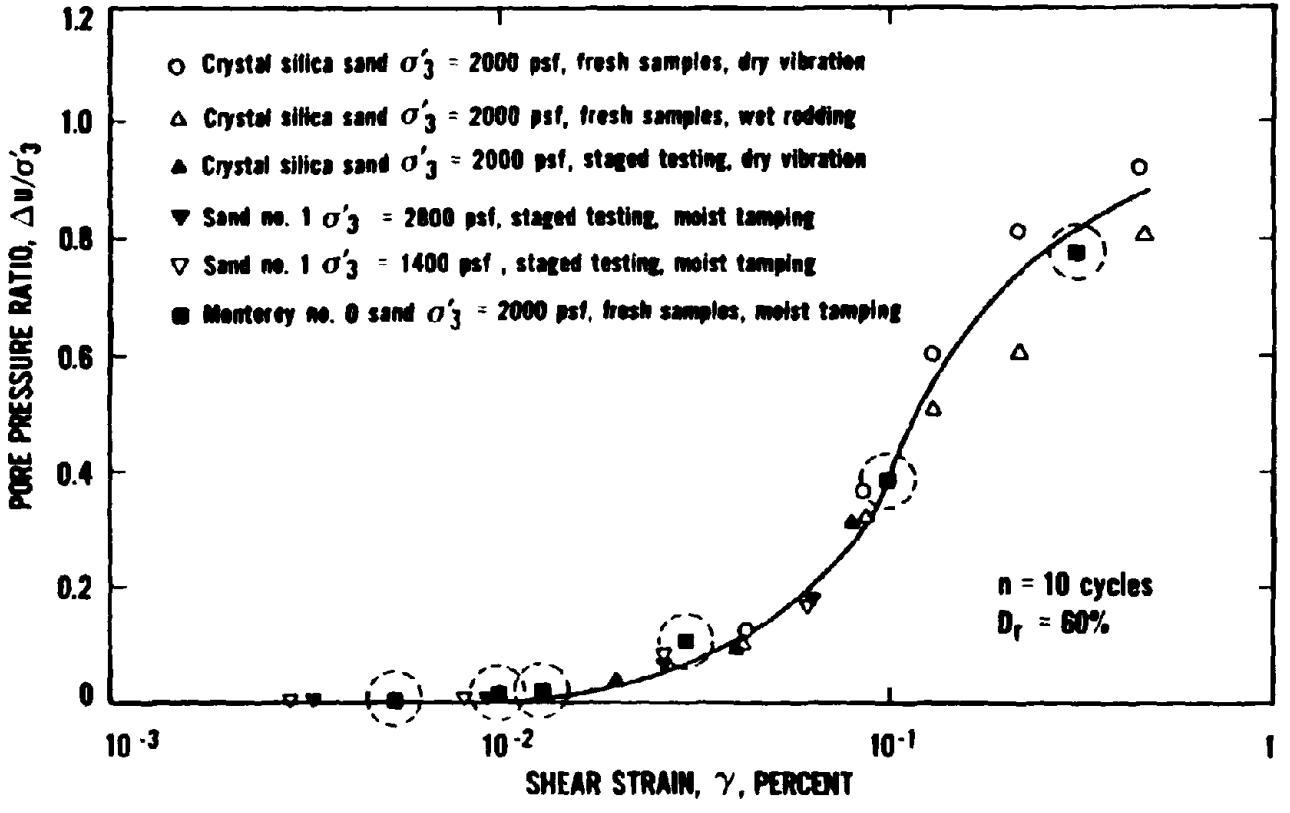

FIG 3.6 INFLUENCE OF TWO DIFFERENT COMPACTION TECHNIQUES ON PORE PRESSURE BUILDUP AFTER 10 CYCLES, DURING STRAIN-CONTROLLED TESTS, FOR VARIOUS SATURATED SANDS AT D_R = 60% (from Dobry and Ladd, 1980).

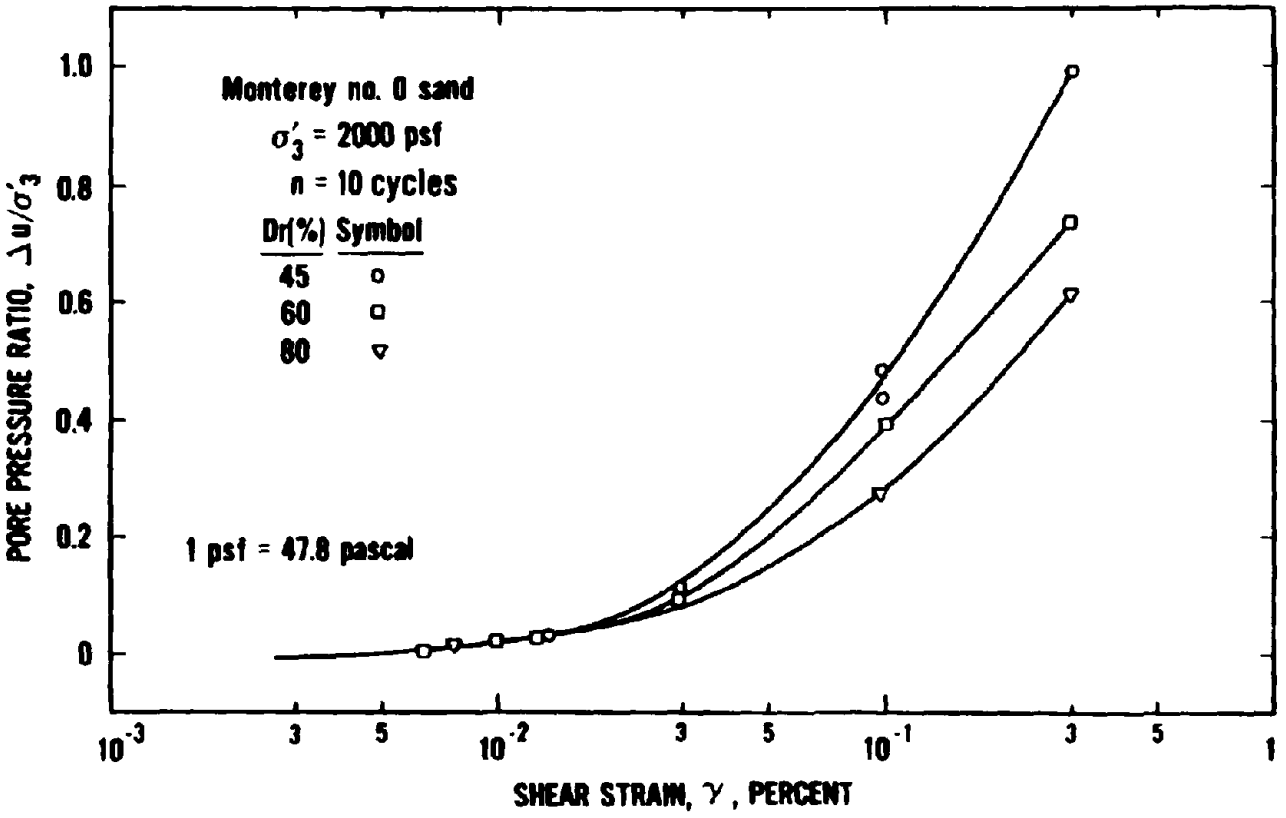

FIG 3.7 INFLUENCE OF RELATIVE DENSITY ON PORE PRESSURE BUILDUP AFTER 10 CYCLES, DURING STRAIN-CONTROLLED TESTS (from Dobry et al., 1982).

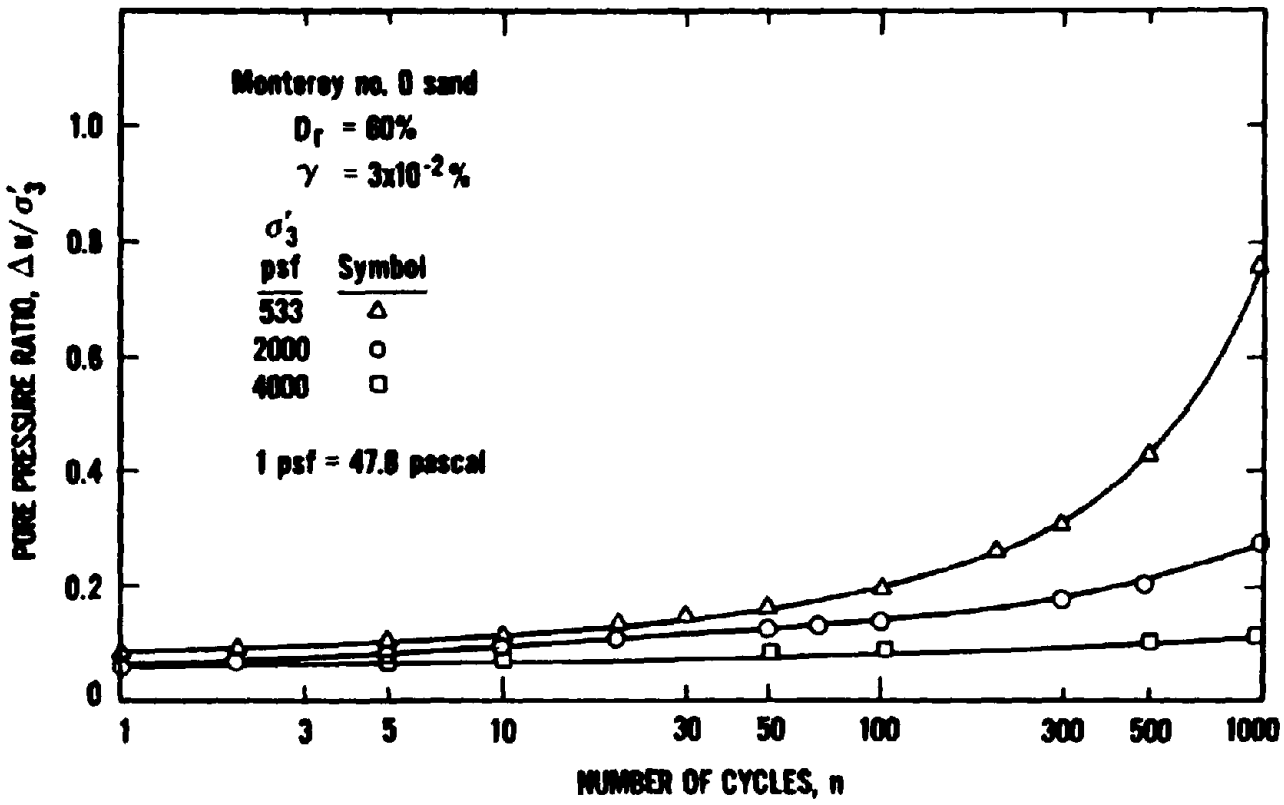

FIG 3.8 INFLUENCE OF EFFECTIVE CONFINING PRESSURE ON PORE PRESSURE BUILDUP AFTER 10 CYCLES, DURING STRAIN-CONTROLLED TESTS (from Dobry et al., 1982).

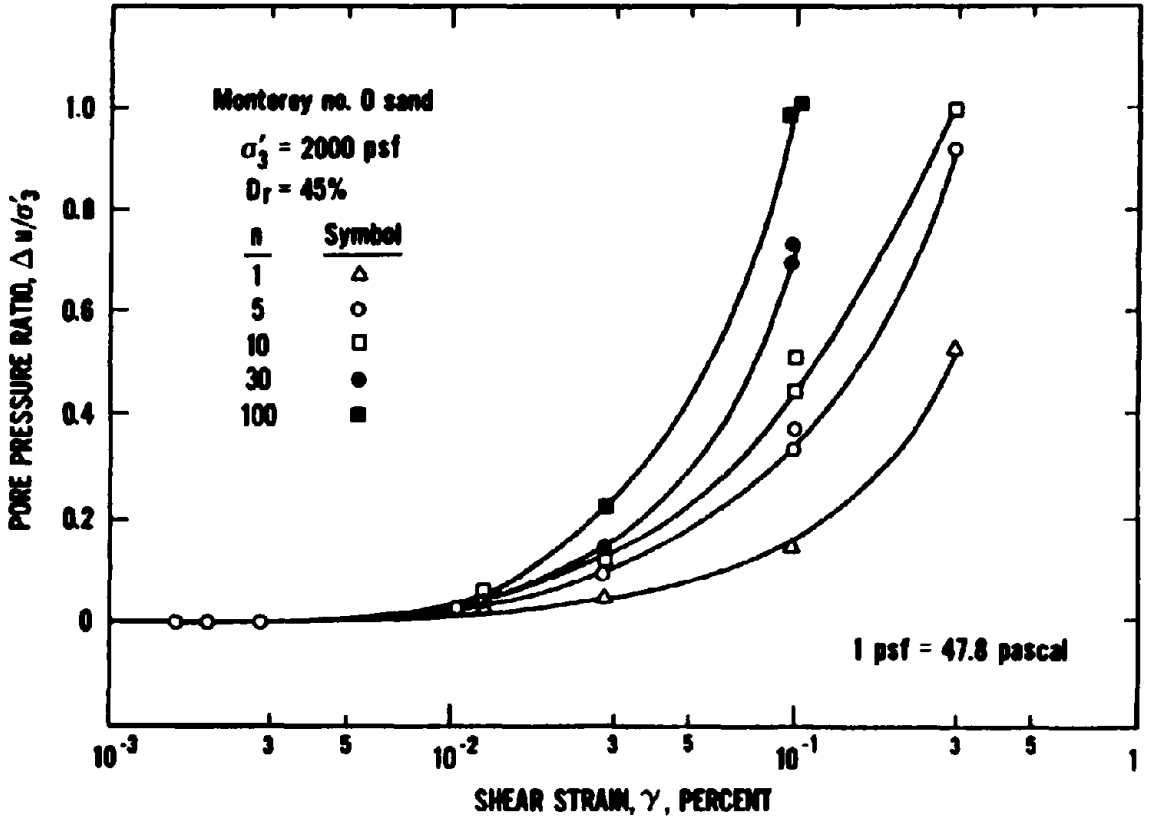

FIG 3.9 PORE PRESSURE BUILDUP IN STRAIN-CONTROLLED TESTS AS A FUNCTION OF SHEAR STRAIN FOR VARIOUS NUMBERS OF CYCLES (from Dobry et al., 1982).

saturated Monterey No. 0 sand (a washed, uniform, medium to fine beach sand composed of quartz and feldspar particles). The sand samples were compacted to relative densities of 45, 60 and 80% and tested at confining pressures of 0.26 ksc (533 psf), 1.0 ksc (2000 psf) and 2.0 ksc (4000 psf). The tests were run at one of three levels of cyclic shear strain: 3×10^{-2}%, 1×10^{-1}%, and 3×10^{-1}%. Dobry, Yokel and Ladd (1981b) also examined the influence of overconsolidation ratio on pore pressure buildup and report that pressures build up much more slowly in overconsolidated sands than in normally consolidated sands.

A further argument in support of the premise that cyclic shear strain is the fundamental parameter controlling pore pressure buildup in sands, is provided by the apparent existence of a threshold shear strain. Ideally, sands cycled at shear strains less than this threshold value will not generate significant pore pressures. The existence of a threshold strain was first noted almost 20 years ago by Drnevich and Richart (1970), Youd (1972) and Pyke (1973), all of whom reported that no detectable densification occurred in dry sand samples cycled at shear strains less than 10^{-2}%. Since volume change in dry sand is directly related to pore pressure change in saturated sands, it may be inferred that significant pore pressures would not have been generated even if the sands had been saturated. The value of threshold strain proposed by these authors is similar in magnitude to values obtained from the results of undrained strain-controlled laboratory tests that were subsequently performed on saturated sand samples. Values of threshold strains for several sands are listed in Table 3.2.

Table 3.2 : Threshold Shear Strains, γ_t, for Dry and Saturated Sands (after Dobry, Stokoe, Ladd and Youd, 1981a)

SAND	TESTING TECHNIQUE	γ_t	REFERENCE
Dry Ottawa Sand	Resonant column	$1\times10^{-2}\%$	Drnevich and Richart (1970)
Dry Crystal Silica Sand	Cyclic Simple Shear	$2\times10^{-2}\%$	Silver and Seed (1971)
Dry and Saturated Ottawa Sand	Cyclic Simple Shear (Drained)	$1\times10^{-2}\%$	Youd (1972)
Dry Monterey Sand	Cyclic Simple Shear Shaking Table	$1\times10^{-2}\%$	Pyke (1973)
Saturated Monterey Sand	Cyclic Triaxial (Undrained)	$1.1\times10^{-2}\%$	Dobry et al. (1982)

The results of strain-controlled laboratory tests indicate that the threshold shear strain is independent of relative density, confining pressure and the magnitude of the initial consolidation shear stresses. For example Dyvik et al (1984) report that samples of Monterey No. 0 sand compacted to relative densities of 20% and 60% exhibited the same values of threshold strain. Other tests (reported by Dobry et al. (1981b) and Dobry et al (1982)) have indicated the same value of threshold strain for Monterey No. 0 sand samples compacted to relative densities of 45% and 80%. Dyvik et al also examined the influence of consolidation stress conditions (represented by values of K_c) on the value of threshold strain and concluded that their influence was negligible. Values of K_c (the ratio of effective vertical consolidation stress to effective horizontal consolidation stress) ranged from 1.0 to 2.5.

One important factor which has been observed to influence the value of threshold strain is the overconsolidation ratio. Results reported by Dobry, Yokel and Ladd (1981b) indicate that the threshold shear strain for overconsolidated sands is significantly higher than the threshold shear strain for normally consolidated samples of the same sand. For example, the threshold shear strain for a sand subjected to an overconsolidation ratio of 8 was measured to be $2.9\times10^{-2}\%$, while the threshold strain for a normally consolidated specimen of the same sand was $1.2\times10^{-2}\%$.

The effect of particle size on threshold strain is reported by Dyvik et al (1984) who compared the threshold shear strains for samples of Banding sand and Monterey No. 0 sand, both of which are uniform clean quartz sands with parallel grain size distribution curves; D_{50} for Banding sand is slightly less than 0.2 mm while the D_{50} for Monterey No. 0 sand is equal to 0.4 mm. Since the threshold strain for Banding sand was reported to vary from $0.8\times10^{-2}\%$ to $0.9\times10^{-2}\%$ and the threshold shear strain for Monterey No. 0 sand is approximately equal to $1\times10^{-2}\%$, it appears that threshold shear strain might decrease slightly with decreasing grain size. Tests performed on reconstituted specimens of Mount St. Helen's volcanic debris (Thomas and Dobry, 1984) have shown that the threshold shear strain for this material is approximately equal to $0.4\times10^{-2}\%$. Thomas and Dobry conclude that shear strains of $0.7\times10^{-2}\%$ to $1.0\times10^{-2}\%$ may be taken as reasonable engineering estimates of γ_t.

3.2.2. Advantages and Disadvantages of the Shear Strain Approach

The principal conceptual advantage associated with using the shear strain approach to evaluate liquefaction potential is that the the pore pressure buildup in saturated sands appears to be more closely related to cyclic shear strain than applied cyclic shear stress. This observation is borne out in the results of laboratory tests which show that the factors which influence the rate of pore pressure buildup in stress-controlled tests have a much smaller influence on the rate of pore pressure buildup in strain-controlled tests. For example, different methods of sample preparation may alter the cyclic stress ratio required to induce liquefaction in n cycles by as much as ± 50%, while such changes in structure appear to influence the pore pressure built up in n cycles (at a constant level of cyclic shear strain) by less than 10%. Since factors such as soil structure, aging and prior seismic history are known to influence a soil's liquefaction resistance and are not observed to significantly influence the rate of pore pressure buildup in strain-controlled tests, these factors are assumed to be taken into account by measuring the shear modulus in the field.

Another advantage that is associated with using the shear strain approach, is the apparent existence of a threshold strain. Since saturated sands cycled at shear strains less than this threshold value are not observed to generate significant pore pressures, it may be concluded that unless the levels of induced cyclic shear strain exceed this value no significant pore pressures will be induced at the site. Laboratory tests have shown that the value of threshold shear strain appears to be relatively insensitive to changes in relative density, overburden pressure, method of sample preparation, and

the effect of aging, and is influenced only slightly by changes in overconsolidation ratio and grain size.

However as with the shear stress approach, the shear strain approach also has several disadvantages. The principal drawback associated with using this approach to evaluate the liquefaction potential of soils subjected to earthquake shaking is that few accepted methods exist for evaluating the magnitude of induced cyclic shear strains. While Equation 3.2 can be used to calculate equivalent uniform strains at low levels of shaking, the strains calculated for high levels of shaking are very approximate since the value at $\frac{G}{G_{max}}$ changes for any given value of γ_e as pore pressures are generated. Because this problem is only encountered when pore pressures are generated, use of Equation 3.2 and the threshold strain concept may still provide an appropriate means of evaluating the minimum amount of shaking required to induce the buildup of pore pressures at any site.

Most of the drawbacks associated with using a strain approach to analyze the liquefaction potential of soils subjected to non-seismically-induced vibrations, are related to the relatively small number of strain-controlled triaxial tests that have been performed on sands. One such disadvantage is caused by the relatively limited amount of information available concerning the buildup of pore pressures under very large numbers of cycles of loading, an important factor considering that some non-seismic sources are capable of generating more than 1 million cycles of loading.

Evaluation of the liquefaction potential of non-seismically-induced ground shaking also hampered by the lack of information on the effect of initial shear stresses. One of the few sets of published results examining the influence of these stresses is reported by Dyvik et al (1984) who performed several anisotropically consolidated, strain-controlled tests on Monterey No. 0 sand. While far from conclusive, their results appear to show that for 20% relative density sand samples, pore pressures develop at a slightly slower rate as the magnitude of the initial shear stresses is increased. This observation appears to contradict the findings of Szerdy (1985), Vaid and Chern (1983), and Castro et al (1982) who report that the cyclic resistance of loose sand reduces significantly as the initial static shear stresses are increased. However, a direct comparison cannot be made without knowing the effect of the initial stresses on the shear modulus of the soil. Since the presence of initial shear stresses does not appear to influence soil behavior in strain-controlled tests, it is presumed that this effect is taken into account by measuring G in the field. As previously discussed, it is important to be able to assess the effect of initial shear stresses on the cyclic resistance of a soil because all of the large scale failures that are listed in Table 1.1, occurred on sloping ground and it may well be that non-seismically-induced ground vibrations are only capable of liquefying sands under these conditions.

In spite of the drawbacks associated with using the shear strain approach to evaluate the liquefaction potential of soils under the effects of non-seismically-induced ground vibrations, this approach might still be more appropriate than using the shear stress approach because of the high frequency content of these ground vibrations. At

such high frequencies, inertial effects of the soil mass are likely to become important and thus cyclic shear strain might provide a better indication of the distress felt by the soil rather than applied cyclic shear stress. The existence of a threshold strain is also likely to be useful when evaluating the liquefaction potential of ground vibrations generated by non-seismic sources because the cyclic shear strains associated with these motions are often similar in amplitude to the threshold strain.

CHAPTER 4

Measurement of Ground Vibration Amplitudes Produced by Trains

4.1. Introduction

As previously noted in Section 2.8, the belief that ground vibrations produced by trains have caused large-scale liquefaction failures appears to be inconsistent with the relatively small amplitudes (of the train-induced ground vibration records) that are reported in the literature. For example, Ames et al. (1976) report that a diesel locomotive generated peak particle velocities of about 3.9 mm/sec (0.153 inches/sec) at a distance of 2 meters from the tracks. Not only are ground vibrations of this size smaller in amplitude than the ground shaking generated by pieces of construction equipment such as jackhammers, but they are also probably incapable of causing liquefaction. Therefore, in an attempt to resolve this inconsistency, it seemed appropriate to measure the amplitude of train-induced ground vibrations in the field and hence determine whether actual levels might exceed the levels of ground vibration reported to date.

To throw some light on this issue, 24 sets of train-induced ground vibration records were recorded at a number of sites and at different distances from the tracks. The results of this investigation are presented in this chapter.

4.2. Vibration Recording Equipment and Data Reduction Procedure

The ground surface accelerations that were generated by the passage of each train, were measured with a force balance accelerometer that was capable of recording motions with amplitudes in the range of $\pm 2g$. Accelerometers of this type have several advantages in that they are highly stable, well calibrated and accurate; however their use may be restricted in some instances since they require a power supply to generate a signal. Because the battery inside the recorder was only capable of supplying power to the accelerometer for about 3 hours, and the investigator often spent more than 7 hours a day recording in the field, the power to the accelerometer was turned off between events and the recorder was manually triggered before the arrival of each train. In contrast, the velocity meters that were also used in the investigation do not require a power supply and thus can be left in the field for extended periods of time with their recorders being set to trigger automatically when the ground shaking exceeds some predetermined base level.

In addition to the surface acceleration records, ground surface velocity records were also obtained during the passage of the same trains. The meter used to record these motions had a velocity gain that was constant for all motions with frequencies above 4.5 Hz but decreased linearly with respect to the log of the frequency at a rate of 12 dB per octave for frequencies below this value. The weakened response for low frequency motions was corrected for when the records were analyzed by enhancing the response of the low frequency components. It is worth noting that the accelerometer used in this investigation provided an acceleration gain which was constant for all frequencies less than 50 Hz.

On arrival at each site, both the accelerometer and the velocity meter were buried about 100mm below the ground surface. This was done to ensure a firm contact with the ground. Similarly, the wires connecting these instruments to their respective recorders were also buried, so that swaying of the wires did not generate additional motions in the records. Both instruments were oriented so as to record the following 3 perpendicular components of ground motion: the vertical component, and two horizontal components perpendicular and parallel to the track.

The ground shaking was recorded (onto digital quality tape cassettes) by modified Sprengnether DR100 Digital Event Recorders which sampled each of the 3 input channels at a rate of 200 samples per second. Since these recorders were equipped with a 5 pole low pass filter at 50 Hz and a 2 pole high pass filter at 0.2 Hz, motions with frequencies outside the range of 0.2 to 50 Hz were heavily damped in the digitized records. The DR100 is a portable instrument which weighs about 35 lbs and therefore was easily moved from site to site.

The ground vibration records were subsequently transferred onto the NMM computer at the Lawrence Berkeley Laboratory (LBL) where the digitized motions were analyzed with the aid of the computer program OPSAS (property of the Center for Computational Seismology at LBL). OPSAS was used to plot both acceleration and velocity time histories for the recorded ground motions and to produce Fourier amplitude spectra for portions of these records. The portions of strongest shaking for each record were subsequently transferred to a MicroVax workstation in the Civil

Engineering Department at U.C. Berkeley where acceleration response spectra were generated for the shortened records.

4.3. Ground Vibration Amplitudes

The 24 sets of train-induced ground vibration records that were obtained during this investigation were recorded on level ground at distances of 6.7m, 7.3m, 9.8m, 13.7m, and 15.5m from the nearest rail. These records were generated by the passage of 4 passenger trains and 20 freight trains and were recorded at the following 4 sites:

Site No. 1: adjacent to the Southern Pacific Railroad track in Albany, California.

Site No. 2: adjacent to the Southern Pacific Railroad tracks, southeast of Brentwood in the San Joaquin River Delta area of Northern California.

Sites Nos. 3 and 4: adjacent to the Atchison Topeka and Santa Fe Railroad tracks, northeast of Brentwood.

The railroad tracks at 3 of these sites were located on top of 1.5m high and 2.5m high embankments which appeared to consist predominantly of sand or gravelly sand and were capped with approximately 0.7m of rock ballast. The tracks at the fourth site, the Albany site, were level with the surrounding ground.

In order to provide the reader with a feel for the nature of the ground shaking generated by trains, a typical ground surface acceleration record is shown in Figure 4.1. This motion was generated by a 4 engine, 49 car freight train passing over a 1.5

meter high embankment and was recorded at a distance of about 7.3 meters from the train; the three acceleration time histories shown in the figure depict the vertical component and the two horizontal components (perpendicular and parallel to the track) of the resulting ground motion. The period of strong shaking seen at the beginning of all 3 traces was generated by the engines, while the remainder of the record was generated by the passage of the railroad cars.

For all but two of the records that were obtained, the ground vibrations generated by the engines were found to be significantly larger in amplitude than those generated by the cars (as shown in Figure 4.1, for example). Such an observation was expected for the following reason: higher axle loads appear to generate ground vibrations of greater amplitudes, and the axle loads for most locomotives are thought to be significantly larger than the axle loads for most railroad cars, few of which are designed to withstand axle loads in excess of 22 tonnes per axle. By way of a comparison, the axle loads for a typical axle locomotive are reported to be about 28 tonnes per axle (Szerdy, 1985).

The observation that railroad cars generated higher levels of acceleration in two of the records can most likely be attributed to a combination of high axle loads and different suspension design. Unfortunately, this supposition cannot be confirmed since neither the axle loads nor the suspension design are known. As noted in Section 2.8, Griffin and Stanworth attribute the higher vibration levels generated by certain engines to the higher unsprung masses of these engines, implying that train-induced ground vibration levels are a function of both axle weight and suspension design.

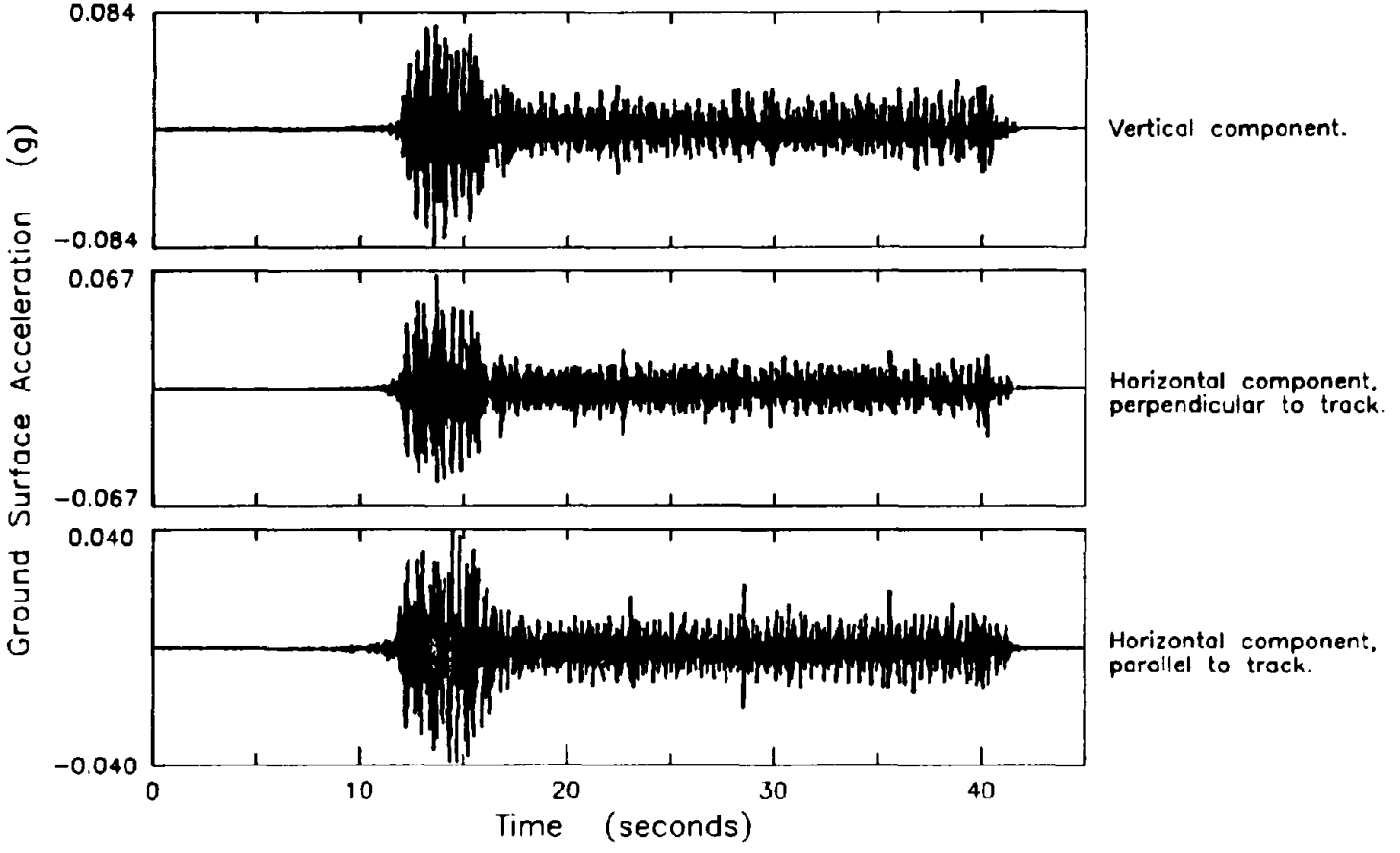

FIG 4.1 THREE PERPENDICULAR COMPONENTS OF A TYPICAL TRAIN-INDUCED GROUND SURFACE ACCELERATION RECORD, RECORDED AT A DISTANCE OF ABOUT 7.3 METERS FROM THE TRACKS DURING THE PASSAGE OF A 4 ENGINE, 49 CAR FREIGHT TRAIN.

The regions of strong shaking for each of the three components shown in Figure 4.1, are also shown in Figure 4.2. When plotted to this time scale, the true cyclic nature of train-induced ground vibrations is readily apparent. Since it appears that all three components contain fairly dominant predominant frequencies, it seems reasonable to conclude that such vibrations may be modelled fairly realistically by a sinusoidal motion of single frequency, an approach used later in this investigation. As is typical of many of the records, the average level of shaking generated by the engines is shown to be about 50% less than the peak ground surface accelerations.

Examination of the records also revealed that close to the tracks (about 7 meters from the nearest rail), the accelerations associated with the vertical components of shaking were significantly larger than those associated with the horizontal components of the same motion. At this distance, for example, the amplitudes of the horizontal accelerations measured both perpendicular and parallel to the track, appear to be about 20% and 40% smaller on average, respectively, than the corresponding vertical ground surface accelerations. This difference in amplitude between the three perpendicular components was noted to be significantly less at greater distances (about 15m) from the tracks, a change which may well be due changes in the frequency content of the vertical components of motion (noted in Section 4.4). The generally similar amplitudes for the three components of recorded motions was also noted by Griffin and Stanworth (1985) who report that trains produce vertical vibrations which are roughly equal in amplitude to the two horizontal components, measured perpendicular and parallel to the tracks.

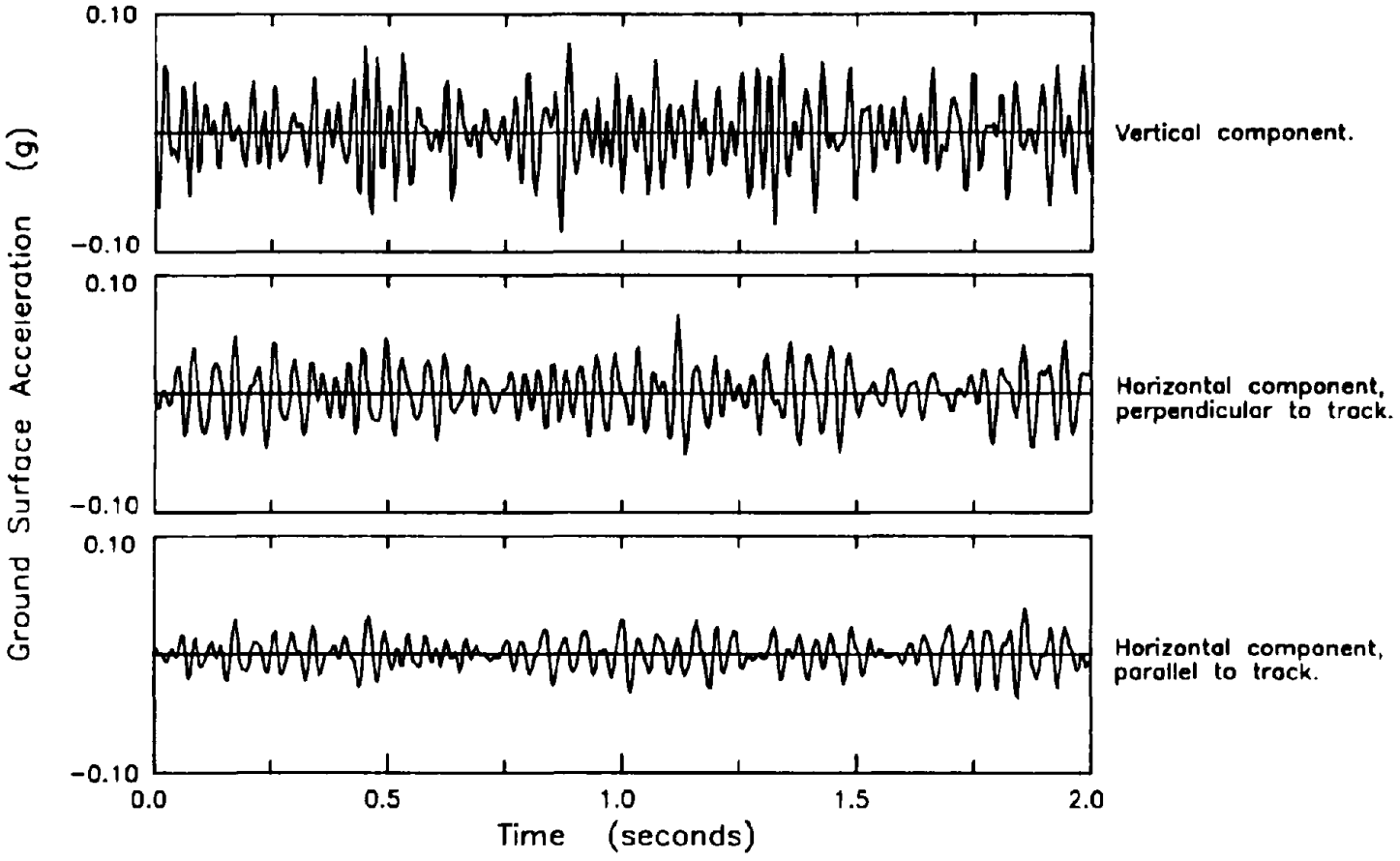

FIG 4.2 REGION OF STRONG SHAKING SHOWN IN FIGURE 4.1, REPLOTTED TO A DIFFERENT TIME SCALE.

The influence of train speed on ground vibration levels was also examined; however no firm conclusions could be drawn from the data due to the following reasons:(1) the small differences in speed between the trains measured at the three San Joaquin River Delta sites and (2), the large number of other factors which also influence ground vibration levels. Comparisons between the motions recorded at the Albany site and those recorded at the San Joaquin River Delta sites revealed that the average amplitude of shaking at the Albany site was approximately 30% less than the average amplitude of the vibrations recorded at the other sites (after the effect of attenuation was accounted for); while this reduction in amplitude might be due to slower train speeds at the Albany site it may also be due to significantly different soil conditions.

The peak ground surface accelerations that were generated by the passage of each train are plotted in relation to the distance, d, at which they were recorded from the nearest rail (see Figures 4.3 and 4.4). When presented in this manner, the data shows a rapid reduction in the magnitudes of the accelerations with increasing distance from the track. It should be pointed out that these figures cannot be used to accurately determine the field attenuation rates for the various sites because each data point represents the passage of a different train and the accelerations were recorded at four different sites. Nonetheless, a rough estimate (of these rates) can probably be obtained from the upper and lower bound curves that are fitted to the data (also shown in Figures 4.3 and 4.4). These curves imply that at least in the near-field region, the amplitudes of train-induced ground vibrations attenuate at some rate proportional to about $d^{-1.4}$.

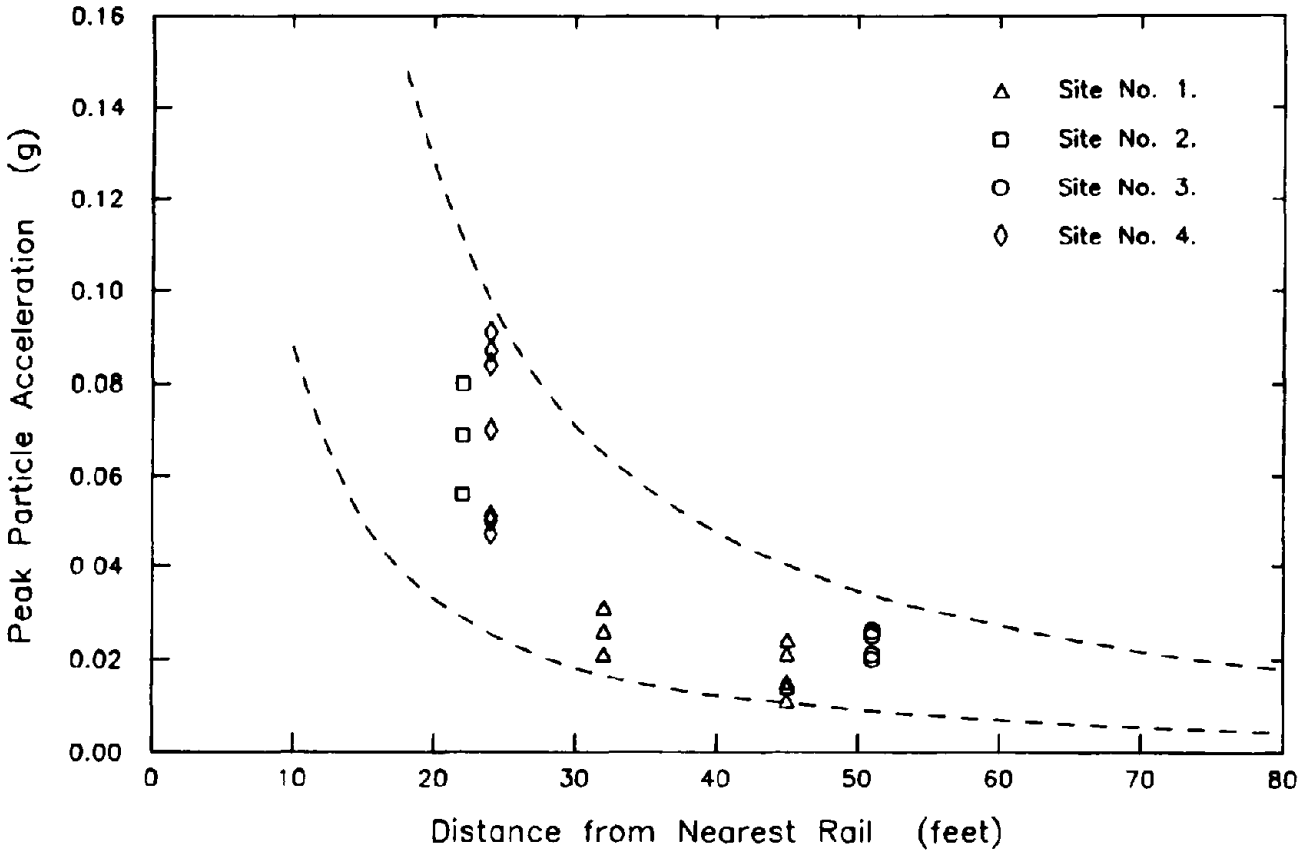

FIG 4.3 PEAK PARTICLE ACCELERATIONS GENERATED BY THE PASSAGE OF EACH TRAIN AND PLOTTED AS A FUNCTION OF DISTANCE FROM THE NEAREST RAIL.

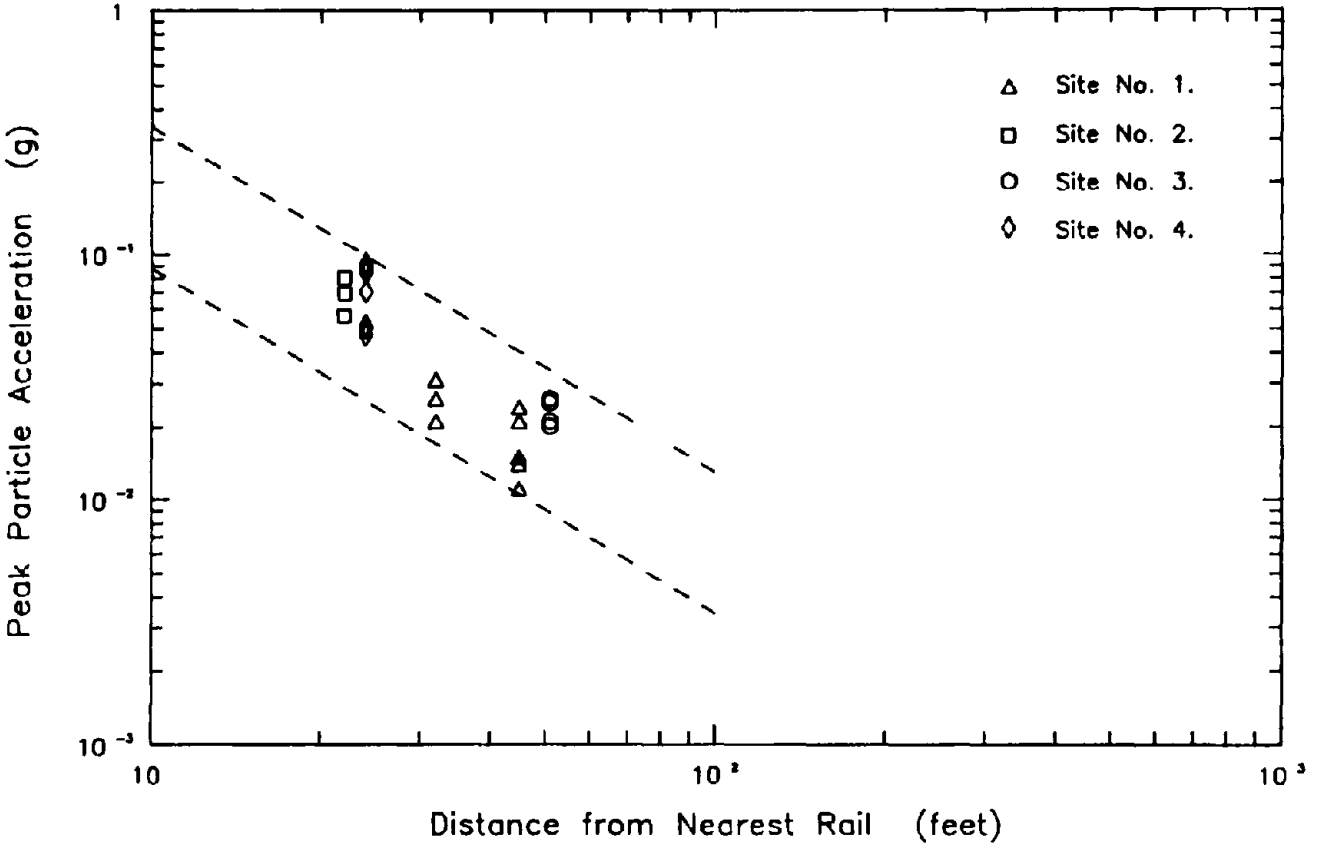

FIG 4.4 PEAK PARTICLE ACCELERATIONS GENERATED BY THE PASSAGE OF EACH TRAIN AND PLOTTED AS A FUNCTION OF DISTANCE FROM THE NEAREST RAIL.

The data shown in Figures 4.3 and 4.4 were obtained from ground vibration records recorded at distances of between about 7 meters and 15 meters from the tracks. Since such distances are small in relation to the length of an average freight train (likely to be about 600m), it might seem reasonable to model trains as line sources in this region. However if this is so, then the contention (made and supported in Section 5.2) that train-induced ground vibrations consist predominantly of Rayleigh waves might appear to be somewhat inconsistent with the attenuation rate determined above. For example, Rayleigh waves generated by a true line source within an ideal, undamped, elastic, homogeneous half-space do not attenuate with distance from the source.

This seemingly high rate of attenuation is possibly due to a combination of the following:

1) Close to the tracks a significant portion of the ground motions is likely to consist of body waves and these waves attenuate in amplitude at a much faster rate than Rayleigh waves.

2) The nature of the data shown in Figures 4.3 and 4.4. As previously mentioned, the data shown in these figures represent the peak particle accelerations generated by the passage of each train. These peak values were usually significantly larger than the average level of shaking generated by either the engines or the railroad cars (see Figures 4.1 and 4.2), thereby suggesting that they were probably generated by a point source such as a

wheel flat or an uneven rail joint. Rayleigh waves generated by this type of source attenuate at a significantly faster rate than those generated by line sources, due to geometrical damping.

In reality, trains can probably be most accurately modelled as a line of point sources with random phasing rather than as a true line source where all points move in phase with each other. However, such a problem is likely to be difficult to analyze since the locations of the point sources vary with time.

Later in this investigation, the average levels of ground shaking are assumed to attenuate at a rate proportional to $d^{-1.4}$. This rate was chosen, even though it was believed that these levels should attenuate at a slower rate than the peak accelerations, because for most sites liquefaction is only predicted to occur within about 6m from the rail. In this region, the ground motion is likely to contain a higher proportion of body waves than at distances of even 7 to 15 meters from the tracks, leading to a higher rate of attenuation in the near-field. This effect may be compensated for by the lower rate of attenuation for average levels of shaking.

It is interesting to note that judging by the peak particle accelerations plotted in Figures 4.3 and 4.4 and the rates of attenuation implied by both the upper and lower bound curves shown in these figures, trains are probably capable of generating peak particle accelerations significantly in excess of 0.1g at distances less than about 6 meters from the nearest rail. This point is mentioned because many people currently believe that earthquake-induced ground vibrations with peak surface accelerations in excess of 0.05g to 0.1g (Section 6.2) are capable of liquefying the sands within certain

sites. However, a direct analogy should not be drawn in this case because train-induced vibrations contain much higher predominant frequencies than seismic motions, resulting in much smaller levels of induced cyclic shear strains and stresses for the same values of surface acceleration.

The peak particle velocities generated at the ground surface by the passage of each train were also measured and these values are shown in Figures 4.5 and 4.6. It may be observed from these figures that as with the ground surface accelerations, the amplitudes of the peak ground surface velocities generated close to the tracks were also significantly larger than the amplitudes reported in the literature. For example, Ames et al report a peak particle velocity of 3.9 mm/sec measured at a distance of about 2 meters from a diesel locomotive, a value which is significantly less than the peak particle velocities of 20 mm/sec at 2m from the nearest rail suggested by Figure 4.6. Further, it is not only believed that velocities of the magnitudes suggested in this figure are reasonable, but that these velocities may still underestimate maximum possible vibration levels. These beliefs are based on the following observations: (1) Ames et al. (1976) also report a peak particle velocity of 1.4 mm/sec (0.055 ips) measured at a distance of 30m from the tracks and this value lies slightly above the upper bound line in Figure 4.6 and (2) the rates of attenuation implied by the curves shown in Figures 4.5 and 4.6 are less than than the rates implied by either Figure 4.4 or Figure 2.21 suggesting that if anything, this curve is likely to underestimate the amplitude of ground vibrations generated close to the tracks.

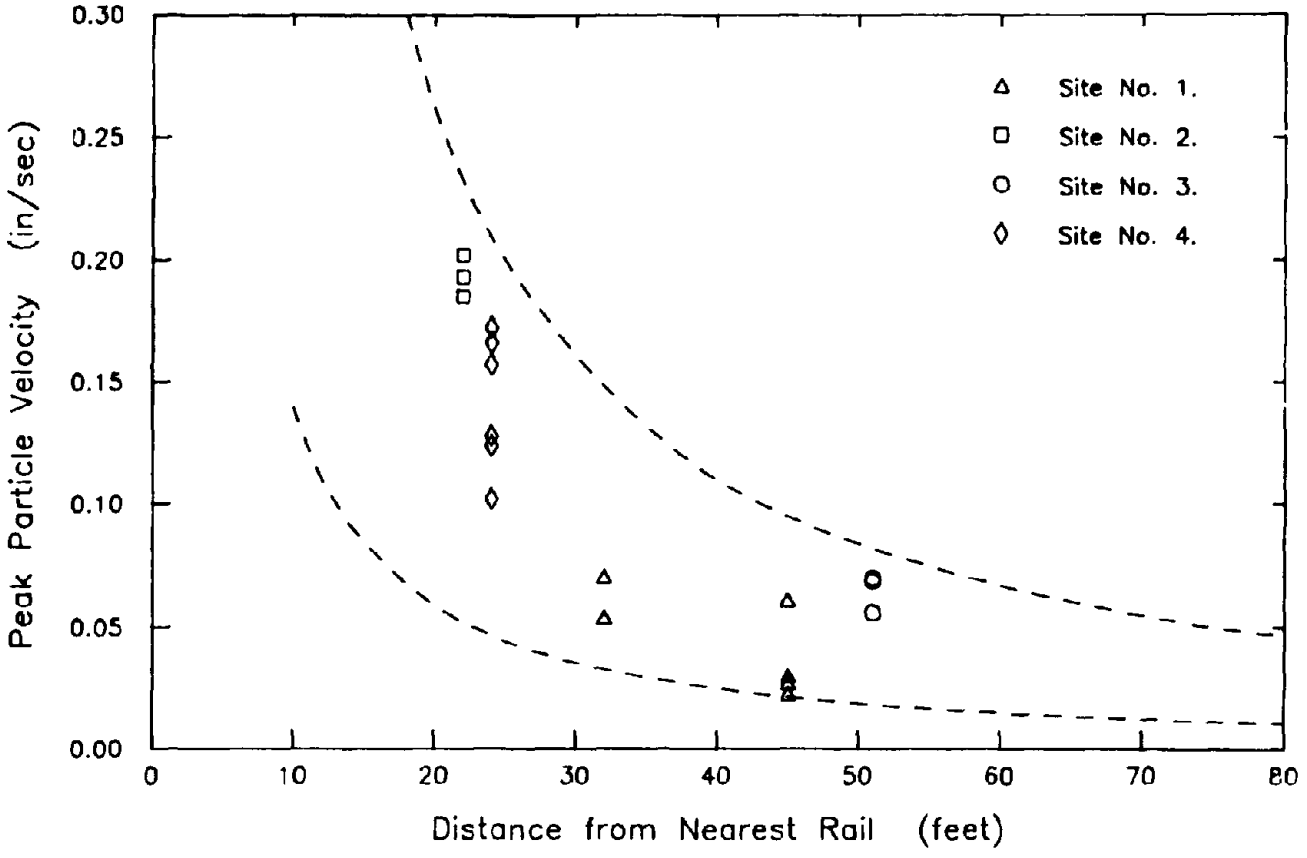

FIG 4.5 PEAK PARTICLE VELOCITIES GENERATED BY THE PASSAGE OF EACH TRAIN AND PLOTTED AS A FUNCTION OF DISTANCE FROM THE NEAREST RAIL.

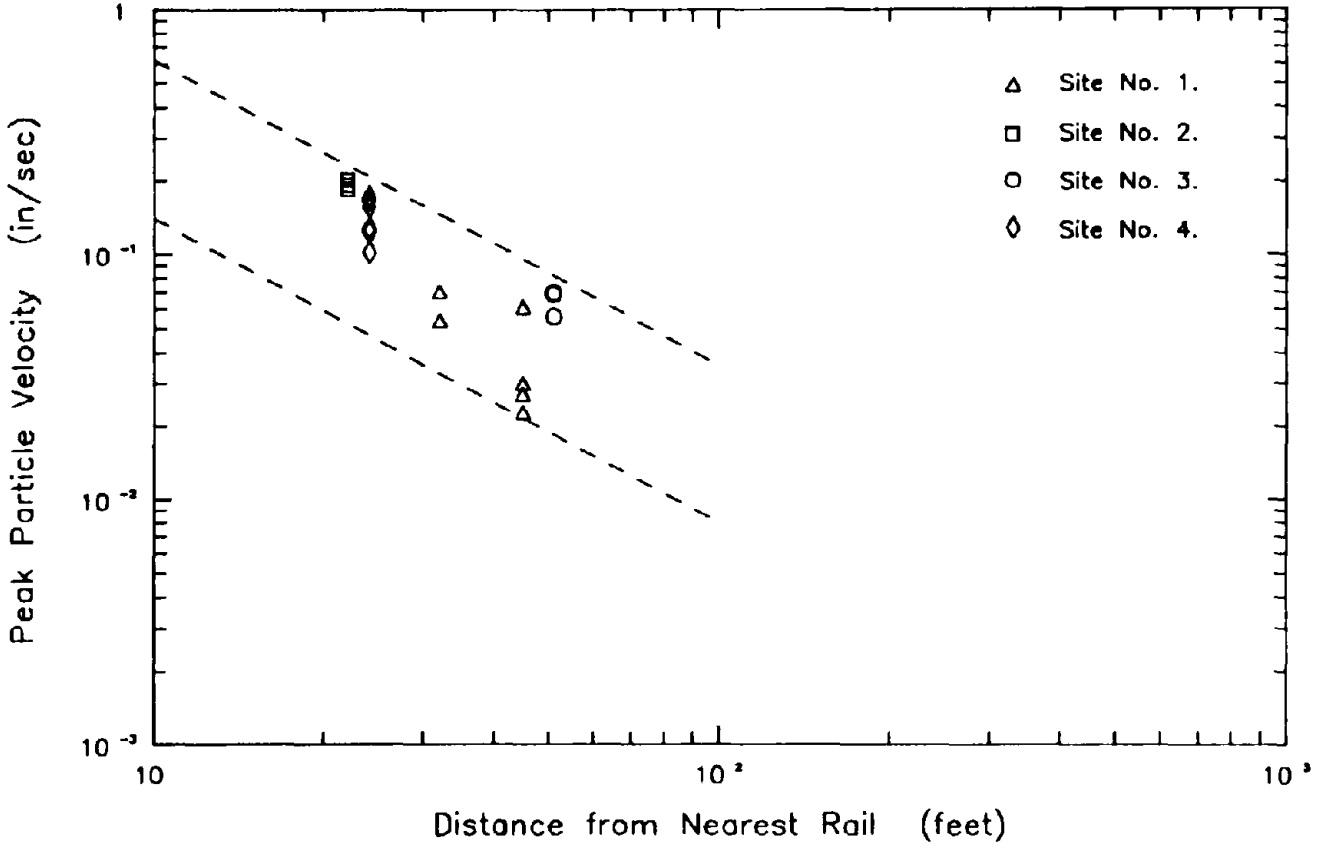

FIG 4.6 PEAK PARTICLE VELOCITIES GENERATED BY THE PASSAGE OF EACH TRAIN AND PLOTTED AS A FUNCTION OF DISTANCE FROM THE NEAREST RAIL.

4.4. Frequency Content of Train-Induced Ground Vibrations

The dominant frequencies of the train-incuced ground vibration records were determined by computing acceleration response spectra for the three perpendicular components of each motion. These spectra show that close to the source, the predominant frequencies for the vertical components were usually significantly higher than the predominant frequencies for either of the two horizontal components of the same motion. As shown in Figure 4.7, the vertical components of these records typically contained predominant frequencies of around 40 Hz while the horizontal components contained predominant frequencies of either 23 or 33 Hz.

The response spectra shown in this figure represent typical spectra for each of the 3 perpendicular components of near-field train-induced ground motions. It may be seen that the spectra for the two horizontal components of motion are somewhat similar in shape, however it should be noted that in some cases they were significantly different. This difference is also noted by Griffin and Stanworth (1985) who report that spectra for horizontal motions recorded parallel to the track, often differ in shape from those for the horizontal component of the same motion recorded perpendicular to the track.

In contrast to train-induced ground shaking recorded close to the source, the predominant frequencies of the vertical components of motions recorded at greater distances (about 15.5 meters from the tracks) were approximately equal to 23 Hz and hence very close to the predominant frequencies of the two horizontal components. This change in predominant frequency with distance, which is clearly illustrated in

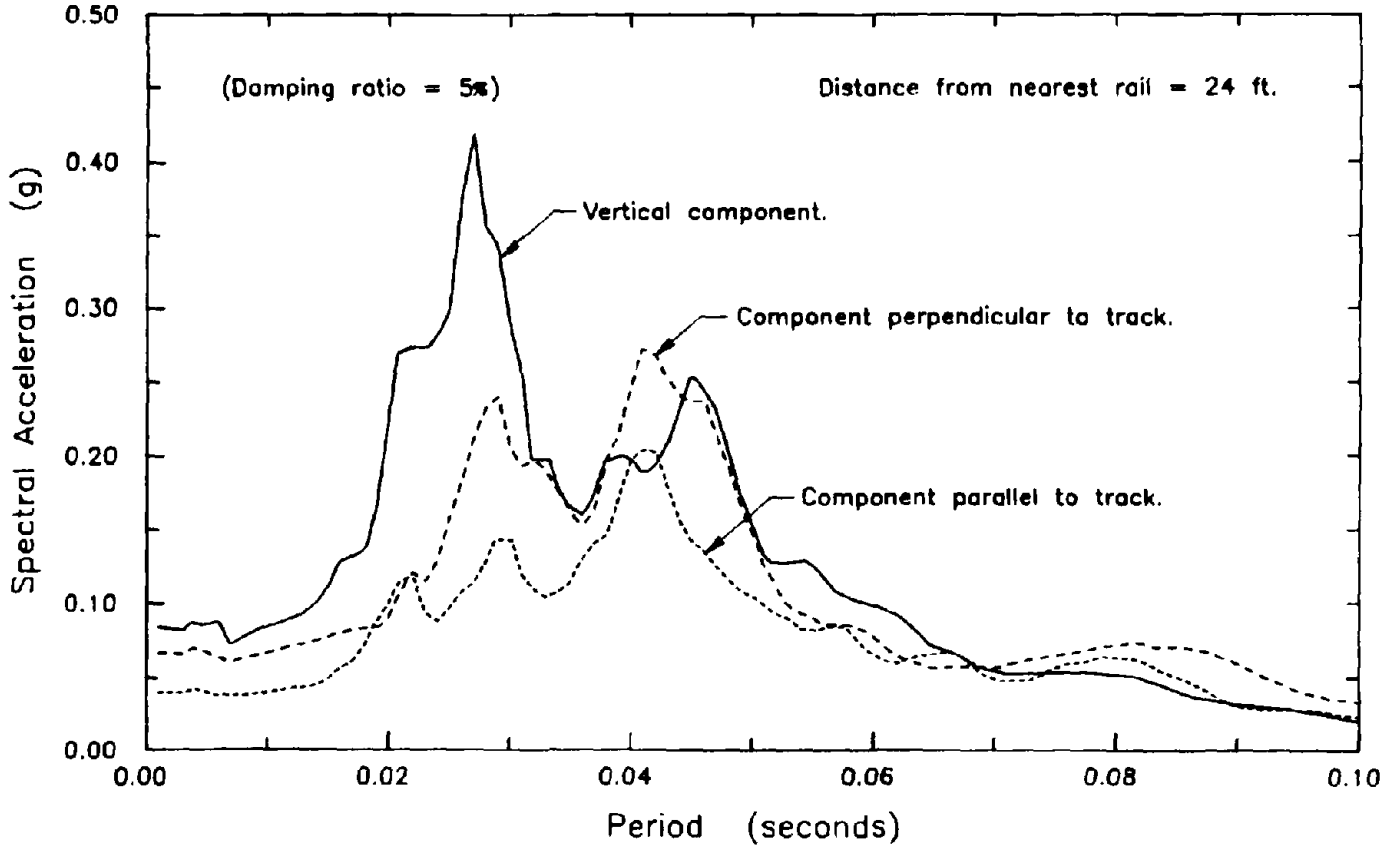

FIG 4.7 TYPICAL ACCELERATION RESPONSE SPECTRA FOR THE THREE PERPENDICULAR FROM COMPONENTS OF TRAIN-INDUCED GROUND VIBRATIONS RECORDED CLOSE TO THE TRACKS.

Figure 4.8, was attributed to the fact that higher frequency motions attenuate much faster with distance than low frequency motions. Thus, at greater distances the low frequency motions tend to dominate.

It is worth noting that most of the response spectra obtained in this investigation, contain dominant frequencies of about 23, 33 and 40 Hz and that all three of these frequencies lie within the range of 10 to 60 Hz, proposed by both Griffin and Stanworth (1985) and Dawn and Stanworth (1979). The latter investigators also proposed a more confined range of 10 to 20 Hz and stated that most of the peaks should occur within this range; however this statement is not supported by the data recorded in this study. Since most of the train-induced ground vibration records contain predominant frequencies around 23 Hz, and frequencies close to the predominant period of the site are predicted to dominate the motion at greater distances from the tracks (as discussed in Section 2.1), it might be inferred that the predominant frequencies of the sites were approximately equal to 23 Hz.

In addition to computing acceleration response spectra for all of the train-induced ground vibration records, the dominant frequencies were also determined by computing Fourier amplitude spectra for the same motions and as shown in Figure 4.9, these latter spectra revealed numerous other dominant frequencies. Several attempts were made to associate these frequencies with repeating features of the track; however all of these attempts were unsuccessful and their failure was attributed to the fact that the speeds of the trains that generated these vibrations were not known, nor could they be determined with an acceptable degree of accuracy from the ground vibration records.

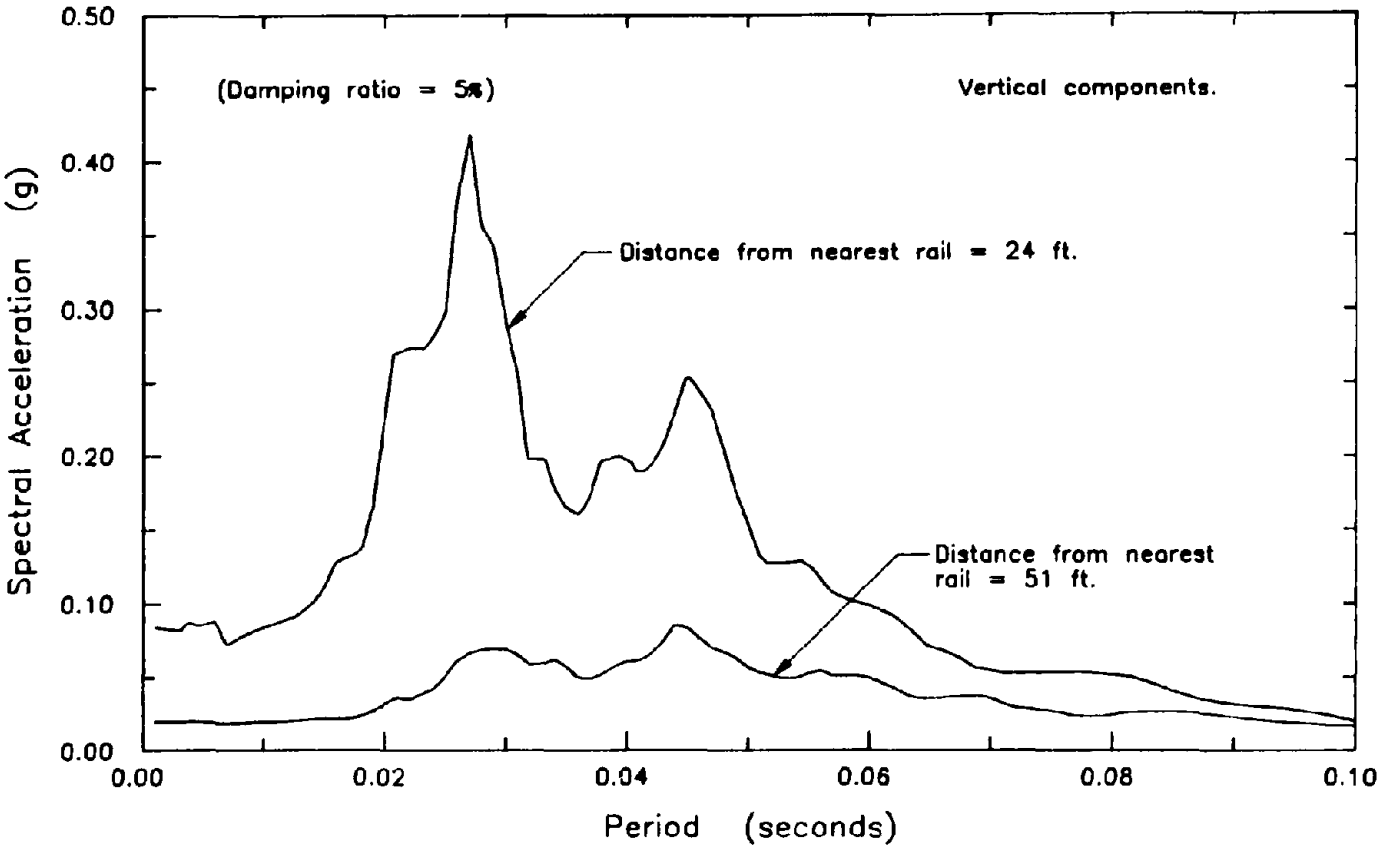

FIG 4.8 COMPARISON OF TYPICAL RESPONSE SPECTRA FOR THE VERTICAL COMPONENTS OF TRAIN-INDUCED GROUND MOTIONS RECORDED AT A DISTANCE OF ABOUT 24 FEET FROM THE TRACKS, WITH THOSE RECORDED AT A GREATER DISTANCE OF ABOUT 51 FEET.

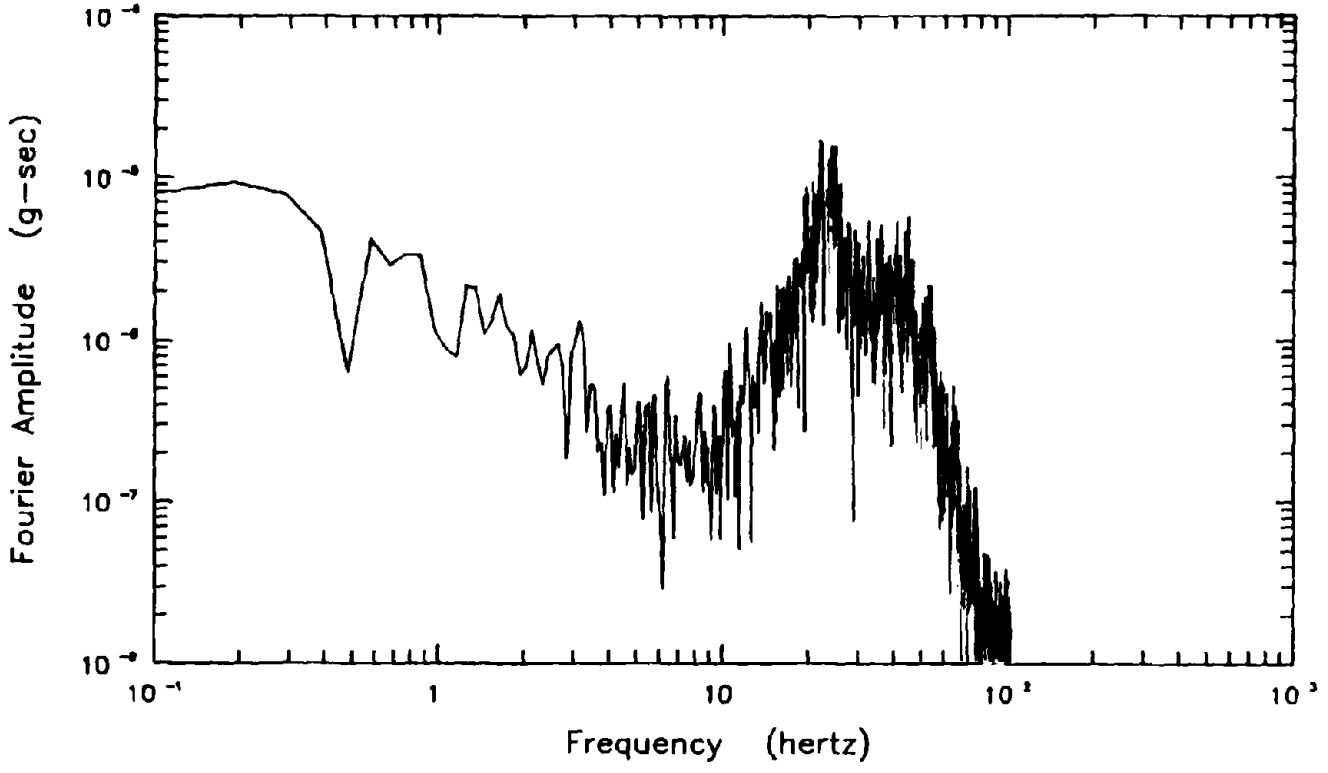

FIG 4.9 FOURIER AMPLITUDE SPECTRUM FOR THE HORIZONTAL COMPONENT, PERPENDICULAR TO THE TRACK, OF A TRAIN-INDUCED GROUND VIBRATION RECORD.

Because the DR 100 recorder contained a 5 pole, 50 Hz low pass filter, none of the records contained significant motions with frequencies greater than 50 Hz, a fact which is clearly illustrated in Figure 4.9.

4.5. Summary

In summary, it may be stated that the amplitudes of train-induced ground vibrations recorded close to the tracks are significantly larger than the amplitudes reported in the literature. For example, the upper bound curve shown in Figures 4.5 and 4.6 implies that at distances of about 2m from the nearest rail, trains may be capable of generating ground shaking with peak particle velocities of about 20 mm/sec. This value is significantly larger than the maximum peak particle velocity of 3.9 mm/sec (recorded at a distance of 2m from a diesel locomotive) reported by Ames et al (1976). Furthermore, since these authors also report a velocity which lies slightly above the upper bound curve shown in these figures, and the rate of attenuation implied by this curve is less than the attenuation rate suggested by Figures 4.4, trains may well be capable of generating ground vibrations with peak particle velocities which exceed the values shown by the upper bound curves in Figures 4.5 and 4.6.

In addition to obtaining ground surface velocity records, ground surface accelerations were also recorded and the peak particle accelerations generated by the passage of each train are plotted in Figures 4.3 and 4.4. These figures show that trains appear to be capable of generating accelerations in excess of 0.1g at distances closer than about 6m from the nearest rail, thus supporting the common belief that trains are

capable of inducing significant levels of ground vibration.

The horizontal components of the train-induced ground motions obtained in this investigation were typically found to contain predominant frequencies of either about 23 Hz or 33 Hz. These frequencies are similar to the predominant frequencies of the vertical components of motion recorded at distances of about 15m from the tracks, but are significantly less than the predominant frequencies for the vertical components measured close to the tracks (usually about 40 Hz).

CHAPTER 5

Liquefaction Potential of Train-Induced Ground Vibrations

5.1. Introduction

The liquefaction potentials of sand deposits subjected to train-induced ground vibrations were evaluated by following both the shear stress approach and the shear strain approach (both of which are outlined in Chapter 3) and the results of these analyses are presented in this chapter. The magnitude of the cyclic shear stresses and cyclic shear strains predicted to be induced within these deposits were calculated assuming that most of the energy imparted to the soil by trains is transmitted as Rayleigh waves. The data on which this assumption was based and the procedure used to calculate the amplitude of these stresses and strains are also outlined in Chapter 5.

5.2. Prediction of Rayleigh Wave Cyclic Shear Strains

The assumption that train-induced ground vibrations consist predominantly of Rayleigh waves is based on the findings of a theoretical study reported by Miller and Pursey (1955). These authors examined the case of a uniformly distributed circular energy source, oscillating vertically on the surface of an ideal, homogeneous, isotropic, elastic half-space and concluded from their study that approximately two-thirds of the energy imparted to the soil was transmitted as Rayleigh waves. Since the energy imparted by trains is also applied vertically at the ground surface, it seemed reasonable

to assume that the ground vibrations generated by this source would also consist predominantly of Rayleigh waves.

The predominance of this wave type is further supported by ground motion attenuation rates measured in the field. For example, Dalmatov et al (1968) conclude from their measurements that most of the energy imparted to the soil by non-seismic sources of vibration is transmitted as Rayleigh waves, and Lo (1976) was able to adequately predict the attenuation of ground vibrations generated by pile driving by using an equation which was developed for Rayleigh waves.

Thus, based on the findings of the Miller and Pursey study, and supported by field attenuation rates, it seemed most appropriate to compute the magnitudes of the induced stresses and strains using Rayleigh wave theory, an approach which was believed to be reasonably accurate at distances greater than about 10 to 15 meters from the train and considered likely to become less accurate at distances closer to the source.

In reality of course, the ground vibrations generated by non-seismic sources probably consist of some combination of both surface waves and body waves. Therefore any calculations made assuming one wave type can only furnish approximate values for the actual levels of induced cyclic shear stress and strain. Despite this fact, the use of such a simplistic approach may still provide an approximate basis for evaluating these effects, even though the relative proportions of the various wave types are unknown. Thus, even if the other wave types were taken into account these levels of strain and stress could not be computed exactly. Use of this approach is further

supported by the observation that the cyclic shear stresses and strains calculated assuming Rayleigh wave theory appear to be similar in magnitude to the stresses and strains calculated using body wave theory (discussed later in this section). Since most ground motions consist predominantly of some combination of these two wave types, the accuracy of this analysis was probably not reduced significantly by the simplifying assumption.

The ground motions associated with each Rayleigh wave mode of vibration may be described by the following equations, where u_x is the horizontal displacement, u_z is the vertical displacement, and $f(z)$ and $g(z)$ are the horizontal and vertical mode shapes respectively:

$$u_x(x,z,t) = f(z) \cdot e^{i(\omega t - kx)} \qquad 5.1$$

$$u_z(x,z,t) = g(z) \cdot e^{i(\omega t - kx)} \qquad 5.2$$

where ω = frequency (rads/sec),
k = wave number,
z = depth,
x = horizontal distance, and
$f(z)$, $g(z)$ are complex functions

In an ideal, homogeneous, elastic half-space, all Rayleigh wave motions propagate with the same normalized mode shape; however, in layered media numerous Rayleigh waves are generated with a wide variety of mode shapes. Each of these mode shapes is associated with a corresponding eigenvalue, k (commonly referred to as the wave number), and it is this eigenvalue that determines the nature of the ground motion in

this numerical formulation. Since k may be a complex number, four wave types can be distinguished in an undamped elastic medium (Waas, 1972):

a) If k is complex, i.e. $k=k_1+ik_2$, and $k_1\neq0$, $k_2\neq0$, the corresponding Rayleigh wave motion propagates in the x direction with the phase velocity $c = \omega/k_1$ and decays or increases in amplitude at an exponential rate of $e^{k_2 x}$. For every wave of this type, a "reciprocal" wave which has the same wave number with opposite sign (i.e. it propagates in the negative x direction and attenuates at the opposite rate) also exists. These wave pairs transmit the same amount of energy away from the source as back to the source, resulting in no net energy transfer.

b) If k is real, i.e. $k=k_1$, and $k_2=0$, the resulting motion is a wave which propagates in the x direction with constant amplitude and phase velocity $c = \omega/k_1$. All horizontal displacements are in phase at a constant distance, x, and are 90 degrees out of phase with the vertical displacements. Real waves do not attenuate with distance and are the only wave types that transmit energy away from the source.

c) If k is purely imaginary, i.e. $k=ik_2$, and $k_2\neq0$, the motion varies exponentially in the x direction and does not propagate. No energy is transmitted.

d) If $k=0$ the ground motion is independent of distance, x, and degenerates to a one-dimensional standing wave. This type of wave can only occur at certain "natural" frequencies of a layered medium over a rigid base. It is not

likely to be generated by the dynamic loading in question.

Most of the energy imparted to a soil by a source goes into exciting the lower modes of vibration and in a damped layered system such as a sand site, these modes tend to be the lower complex modes. However, provided that the damping is small (as is the case for train-induced ground vibrations) the imaginary parts of the wave numbers for these modes are also very small. Further, these modes are similar in shape to the real modes computed for an undamped system. Thus it seems appropriate to predict the levels of cyclic shear strain generated within a real system using the real modes determined for an undamped system.

The various mode shapes predicted to exist within an undamped layered site can be computed using the finite element program GROUND-2D. This program (which is still under development at U.C.Berkeley) is based on a computer program written by Waas (1972) and is being developed to perform 2-dimensional site response analyses for sites subjected to shaking by surface waves. Once the mode shapes are known, the cyclic shear strains that are associated with each Rayleigh wave mode of vibration can be calculated using Equations 5.3 and 5.4:

$$\max \gamma_{90^\circ} = \left| \gamma_{zx} \right| = \left| f'(z) - i \cdot k \cdot g(z) \right| \qquad 5.3$$

$$\max \gamma_{45^o} = \left| \gamma_{45^o} \right| = \left| k \cdot f(z) - i \cdot g'(z) \right| \qquad 5.4$$

where γ_{zx} = horizontal and vertical shear strain,
γ_{45^o} = shear strain on a 45^o plane, and
$f'(z)$, $g'(z)$ = derivatives of $f(z)$, $g(z)$ w.r.t. z

Derivations for both of these equations are provided in the Appendices. It can be shown that the maximum strains induced by Rayleigh waves occur on either the vertical and horizontal planes, or the 45 degree plane.

Because GROUND-2D performs an elastic analysis using constant values of shear moduli, and the shear moduli of sands are strain dependent, the site response was determined iteratively. The values of shear moduli used as input for each iteration were determined from Figure 5.1, using the shear strains computed in the previous iteration and the value of G_{max} calculated (using Equation 5.7) for each layer. The analysis was stopped when the shear moduli varied in magnitude by less than 5% between successive iterations since changes in modulus of this magnitude were judged to have only a minor effect on the computed site response; site response is dependent primarily on shear wave velocity which is a function of the square root of the shear modulus.

Thus, estimates for Rayleigh wave motions likely to occur within a loose ($D_R \approx 35\%$) sand site were obtained by using GROUND-2D to compute the response of the model site defined in Table 5.1. The depth of the model was chosen (using Equation 5.5) to be slightly greater than twice the wavelength of the expected funda-

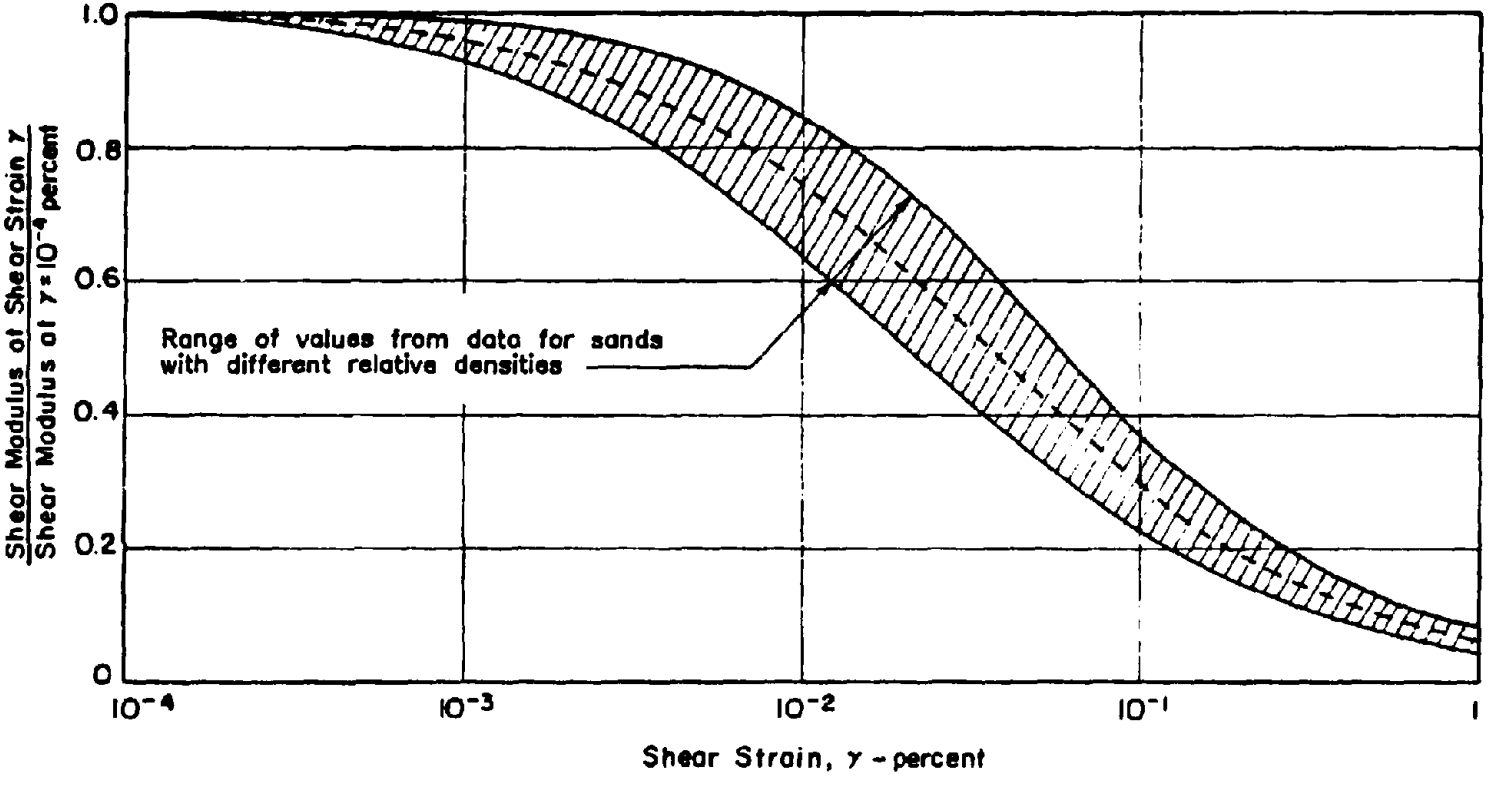

FIG 5.1 VARIATION OF SHEAR MODULUS WITH SHEAR STRAIN FOR SANDS (from Seed and Idriss, 1970).

mental mode of vibration:

$$H > \frac{2\,V_{site}}{f} \tag{5.5}$$

$$V_{site} = \frac{H}{\int_0^H \frac{dz}{V_z}} \tag{5.6}$$

where H = depth of the site,
f = frequency (hz),
V_z = shear wave velocity at depth z, and
V_{site} = average shear wave velocity for site

This was done to ensure that the base of the model did not influence either the wave number or the mode shape for this mode.

As shown in Table 5.1, the model site was divided into 20 layers which ranged in thickness from 2 inches at the surface to 130 inches at the base. The small strain shear moduli for each of these layers were calculated from the following equation assuming that $(K_{2)max} = 37$ (after Seed et al, 1984, for a sand with $D_R = 35\%$):

$$G_{max} = 1000 \cdot (K_2)_{max} \cdot (\sigma'_m)^{\frac{1}{2}} \tag{5.7}$$

where G_{max} = shear modulus for sand (psf)
and σ'_m = mean effective stress (psf)

The computer analyses were performed with the aid of Mr. Nan Deng and were supervised by Professor J. Lysmer.

Table 5.1 : Model Site Used to Compute Rayleigh Wave Mode Shapes

Layer No.	Layer Thickness (ft)	Depth to Base of Layer (ft)	Density (pcf)	V_s (fps)	V_p (fps)
1	0.1667	0.1667	120	130	5000
2	0.2500	0.4167	120	182	5000
3	0.3333	0.7500	120	214	5000
4	0.4167	1.1667	120	240	5000
5	0.5000	1.6667	120	259	5000
6	0.5833	2.2500	120	275	5000
7	0.6667	2.9167	120	291	5000
8	0.7500	3.6667	120	308	5000
9	0.8333	4.5000	120	331	5000
10	1.0000	5.5000	120	357	5000
11	1.1667	6.6667	120	392	5000
12	1.3333	8.0000	120	411	5000
13	1.5000	9.5000	120	434	5000
14	1.6667	11.1667	120	454	5000
15	2.0000	13.1667	120	478	5000
16	2.5000	15.6667	120	499	5000
17	3.3333	19.0000	120	522	5000
18	5.0000	24.0000	120	550	5000
19	7.5000	31.5000	120	586	5000
20	10.8333	42.3333	120	629	5000

The three real modes of vibration computed to occur within the model sand site are shown in Figures 5.2, 5.3 and 5.4; the horizontal mode shapes, $f(z)$ are shown as solid lines and the vertical mode shapes, $g(z)$ are shown as dashed lines. These waves were determined for a peak ground surface acceleration of 0.1g and a ground vibration frequency of 20 Hz. The magnitudes of the induced cyclic shear strains associated with each of these modes were computed from Equations 5.3 and 5.4 by scaling both the vertical and the horizontal mode shapes (for each mode) by the same factor to give a peak horizontal ground surface acceleration of 0.1g. These strains are shown in Figures 5.5, 5.6 and 5.7.

A further 9 complex modes and 19 purely imaginary modes were also generated by the computer analysis. However these modes were not included in the analysis because it would have been both unnecessary and impractical to try to combine all 31 Rayleigh wave modes in varying proportions (as discussed later). The justification for neglecting these modes is provided by the following observations:

1) Both the complex and the purely imaginary modes attenuate very rapidly with increasing distance from the source, and

2) in a similar manner to the earthquake response of structures, most of the energy imparted to the soil by a source goes into exciting the lower modes of vibration. Successively smaller amounts of energy go into exciting the higher modes. Thus, since the real modes are the first, second and third modes of vibration, these three modes will probably tend to dominate the resulting ground motion.

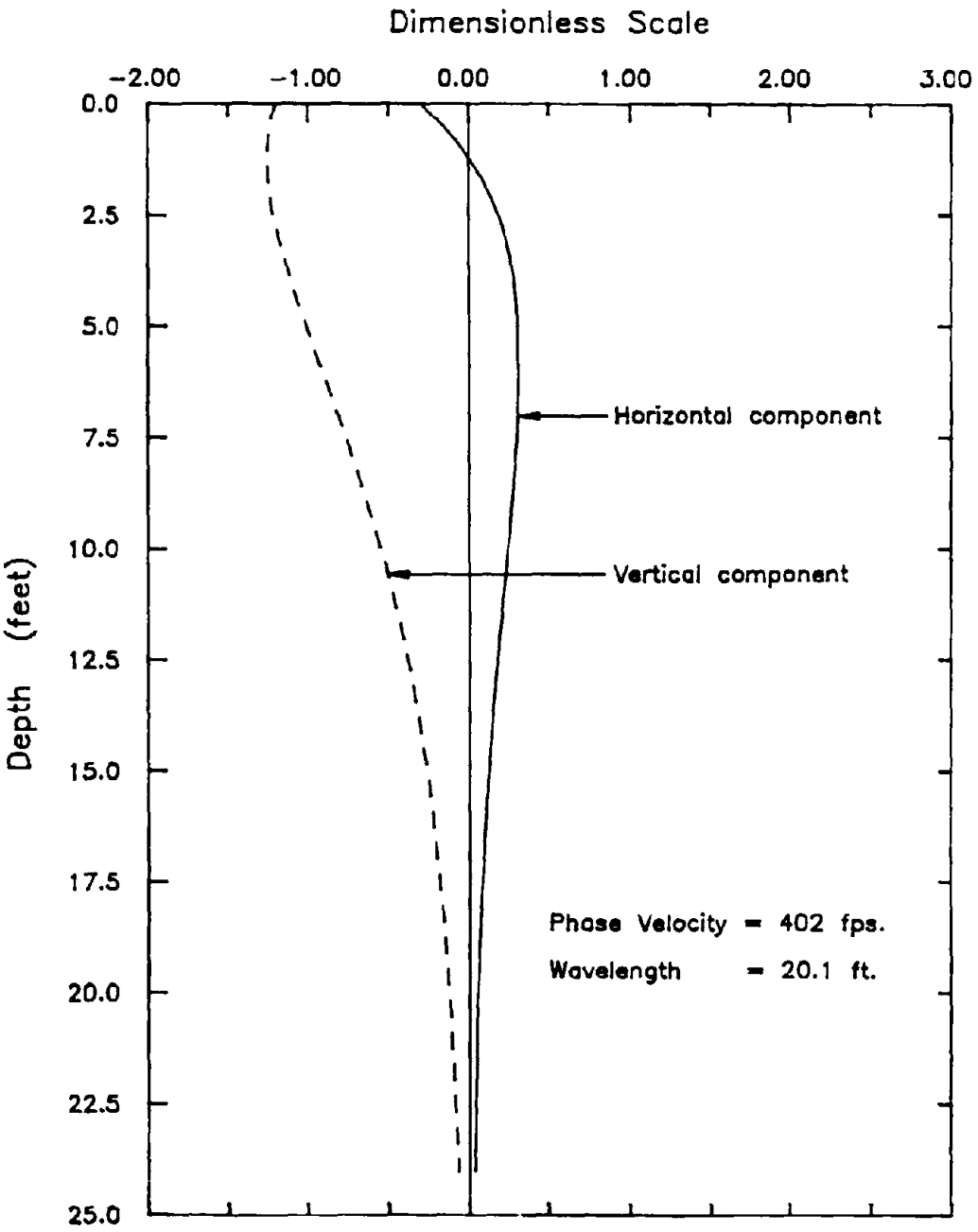

IG 5.2 HORIZONTAL AND VERTICAL MODE SHAPES FOR THE FIRST REAL RAYLEIGH WAVE MODE OF VIBRATION.

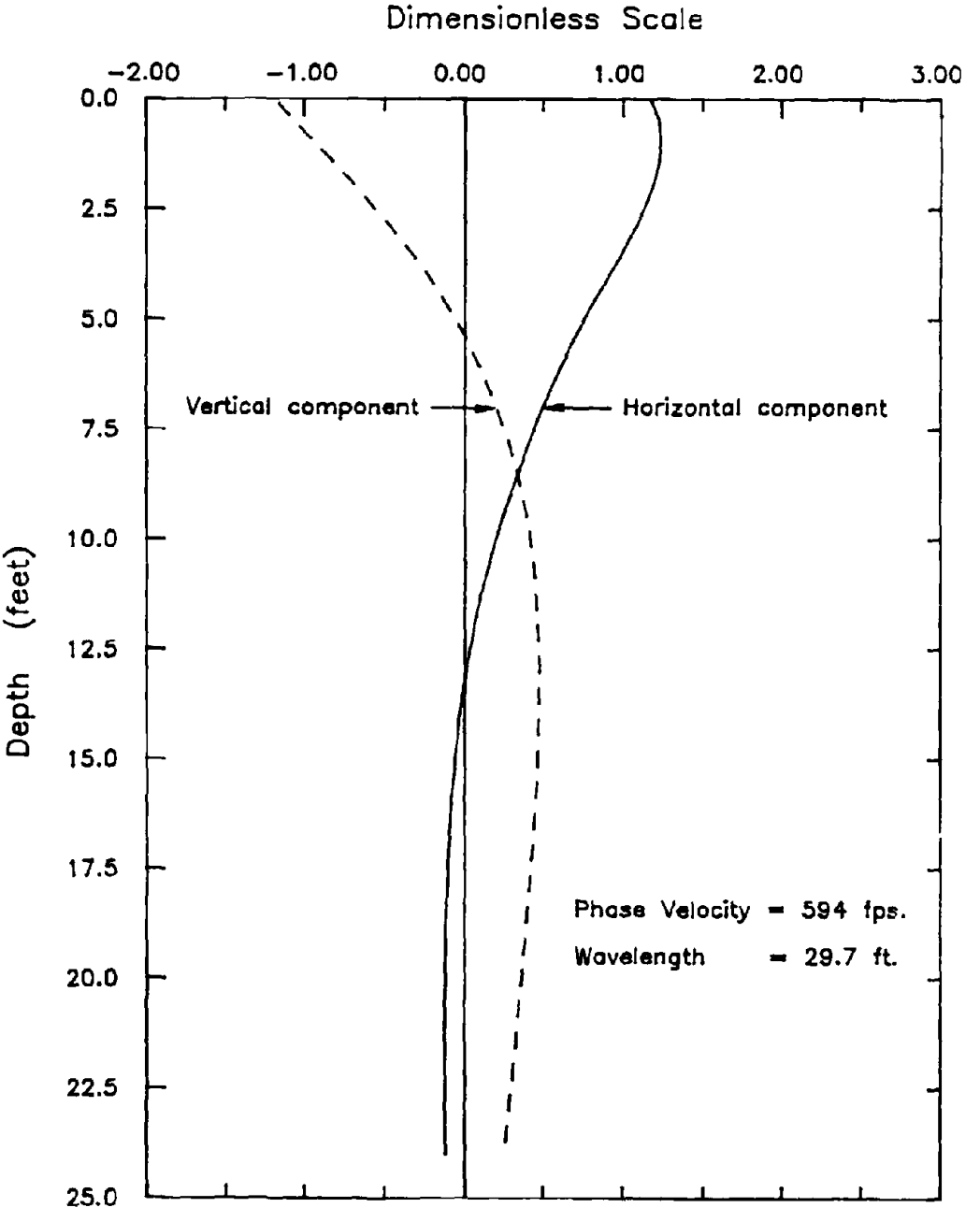

FIG 5.3 HORIZONTAL AND VERTICAL MODE SHAPES FOR THE SECOND REAL RAYLEIGH WAVE MODE OF VIBRATION.

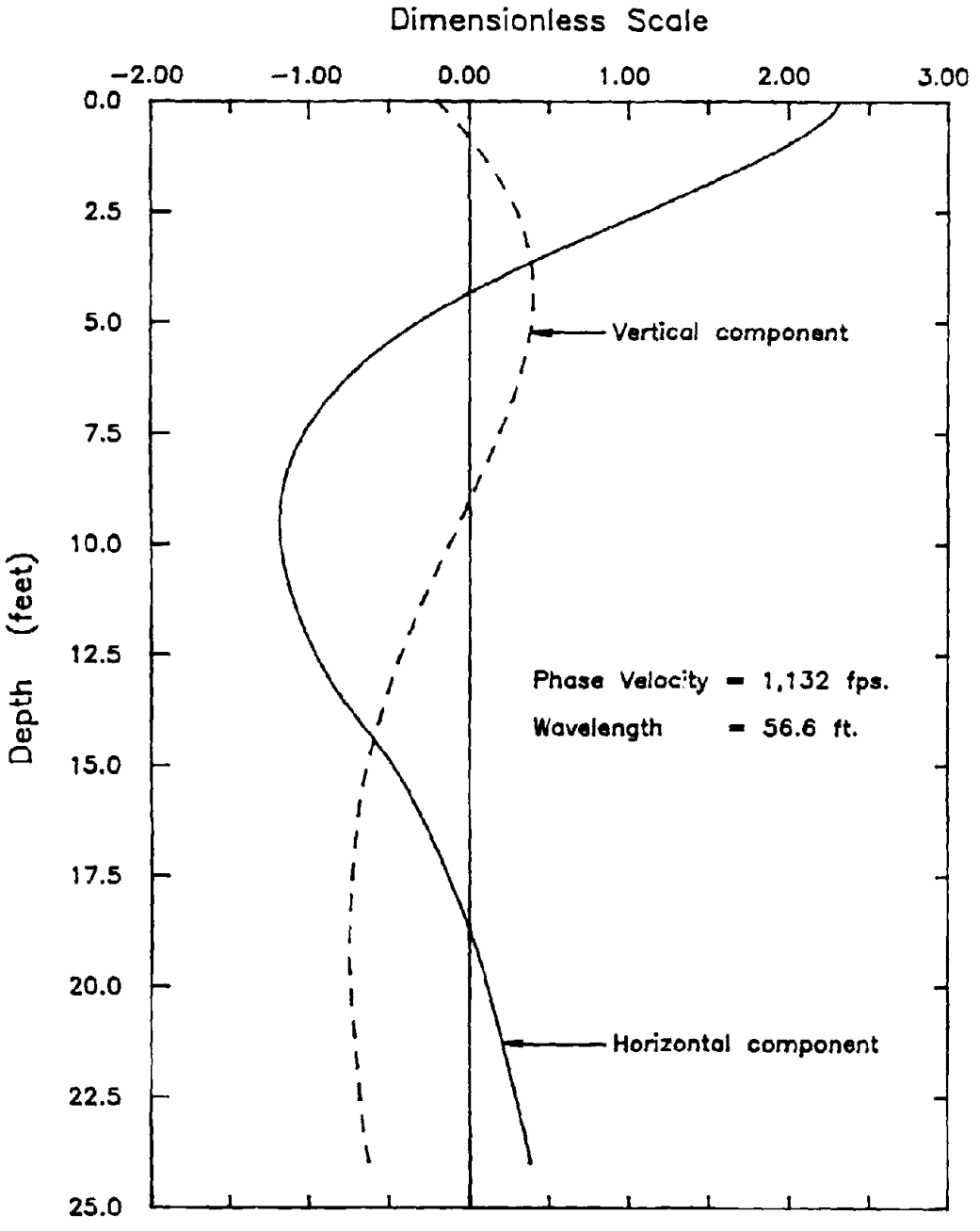

FIG 5.4 HORIZONTAL AND VERTICAL MODE SHAPES FOR THE THIRD REAL RAYLEIGH WAVE MODE OF VIBRATION.

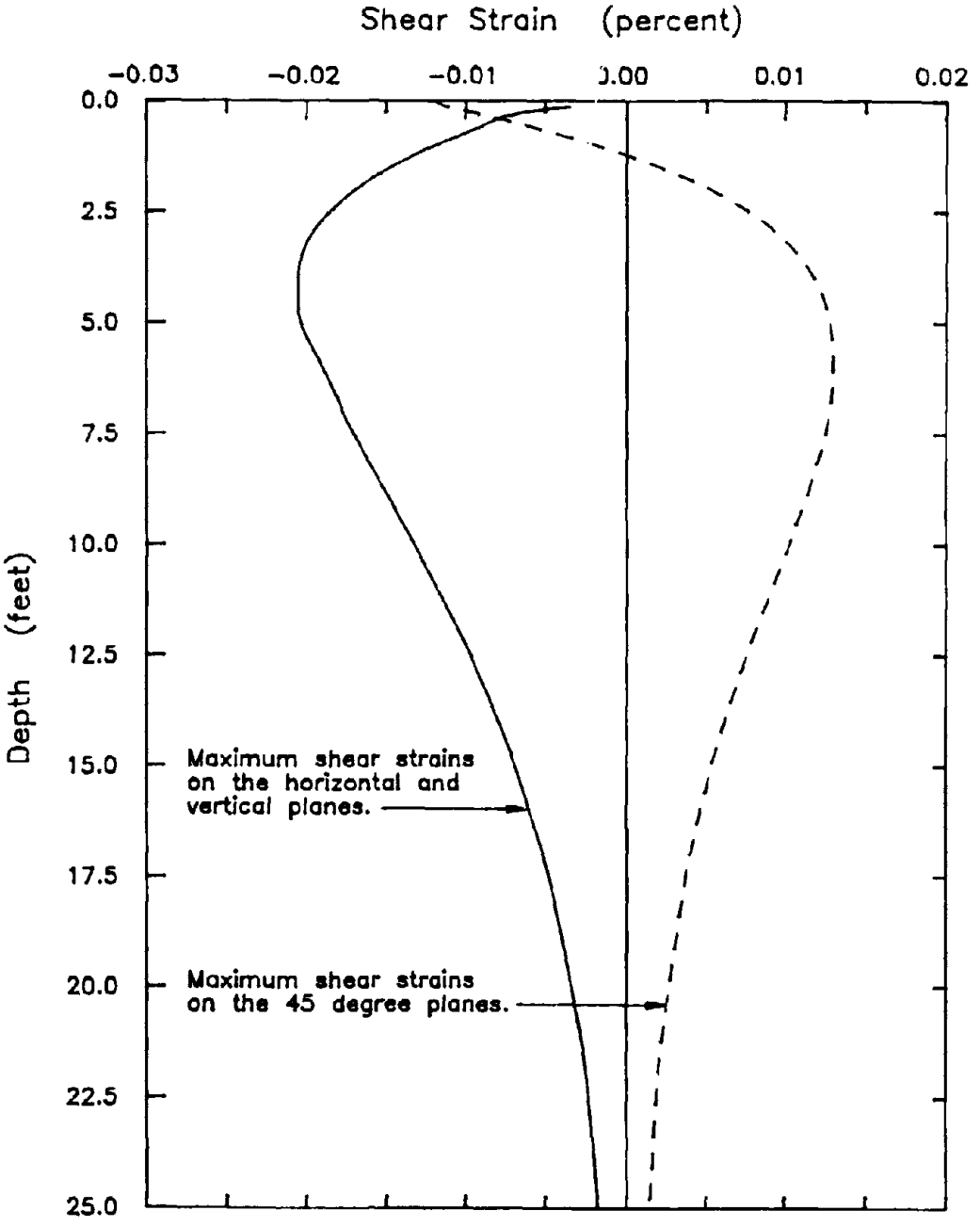

FIG 5.5 MAXIMUM CYCLIC SHEAR STRAINS GENERATED BY THE FIRST REAL RAYLEIGH WAVE MODE OF VIBRATION, FOR A PEAK GROUND SURFACE ACCELERATION OF 0.1g.

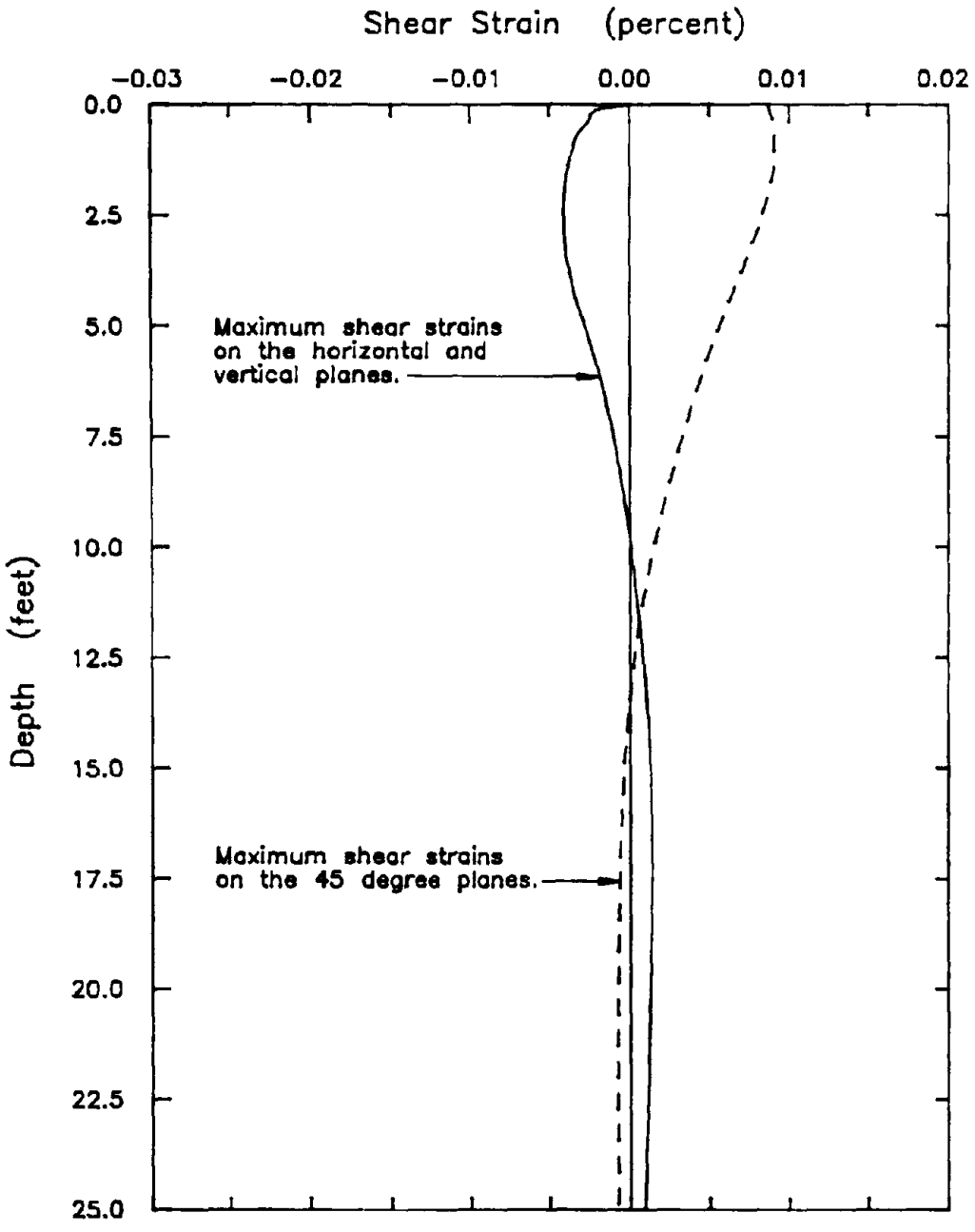

FIG 5.6 MAXIMUM CYCLIC SHEAR STRAINS GENERATED BY THE SECOND REAL RAYLEIGH WAVE MODE OF VIBRATION, FOR A PEAK GROUND SURFACE ACCELERATION OF 0.1g.

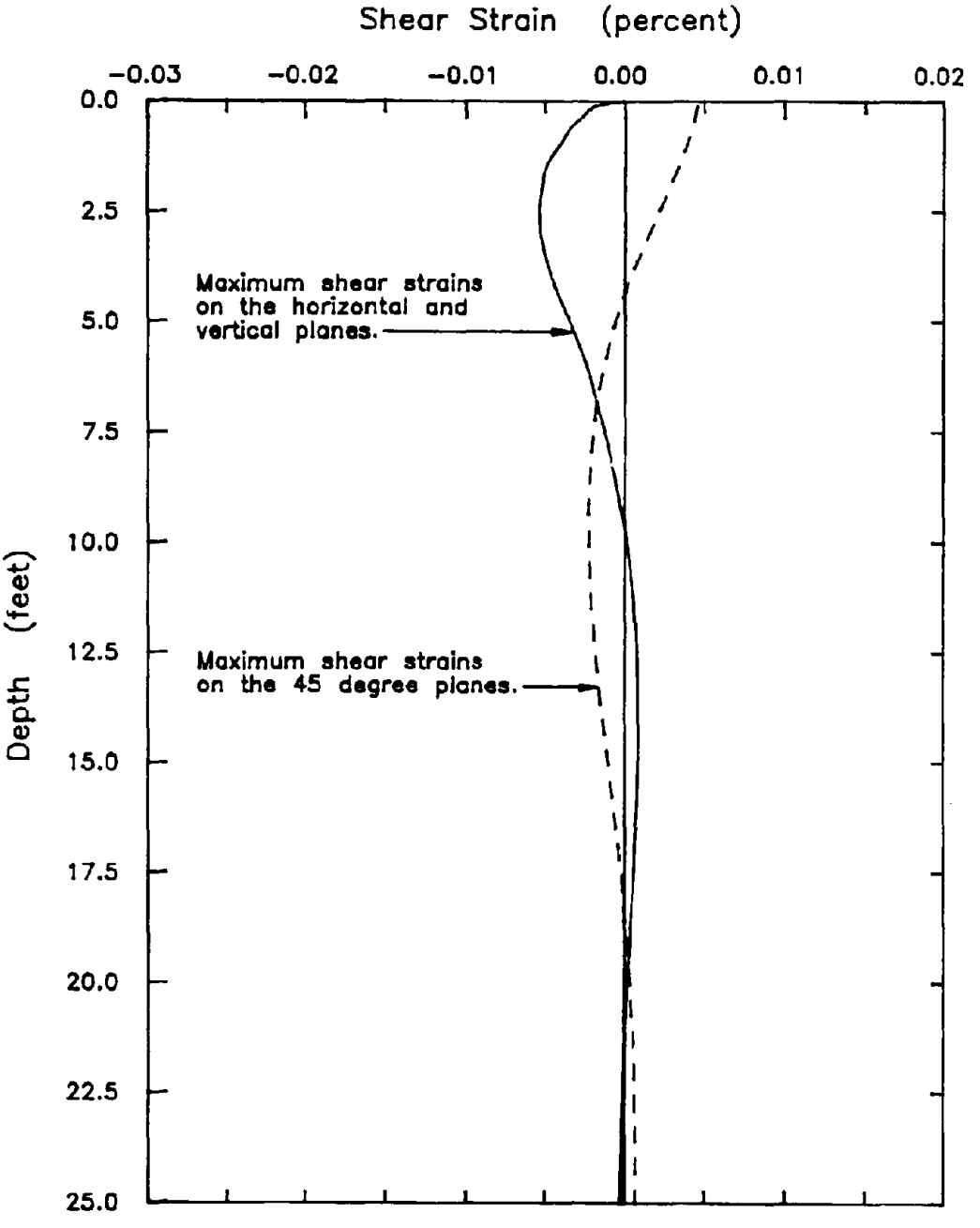

FIG 5.7 MAXIMUM CYCLIC SHEAR STRAINS GENERATED BY THE THIRD REAL RAYLEIGH WAVE MODE OF VIBRATION, FOR A PEAK GROUND SURFACE ACCELERATION OF 0.1g.

Thus, the cyclic shear strains induced within the site are predicted to be some combination of the strains (shown in Figures 5.5, 5.6, and 5.7) associated with the three real modes of vibration. Unfortunately the exact magnitude of these induced strains cannot be determined because the computer analysis provides no information on the relative proportions of ground shaking generated by each mode. It should be pointed out that the lines shown in Figures 5.2, 5.3, and 5.4 merely depict the relative amplitudes of the vertical component of ground motion with respect to the horizontal component of ground motion for the same mode of vibration.

In order to overcome this limitation, it seemed most appropriate to calculate an approximate upper bound for the magnitude of the cyclic shear strains likely to be induced at the site. This upper bound was obtained by combining the three real modes of vibration in varying proportions which satisfied the ratio of vertical ground motion to horizontal ground motion at the ground surface (as determined from the train-induced ground vibration records described in Chapter 4), while still maintaining a peak horizontal ground surface acceleration of 0.1g. Examination of the train-induced ground vibration records revealed that on average, the vertical ground surface accelerations generated by trains were approximately 20% greater in amplitude than the horizontal ground surface accelerations measured perpendicular to the track.

The cyclic shear strains associated with the six modal combinations (that satisfied the constraints described above) were calculated by superimposing the strains computed for the three real modes of vibration (shown in Figures 5.5, 5.6 and 5.7). These combined strain profiles were then compared and the maximum strains generated at

any given depth were determined. Figure 5.8 shows the maximum cyclic shear strains generated on horizontal planes at various depths in this deposit, while the curve shown in Figure 5.9 depicts the maximum cyclic shear strains that were predicted to be generated on 45 degree planes. It is worth noting at this point that while the curves shown in Figures 5.8 and 5.9 are believed to provide an approximate upper bound for the levels of induced cyclic shear strain, the strains implied by these curves are probably not significantly larger in magnitude than the actual cyclic shear strains induced within the site. Such a belief is held because the three real modes of vibration propagate with different wavelengths and therefore probably combine in widely varying proportions at different distances from the tracks.

Having completed the Rayleigh wave analysis (of the 13 meter, 35% relative density sand site) and calculated what appears to be a reasonable estimate for the magnitudes of the cyclic shear strains actually induced within the site by train-induced ground vibrations with peak ground surface accelerations of about 0.1g, it was decided to repeat the analysis assuming that the ground motions consisted entirely of vertically propagating shear waves. This latter analysis was performed in order to compare the levels of cyclic shear strain induced by the two wave types, and hence assess the effect of the initial assumption that most of the energy imparted to the soil by trains was transmitted as Rayleigh waves.

The magnitudes of the cyclic shear strains induced by vertically propagating shear waves, were determined by creating an artificial sinusoidal ground vibration record and then deconvolving the motion down through the site using the computer program

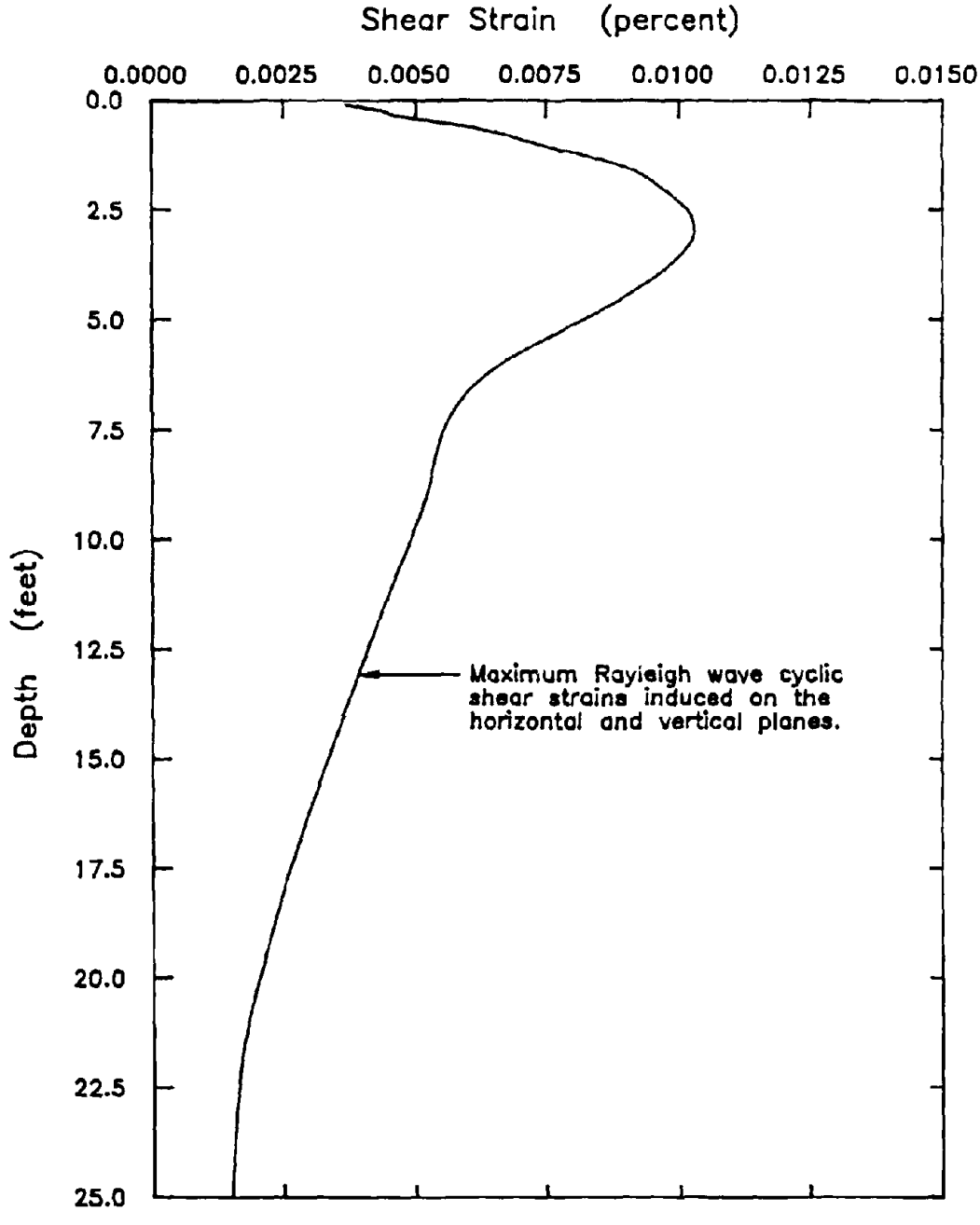

FIG 5.8 MAXIMUM ABSOLUTE CYCLIC SHEAR STRAINS GENERATED ON THE HORIZONTAL AND VERTICAL PLANES BY ANY ONE OF THE SIX MODAL COMBINATIONS THAT WERE CONSIDERED.

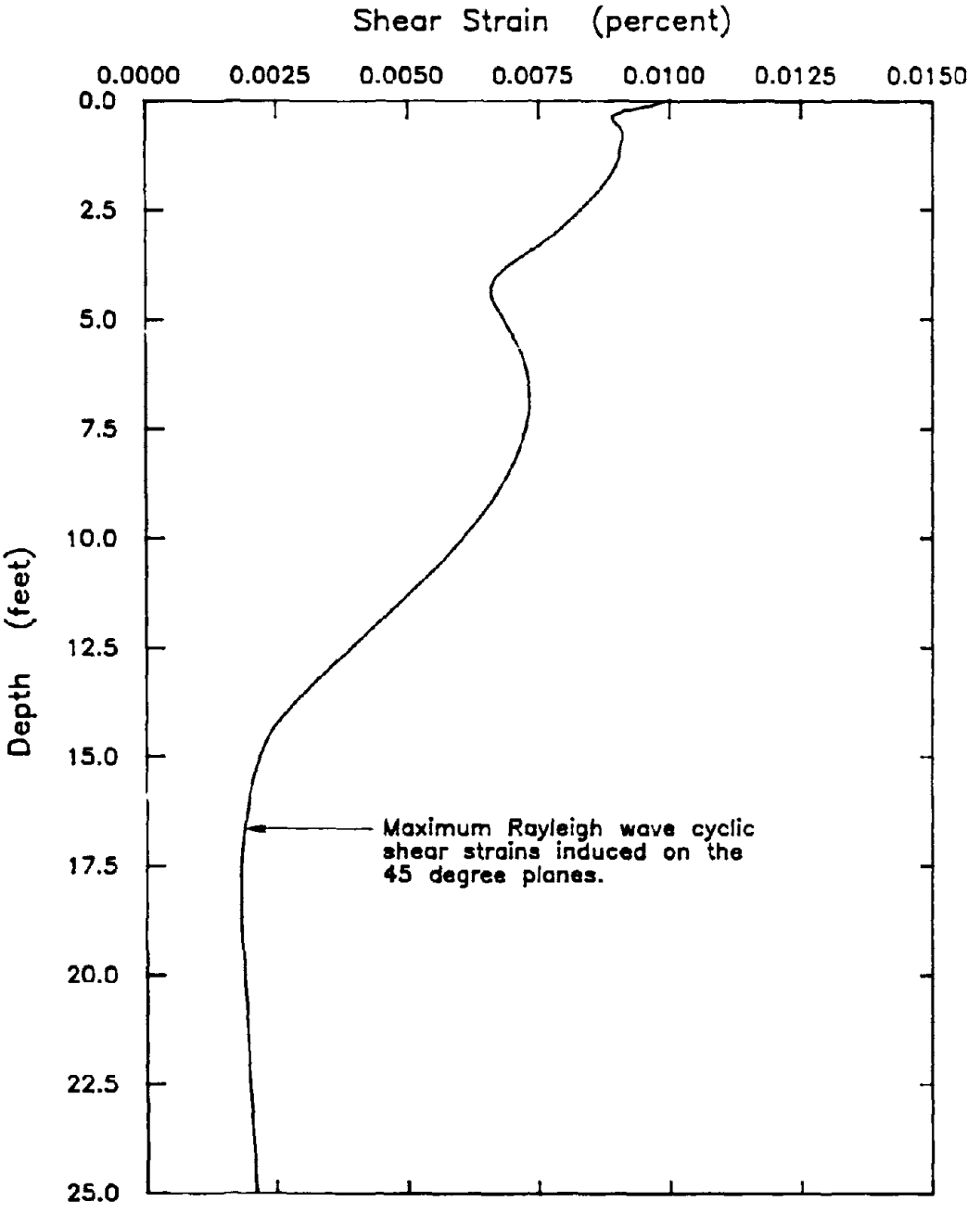

FIG 5.9 MAXIMUM ABSOLUTE CYCLIC SHEAR STRAINS GENERATED ON 45 DEGREE PLANES BY ANY ONE OF THE SIX MODAL COMBINATIONS THAT WERE CONSIDERED.

SHAKE. This ideal surface motion was chosen to have a constant amplitude of 0.1g and a predominant frequency of 20 Hz. The strains calculated by this approach are shown by the dashed line in Figure 5.10, and are presented together with the approximate upper bound curves that were computed using Rayleigh wave theory (also shown in the previous figure). It should be pointed out that the unusually low values of shear strain at depths of about 7.5 ft and 19 ft indicate the presence of nodes at these points and are due to the fact that the input motion from which the site response was calculated, was a pure 20 Hz motion. With a less uniform frequency as is present in train vibrations, this marked difference at a depth of 7.5 ft would be ameliorated.

The effect of using an ideal 20 Hz, sinusoidal record to predict site response was investigated by comparing the cyclic shear strains computed for the ideal motion with those computed by assigning actual train-induced ground vibration records as the ground surface motions. All records were scaled to give the same peak horizontal surface acceleration of 0.1g. As shown in Figure 5.11, it was found that the shear strains associated with the ideal surface motion are somewhat higher than those associated with the actual train-induced records. This is probably due to the higher predominant frequencies of the latter records. As is expected, the nodes are no longer evident at depths of about 7.5 ft and 19 ft because of the range of frequencies present in the real motion. The train-induced ground motion used to compute the strains shown in Figure 5.11 was recorded parallel to the tracks.

From the comparisons shown in Figure 5.10 it may be concluded that:

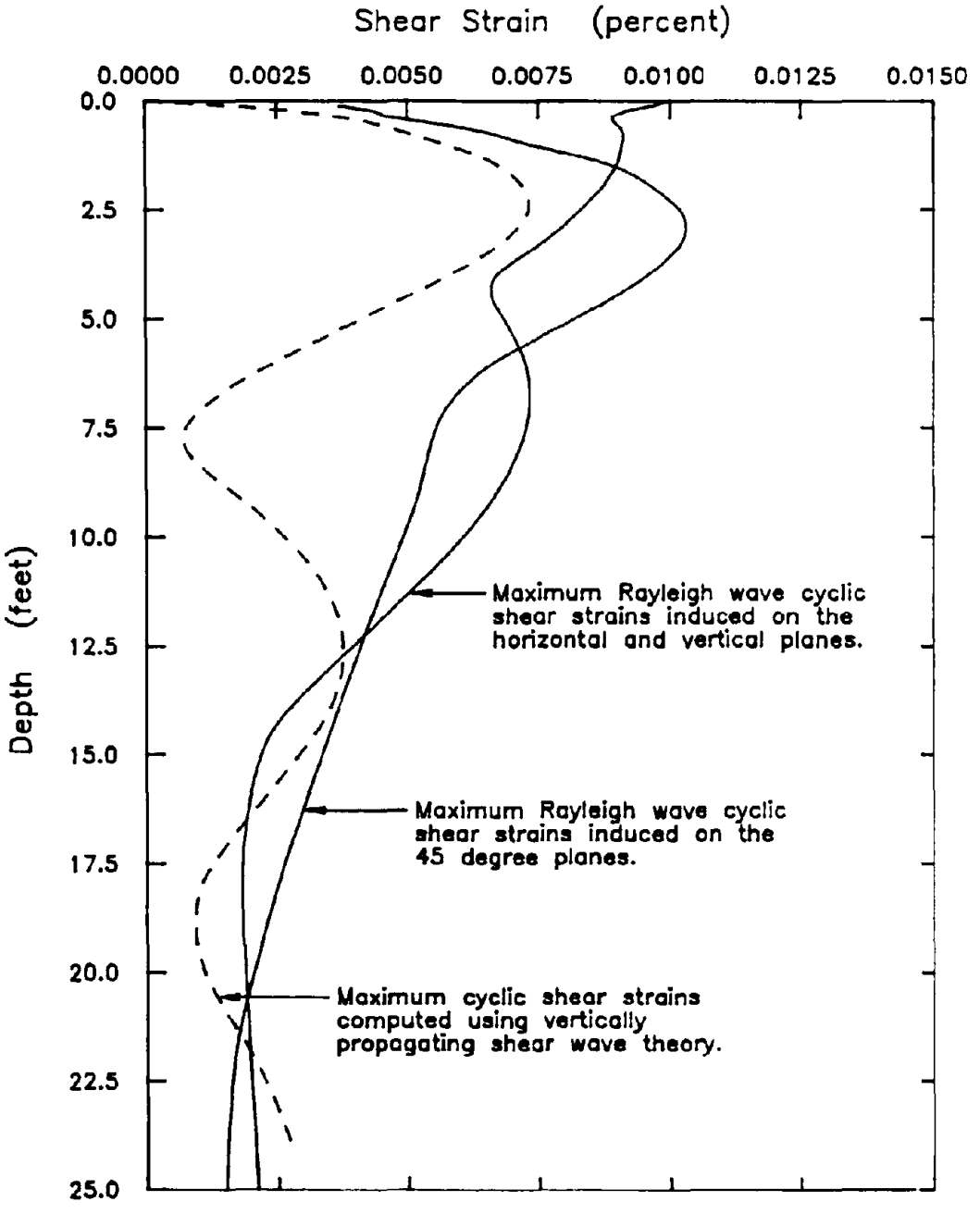

FIG 5.10 COMPARISON OF THE MAXIMUM ABSOLUTE CYCLIC SHEAR STRAINS COMPUTED USING RAYLEIGH WAVE THEORY WITH THOSE COMPUTED USING VERTICALLY PROPAGATING SHEAR WAVE THEORY.

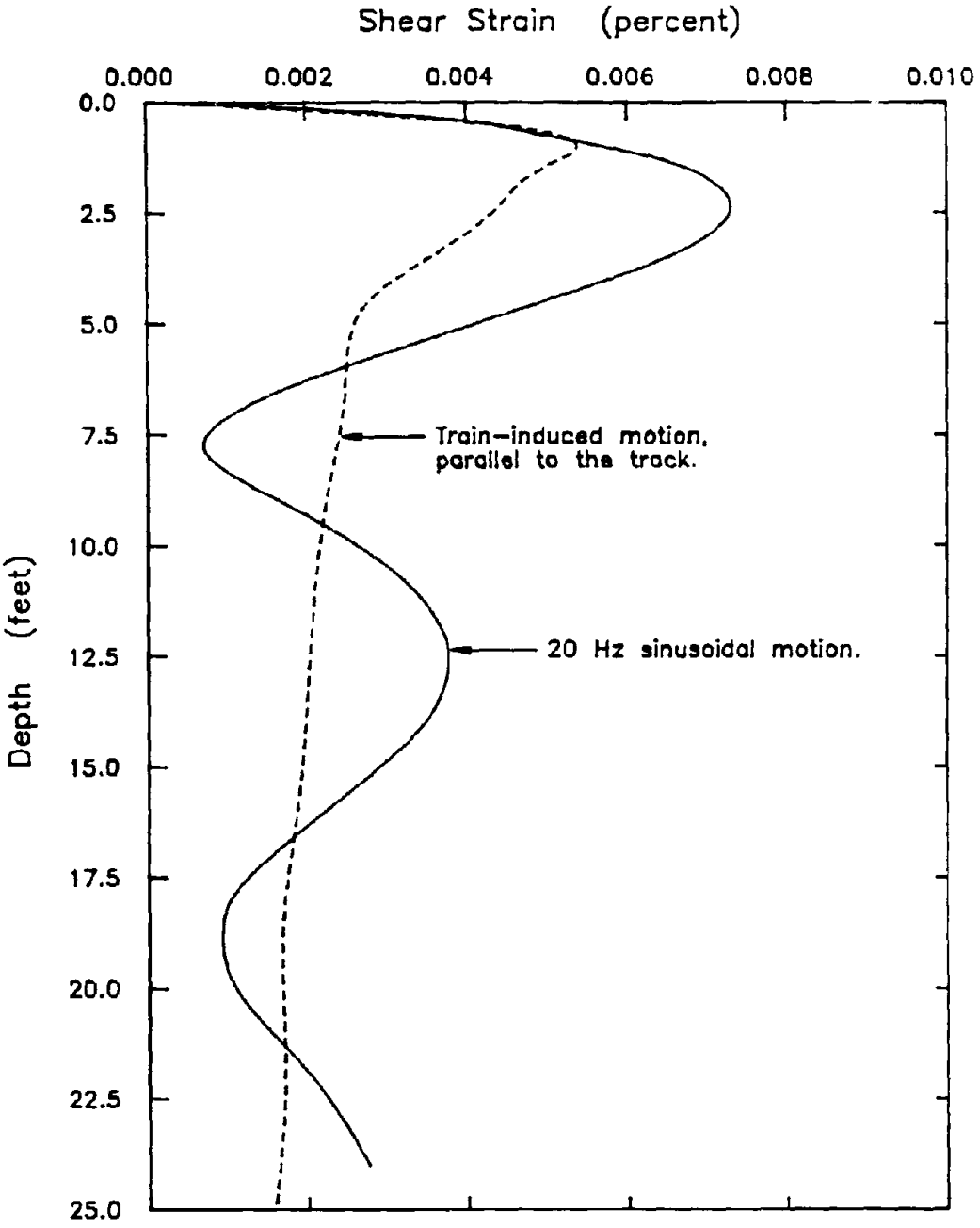

FIG 5.11 COMPARISON OF THE MAXIMUM ABSOLUTE CYCLIC SHEAR STRAINS COMPUTED FOR AN IDEAL 20Hz SURFACE MOTION WITH THOSE COMPUTED FOR AN ACTUAL TRAIN-INDUCED GROUND VIBRATION RECORDED PARALLEL TO THE TRACKS.

) The maximum cyclic shear strains calculated using vertically propagating shear wave theory are quite similar in magnitude to the upper bound cyclic shear strains calculated using Rayleigh wave theory.

2) Since both Rayleigh wave theory and vertically propagating shear wave theory (V.P.S.W. theory) predict similar levels of induced cyclic shear strain, and most ground motions are believed to consist predominantly of some combination of surface waves and body waves, it seems probable that the magnitudes of the strains calculated using Rayleigh wave theory are close in magnitude to the strains actually generated by train-induced ground vibrations.

Thus, based on the above conclusions, and given that V.P.S.W. analyses require significantly less computational effort to perform than Rayleigh wave analyses, it seemed appropriate to use vertically propag ting shear wave theory to estimate the magnitude of the cyclic shear strains generated by trains for the remainder of the analyses. The observation that both theories predict similar levels of induced cyclic shear strain seems plausible since most of the energy transmitted by Rayleigh waves is propagated at depth where the shear modulus of the sand is higher. Therefore, the deeper layers drive the motions in the layers closer to the surface in a similar manner to that developed by near-vertically propagating shear waves.

5.3. Evaluation of Liquefaction Potential Using the Shear Strain Approach

In light of the above results, the liquefaction potentials of sand sites subjected to train-induced ground vibrations were evaluated by first estimating the levels of induced Rayleigh wave cyclic shear strains using vertically propagating shear wave theory. These levels were then compared with the levels of cyclic shear strain required to liquefy the sand in-situ. Comparisons were made at distances of 10 and 20 ft from the nearest rail but were not undertaken at distances closer to the tracks since it is believed that in this near-field range, the soil behavior is likely to be dominated by the weight of the train. Szerdy (1985) has already shown that these static stresses are capable of causing liquefaction of saturated sand embankments.

The magnitudes of the strains induced at these distances were computed by scaling the 20 Hz record to produce motions of different amplitudes and deconvolving these motions down through the site using the computer program SHAKE. The acceleration amplitudes were determined with the aid of Figure 4.4 which indicates that trains are probably capable of generating peak ground surface accelerations of about 0.3g and 0.1g at distances of 10 ft and 20 ft from the nearest rail respectively. These accelerations were reduced by 50% to represent average levels of shaking and thus ideal sinusoidal surface motions with maximum amplitudes of 0.15g and 0.05g were applied at distances of 10 ft and 20 ft from the tracks respectively. Examination of the train-induced ground vibration records presented in Chapter 4 revealed that the average level of ground shaking generated by the engines was typically half the peak particle acceleration.

The 20 Hz frequency chosen for the sinusoidal surface motion was determined from the acceleration response spectra computed during this investigation. These spectra show that most of the train-induced ground vibration records contain dominant frequencies of about 40 Hz, 33 Hz and 23 Hz (as discussed in Section 4.4 and shown in Figures 4.7 and 4.8). Because several of the ground vibration records contained dominant frequencies of approximately 20 Hz, and the magnitude of the induced cyclic shear strains was found to drop significantly as the frequency of the input surface motion was increased, while holding the peak ground surface acceleration constant, it seemed most appropriate to use an artificial surface motion with a frequency of 20 Hz in the analyses.

The cyclic shear strains computed using one dimensional vertically propagating shear wave theory to occur within a 35% relative density saturated sand site (with a water table at the ground surface) at distances of 10 and 20 ft from the tracks are shown by the solid lines in Figures 5.13 and 5.14 respectively. These curves were then adjusted (with the aid of the comparison presented in Figure 5.10) to determine estimates for the magnitudes of the Rayleigh wave-induced cyclic shear strains at these distances, and hence what are believed to be reasonable values for the actual levels of train-induced shear strains. The estimated Rayleigh wave strains are shown by the dashed lines in the same figures. The same procedure was also used to estimate the magnitudes of the Rayleigh wave cyclic shear strains likely to be induced within the same sand site with water tables at depths of 2.0 ft and 5.0 ft and the results for all three site conditions are summarized in Figures 5.15 and 5.16.

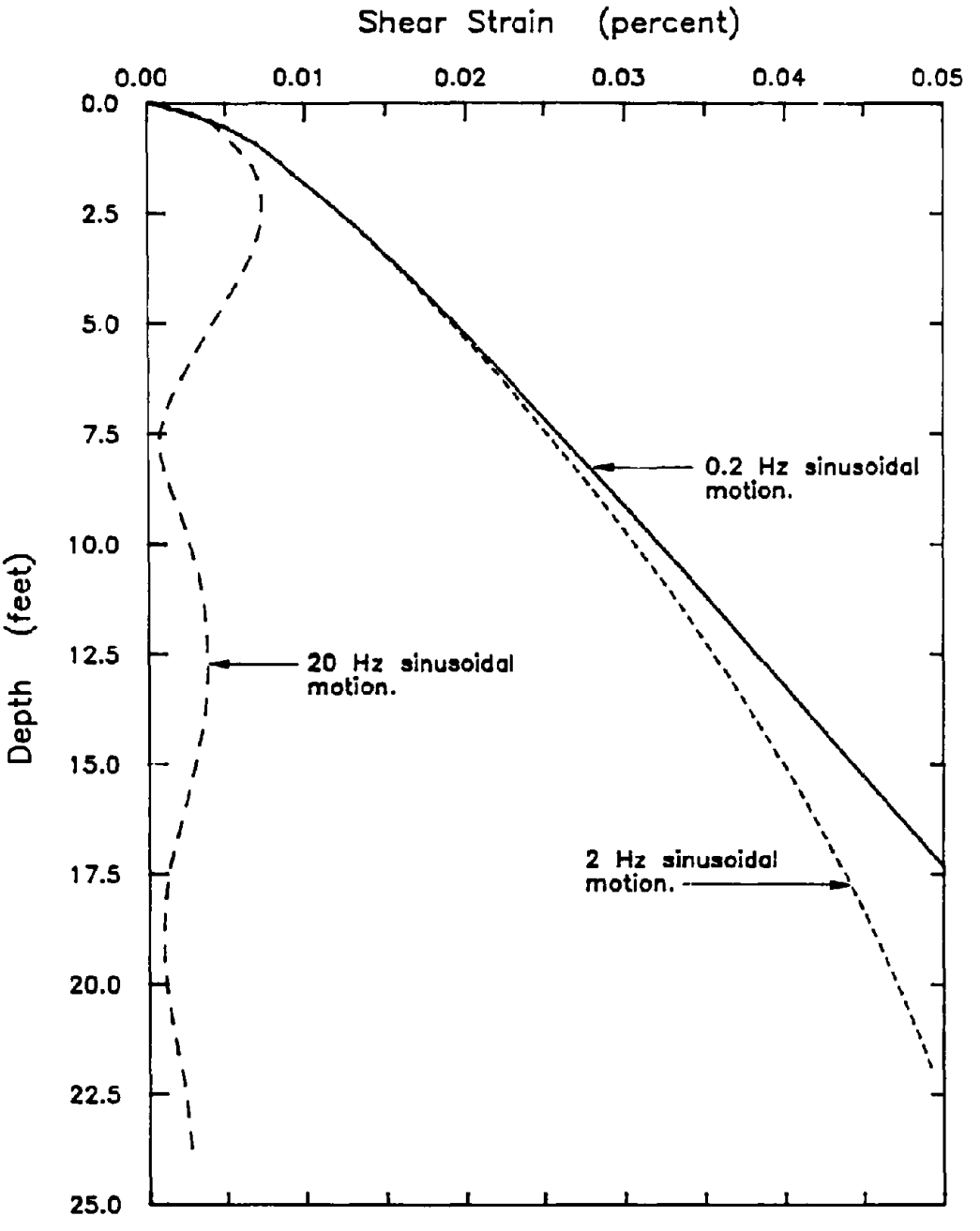

FIG 5.12 MAXIMUM ABSOLUTE CYCLIC SHEAR STRAINS GENERATED BY VERTICALLY PROPAGATING SHEAR WAVES WITH PEAK GROUND SURFACE ACCELERATIONS OF 0.1g AND PREDOMINANT FREQUENCIES OF 0.2, 2, and 20 Hz.

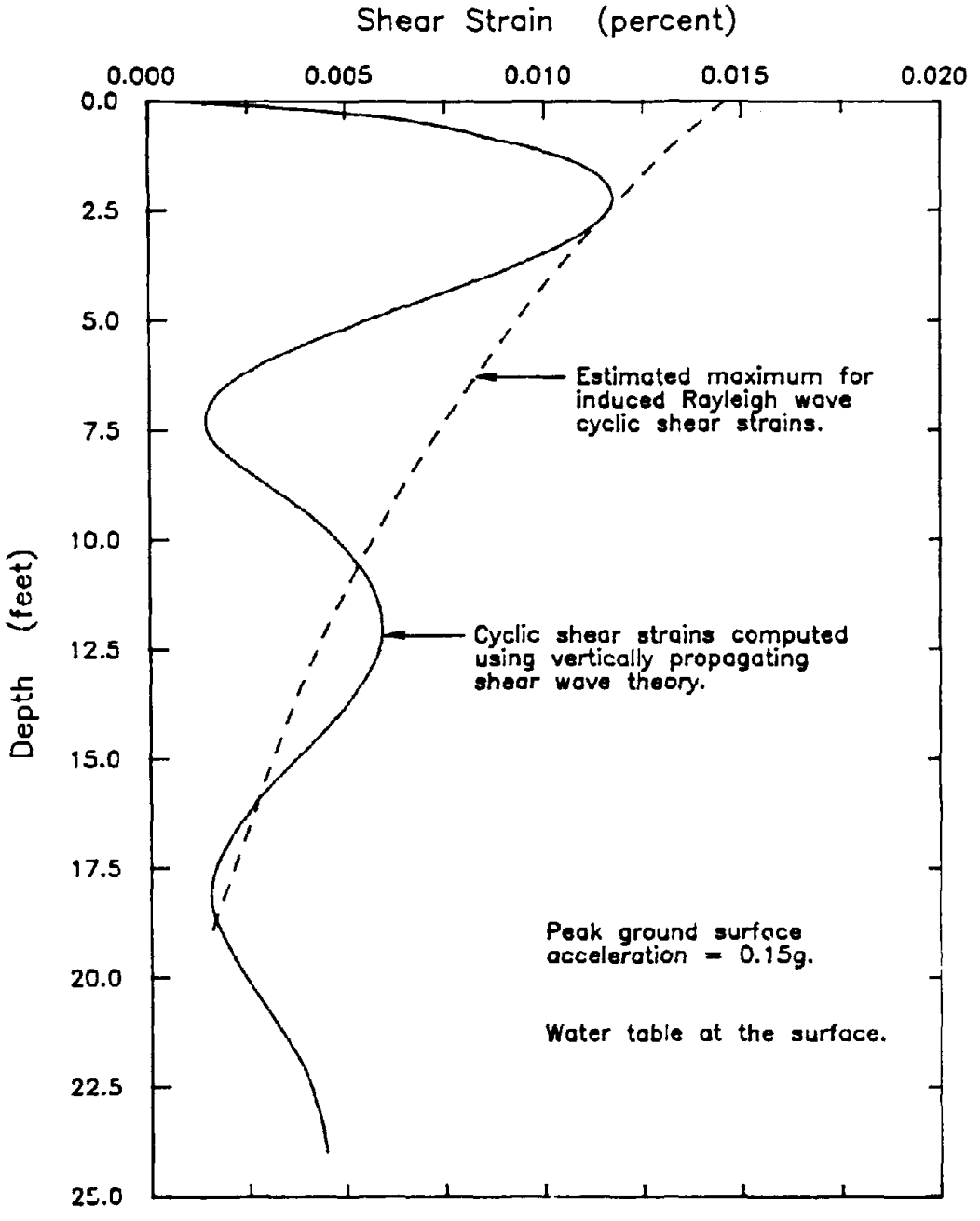

FIG 5.13 MAXIMUM RAYLEIGH WAVE CYCLIC SHEAR STRAINS PREDICTED TO OCCUR AT DISTANCES OF ABOUT 10 FEET FROM THE TRACKS.

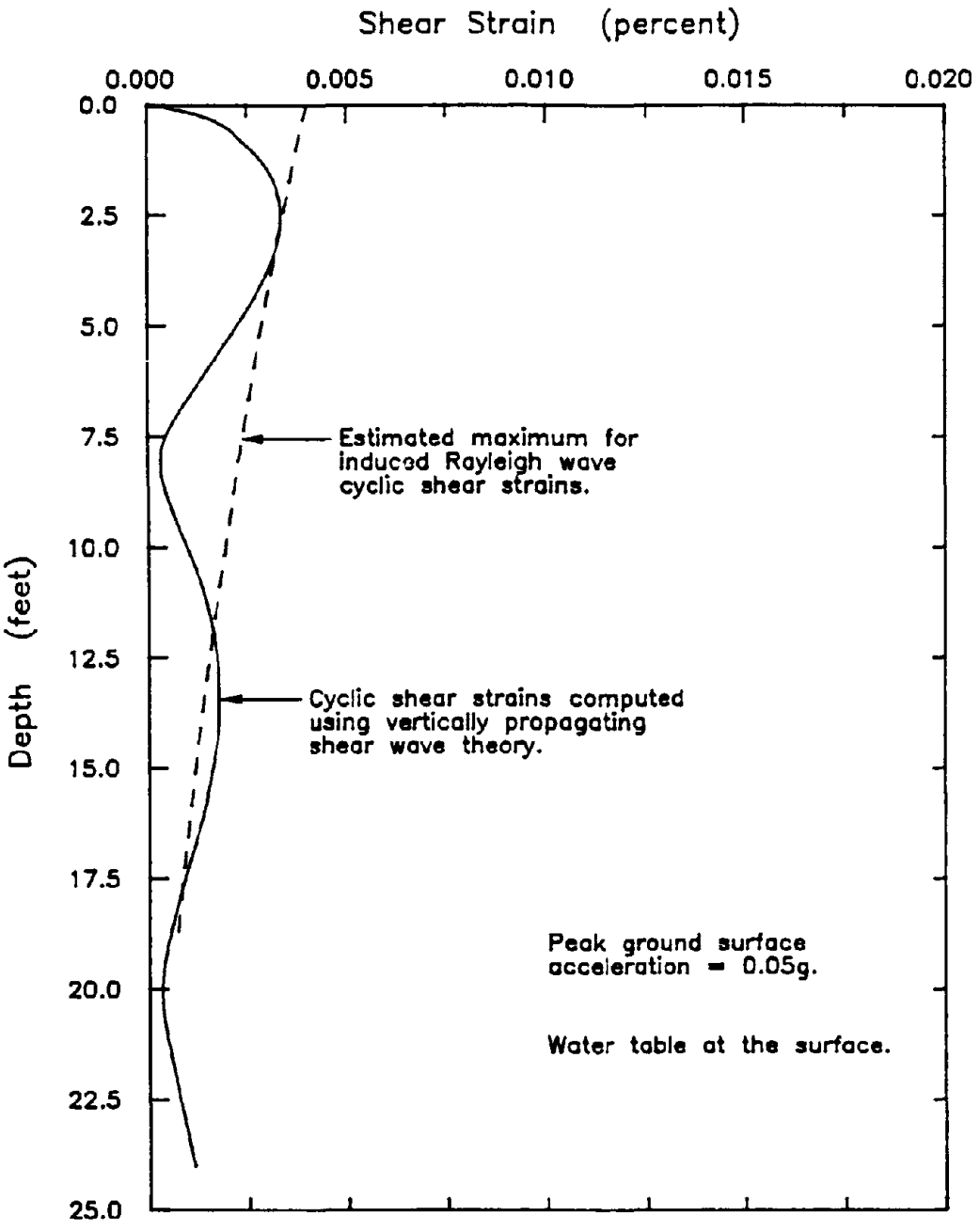

FIG 5.14 MAXIMUM RAYLEIGH WAVE CYCLIC SHEAR STRAINS PREDICTED TO OCCUR AT DISTANCES OF ABOUT 20 FEET FROM THE TRACKS.

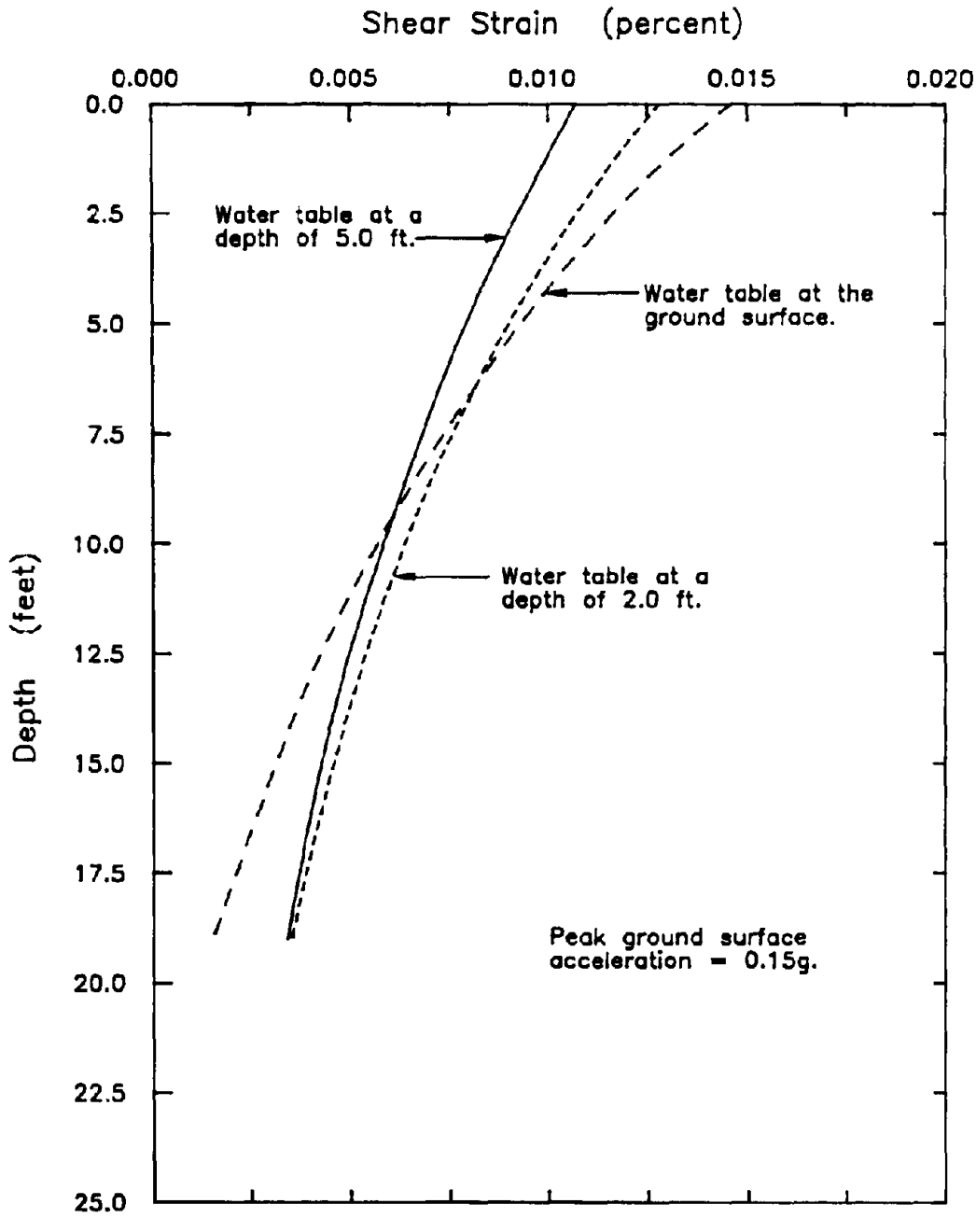

FIG 5.15 MAXIMUM RAYLEIGH WAVE CYCLIC SHEAR STRAINS PREDICTED TO OCCUR AT DISTANCES OF ABOUT 10 FEET FROM THE TRACKS WITHIN SAND SITES WITH WATER TABLES AT DEPTHS OF 0, 2, AND 5 FEET.

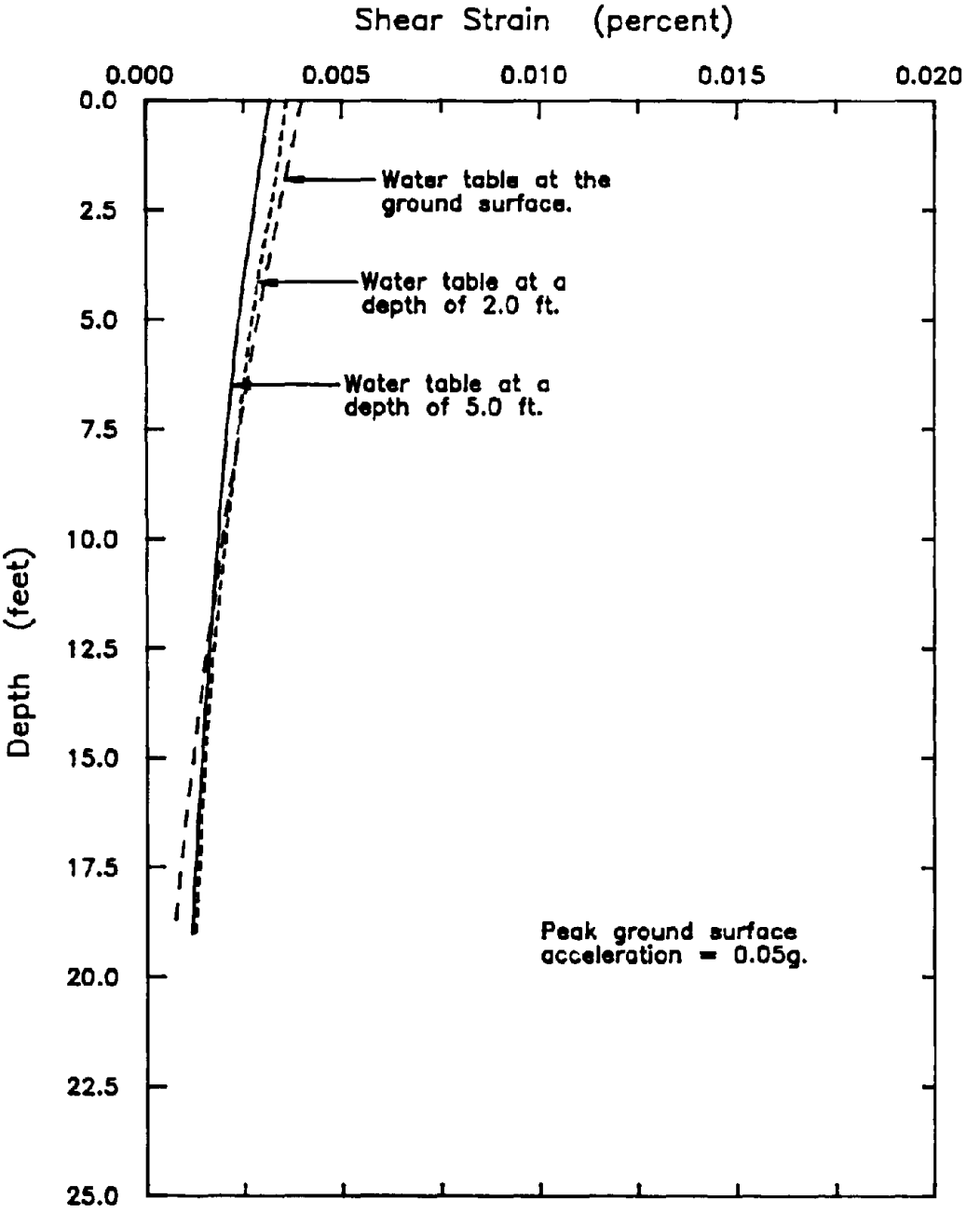

FIG 5.16 MAXIMUM RAYLEIGH WAVE CYCLIC SHEAR STRAINS PREDICTED TO OCCUR AT DISTANCES OF ABOUT 20 FEET FROM THE TRACKS WITHIN SAND SITES WITH WATER TABLES AT DEPTHS OF 0, 2, AND 5 FEET.

As shown in these figures, the magnitudes of the cyclic shear strains predicted to be induced within level, loose sand deposits are relatively small. In fact, even at distances as close as 10 ft from the nearest rail these strains are not predicted to exceed a value of about $1.5\times10^{-2}\%$, a strain which is only slightly larger than the threshold strains of many sands. For example, the threshold strains for most of the sands for which data are presented in Table 3.2, may be seen to be about $1.0\times10^{-2}\%$. In addition, experimental data has shown that even after 100 cycles of loading at a maximum strain of $1.5\times10^{-2}\%$, the pore pressure ratio generated within a 45% relative density Monterey No. 0 sand sample did not exceed a value of about 0.1 (refer to Figure 3.9). Since changes in the relative density from 45% to 80% have been shown to have a relatively minor effect on the rate of pore pressure build-up at such low strain levels (see Figure 3.7), it seems likely that the excess pore pressures generated within loose ($D_R \simeq 35\%$) sand samples would also be small.

Thus it appears that according to the shear strain analysis, the ground vibrations generated by trains are not only incapable of liquefying level, loose sand deposits located at distances greater than about 10 ft from the nearest rail, but they are also probably incapable of generating significant pore pressures within sands at these distances. Such a conclusion is consistent with the observation that no case histories are known to have been reported where ground vibrations generated by trains have liquefied level sand sites.

5.4. Evaluation of Liquefaction Potential Using the Shear Stress Approach

The liquefaction potentials of sand deposits subjected to train-induced ground vibrations were also evaluated using the shear stress approach. This approach was employed for the following reasons: (1) in order to compare the conclusions reached by following both the shear strain and the shear stress approaches and (2), to enable the effects of initial static shear stresses on the liquefaction potential of the deposits to be taken into account. The ability to account for these stresses was perceived to be important because all of the large-scale liquefaction failures listed in Table 1.1 occurred on sloping ground, and it was believed that non-seismic sources of vibration might only be capable of liquefying sands that were subjected to high initial shear stress/normal stress ratios.

The magnitudes of the induced cyclic shear stresses predicted to occur within the 35% relative density sand site were calculated from the values of induced cyclic shear strain shown in Figures 5.15 and 5.16. These stresses were computed with the aid of the Seed and Idriss (1970) curve of normalized shear modulus versus cyclic shear strain (shown in Figure 5.1) and the values of the maximum (i.e. small strain) shear moduli calculated from Equation 5.7. The induced cyclic stress ratios calculated by this approach and shown in Figures 5.17 and 5.18 were subsequently compared with the levels of cyclic stress ratio that were thought to be capable of inducing liquefaction.

In contrast to the shear strain approach, where the value of threshold strain appears to be independent of the number of cycles of applied loading, the level of

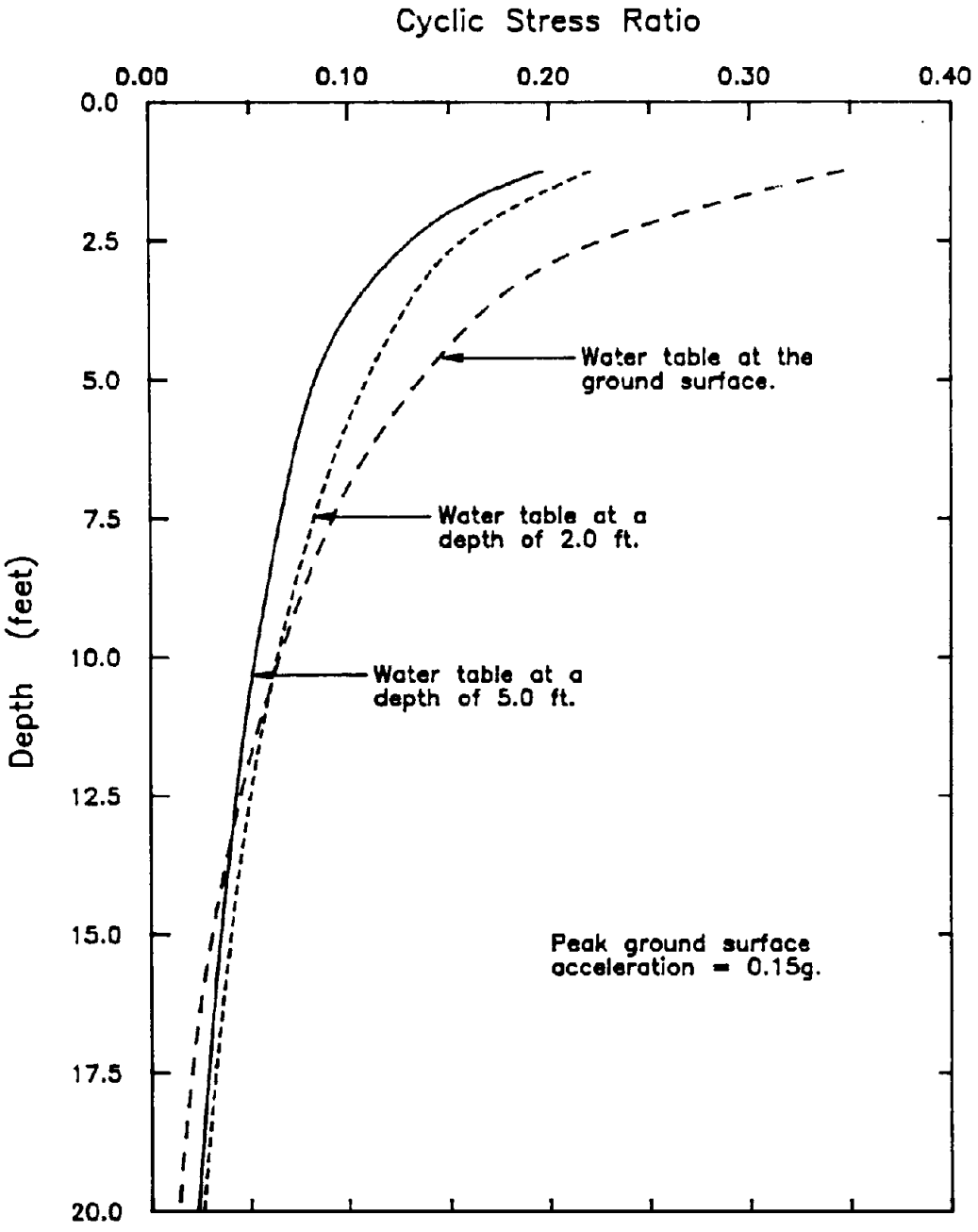

FIG 5.17 MAXIMUM CYCLIC STRESS RATIOS PREDICTED TO BE INDUCED BY TRAINS AT DISTANCES OF ABOUT 10 FEET FROM THE TRACKS, WITHIN SAND SITES WITH WATER TABLES AT VARIOUS DEPTHS.

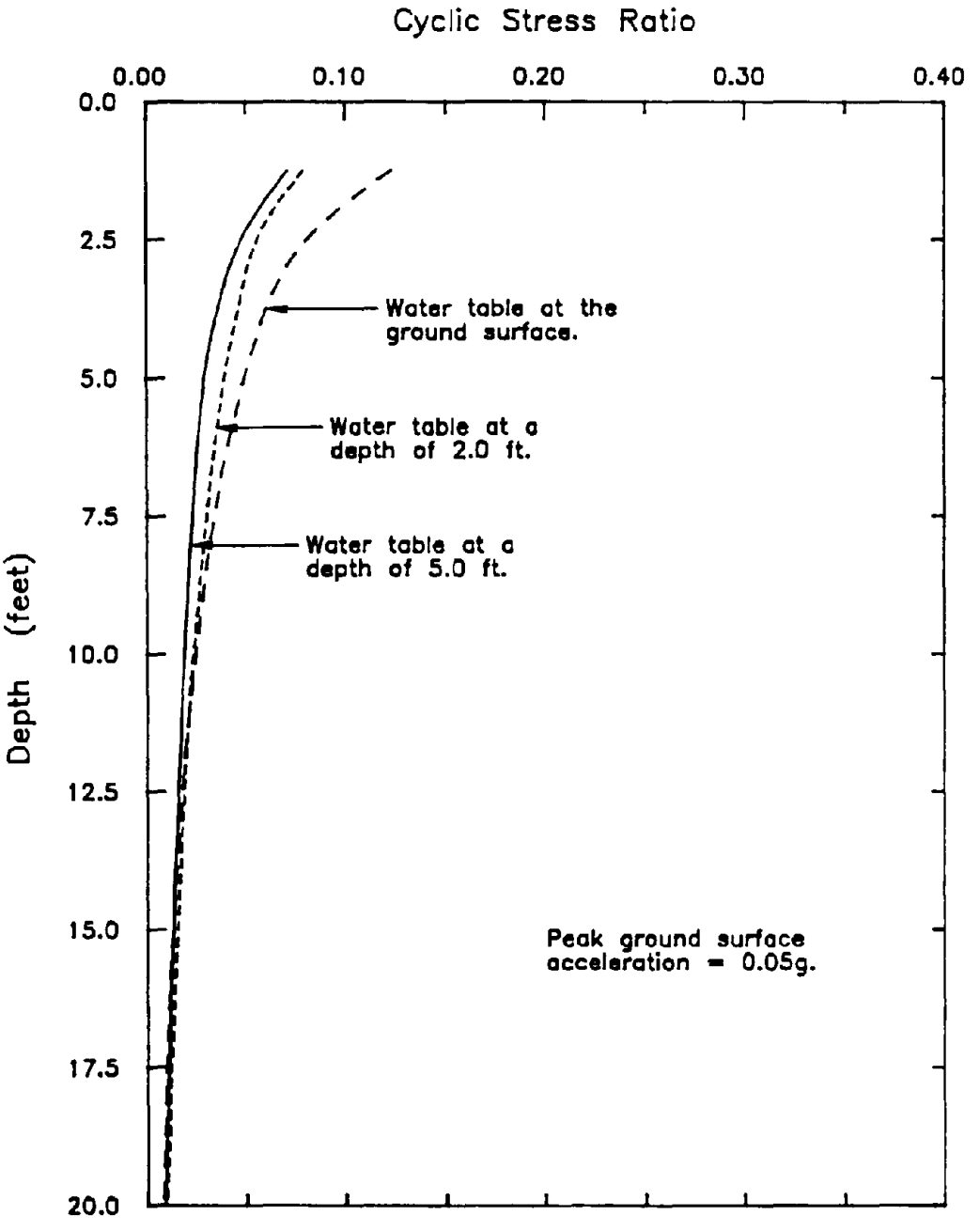

FIG 5.18 MAXIMUM CYCLIC STRESS RATIOS PREDICTED TO BE INDUCED BY TRAINS AT DISTANCES OF ABOUT 20 FEET FROM THE TRACKS, WITHIN SAND SITES WITH WATER TABLES AT VARIOUS DEPTHS.

cyclic shear stress that is required to liquefy a sand is heavily dependent on this number of cycles. Therefore, before the level of required shaking could be determined it was necessary to estimate the number of representative cycles of loading likely to be produced by an average freight train. Based on the observation that freight trains of moderate length are typically powered by four engines which generate about 5 seconds of strong ground shaking, and given that these motions are represented by an ideal 20 Hz sinusoidal surface motion, it seemed reasonable to assume that the passage of such a train would generate about 100 representative cycles of shaking.

While it might appear from this description that the ground shaking generated by railroad cars was ignored, this is not the case. Rather, it was determined that the shaking generated by the cars was likely to impose a relatively insignificant amount of distress on the soil when compared to the amount of distress imposed by the engines. This belief is based on the observation that the ground surface accelerations generated by the cars were usually about one-half to two-thirds of the magnitude of the average levels of shaking generated by the engines. Applied cyclic stress ratios, two-thirds of the magnitude of the stress ratios required to induce liquefaction in 100 cycles are probably incapable of liquefying the same sand in any number of cycles (see Figure 3.3).

The magnitudes of the applied cyclic stress ratios required to liquefy a 35% relative density saturated sand deposit, in situ, were determined approximately from the field performance plots shown in Figures 3.1 and 3.2. Given that the standard penetration resistance of such a sand is approximately equal to 5 (for a $D_R \approx 35\%$ sand), the

cyclic stress ratio required to liquefy this sand in 15 cycles of loading is estimated (from Figure 3.1) to be about 0.07. Since trains typically generate around 100 representative cycles of loading, and the stress ratio required to liquefy a sand in 100 cycles is about three-quarters of that required to liquefy the same sand in 15 cycles (see Figure 3.3), the value obtained above was multiplied by a factor of 0.75. Therefore the applied cyclic stress ratio required to liquefy a 35% relative density saturated sand (subjected to an overburden pressure of approximately 1 ksc) in-situ in 100 cycles, was estimated to be $0.07 \times 0.75 = 0.05$. The resulting values of cyclic loading resistance plotted as the dashed lines in Figures 5.19, 5.20, and 5.21 were obtained by adjusting this value of 0.05 for overburden effects using the values of K_σ shown in Figure 3.4.

It may be seen from these figures that analyses using the shear stress approach indicate that trains be capable of liquefying sands within level sites to distances somewhat greater than 10 ft from the tracks. For example, ground motions with peak surface accelerations of about 0.04g are predicted to cause liquefaction within the upper 2 ft of a loose sand deposit (see Figure 5.19), thereby suggesting that liquefaction may occur within such deposits, provided that the water table is at the ground surface, at distances as far as about 25 ft from the nearest rail (refer to Figure 4.4). Because the stresses generated by Rayleigh waves decrease rapidly with depth, liquefaction is confined mainly to the surface layers, and hence the maximum distance of liquefaction is computed to be heavily dependent on the depth of the water table.

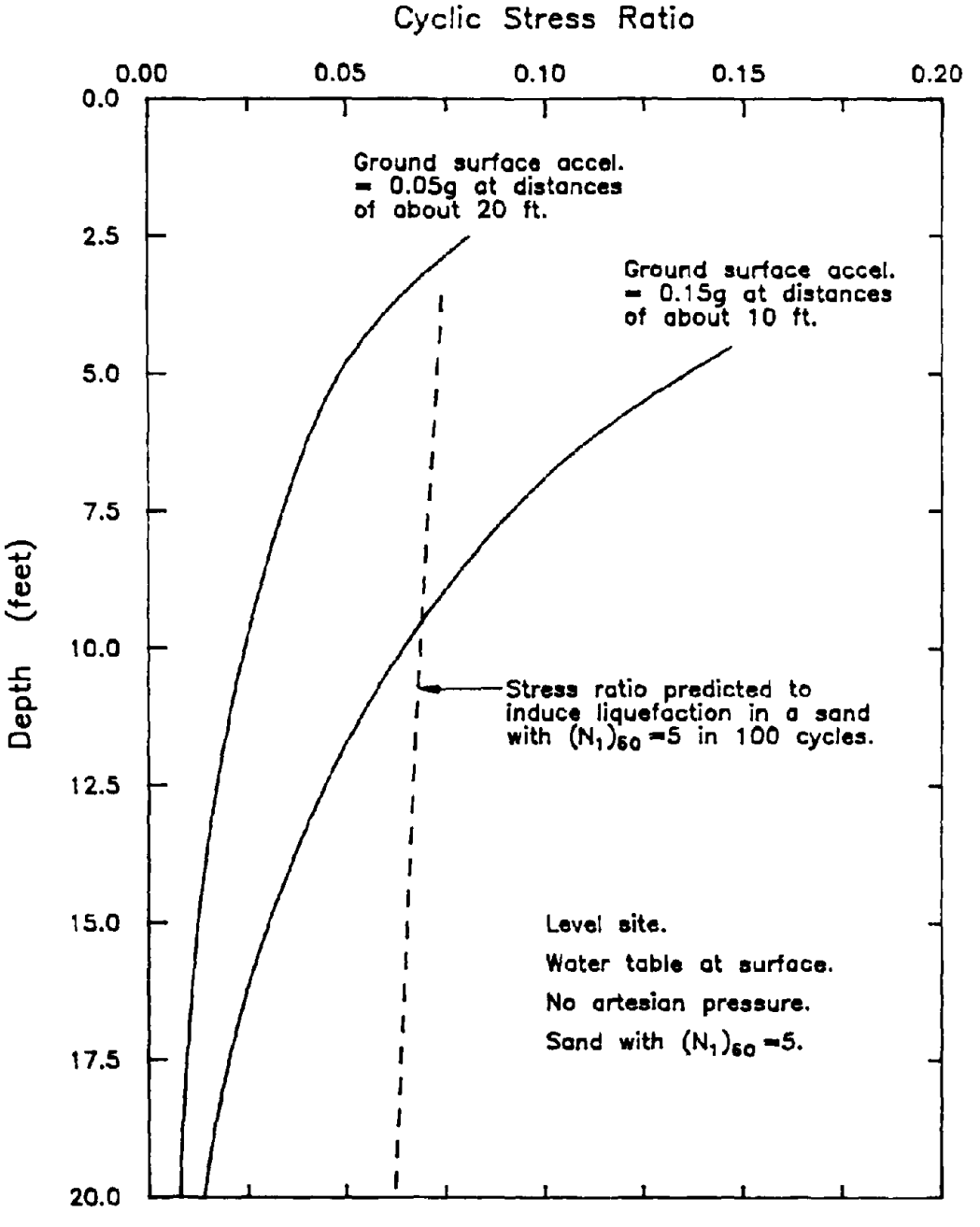

FIG 5.19 COMPARISON OF THE MAXIMUM CYCLIC STRESS RATIOS INDUCED WITHIN LEVEL SAND SITES WITH WATER TABLES AT THE SURFACE, WITH THE CYCLIC STRESS RATIOS REQUIRED TO CAUSE LIQUEFACTION.

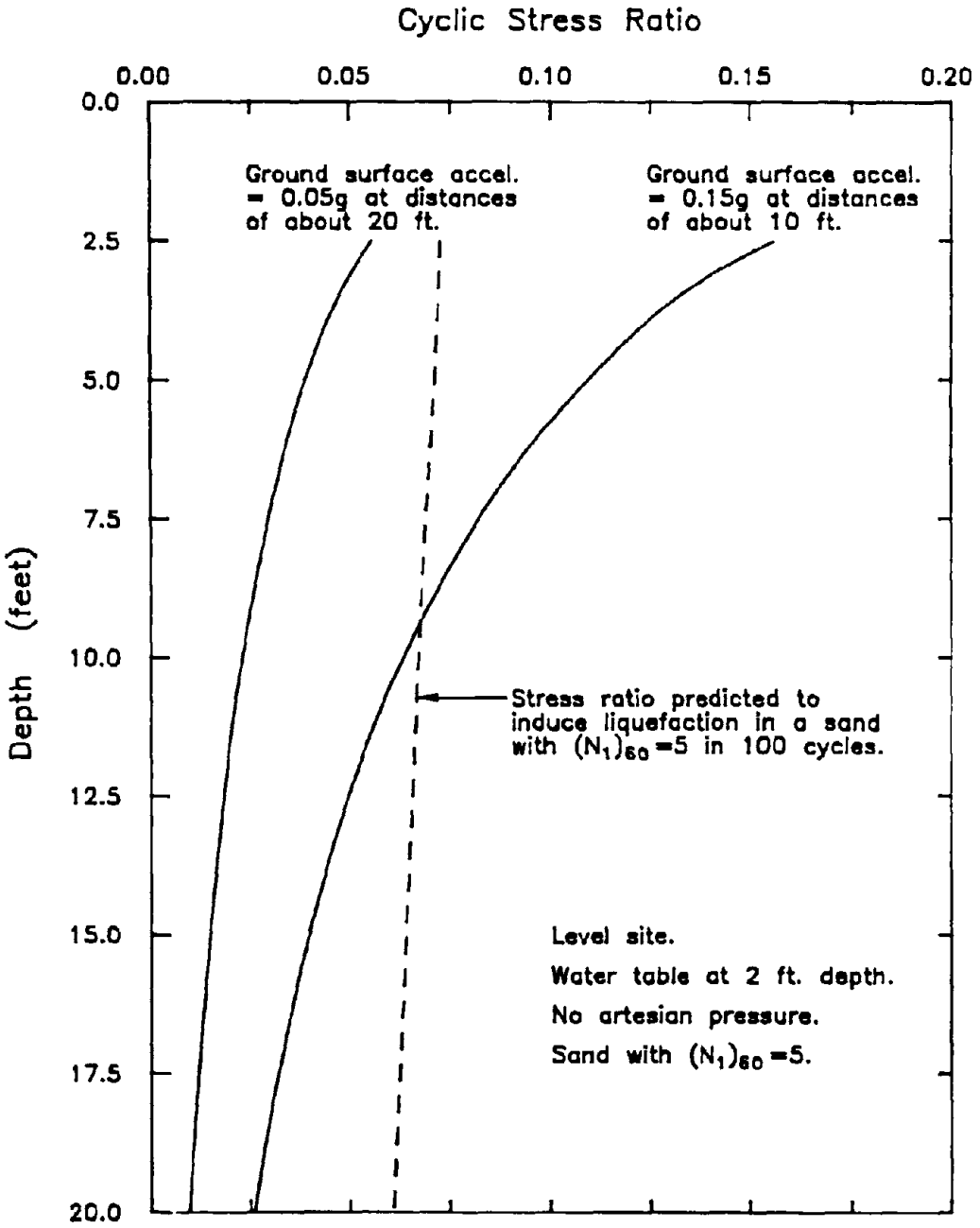

FIG 5.20 COMPARISON OF THE MAXIMUM CYCLIC STRESS RATIOS INDUCED WITHIN LEVEL SAND SITES WITH WATER TABLES AT 2 FEET DEPTH, WITH THE CYCLIC STRESS RATIOS REQUIRED TO CAUSE LIQUEFACTION.

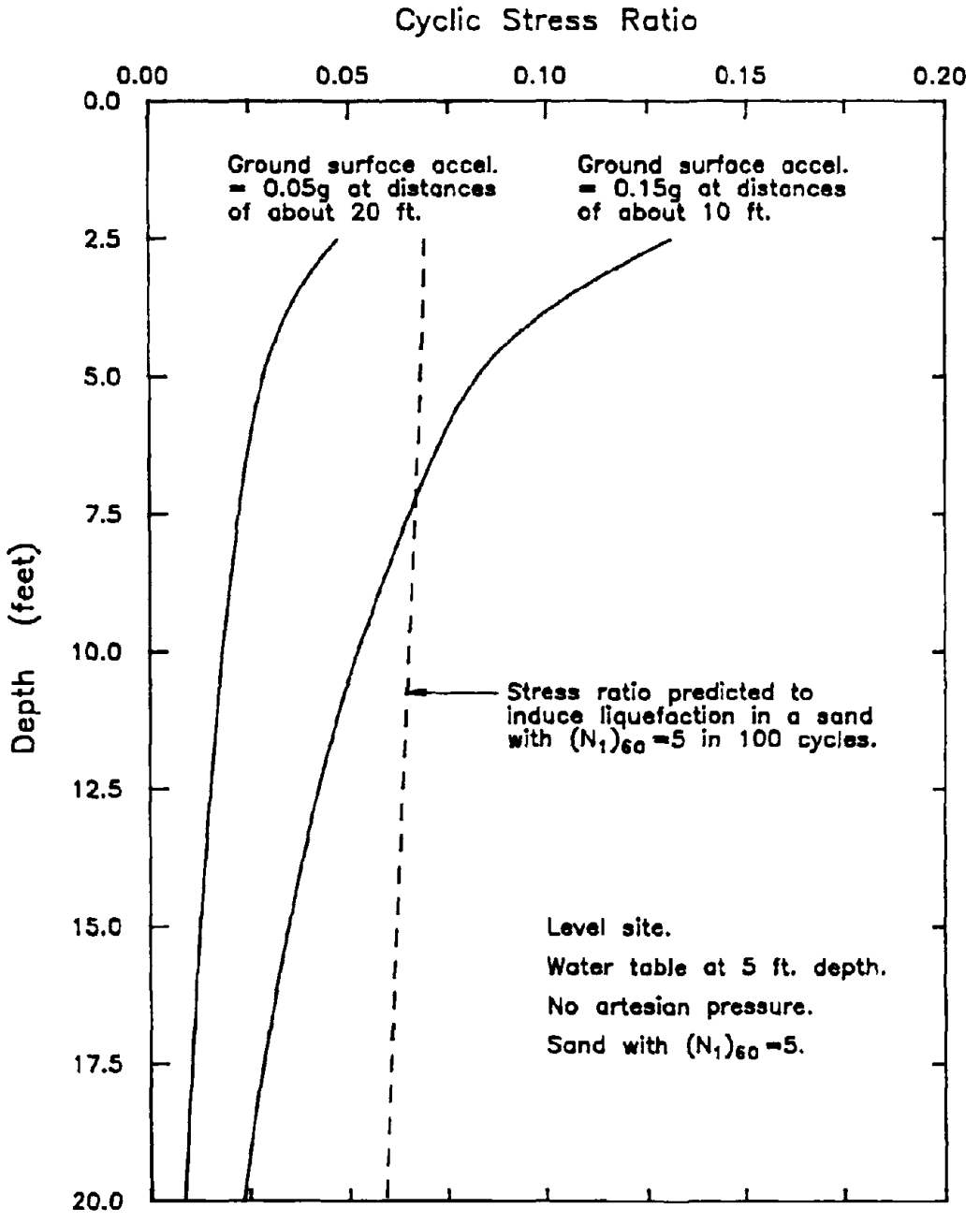

FIG 5.21 COMPARISON OF THE MAXIMUM CYCLIC STRESS RATIOS INDUCED WITHIN LEVEL SAND SITES WITH WATER TABLES AT 5 FEET DEPTH, WITH THE CYCLIC STRESS RATIOS REQUIRED TO CAUSE LIQUEFACTION.

The practical significance of this result, however, requires that consideration be given to the effects of several other factors including: (1) the fact that very few railroad tracks are likely to pass over 35% relative density sand deposits; (2) the water table at most sites is very rarely coincident with the ground surface; and (3) most sands adjacent to railroad tracks have probably been subjected to a significant number of cycles of prior shaking during construction and during the passage of trains. The effects of these additional factors may cause the preceding analytical results to be more apparent than real.

The effect of water table height on the liquefaction potential of sand deposits subjected to train-induced ground vibrations is illustrated in Figures 5.19, 5.20 and 5.21. These figures show that as the depth of the water table (below the ground surface) is increased, the level of shaking required to induce liquefaction is also increased, resulting in a marked reduction in the maximum distance at which liquefaction is predicted to occur. For example, the cyclic shear stresses induced within a level sand site with a water table at a depth of 5 ft, at a distance of 10 ft from the tracks, are unlikely to exceed the levels of applied cyclic shear stress required to liquefy a 35% relative density sand (Figure 5.21). In comparison, when the water is at the ground surface, liquefaction is predicted to occur at distances as great as 25 ft from the tracks (see Figure 5.19). Since the water tables at most sand sites are located significantly below the ground surface, liquefaction is unlikely to occur at distances of 25 ft for the majority of level sites.

The other factor which can be expected to affect (increase) the liquefaction resistance of a loose saturated sand deposit is prior shaking, and this effect was taken into account by adjusting the liquefaction resistance values as described later. The effect of prior shaking is particularly significant when analyzing train-induced ground vibrations, because (as previously noted) the prior passage of a single train may have generated over 100 cycles of loading. Since water tables at, or above the ground surface (the most critical case), are most likely to have arisen as a result of either flooding or exceptionally high precipitation, the sand near the surface was probably shaken by the passage of earlier trains while it was in an unsaturated state.

The effect of such dry pre-loading on the liquefaction resistance of loose sands was examined by Szerdy (1985), who conducted laboratory tests on samples of Sacramento River fine sand. These tests showed that the cyclic stress ratio required to liquefy 35% relative density sand samples in 100 cycles, after 1000 cycles of dry preloading at the same level of cyclic shear stress, is approximately 60% larger in magnitude than the cyclic stress ratio required to liquefy the same sand, subjected to no preloading, in the same number of cycles. Thus, the values of cyclic stress ratio required to induce liquefaction (and shown in Figures 5.19, 5.20 and 5.21) were also increased by about 60%. The modified values are plotted in Figures 5.22, 5.23 and 5.24 for comparison with the train-induced stresses.

Examination of these latter figures shows that when the effect of prior shaking is taken into account, the maximum distance at which liquefaction is predicted to occur is significantly reduced. For example, Figure 5.22 implies that for level sites, even with

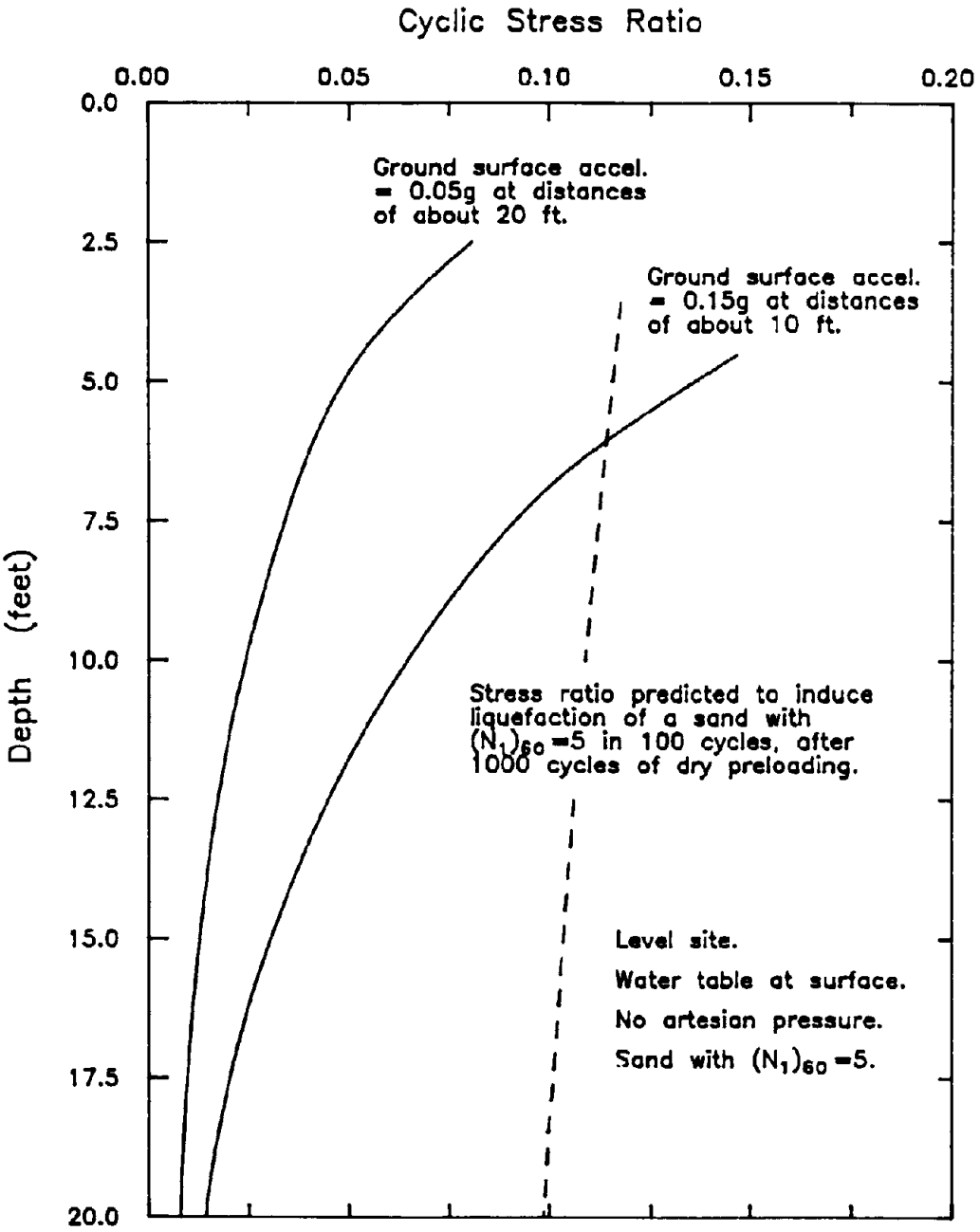

FIG 5.22 COMPARISON OF THE MAXIMUM CYCLIC STRESS RATIOS INDUCED WITHIN LEVEL SAND SITES WITH WATER TABLES AT THE SURFACE. WITH THE CYCLIC STRESS RATIOS REQUIRED TO CAUSE LIQUEFACTION AFTER 1000 CYCLES OF DRY PRELOADING.

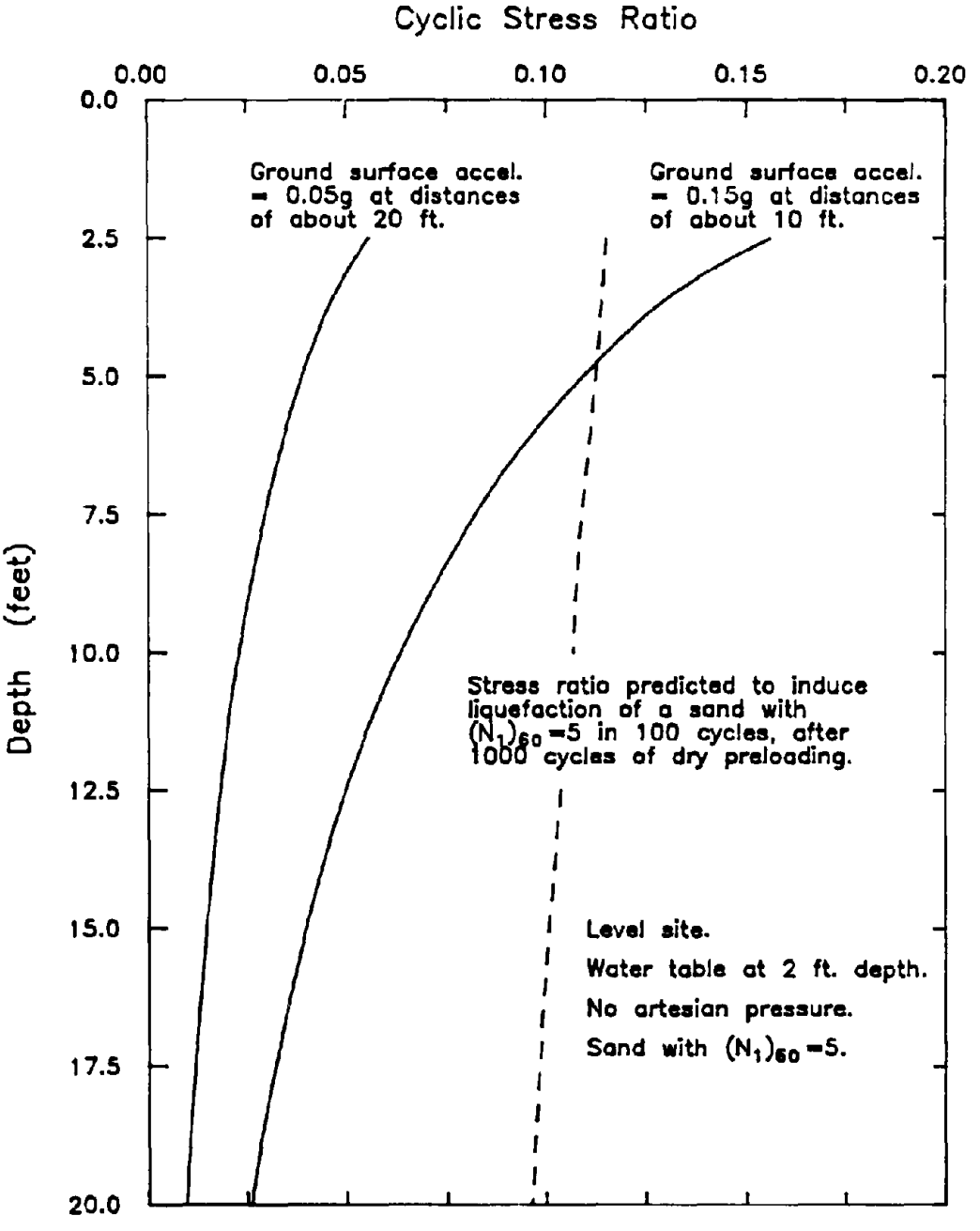

FIG 5.23 COMPARISON OF THE MAXIMUM CYCLIC STRESS RATIOS INDUCED WITHIN LEVEL SAND SITES WITH WATER TABLES AT 2 FEET DEPTH, WITH THE CYCLIC STRESS RATIOS REQUIRED TO CAUSE LIQUEFACTION AFTER 1000 CYCLES OF DRY PRELOADING.

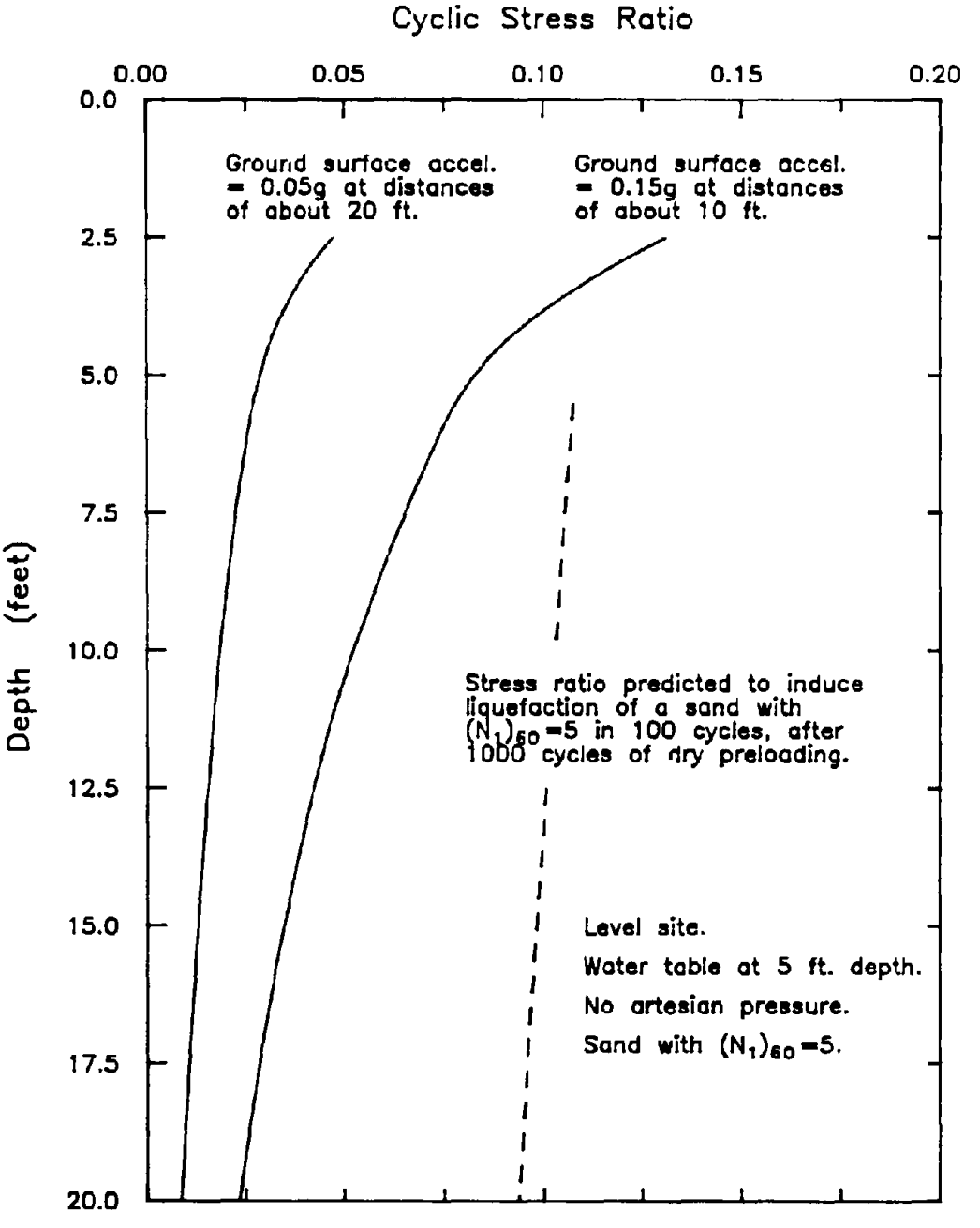

FIG 5.24 COMPARISON OF THE MAXIMUM CYCLIC STRESS RATIOS INDUCED WITHIN LEVEL SAND SITES WITH WATER TABLES AT 5 FEET DEPTH, WITH THE CYCLIC STRESS RATIOS REQUIRED TO CAUSE LIQUEFACTION AFTER 1000 CYCLES OF DRY PRELOADING.

a water table coincident with the ground surface, liquefaction is unlikely to occur at distances greater than about 15 ft from the tracks and that it is limited to the upper 6 ft of the sand deposit at a distance of about 10 ft from the tracks. In comparison, Figure 5.19 implies that trains might be capable of liquefying loose saturated sands (within the same site) subjected to no preshaking at distances up to about 25 ft and down to a depth of about 9 ft at a distance of 10 ft from the tracks. It is important to note that when the effects of prior shaking are taken into account, liquefaction is not predicted to occur, even at distances as close as 10 ft from the nearest rail, within loose sand sites with water tables more than 3 ft below the surface.

Thus, in summary, it appears that according to the shear stress approach, the ground vibrations generated by trains are probably incapable of liquefying level, saturated, loose sand deposits located at distances greater than about 10 ft from the tracks in all but exceptional cases. This prediction seems to be reasonable since it is both similar to the conclusion reached by following the shear strain approach, and consistent with the fact that no case histories involving train-induced liquefaction failures of level ground were found in the literature.

5.5. Effects of Train Vibrations on Liquefaction Potential for Sloping Sites

While no effects of liquefaction appear to have been reported for level ground, it seems likely that the ground vibrations generated by trains have caused sloping deposits to liquefy at significantly greater distances from the tracks. Several such failures are listed in Table 1.1. The suggestion that these vibrations might be capable of

triggering liquefaction within one type of site and not the other is considered to be plausible for the following reasons: (1) the sands within sloping deposits may be subjected to reasonably high values of initial static shear stress while no such stresses are likely to exist within level sites and (2), recent research has shown that the cyclic liquefaction resistance of loose sands decreases significantly with increasing level of initial shear stress/normal stress ratio (refer to Figure 3.5).

The possible effects of these initial static shear stresses on the liquefaction potential of sand deposits subjected to train-induced ground shaking were evaluated by first computing the magnitudes of the cyclic stress ratios induced within a hypothetical, 10 degree, 35% relative density saturated sand slope. These ratios were then compared with the magnitudes of the cyclic stress ratios required to cause liquefaction of the sand within the slope. The effect of these stresses could not be evaluated by performing shear strain analyses because the strain approach appears to account for the presence of initial shear stresses by measuring shear moduli in-situ and no relationships relating changes in initial shear stress to changes in shear moduli were found.

The magnitudes of the initial static shear stress/normal stress ratios present within a slope (on any plane parallel to the ground surface) may be determined approximately from Equations 5.8 and 5.9 below, both of which were derived using infinite slope theory. Equation 5.8 applies to submerged slopes while Equation 5.9 applies to slopes with water tables coincident with the ground surface and seepage occurring down the slope and parallel to the surface.

$$\frac{\tau_\alpha}{\sigma'_{n\alpha}} = \frac{\gamma' \cdot h_v \cdot \cos\alpha \cdot \sin\alpha}{(\gamma' \cdot h_v \cdot \cos^2\alpha) - u_e} \qquad 5.8$$

$$\frac{\tau_\alpha}{\sigma'_{n\alpha}} = \frac{\gamma_b \cdot h_v \cdot \cos\alpha \cdot \sin\alpha}{(\gamma' \cdot h_v \cdot \cos^2\alpha) - u_e} \qquad 5.9$$

where $\frac{\tau_\alpha}{\sigma'_{n\alpha}}$ = initial shear stress/normal stress ratio acting on any plane parallel to the ground surface,
γ_b = bulk density of soil,
γ' = effective density of soil,
h_v = vertical height from plane to surface,
α = slope of ground surface, and
u_e = excess pore pressure acting at depth of plane being considered

These values may then be used in conjunction with Figure 3.5 and the field performance plots shown in Figures 3.1 and 3.2 to determine the liquefaction resistance of the sands within various slopes. For example, the initial shear stress/normal stress ratio predicted to exist (on any plane parallel to the ground surface) within the submerged 10 degree slope when there are no artesian pressures present in the deposit, is calculated to be about 0.18 (from Equation 5.8). Referring to Figure 3.4, this value implies that the cyclic stress ratios required to liquefy loose sands within such a slope may be about 25% smaller in magnitude than the stress ratios required to liquefy the same sand within a level site. Since the cyclic stress ratios induced on any plane parallel to the ground surface (within the 10 degree slope) are only slightly smaller in magnitude than the ratios induced within level sites (subjected to the same level of shaking), it therefore appears that significantly lower levels of shaking are required to

liquefy the sands within sloping sites than the same sands within level sites.

The magnitudes of the cyclic stress ratios required to cause liquefaction within the 10 degree slope described above, were obtained by multiplying the values of required cyclic stress ratio shown in Figures 5.19 and 5.22 for level sites by a factor of 0.75, as indicated previously. These corrected ratios are shown in Figures 5.25 and 5.26 together with the values of cyclic shear stress ratio predicted to be induced within the site on planes parallel to the ground surface. It may be seen from these latter figures that reducing the required cyclic stress ratios by a factor of 25% significantly increases the distance at which liquefaction is predicted to occur from the tracks. For example, Figure 5.26 implies that the cyclic shear stresses associated with peak ground surface accelerations greater than about 0.06g are capable of liquefying loose saturated sands more than 2 ft below the ground surface, thereby suggesting that the ground vibrations generated by trains may be capable of liquefying loose sands at distances up to about 20 ft from the nearest rail (see Figure 4.4). As a comparison, train-induced ground vibrations are predicted to be incapable of liquefying the same loose sands within level sites at distances greater than about 15 ft from the tracks (refer to Figure 5.22). Both of these latter analyses include the effect of 1000 cycles of dry preshaking on the liquefaction resistance of the sand.

The same approach was also used to evaluate the liquefaction potential of a hypothetical 10 degree loose sand slope with seepage down the slope, and since the initial shear stresses that are present within such slopes are significantly larger in magnitude that the initial shear stresses present within submerged slopes, the maximum

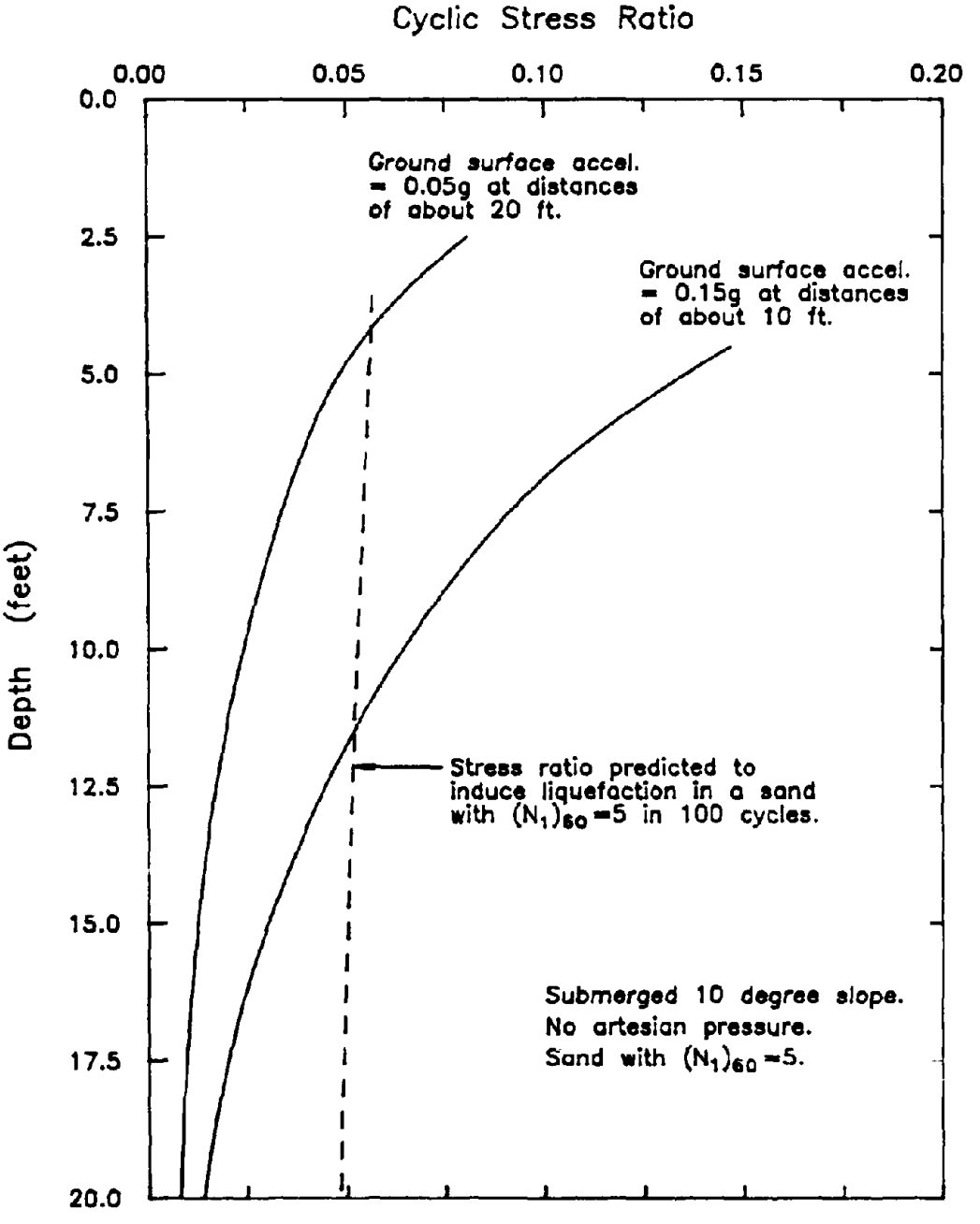

FIG 5.25 COMPARISON OF THE MAXIMUM CYCLIC STRESS RATIOS INDUCED WITHIN SUBMERGED, 10 DEGREE, SAND SLOPES, WITH THE CYCLIC STRESS RATIOS REQUIRED TO CAUSE LIQUEFACTION IN 100 CYCLES.

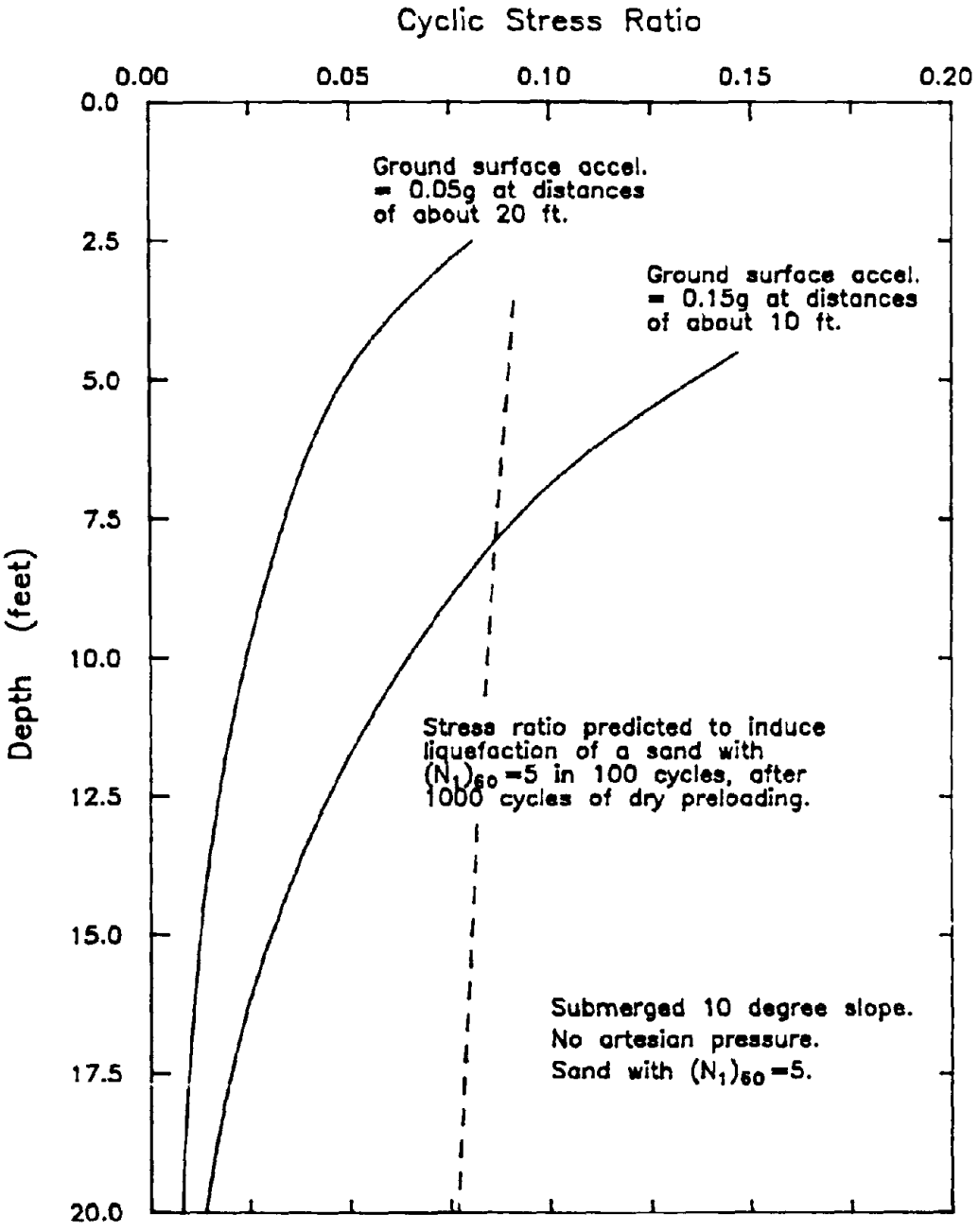

FIG 5.26 COMPARISON OF THE MAXIMUM CYCLIC STRESS RATIOS INDUCED WITHIN SUBMERGED, 10 DEGREE, SAND SLOPES, WITH THE CYCLIC STRESS RATIOS REQUIRED TO CAUSE LIQUEFACTION IN 100 CYCLES, AFTER 1000 CYCLES OF DRY PRELOADING.

distances at which liquefaction is predicted to occur are also much greater. The results of this seepage analysis are summarized in Figures 5.27 and 5.28 and these figures show that the maximum distance from the tracks at which liquefaction was predicted to occur is about 80 ft. Since the effect of prior shaking was not taken into account when computing this distance, 80 ft probably represents an extreme value for 10 degree slopes and a value of about 45 ft is considered to be a more realistic maximum.

Thus, it may be concluded from the shear stress analysis that even though train-induced ground vibrations do not appear to be capable of liquefying the majority of level, loose sand deposits, they may well be capable of inducing liquefaction in similar deposits that are subjected to high values of initial static shear stress. For example, the applied cyclic shear stresses generated by trains are predicted to be capable of causing the liquefaction of loose sands within 10 degree slopes (with downslope seepage) at distances of up to about 45 ft from the tracks, and possibly up to about 80 ft in extreme cases. Because steeper slopes tend to contain higher initial shear stress/normal stress ratios than flatter slopes (with similar seepage conditions), and the liquefaction resistance of loose sands decreases as the magnitudes of these ratios are increased, trains are theoretically capable of liquefying more critical sand deposits at distances greater than 80 ft from the tracks.

5.6. Summary

Despite the fact that trains are commonly perceived to be a source of significant ground vibrations, the ground vibrations generated by trains appear to have caused a

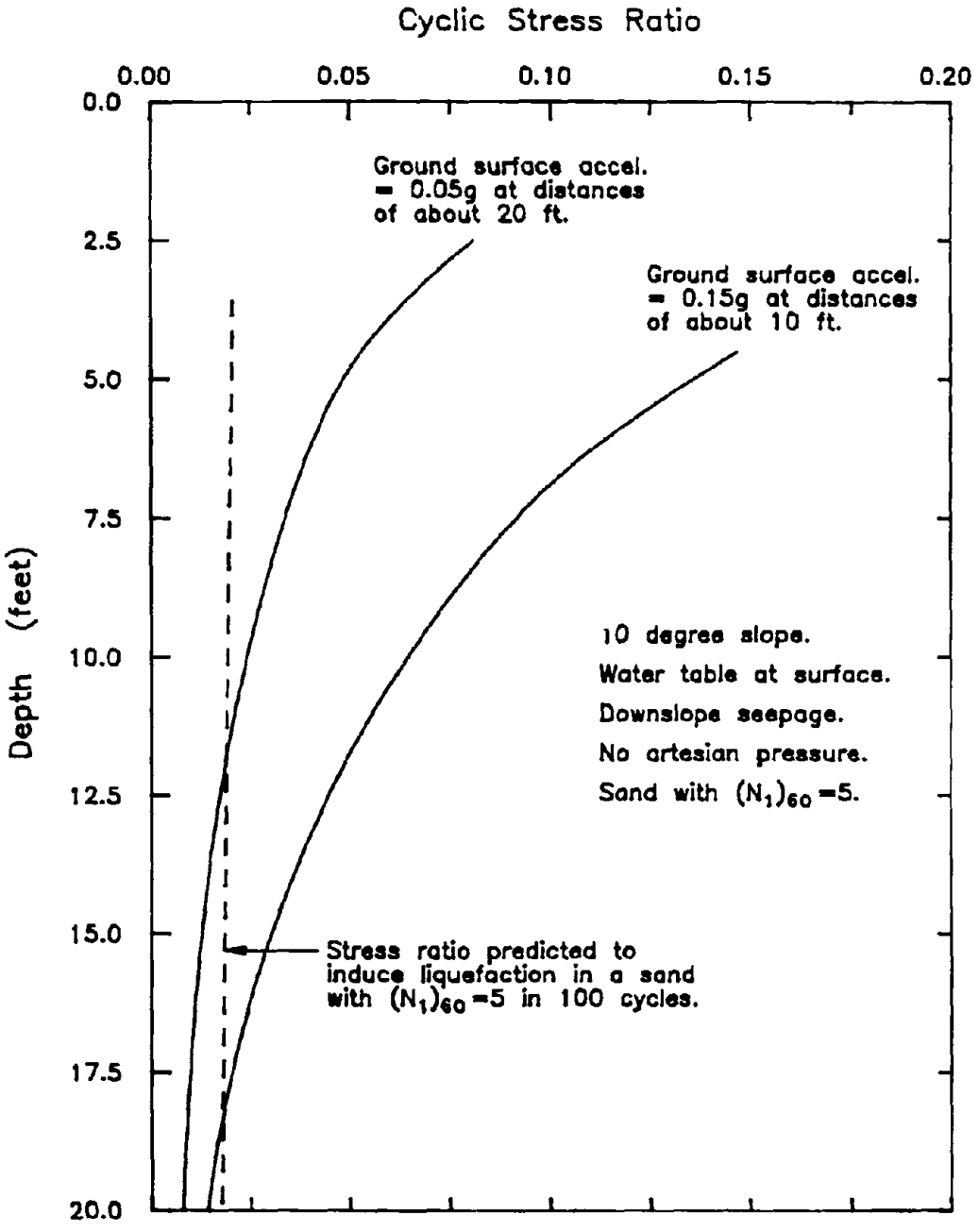

FIG 5.27 COMPARISON OF THE MAXIMUM CYCLIC STRESS RATIOS INDUCED WITHIN SUBMERGED, 10 DEGREE, SAND SLOPES WITH SEEPAGE OCCURING DOWN THE SLOPE, WITH THE CYCLIC STRESS RATIOS REQUIRED TO CAUSE LIQUEFACTION IN 100 CYCLES.

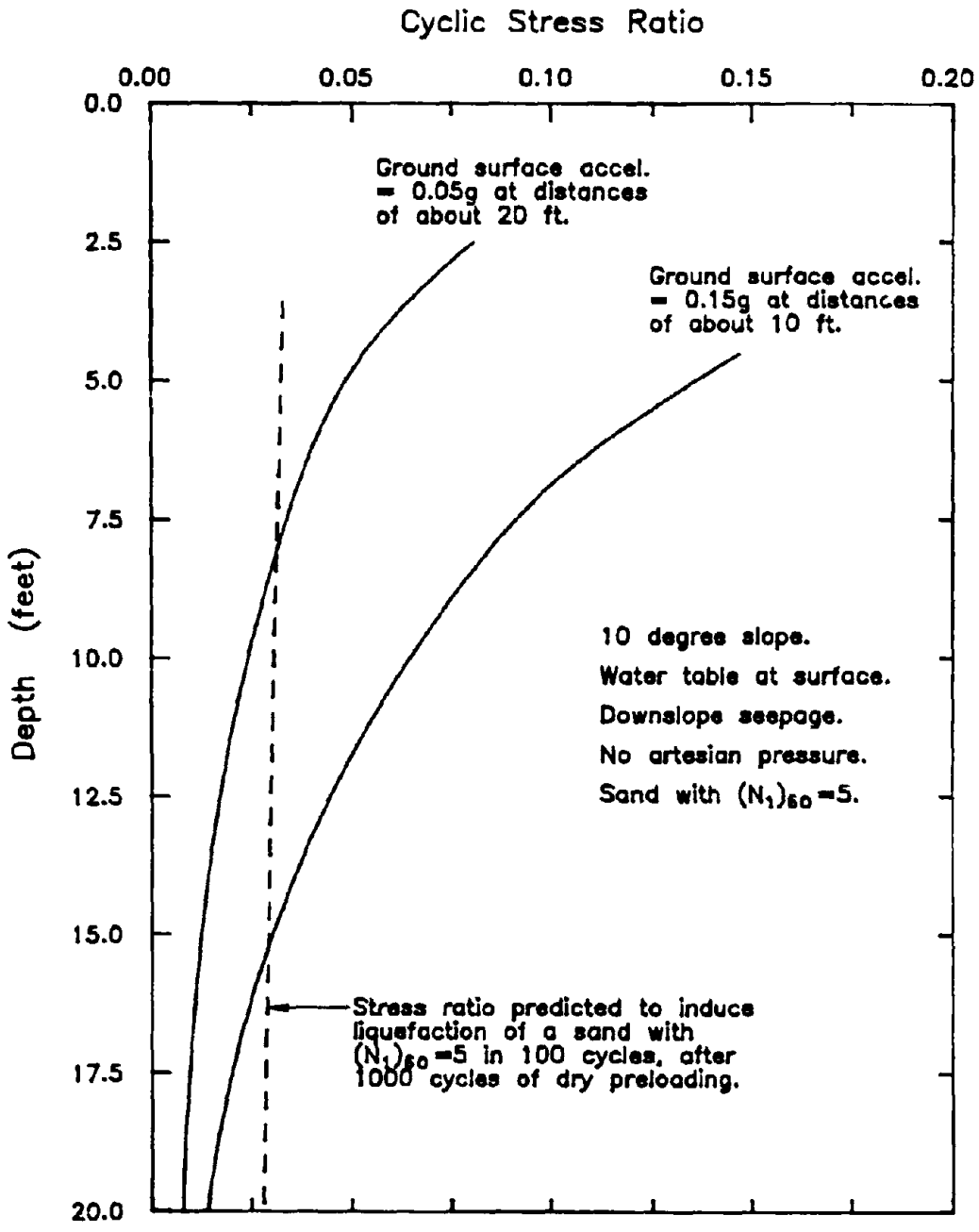

FIG 5.28 COMPARISON OF THE MAXIMUM CYCLIC STRESS RATIOS INDUCED WITHIN SUBMERGED, 10 DEGREE, SAND SLOPES WITH SEEPAGE OCCURING DOWN THE SLOPE, WITH THE CYCLIC STRESS RATIOS REQUIRED TO CAUSE LIQUEFACTION IN 100 CYCLES, AFTER 1000 CYCLES OF DRY PRELOADING.

relatively small number of liquefaction failures (several are listed in Table 1.1). All of these failures seem to have occurred within deposits containing sloping sand seams or layers. Because the sands within such deposits are subject to initial static shear stresses and the liquefaction resistance of loose sands subjected to such stresses is reported to decrease as the magnitudes of the initial static shear stress/normal stress ratios are increased, it may well be that train-induced ground vibrations are only capable of liquefying loose sand deposits subjected to reasonably high values of initial static shear stress, a supposition that is generally supported by the shear strain and shear stress analyses, described in this chapter.

The liquefaction potentials of level loose sand sites subjected to train-induced ground vibrations, for example, were evaluated by following both the shear strain and the shear stress approaches and since the levels of cyclic shear strain, predicted to be generated within the level sites that were analyzed, were only slightly greater in magnitude than the threshold strains for most sands, it seemed reasonable to conclude that the ground vibrations generated by trains are probably incapable of liquefying sands at distances greater than about 10 ft from the nearest rail; analyses were not performed at distances closer than 10 ft from the rail.

The same general conclusion was also reached for those level sites analyzed using the shear stress approach. However while none of the shear strain analyses predicted that these sites would liquefy at distances beyond 10 ft from the tracks (see Figure 5.29), analyses using the shear stress approach indicated that liquefaction might occur up to distances of about 20 ft from the track under certain site conditions (Figure

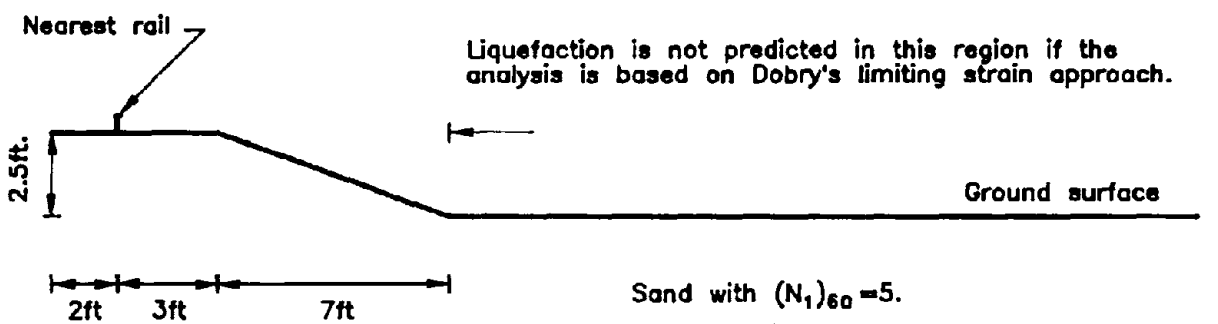

FIG 5.29 MAXIMUM DISTANCE AT WHICH TRAINS ARE LIKELY TO INDUCE LIQUEFACTION WITHIN LEVEL, LOOSE SAND SITES, ACCORDING TO SHEAR STRAIN THEORY.

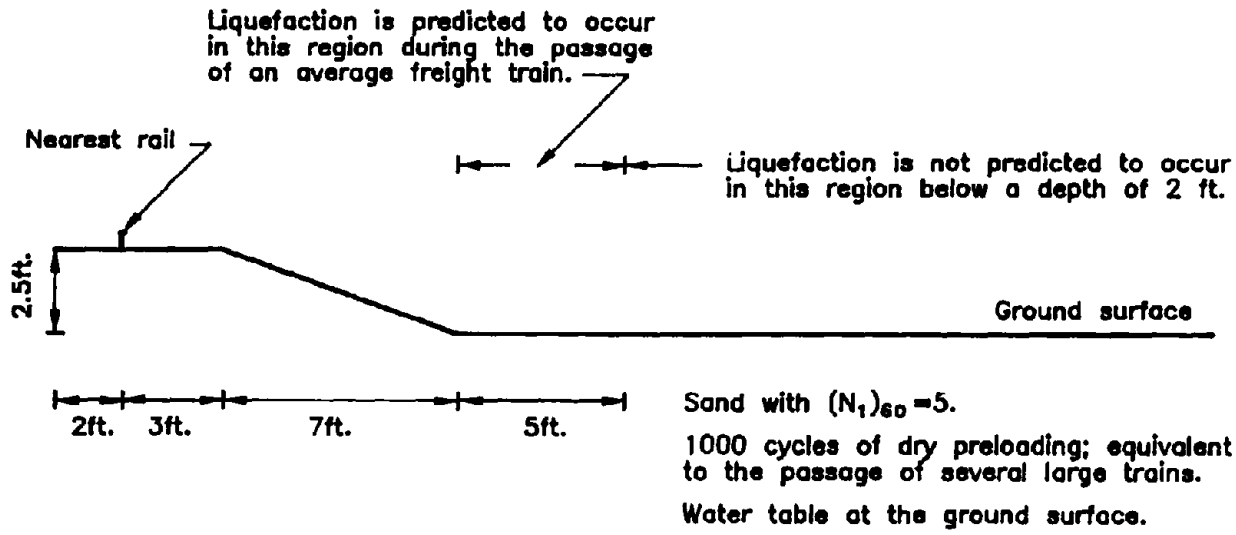

FIG 5.30 MAXIMUM DISTANCE AT WHICH TRAINS ARE LIKELY TO INDUCE LIQUEFACTION WITHIN LEVEL, LOOSE SAND SITES WITH WATER TABLES AT THE GROUND SURFACE, ACCORDING TO SHEAR STRESS THEORY.

5.30). Because the water tables at most sand sites probably lie more than 3 ft below the ground surface and the sands at all sites have almost certainly been subjected to thousands of cycles of prior shaking, most level sand sites are not predicted to liquefy at distances greater than about 10 ft from the tracks as shown in Figure 5.31.

The results of the shear stress analyses performed for sloping ground are summarized in Figures 5.32, 5.33, and 5.34 and as noted previously, the findings of these analyses support the observation that the ground vibrations generated by trains appear to be capable of liquefying loose sand deposits subjected to initial static shear stresses. For example, Figure 5.33 shows that in extreme cases train-induced ground vibrations may well be capable of liquefying loose sands within 10 degree slopes (with seepage down the slope) to depths of about 20ft at a distance of about 10 ft from the tracks. At shallower depths, liquefaction may occur as much as 80 ft from the tracks. Since prior shaking significantly increases the cyclic loading resistance of loose sands, this maximum distance is probably closer to 45 ft in reality; however liquefaction is still predicted to occur down to depths of about 15 ft at 10 ft from the tracks. This maximum depth is important because two of the large scale liquefaction failures associated with trains and listed in Table 1.1, were attributed to the liquefaction of sand seams and lenses within the soil profile (Fellenius, 1953, Broms, 1978).

The first of these slides which occurred in the town of Surte, Sweden on September 29, 1950 involved the movement of approximately 4 million cubic yards of soil over distances up to about 500 ft (150 m). Sliding commenced as a train was pulling out of the station, a bus was arriving at the bus stop and pile driving was also in

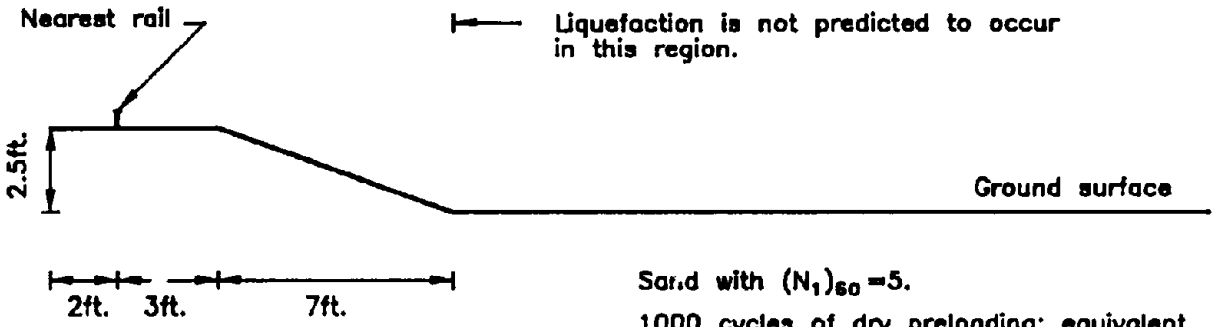

FIG 5.31 MAXIMUM DISTANCE AT WHICH TRAINS ARE LIKELY TO INDUCE LIQUEFACTION WITHIN LEVEL, LOOSE SAND SITES WITH WATER TABLES AT DEPTHS GREATER THAN ABOUT 3 FEET, ACCORDING TO SHEAR STRESS THEORY.

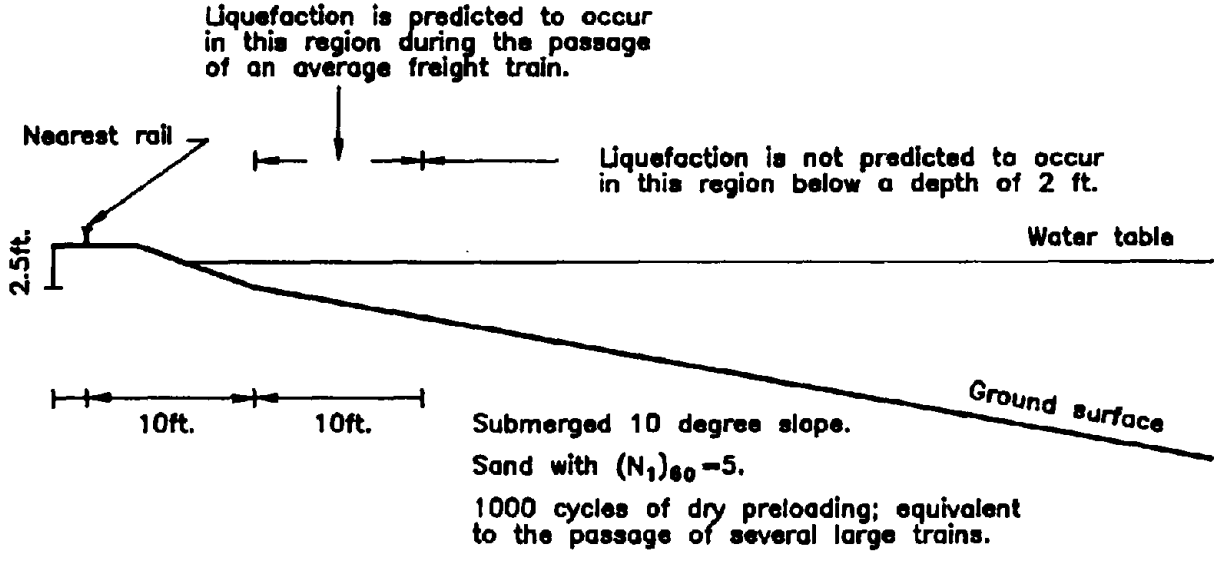

FIG 5.32 MAXIMUM DISTANCE AT WHICH TRAINS ARE LIKELY TO INDUCE LIQUEFACTION WITHIN SUBMERGED, 10 DEGREE, LOOSE SAND SLOPES, ACCORDING TO SHEAR STRESS THEORY.

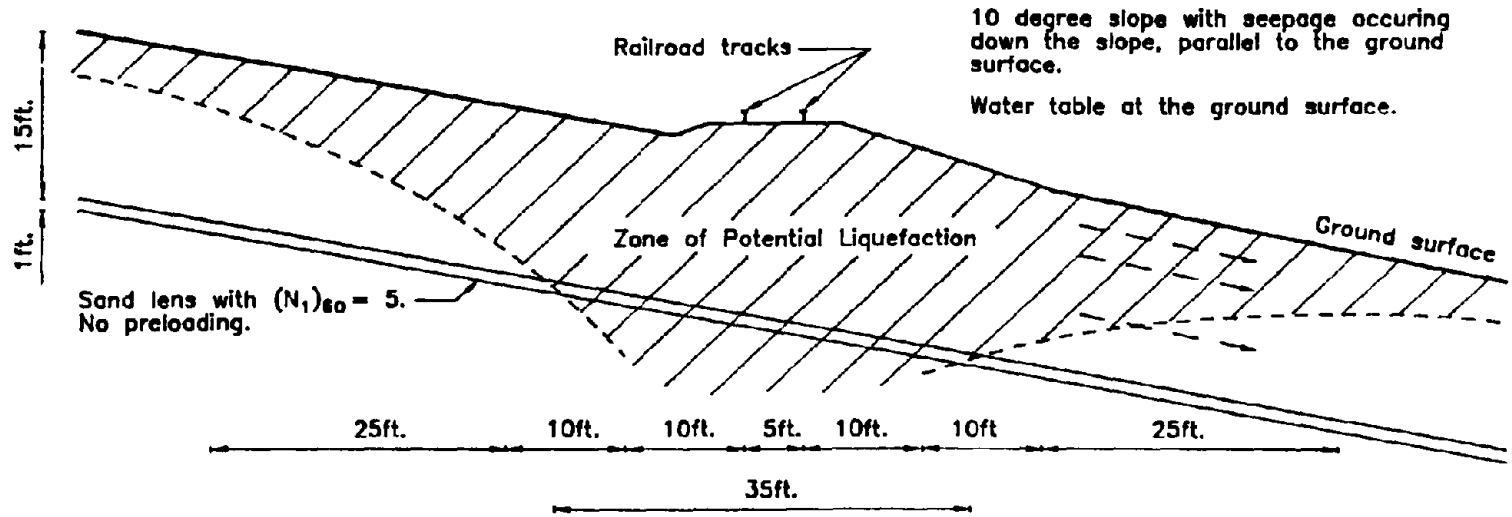

FIG 5.33 MAXIMUM DISTANCE AT WHICH TRAINS ARE LIKELY TO INDUCE LIQUEFACTION WITHIN 10 DEGREE, LOOSE SAND SLOPES (SUBJECTED TO NO PRELOADING) WITH SEEPAGE OCCURING DOWN THE SLOPE, ACCORDING TO SHEAR STRESS THEORY.

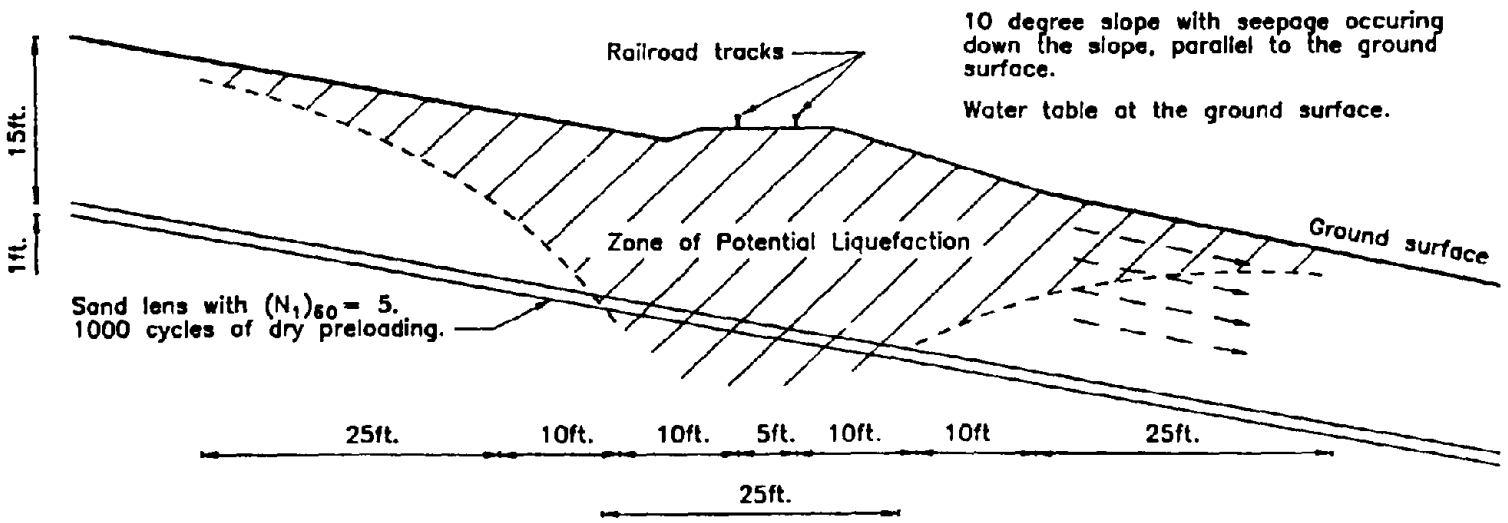

FIG 5.34 MAXIMUM DISTANCE AT WHICH TRAINS ARE LIKELY TO INDUCE LIQUEFACTION WITHIN 10 DEGREE, LOOSE SAND SLOPES (SUBJECTED TO 1000 CYCLES OF DRY PRELOADING) WITH SEEPAGE OCCURING DOWN THE SLOPE, ACCORDING TO SHEAR STRESS THEORY.

progress in the upper area of the slide (see Figure 5.35). Measurements made after the failure revealed that the soil profile consisted of about 35 ft (10 m) of normally consolidated sensitive clay overlying a similar clay containing sand and gravel lenses and seams. These lenses and seams contained significant excess pore pressures and the prevalent belief at the time was that these pressures were due to an artesian pressure condition existing in the slide before the failure. Cores taken at the site showed many slip surfaces but some of these may have been from earlier slides.

Several authors, including Szerdy (1985) and Broms (1978), suggest that the Surte failure probably resulted from the liquefaction of one or more of the saturated sand seams located between 35 ft and 60 ft below the ground surface. They also indicate that this liquefaction may have been caused by the ground vibrations generated by trains. However given that trains appear to be incapable of causing liquefaction over a significant area at depths greater than about 35 ft (implied by Figure 5.34) it seems unlikely that train-induced ground vibrations were responsible for this failure. Rather the ground vibrations generated by pile driving are considered to be a much more likely cause, a belief supported by the observation that the slide initiated close to the point where the piles were being driven (Broms, 1978). Most of the energy imparted by piles is applied at depth (as discussed in Section 2.5) and therefore is not confined to the surface layers as with trains.

The second slide occurred 3 years later along the banks of the Guntorp Brook in Sweden and involved around 30 thousand cubic yards of soil. This slide took place shortly after a train had passed across the top of the slide area. The soil profile at the

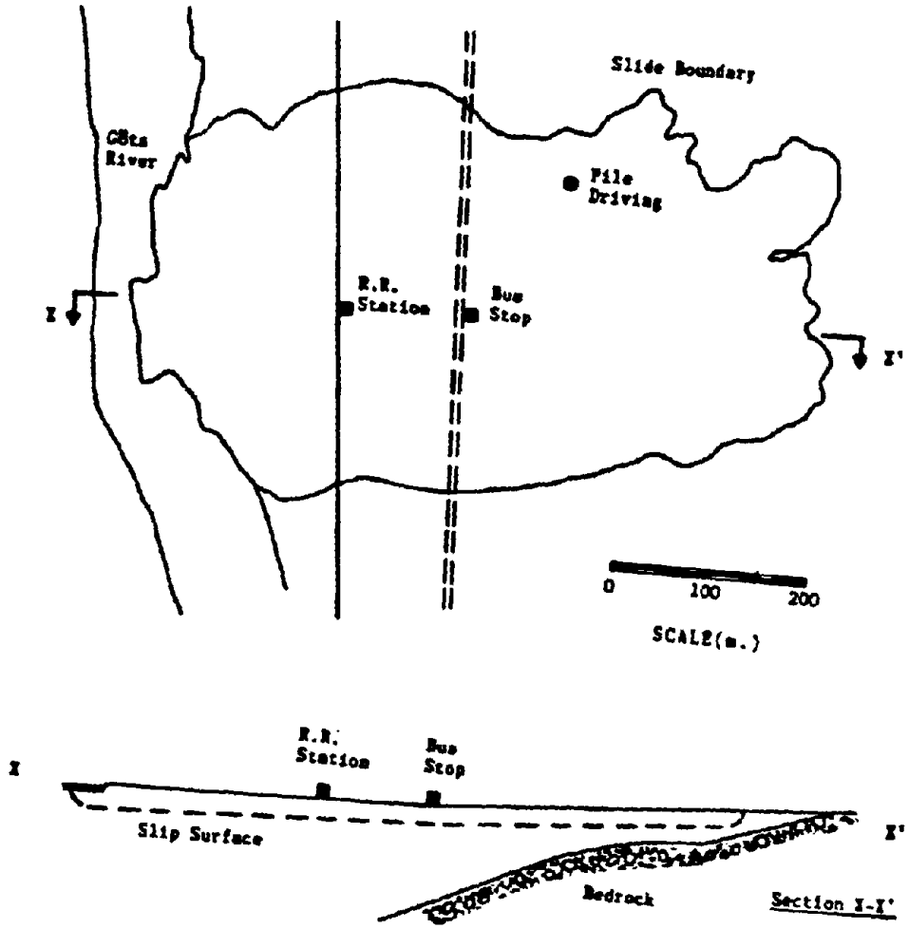

FIG 5.35 LANDSLIDE AT SURTE (after Jakobsen, 1952).

site consisted of a 35 to 50 ft (10 to 15 m) thick deposit of quick clay underlain by bedrock. Running through this layer was a 4 inch thick silt seam and within it, a 0.5 inch thick sand parting. Failure is believed to have occurred along this sand parting which varied in depth from about 15 ft to 40 ft (5 to 12 m) beneath the ground surface. Adjacent to the base of the embankment, about 50 ft from the nearest rail, this parting was only 15 ft below the surface; directly beneath the tracks, the same seam was at a depth of about 35 ft. Thus applying the results summarized in Figure 5.34 it seems improbable once again, that the ground vibrations generated by the train could have caused this failure.

However, around two months prior to the failure the railroad embankment at the top of the slide had settled about 2 to 4 inches (5 to 10 cm) and a large crack had appeared in the embankment, only days before the event. Therefore it was concluded that the slide was already moving and would have failed without the passage of the train, but that the train triggered the slide (Fellenius, 1953). Given that the slide was on the point of failure, the initial shear stress/normal stress ratios present within the sand parting would have been almost twice the value of those within the 10 degrees slope with seepage downslope. Since the cyclic shear stresses required to liquefy a loose sand decrease rapidly as the magnitudes of the initial static shear stress/normal stress ratios the sand are increased, it is therefore possible that these vibrations triggered the failure in this case.

CHAPTER 6

Effects of Artesian Pressure Conditions and Initial Static Shear Stresses on the Liquefaction Potential of Sand Sites Subjected to Earthquake Shaking

6.1. Introduction

Many researchers currently believe that liquefaction will not occur within a sand site unless the ground surface accelerations generated at the site exceed a value of about 0.05g to 0.10g. However, some evidence appears to suggest that accelerations as small as 0.02g may have been associated with liquefaction failures. The data supporting the various minimum levels are presented in this chapter together with the results of analytical studies undertaken to examine the effects of artesian pressure conditions and initial static shear stresses on the liquefaction potential of loose sand sites. These analyses were performed for both magnitude 8 and magnitude 5.25 earthquakes.

Unless otherwise stated, the minimum level of earthquake shaking capable of causing liquefaction in the field will simply be referred to as "the minimum level of shaking" and will be expressed in terms of the peak ground surface accelerations.

6.2. Evidence Supporting the Various Minimum Levels of Earthquake Shaking

The upper bound of the minimum level of shaking required to cause liquefaction is based on the relationships between Intensity (say as measured on the Modified

Mercalli Scale) and observed field performance. For example, the field evidence associated with Modified Mercalli (M.M.) shaking intensities VI and VII (as summarized by Brazee, 1980), are shown in Table 6.1. It may be seen from this table that Intensity VII is associated with "wet ground cracked", "water in streams and ponds became turbid and muddy" and "sand and mud are shifted horizontally on beaches on flat land"; all of these phenomena may be taken to be evidence of soil liquefaction. In contrast, M.M. shaking intensities of VI and smaller are not associated with any such evidence of possible liquefaction, leading to the conclusion that earthquake shaking of these intensities is never associated with soil liquefaction. Ground shaking of Modified Mercalli Intensity VI has been related to ground surface accelerations of the order of 0.06g (after Trifunac and Brady, 1975) and 0.08g (Krinitzky and Chang, 1987). From this it may be inferred that this level of shaking may be the minimum level of shaking capable of liquefying sand deposits in the field.

Support for what may be a relatively high minimum level (as discussed later), is also provided by the results of studies such as those reported by Iwasaki et al (1978b), Tokimatsu and Yoshimi (1983), and Dobry et al (1981a). The first two studies examined the relationship between the liquefaction characteristics of sands as determined from field tests, laboratory tests on undisturbed samples, and standard penetration resistance. The results of these studies led the investigators to conclude that a cyclic stress ratio (τ_{av} / σ_o') of about 0.05 is required to cause liquefaction of a 20 to 25% relative density sand under level site conditions. Sands of this density are probably as loose as the loosest natural deposits. The relationship between peak ground surface

Table 6.1 : Earthquake Effects According to Intensity (MM) (after Brazee, 1980)

"MM Intensity"		"Earthquake Effects"
VI	a.	Liquids were spilled from containers.
	b.	Roaring sounds were reported.
	c.	Slight damage was incurred. Poor construction was sometimes specified.
	e.	Buildings trembled throughout.
	f.	Small, unstable objects were overturned.
	g.	Some furniture of moderately heavy kind (chairs, tables, small sofas, small dressers, etc.) were moved from position.
	h.	Water or gas pipes were broken in isolated instances.
	i.	Trees and bushes were shaken strongly.
	j.	Plaster fell in small-to-moderate amounts. Chimneys were cracked.
	k.	Some dishes, glassware, and windows were broken.
	l.	Damage was negligible in well-designed structures and structures of good construction.
	m.	Vibrations were reported comparable to those caused by heavy or heavily loaded trucks.
VII	a.	Free-standing and exterior masonary walls were cracked.
	b.	Well-built ordinary structures were damaged slightly to moderately.
	c.	Cornices, brickwork, tiles and stones fell from exterior walls and parapets of buildings.
	d.	Several landslides were reported. Small quantities of rocks and boulders were shaken from hillsides and embankments in single instances.
	e.	Chimneys were broken. Chimneys with a ratio of height above roof to lateral dimension at roof exceeding 5, were broken sharply at roof-line.
	f.	Wet ground cracked (no qualifying adjectives).
	g.	Some found it difficult to stand. Persons were made to move unsteadily.
	h.	Water in streams and ponds became turbid and muddy.
	i.	Waves were produced on ponds, lakes, reservoirs and running water.
	j.	Sand and mud were shifted horizontally on beaches and flat land.

acceleration and the cyclic stress ratio applied to a representative element of sand within a sand deposit, may be determined from the following equation:

$$\frac{\tau_{av}}{\sigma_o'} \approx 0.65 \cdot \frac{\sigma_o}{\sigma_o'} \cdot \frac{a_{max}}{g} \cdot r_d \qquad 6.1$$

Assuming the water table to be about 4 ft below the ground surface and considering a representative element at a depth of 15 ft, this equation leads to (since $r_d \approx 0.95$ at a depth of 15 ft, Seed and Idriss, 1983):

$$\tau_{av} \approx 0.65 \cdot \frac{1800\ psf}{1140\ psf} \cdot \frac{a_{max}}{g} \cdot 0.95 \approx \frac{a_{max}}{g} \qquad 6.2$$

Thus liquefaction is not predicted to occur unless:

$$\tau_{av} \approx \frac{a_{max}}{g} > 0.05 \qquad 6.3$$

$$i.e. \quad a_{max} > 0.05g$$

The other set of studies referred to, are those reported by Dobry et al (1981) and as previously noted in Section 3.2 (and summarized in Table 3.1), these studies imply that sands are unlikely to liquefy unless the applied cyclic shear strain exceeds a value of about 0.01% (the threshold strain for the sand). Further, since significant pore pressures do not appear to be generated unless the applied shear strain significantly exceeds this value (see Figure 3.9), the level of shaking computed using the threshold strain, γ_{th}, supposedly represents a lower bound for the actual minimum level of shaking. Once again considering a representative element of sand at a depth of 15 ft within the same site described above, the peak ground surface acceleration required to

induce liquefaction may be determined as follows:

Given that $(K_2)_{max} = 30$ (for a sand with $D_R = 25\%$, after Seed et al, 1984) and $\sigma_o' \approx 1140\ psf$ at a depth of 15 ft,

$$G_{max} \approx 1000 \cdot (K_2)_{max} \cdot (\sigma_m')^{\frac{1}{2}} \qquad 5.7$$
$$\approx 7.8 \times 10^5\ psf$$

At a strain of about 0.01% (see Figure 5.1)

$$G_{eff} \approx 0.75 \cdot G_{max} \approx 5.9 \times 10^5\ psf \qquad 6.4$$

Thus, if the threshold strain, $\gamma_{th} \approx 0.01\%$

$$\gamma_{th} = \frac{\tau_{th}}{G_{eff}} \approx 0.01 \times 10^{-2} \qquad 6.5$$

and the corresponding threshold shear stress,

$$\tau_{th} \approx 0.01 \times 10^{-2} \times 5.9 \times 10^5\ psf$$
$$\approx 59\ psf$$

The average shear stress, τ_{av}, induced by earthquake shaking at a depth of 15 ft, may be determined by the relationship (using $\sigma_o \approx 1{,}800$ psf and $r_d \approx 0.95$ as before):

$$\tau_{av} \approx 0.65 \cdot \frac{a_{max}}{g} \cdot \sigma_o \cdot r_d \qquad 3.1$$

$$\approx 1100 \cdot \frac{a_{max}}{g}\ (psf) \qquad 6.6$$

Thus, in order for liquefaction to occur, the average induced shear stress, τ_{av}, must exceed the threshold shear stress, τ_{th}, i.e.

$$i.e. \qquad 1100 \cdot \frac{a_{max}}{g} > 59$$

$$or \qquad a_{max} > 0.05g$$

Thus, based on the field observations associated with Modified Mercalli Intensity, and supported by the studies listed above, it seems reasonable to conclude that unless the peak ground surface accelerations (generated at a site by earthquake shaking) exceed some value between about 0.05g and 0.1g liquefaction will not occur.

However, having shown support for this minimum level it should also be pointed out that significantly lower levels of shaking are probably capable of inducing liquefaction. For example, Figure 2.2 shows that magnitude 8.5 earthquakes have caused liquefaction at sites as far as about 700 kms (440 miles) from the epicenters of these earthquakes. Since the peak ground surface accelerations generated at this distance are indicated by empirical data to only be about 0.02g, the field performance data imply that the minimum level of shaking may actually be about one-half to one-fifth of the levels computed above.

Further support for this lower minimum level is provided by the observation that over the past four decades, a number of large scale liquefaction failures have been induced by non-seismic sources of ground vibration (refer to Table 1.1). Such sources of vibration generate much lower levels of ground shaking than the shaking produced by even small (magnitude. 5) earthquakes. For example, the analyses presented in Chapter 5 suggest that trains might cause liquefaction (albeit at shallow depths) if the ground surface accelerations exceed a value of about 0.05g (see Figure 5.26). Because train-induced ground vibrations contain much higher predominant frequencies than

seismic ground motions, the magnitudes of the shear strains induced by trains are much lower than those generated by earthquake shaking of a similar magnitude (refer to Figure 5.12), thereby suggesting that the minimum level of earthquake shaking which could induce similar liquefaction is significantly lower than 0.05g.

Thus, it indeed seems probable that levels of earthquake shaking significantly less than about 0.05g to 0.10g are both capable of, and have caused liquefaction, and that this minimum level of shaking may well be as low as about 0.02g.

It should be noted at this point that at least in the case of the minimum levels determined using experimental data (e.g. Iwasaki et al, Tokimatsu and Yoshimi and Dobry et al), the discrepancy between these levels and the more probable minimum level may be more apparent than real. In fact, this difference can most likely be explained by considering the effects of two factors: (1) the presence of artesian pressure conditions, and (2) the presence of initial static shear stresses which are in turn a function of the geography of the site and the magnitude of any artesian pore pressures (Equations 5.8 and 5.9). The effects of these factors are automatically included in the field observations but were not taken into account when computing the minimum levels discussed above. Referring to Figure 3.5 it may be seen that the liquefaction resistance of a loose sand decreases markedly as the magnitude of the initial shear stress/normal stress ratio is increased.

In view of the potentially significant effects of these factors, it seems appropriate to recompute the minimum levels of earthquake shaking taking into account the effects of both artesian pressure conditions and initial static shear stresses. Accordingly,

analyses were performed for both magnitude 8 earthquakes and magnitude 5.25 earthquakes, because the minimum level of shaking appears to be heavily dependent on the magnitude of the earthquake that generated the ground motions (see Figure 2.3). This dependence is most probably due to the different numbers of representative cycles of shaking typically generated by earthquakes of different magnitudes.

The effects of these factors were examined by following the shear stress approach. The shear strain approach was not used because it appears to account for the presence of initial static stresses by measuring shear moduli in the field and no relationships were found relating shear moduli to initial static shear stress.

6.3. Minimum Level of Shaking for Magnitude 8 Earthquakes

The effects of both artesian pore pressures and initial static shear stresses on the liquefaction potential of sand sites were determined by computing the response of loose sand deposits to earthquake shaking. Analyses were only performed for loose sands for the following reasons: (1) dense sands have a much higher cyclic loading resistance than loose sands, and thus require a significantly greater level of shaking to cause them to liquefy, and (2) the presence of initial static shear stresses within medium-dense to dense sands appears to increase their resistance (Szerdy, 1985, Vaid and Finn, 1979, Seed et al., 1973, Vaid and Chern, 1983) rather than reduce it as is the case for loose sands.

The rock acceleration record that was used to compute the site response (for all the magnitude 8 earthquake analyses) is the CUMV NS Mexico City record, a ground

motion recorded on rock at a distance of about 300 kms (190 miles) from the epicentral region of the magnitude 8.1 earthquake that occurred off the coast of Mexico on September 19, 1985. This motion was chosen because it is one of the few high quality rock records recorded at such large distances from the epicenters of large (approximately magnitude. 8) earthquakes. Further, the acceleration response spectrum (shown in Figure 6.1) for the CUMV NS motion is similar in shape to the average response spectrum computed for all of the rock records recorded in Mexico city during the same earthquake (Seed et al., 1987), thereby suggesting that this motion is the most representative long distance record for magnitude 8 earthquakes.

The magnitudes of the cyclic shear stresses induced at such large distances (by magnitude 8 earthquakes) may be determined approximately by scaling the CUMV NS record to produce different peak accelerations and then using these scaled motions as input for the computer program SHAKE. The levels of acceleration generated at the surface of loose sand deposits by such low levels of shaking are found to be about twice the magnitude of the peak accelerations, associated with the corresponding rock outcrop motions. Thus, since the minimum level of earthquake shaking causing liquefaction appeared to be about 0.03g (see Figure 2.3), it seemed appropriate to compute the strains for peak rock outcrop accelerations of 0.01g, and 0.02g.

The performances of the various sites were evaluated by comparing the magnitudes of the induced cyclic shear stresses with the magnitudes of the stresses required to liquefy the sands in-situ. However in order to compute the values of required stress, it is first necessary to determine the number of representative cycles of loading

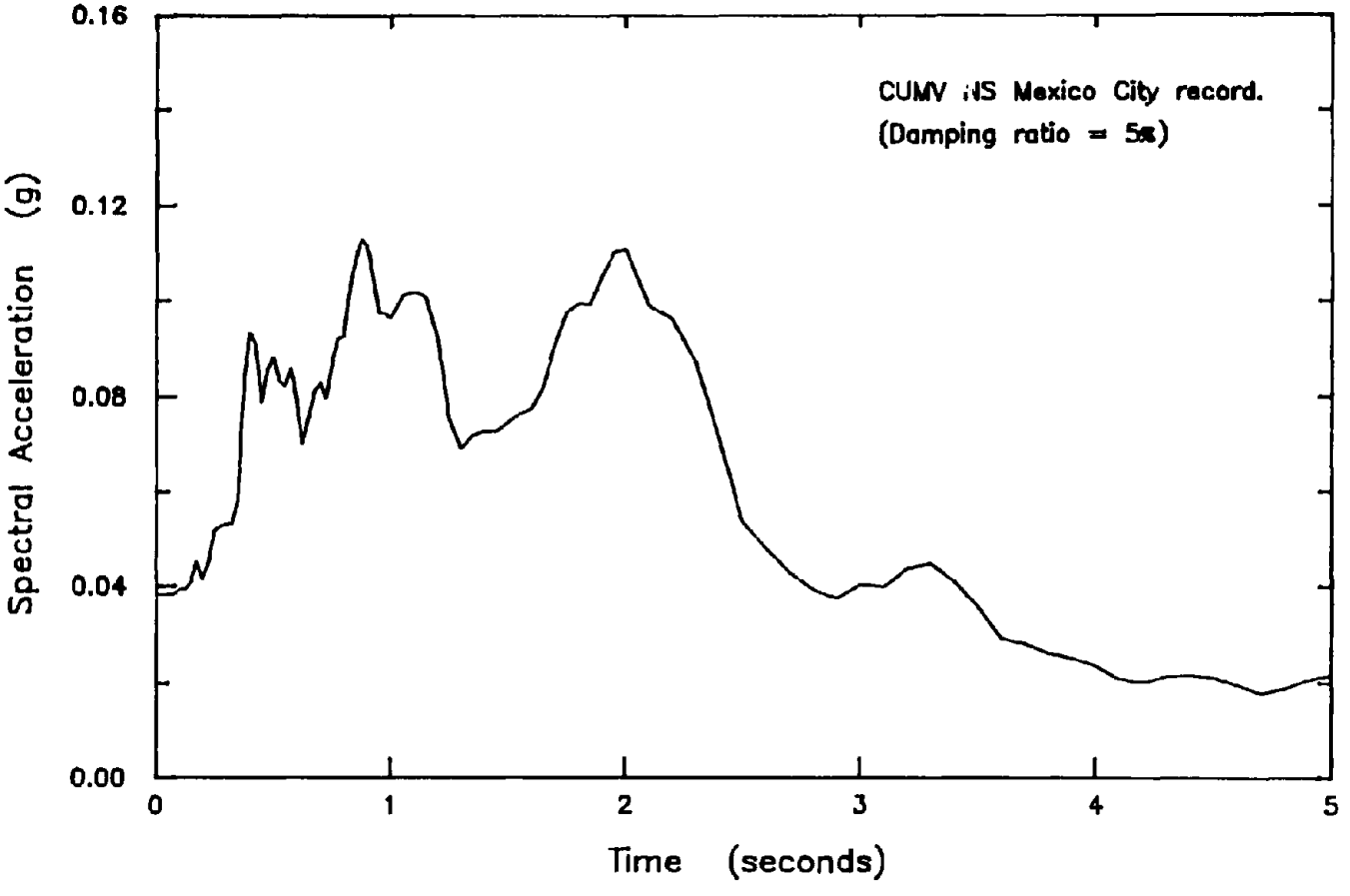

FIG 6.1 ACCELERATION RESPONSE SPECTRUM FOR THE CUMV NS MEXICO CITY RECORD.

typically generated at such large distances by magnitude 8 earthquakes. This number can be obtained from a ground surface acceleration time history using the procedure described by Seed et al (1975).

The computed response of a 100 ft deep, level sand deposit having a water table at ground surface and a penetration resistance $(N_1)_{60} = 5$, to the CUMV NS motion scaled to give a peak rock outcrop acceleration of 0.02g, is shown in Figure 6.2. Using the liquefaction evaluation procedure proposed by Seed et al, 1983, the number of representative cycles at a constant cyclic stress level of 0.65 τ_{max} is computed to be about 7, a somewhat surprising value in view of the fact that magnitude 8 earthquakes are commonly believed to generate about 20 such cycles of loading (inferred from Table 3.1). However while this value may appear to be unusually low, it is probably a more realistic number than the higher number of representative cycles commonly associated with such earthquakes for the following reasons:

(1) the higher number of cycles was determined for acceleration records of large magnitude earthquakes recorded at distances much closer than 300 kms from the epicenter of the earthquake, and

(2) the CUMV NS record is one of the few high quality rock acceleration records that have been recorded at such great distances from the epicenters of large (magnitude 8) earthquakes, and the earthquake that generated this record is, itself, believed to have generated a relatively long duration of ground shaking (Seed et al., 1987).

The Seed et al procedure was also used to calculate the number of representative cycles of loading generated within a 50 ft deep loose sand site and a 250 ft deep site. These values are calculated to be about 12 and 6 respectively. Thus, averaging the values for the three sites, and making some allowance for the fact that magnitude 8 earthquakes are commonly believed to generate about 20 cycles of loading, it was concluded that magnitude 8 earthquakes generate about 10 representative cycles of loading, at a constant level of cyclic shear stress of 0.65 τ_{max}, at epicentral distances of about 400 kms (250 miles).

The observation that the same rock outcropping record appears to generate almost twice the number of representative cycles of loading in the 50 ft site as in the 100 ft site is interesting to note and is probably due to the shorter natural period of the shallower site. Since components of bedrock motions with periods close to the natural period of a site are amplified as they propagate up through the site, and shallower sites tend to have shorter natural periods than deeper sites, the motions generated within shallow sites tend to contain more dominant high frequency components. Thus, shallow sites are likely to be subjected to more cycles of loading for the same total duration of bedrock motion. For example, the surface motions computed for the 50 ft site (which had a natural period of about 0.5 sec) have predominant frequencies of about 2 Hz, while the surface motions computed for the 100 ft site, with a 0.9 second natural period, have predominant frequencies of about 1 Hz (see Figure 6.2).

It seems logical to conclude from such an observation that the level of shaking required to cause liquefaction of shallow sites might therefore be significantly less than

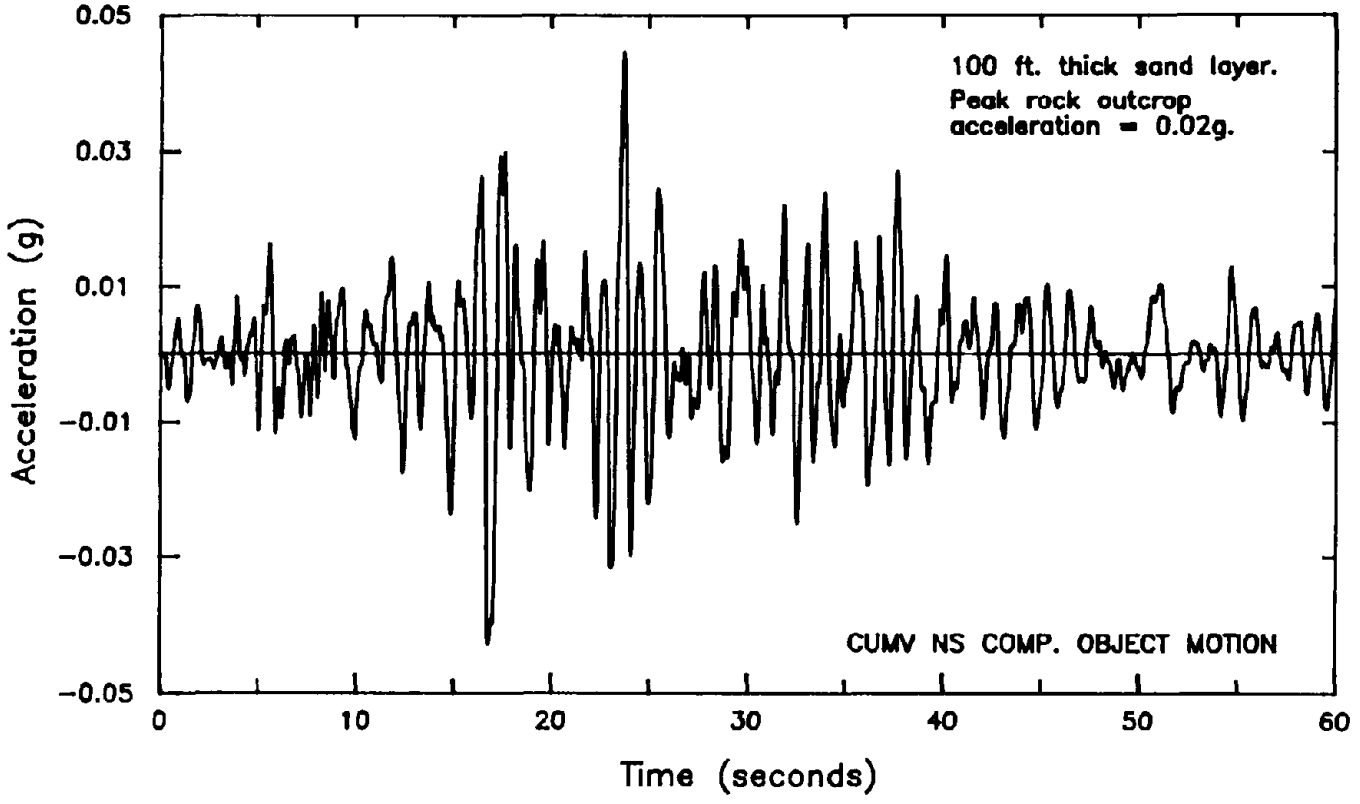

FIG 6.2 COMPUTED SURFACE RESPONSE OF A 100FT DEEP, LEVEL SAND DEPOSIT HAVING A WATER TABLE AT THE GROUND SURFACE AND A PENETRATION RESISTANCE $(N_1)_{60}$ = 5, TO THE CUMV NS MOTIONS SCALED TO GIVE A PEAK ROCK OUTCROP ACCELERATION OF 0.02g.

the level of shaking required to cause liquefaction for deeper sites. However this does not appear to be the case. Rather, the magnitudes of the shear stresses induced within shallow sites are also computed to be less, thereby tending to compensate for the larger number of applied cycles of loading. For example, the analyses summarized in Figure 6.3 show that the cyclic shear stresses generated within both 100 ft deep and 250 ft deep loose sand deposits may be about 25% larger in magnitude than those generated within 50 ft deep deposits. Since the cyclic stress ratio required to cause liquefaction of a sand in 6 cycles is approximately 20% greater than the stress ratio required to liquefy the same sand in 12 cycles (Figure 3.3), these effects tend to cancel. Thus, the results of analyses based on one depth of site are probably also valid for similar deposits of other depths.

As discussed in Section 3.1, the values of cyclic stress ratio required to induce liquefaction of a sand, in-situ, can probably be determined most accurately from the field performance plots shown in Figures 3.1 and 3.2. Assuming a standard penetration resistance for the sand of $(N_1)_{60} = 5$, the cyclic stress ratio required to liquefy this sand in 15 cycles is approximately equal to 0.07 (see Figure 3.1). Since the stress ratio required to liquefy a sand in 10 cycles appears to be about 10% greater than the ratio required to liquefy the same sand in 15 cycles (Figure 3.3), the cyclic stress ratio required to liquefy the same sand in 10 cycles is estimated to be about $0.07 \times 1.10 \approx 0.08$. Thus, the cyclic stress ratios required to liquefy a level loose ($(N_1)_{60} = 5$) sand site were determined by adjusting this value for overburden effects using the K_σ curve shown in Figure 3.4; these ratios are shown by the solid line in Figure 6.4.

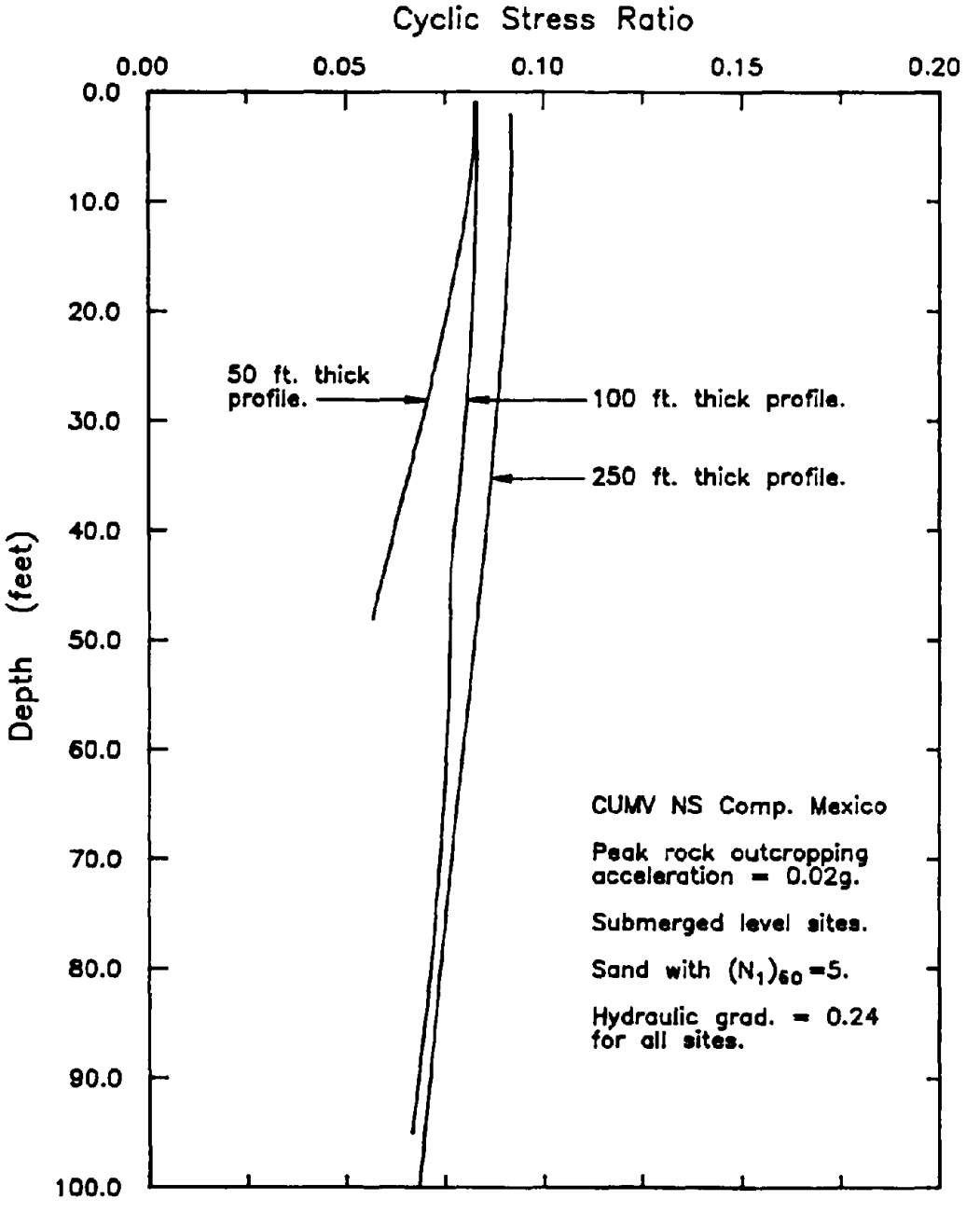

FIG 6.3 AVERAGE INDUCED CYCLIC STRESS RATIO AS A FUNCTION OF DEPTH FOR SITES WITH DIFFERENT DEPTHS. SUBJECTED TO THE SAME BEDROCK MOTION.

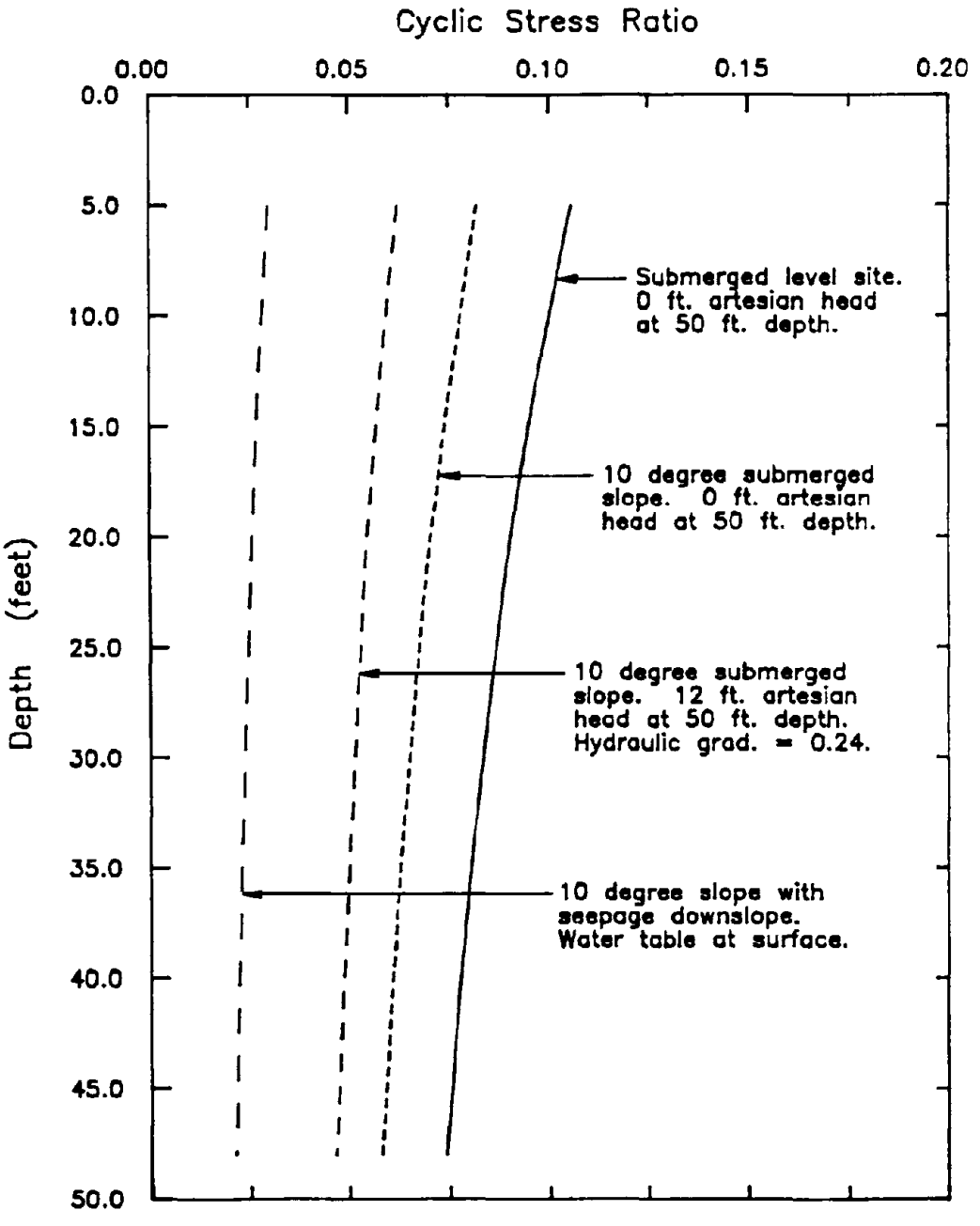

FIG 6.4 CYCLIC STRESS RATIO REQUIRED TO CAUSE LIQUEFACTION OF A SAND WITH $(N_1)_{60}$ = 5 IN 10 CYCLES, FOR FOUR DIFFERENT SITE CONDITIONS.

Also shown in this figure are the cyclic stress ratios required to liquefy the $(N_1)_{60} = 5$ sand within submerged 10 degree slopes, with or without artesian pressure conditions, and within 10 degree slopes with the water table at the surface and seepage occurring down the slope, parallel to the ground surface. These stress ratios (shown by the dashed lines) were computed by scaling the required cyclic stress ratios (shown by the solid line in the same figure) for the level site by a constant factor to take into account the effects of the initial static shear stresses imposed on the sands within these slopes. For example, the initial shear stress/normal stress ratio imposed upon the sand within a submerged infinite 10 degree slope is computed to be about 0.18 (from Equation 5.8) and Figure 3.5 implies that the cyclic stress ratios required to liquefy loose sands subjected to ratios of about 0.18 are approximately 20% smaller than the ratios required to liquefy the same sand when subjected to zero initial shear stress. Thus, the ratios required to liquefy a $(N_1)_{60} = 5$ sand within submerged 10 degree slopes with no artesian pressure conditions may be computed by multiplying the ratios for level sites by a factor of 0.8.

The dramatic reduction in the levels of required cyclic stress ratio (for loose sands) as a result of an increase in the magnitudes of the initial imposed shear stresses is also clearly shown in Figure 6.5. The solid curve shown in this figure is identical to the proposed average curve shown in Figure 3.5 and as such, is believed to provide the best indication of the reduction in liquefaction resistance for loose sands subjected to initial shear stresses. The cyclic stress ratios required to liquefy a saturated sand with

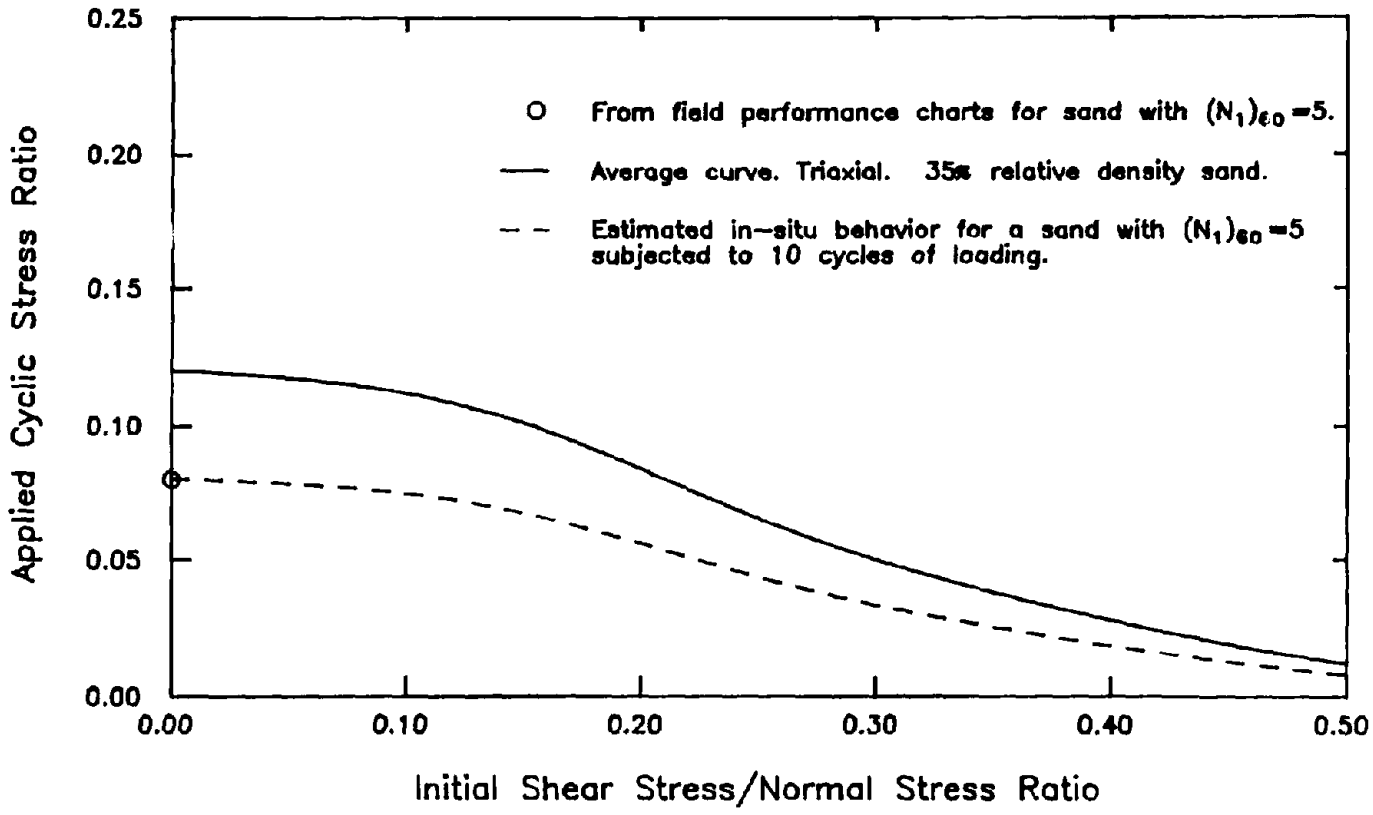

FIG 6.5 CYCLIC STRESS RATIO REQUIRED TO CAUSE LIQUEFACTION OF A LOOSE SAND IN 10 CYCLES AS A FUNCTION OF INITIAL SHEAR STRESS/NORMAL STRESS RATIO.

$(N_1)_{60}$ = 5, in-situ, in 10 cycles may be determined by scaling the solid curve to give an applied cyclic stress ratio of 0.08 (determined above) at an initial static shear stress/normal stress ratio equal to zero. These modified values are shown by the dashed line in this figure. It should be pointed out that the dashed curve was obtained by multiplying the solid curve by a constant factor for all values of initial imposed stress because the field performance plots only apply to sands subjected to zero initial shear stress and no field data exist for sands subjected to such stresses.

6.3.1. Effects of Artesian Pressures on Liquefaction Potential of Sand Deposits

One of the phenomena that are thought to be responsible for the discrepancy between the observed minimum levels of earthquake shaking, and those determined in Section 6.2 from experimental studies, is the presence of artesian pressure conditions. Such conditions not only increase the magnitudes of the initial static shear stress/normal stress ratios present within a site (refer to Equations 5.8 and 5.9), thus significantly reducing the liquefaction resistance of sloping sites (Figure 6.4), but they also appear to result in higher induced cyclic stress ratios for the same rock motion, as shown in Figure 6.6.

It may be observed from this figure that the cyclic stress ratios induced within a loose sand site with a 12 ft artesian head acting at a depth of 50 ft (hydraulic gradient, i, = 0.24), are computed to be about 25% larger than the cyclic stress ratios induced within the same site with no artesian pressures. Since the presence of such pressures

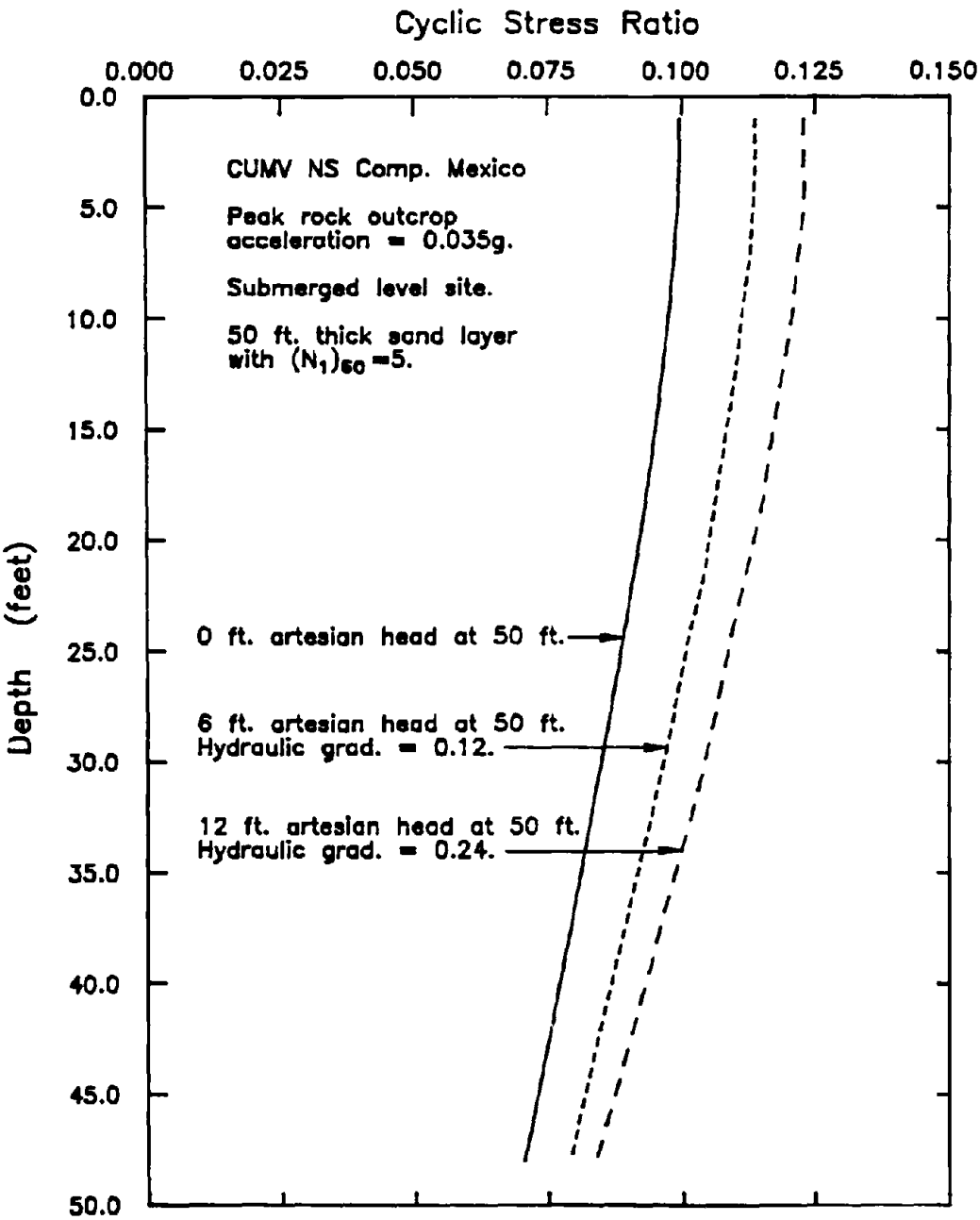

FIG 6.6 EFFECT OF ARTESIAN PRESSURE CONDITIONS ON THE MAGNITUDES OF THE INDUCED CYCLIC STRESS RATIOS - EARTHQUAKE MAG. ≈ 8.

has only a minor effect on the liquefaction resistance of level sites, level sites containing artesian pressure conditions appear to be more susceptible to liquefaction. The analyses summarized in this figure were performed for a 50 ft deep, $(N_1)_{60} = 5$ sand deposit shaken by the CUMV NS record scaled to contain a peak acceleration of 0.035g. This deposit was underlain by a 10 ft thick gravel layer overlying bedrock.

The magnitudes of the cyclic shear stresses generated within sites containing artesian pressures were computed by modifying the shear moduli for the sands to account for the presence of these pressures. Such an effect could have been achieved by reducing the density of the sands and thus the effective stresses (see Equation 5.7); however this approach is undesirable since the mass of a site would also be affected and this is not the case in reality. Instead it was achieved by modifying the values of $(K_2)_{max}$, also supplied as input for the computer program SHAKE, using the following equation:

$$(K_2)_{new} = (K_2)_{max} \cdot \frac{\sqrt{\sigma_o' - 1.5u_e}}{\sqrt{\sigma_o'}} \qquad 6.7$$

where σ_o' = effective overburden pressure
u_e = artesian pore pressure

The magnitudes of the cyclic stress ratios predicted to be induced within the 50 ft deep site are shown in Figures 6.7 and 6.8, together with the values of cyclic stress ratio required to cause liquefaction (shown in Figure 6.4). It may be seen from these figures that liquefaction is not predicted to occur within level loose sand deposits containing no artesian pore pressures, unless the corresponding peak rock outcropping

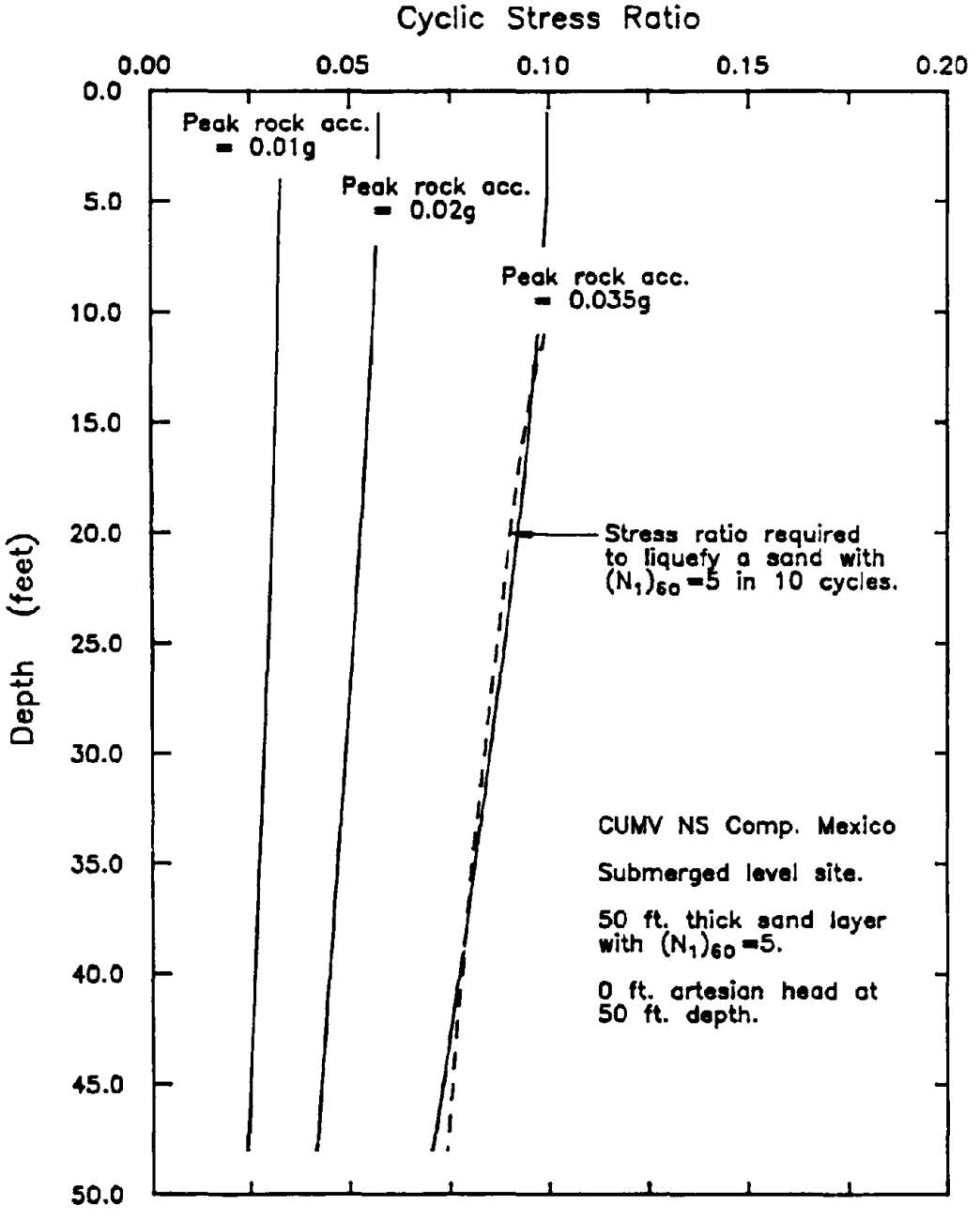

FIG 6.7 AVERAGE INDUCED CYCLIC STRESS RATIO AS A FUNCTION OF DEPTH FOR DIFFERENT LEVELS OF BEDROCK ACCELERATION - LEVEL SITE WITH NO ARTESIAN PRESSURES - EARTHQUAKE MAG. ≈ 8.

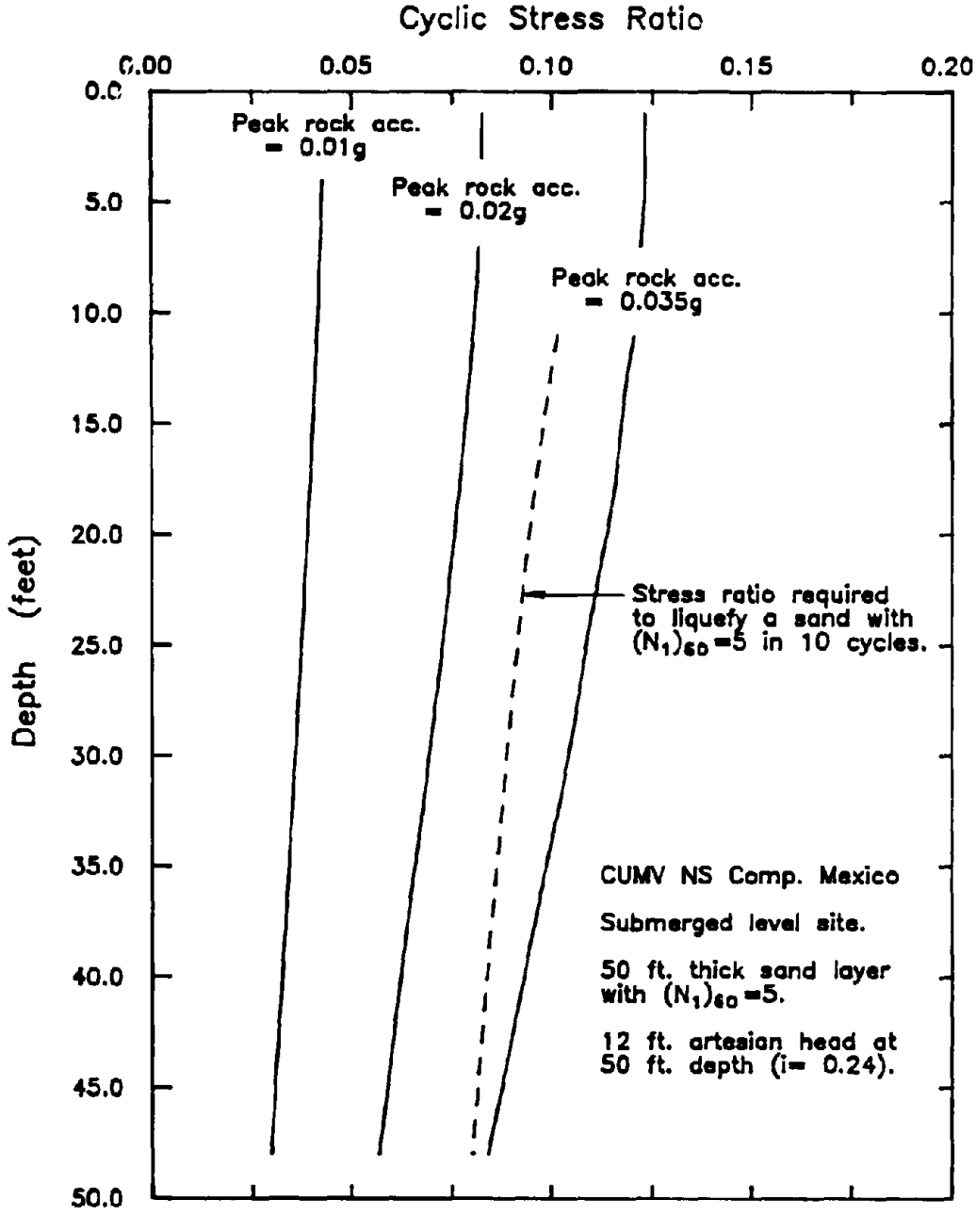

FIG 6.8 AVERAGE INDUCED CYCLIC STRESS RATIO AS A FUNCTION OF DEPTH FOR DIFFERENT LEVELS OF BEDROCK ACCELERATION - LEVEL SITE WITH ARTESIAN PRESSURE CONDITIONS - EARTHQUAKE MAG. = 8.

accelerations exceed a value of about 0.035g. Since the ground surface accelerations are approximately 100% larger in magnitude than the associated rock outcropping accelerations, this value implies that the minimum level of earthquake shaking required to liquefy such a site is about 0.07g. If the effect of artesian pore pressures is taken into account, the minimum level of shaking required to cause liquefaction may still only be as low as 0.025g in rock, or 0.05g at the ground surface for a site with 12 ft of artesian head acting at a depth of 50ft (i = 0.24, Figure 6.8). This suggests that presence of artesian pore pressures, alone, is not sufficient to account for the discrepancy between the minimum levels calculated as described above, and those determined from field observations (about 0.03g as shown in Figure 2.3).

6.3.2. Effect of Initial Shear Stresses

The other factor believed to have a significant effect on the minimum level of earthquake shaking required to cause liquefaction is the presence of initial static shear stresses and the effects of such stresses are shown in Figures 6.9, 6.10, and 6.11. As with the analyses performed for level sites, the induced cyclic stress ratios shown in these figures were computed for a 50 ft deep, $(N_1)_{60} = 5$ sand deposit. However in this case, the deposits were located within 10 degree slopes with water tables, level with and above the ground surface.

Referring to Figure 6.9 it may be seen that the ground vibrations generated by magnitude 8 earthquakes appear to be capable of causing liquefaction within loose sand slopes, with no artesian pore pressures, at distances where the peak rock outcrop

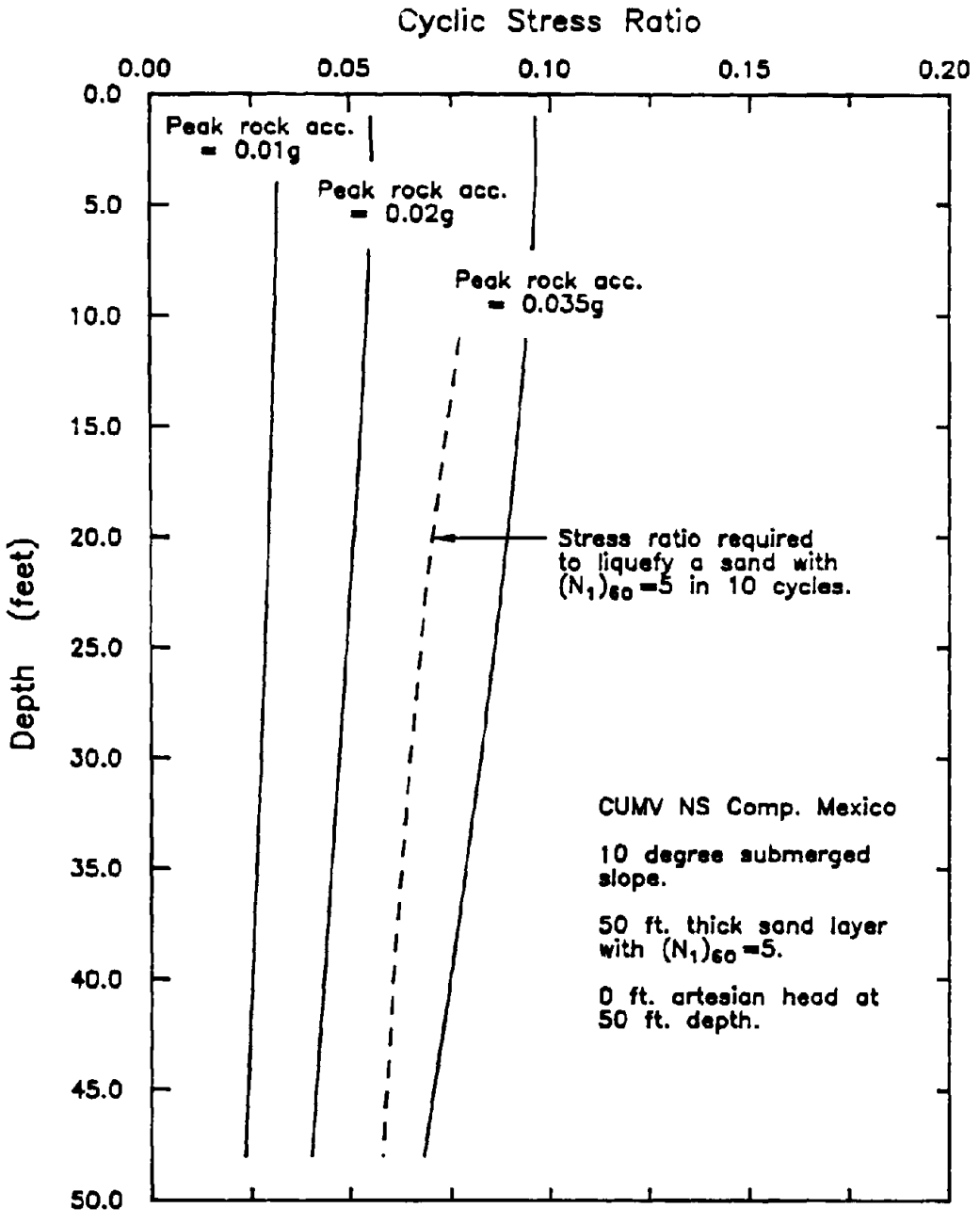

FIG 6.9 AVERAGE INDUCED CYCLIC STRESS RATIO AS A FUNCTION OF DEPTH FOR DIFFERENT LEVELS OF BEDROCK ACCELERATION - SLOPING SAND LAYER WITH NO ARTESIAN PRESSURES - EARTHQUAKE MAG. ≈ 8.

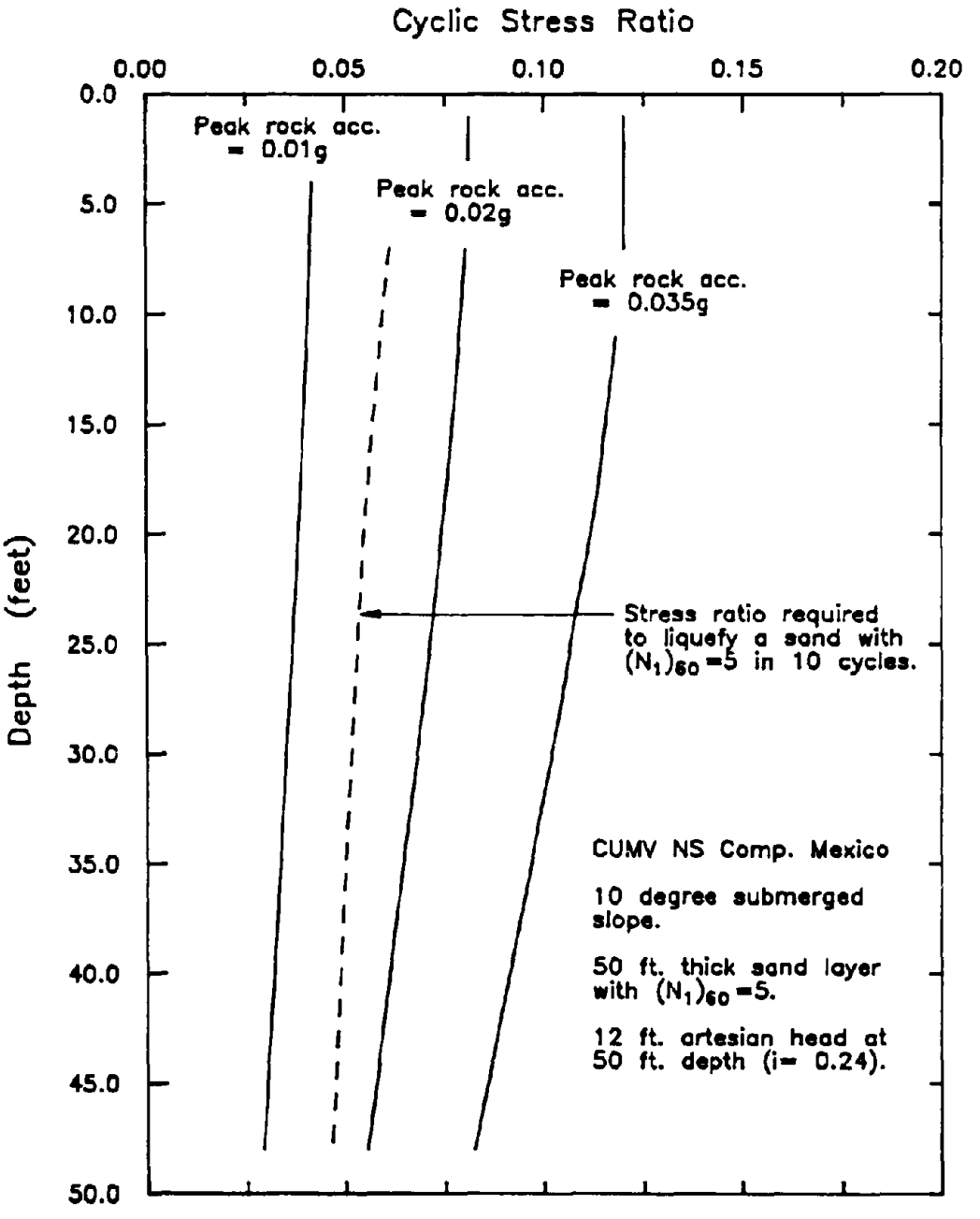

FIG 6.10 AVERAGE INDUCED CYCLIC STRESS RATIO AS A FUNCTION OF DEPTH FOR DIFFERENT LEVELS OF BEDROCK ACCELERATION - SLOPING SAND LAYER WITH ARTESIAN PRESSURE CONDITIONS - EARTHQUAKE MAG. = 8.

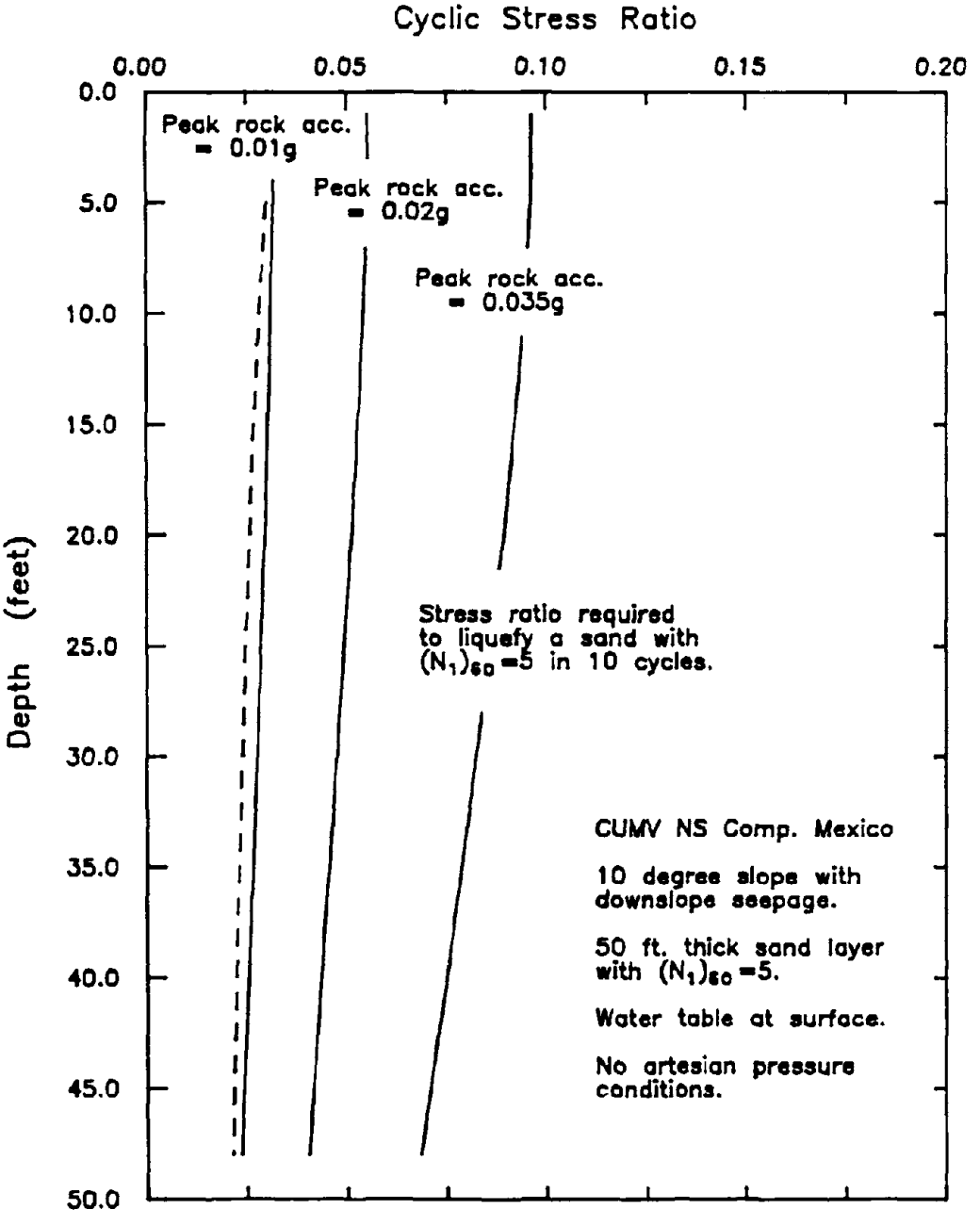

FIG 6.11 AVERAGE INDUCED CYCLIC STRESS RATIO AS A FUNCTION OF DEPTH FOR DIFFERENT LEVELS OF BEDROCK ACCELERATION - SLOPING SAND LAYER WITH DOWNSLOPE SEEPAGE - EARTHQUAKE MAG. = 8.

accelerations exceed a value of about 0.025g. It was shown in Figure 6.8 that the same level of shaking may also be capable of causing the liquefaction of level sites containing significant artesian pore pressures. This observation is not surprising because the reduction in the magnitudes of the cyclic stress ratios required to cause liquefaction in sloping deposits (due to the presence of initial shear stresses) is offset by the higher applied cyclic shear stresses generated within level sites as a result of the artesian pressures.

For the case of 10 degree slopes with artesian pore pressures, however, the minimum levels of earthquake shaking required to cause liquefaction are greatly reduced. For example, Figure 6.10 indicates that liquefaction of submerged, 10 degree loose sand slopes with 12 ft artesian heads acting at depths of 50 ft (hydraulic gradient, i, =0.24), may be caused by bedrock motions with peak rock outcropping accelerations of about 0.015g, corresponding to ground surface accelerations of about 0.03g. This value is approximately 40% smaller in magnitude than the peak accelerations associated with the failure of the same slope without artesian pore pressures.

Thus, when the effects of both artesian pore pressures and initial static shear stresses are taken into account, levels of earthquake shaking similar to the minimum levels determined from field performance observations are computed, using current liquefaction theory, to cause the liquefaction of certain, relatively critical loose sand slopes. This prediction indirectly implies that some of the sites depicted as data points in Figure 2.2 were probably sloping sites and possibly contained artesian pressures.

Similarly, the results of the analyses presented in Figure 6.11, for seepage parallel to the surface of the slope, indicate that magnitude 8 earthquakes may be capable of liquefying such loose sand sites when the peak ground surface accelerations exceed a value as low as about 0.02g (approximately twice the peak rock outcrop acceleration). These analyses were performed for the same 50 ft deep, loose sand deposit located within a 10 degree slope with a water table at the surface and seepage occurring down the slope, parallel to the ground surface.

Such a low predicted minimum level of shaking is due to the high initial shear stresses present within this slope and the significant effects of these stresses on the liquefaction resistance of loose sands. Given that the initial shear stress/normal stress ratios on any plane parallel to the ground surface, τ_i/σ_{ni}' are about 0.37 (Equation 5.9), Figure 3.5 shows that the applied cyclic shear stresses required to liquefy this sand are approximately 60% less than the stresses required to liquefy the same sand within the submerged 10 degree slope with no artesian pore pressures (where $\tau_i / \sigma_{ni}' = 0.18$). Since similar levels of cyclic shear stress are generated within both slopes, this implies that sloping loose sand sites with seepage down the slope may be liquefied at much greater epicentral distances than submerged slopes with similar deposits (subjected to the same level of shaking) and no artesian pressure conditions.

In the light of these results, it would appear that analytical prediction of liquefaction potential can provide results in accord with the maximum observed distances of liquefaction occurring for some types of site conditions.

The fact that analyses of the type described above appear to be capable of making reasonable predictions for the field performance of sand deposits subjected to earthquake shaking, seems to indicate that analyses based on liquefaction theory provide reasonable results. Thus, the apparent existence of an upper bound distance beyond which liquefaction is unlikely to occur, is most probably due to either one of the following:

1) A practical minimum level of required earthquake shaking that is relatively independent of the stress state imposed on the soil and probably results from some characteristic soil property such as threshold strain, or

2) That liquefaction failures could have been induced (by magnitude 8 earthquakes) at epicentral distances greater than about 400 kms but that in historic time, the motions have not been induced in sufficiently critical deposits.

The peak cyclic shear strains that are predicted to occur within loose sand sites (with artesian pressure conditions for which these strains are largest) at epicentral distances of about 400 kms are approximately equal to 0.02%. Since this value is only slightly larger than the threshold strains for many sands (Table 3.1), it might initially appear that the minimum level of earthquake shaking is directly related to the concept of a threshold strain. However it should also be pointed out that loose sands cycled at this level of strain for about 10 cycles, are not predicted to liquefy. In fact, given that the rate of pore pressure buildup at low levels of cyclic shear strain is only slightly influenced by relative density (Figure 3.7), the pore pressure ratios built up within

loose ($D_R = 30 - 35\%$) sands cycled at a constant maximum shear strain of $1.3 \times 10^{-2}\%$ ($0.65 \times 0.02\%$) are not even expected to exceed a value of about 0.05, possibly even after 100 cycles of loading (see Figure 3.9). Therefore, unless magnitude 8 earthquakes generate peak ground surface accelerations significantly in excess of 0.03g (at epicentral distance of about 400 kms), which seems unlikely, the minimum levels of shaking determined using shear strain theory are likely to be significantly higher than the minimum levels determined from field observations (as shown in Section 6.2). It may be that the value of threshold strain is in fact influenced by the magnitudes of the initial static shear stresses; however data presented to date seems to refute this concept (Dyvik et al., 1984).

The apparent existence of an apparent upper bound distance can probably best be explained by the second suggestion; i.e. that liquefaction may be induced at greater distances if sufficiently critical site conditions exist. Such a premise appears to be even more likely when the following are considered:

1) The line drawn in Figure 2.3 is only an upper curve drawn to fit the available extreme data and would change significantly if one or two data points were to plot above this line.

2) Epicentral distance is plotted on a log scale; this gives the impression that several earthquake-induced liquefaction failures have occurred at epicentral distances similar to the upper bound distance when in reality, these failures occurred at epicentral distances which differ by as much as several hundred kilometers (for magnitude 8 earthquakes).

3) Very few, if any, sufficiently sensitive sites are likely to exist, especially in areas where there is a history of seismic shaking, thereby suggesting that only a small number of earthquake-induced liquefaction failures may even occur at distances further than about 400 kms.

Thus, based on the results of the analytical studies, and supported by the suggestion that liquefaction may well have occurred at greater epicentral distances, it seems reasonable to conclude that the ground shaking generated by magnitude 8 earthquakes is probably capable of liquefying certain critical sites at epicentral distances significantly greater than 400 kms. For example, the distances at which the four sites analyzed in this section may be liquefied, are presented in Table 6.2. These distances were obtained by using the attenuation relationships listed in Section 2.1 to predict the distances at which the required levels of shaking might be generated. It should be cautioned that these values are very approximate.

6.4. Minimum Level of Shaking for Magnitude 5.25 Earthquakes

The effects of artesian pore pressures and initial static shear stresses on the minimum level of shaking required to cause liquefaction were also evaluated for magnitude 5.25 earthquakes. As for the magnitude 8 earthquake study, this evaluation is based on the computed responses of loose ($(N_1)_{60} = 5$) sand deposits to earthquake shaking. The deposits that were analyzed contained a range of artesian pressure conditions and were located within both level sites and 10 degree slopes.

Table 6.2 : Approximate Upper Bound Distances for Liquefaction Occurring in Magnitude 8 Earthquake Shaking

Site	Static Shear Stress/ Normal Stress Ratio	Min. level of Shaking	Epicentral Dist. (kms)
Level ground Zero hydraulic grad.	0.0	0.07g	200
Level ground Hydraulic grad. = 0.24	0.0	0.05g	275
10 degree slope Zero hydraulic grad.	0.18	0.05g	275
10 degree slope Hydraulic grad. = 0.24	0.24	0.03g	400
10 degree slope seepage downslope	0.37	0.02g	575

An initial estimate for the level of shaking required to liquefy such deposits was determined from the field performance data presented in Figure 2.2. This data appears to imply that magnitude 5.25 earthquakes might only be capable of causing liquefaction failures at epicentral distances less than about 11 kms. The peak ground surface accelerations generated at this distance by earthquakes of this magnitude are expected to be about 0.15g (Figure 2.3).

Since the ground motions generated at the surface of loose sand sites (by shaking of this magnitude) are found to be about 130% larger in magnitude than the corresponding bedrock motions, the field data further imply that liquefaction might only occur at distances where the peak rock outcrop accelerations (generated by magnitude 5.25 earthquakes) exceed a value of about 0.065g. However, given that the minimum levels for magnitude 8 earthquakes were computed to be significantly less

than those implied by Figure 2.3, it seemed probable that lower levels would also be predicted for magnitude 5.25 earthquakes. Thus, the various sites were analyzed for bedrock motions with peak rock outcrop accelerations of 0.10g, 0.065g, and 0.025g.

The rock outcrop motion that was used to compute the site response is the S80E component of the Golden Gate Park record of the San Francisco earthquake of March 22, 1957. This motion was recorded at a distance of about 11 kms from the epicenter of the earthquake. The predominant period of the record is approximately 0.18 secs and the peak particle acceleration is about 0.105g. The motion was therefore scaled to give one of the three desired peak accelerations (listed above) and the modified records were then used as input for the computer program SHAKE.

The levels of induced cyclic shear stress, calculated by this approach were compared with the levels of cyclic stress required to cause liquefaction of the sand, in-situ. From these comparisons it was possible to estimate the minimum levels of required shaking for each site, and hence, determine an approximate value for the minimum level of magnitude 5.25 earthquake shaking for all sites.

The magnitudes of the cyclic shear stresses required to cause liquefaction of sand with $(N_1)_{60} = 5$ in a Magnitude 5.25 earthquake, can probably be determined most accurately from the levels already obtained for magnitude 8 earthquakes (shown by the solid line in Figure 6.5 and the dashed line in Figure 6.12). This can be achieved by adjusting the latter values to account for the different numbers of cycles of loading generated by the different sources. As previously noted (Section 6.2), magnitude 8 earthquakes at large distances probably generate about 10 representative cycles of loading at a constant stress level of 0.65 τ_{max}.

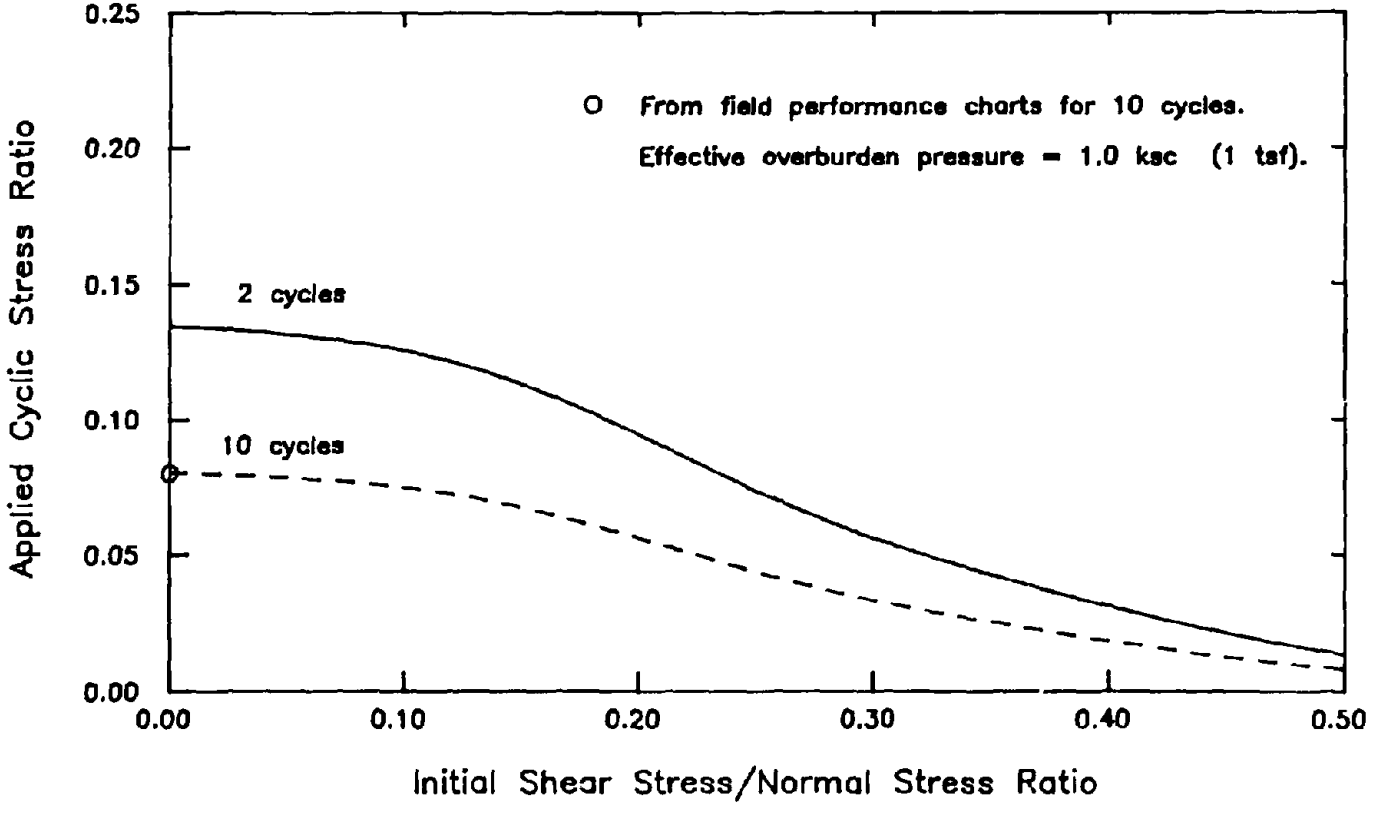

FIG 6.12 CYCLIC STRESS RATIO REQUIRED TO CAUSE LIQUEFACTION OF A LOOSE SAND IN 2 CYCLES AND IN 10 CYCLES AS A FUNCTION OF INITIAL SHEAR STRESS/NORMAL STRESS RATIO.

For the purpose of this analysis, magnitude 5.25 earthquakes were assumed to generate about 2 representative cycles of loading at the same stress level. This number was chosen, even though earthquakes of this magnitude are reported to generate a slightly higher number of cycles (2 to 3 cycles, refer to Table 3.1), for the following reasons: (1) this investigation is primarily concerned with the minimum level of shaking and hence the maximum distance at which liquefaction can occur, and (2) the number of cycles probably decreases with increasing distance from the source, as was found for magnitude 8 earthquakes.

The cyclic stress ratio required to liquefy a sand in 2 cycles is approximately 70% larger than the ratio required to liquefy the same sand in 10 cycles (Figure 3.3). Thus, the required cyclic stress ratios for magnitude 5.25 earthquake shaking were obtained by multiplying the ratios represented by the dashed line in Figure 6.12 by a constant factor of 1.7 (for all values of initial shear stress/normal stress ratio). These modified ratios are shown by the solid line in the same figure. It should be pointed out that the dashed line was obtained (as described in Section 6.2) by scaling the average curve determined for loose ($(N_1)_{60}$ = 5) sands (from experimental results) to give an applied cyclic stress ratio of 0.08 (determined from field performance data) at zero initial shear stress, and as such, it is believed to provide a reasonable representation for the in-situ liquefaction resistance of such sands. Therefore it also follows that the solid line is likely to be equally valid for predicting magnitude 5.25 earthquake resistance. Both curves pertain to sands subjected to overburden pressures of about 1 ksc (1 tsf).

The cyclic stress ratios required to cause liquefaction of the $(N_1)_{60} = 5$ sand deposit for four different site conditions are shown in Figure 6.13. These curves were generated (as previously described Sections 5.4 and 6.2) by adjusting the cyclic stress ratios obtained from the solid line shown in Figure 6.12, for overburden effects using the K_σ curve presented in Figure 3.4. The magnitudes of the initial static shear stress/normal stress ratios within the sites (on planes parallel to the ground surface) were calculated using Equations 5.8 and 5.9. It may be seen from this figure that as expected, the presence of initial static shear stresses is predicted to have a significant effect on the liquefaction resistance of loose sand deposits. Furthermore, since the initial stresses are a function of the artesian pore pressure conditions (see Equations 5.8 and 5.9), such pressures are also predicted to influence the liquefaction resistance of sloping sites.

However, it is interesting to note that in contrast to the findings of the magnitude 8 study, the induced cyclic stress ratios for level sites in Magnitude 5.25 earthquakes does not appear to be greatly influenced by the magnitude of the artesian pressures. For example, Figure 6.14 shows that similar levels of cyclic stress ratios are likely to be induced (by the same bedrock motion) within loose sand deposits containing significantly different artesian pressure conditions. These stresses were computed for a bedrock motion with a peak rock outcrop acceleration of 0.10g. Since the levels of cyclic stress ratio required to cause liquefaction at level sites are only slightly affected by the magnitudes of the artesian pressures (due to the effect of the factor, K_σ), it

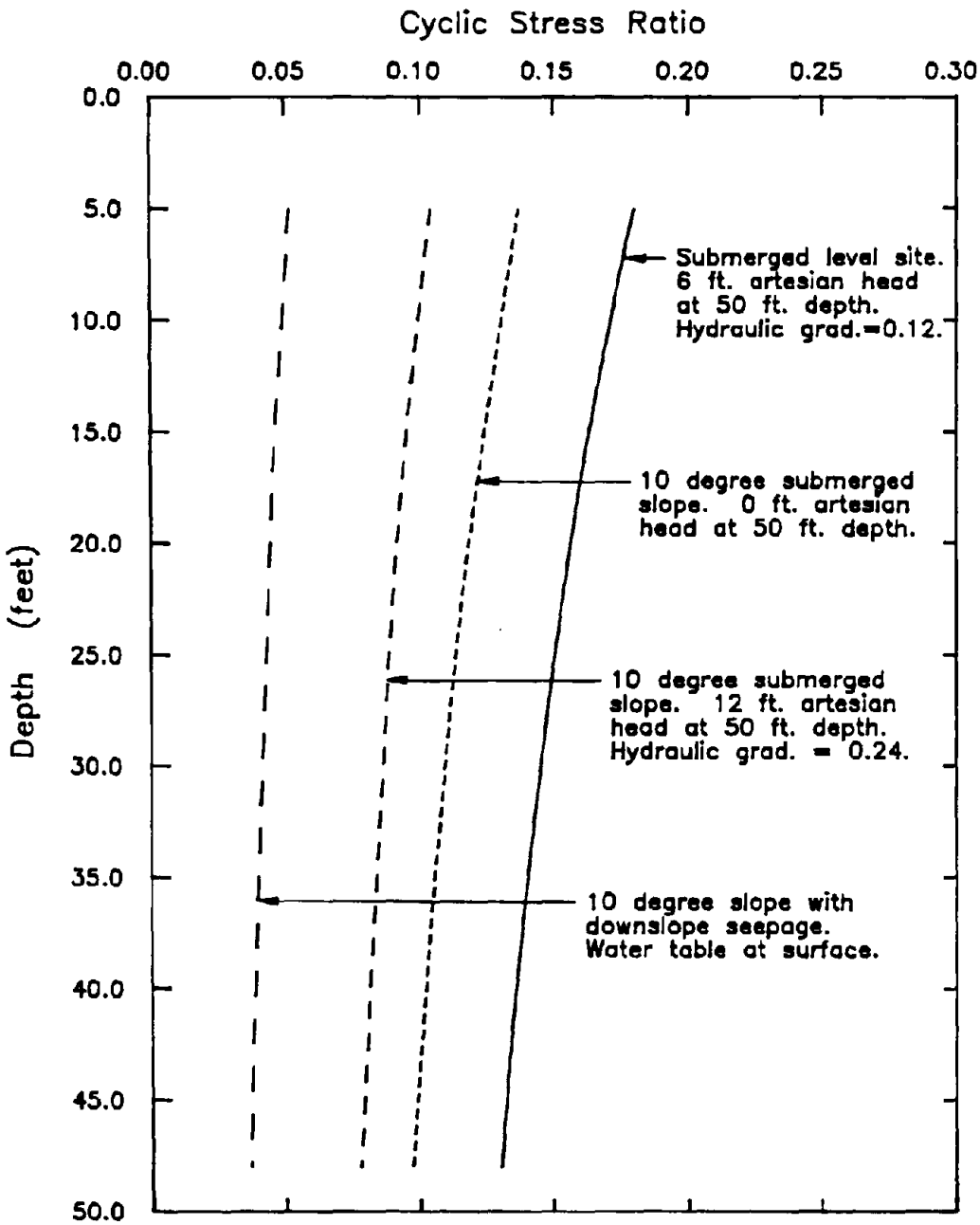

FIG 6.13 CYCLIC STRESS RATIO REQUIRED TO CAUSE LIQUEFACTION OF A SAND WITH $(N_1)_{60}$ = 5 IN 2 CYCLES, FOR FOUR DIFFERENT SITE CONDITIONS.

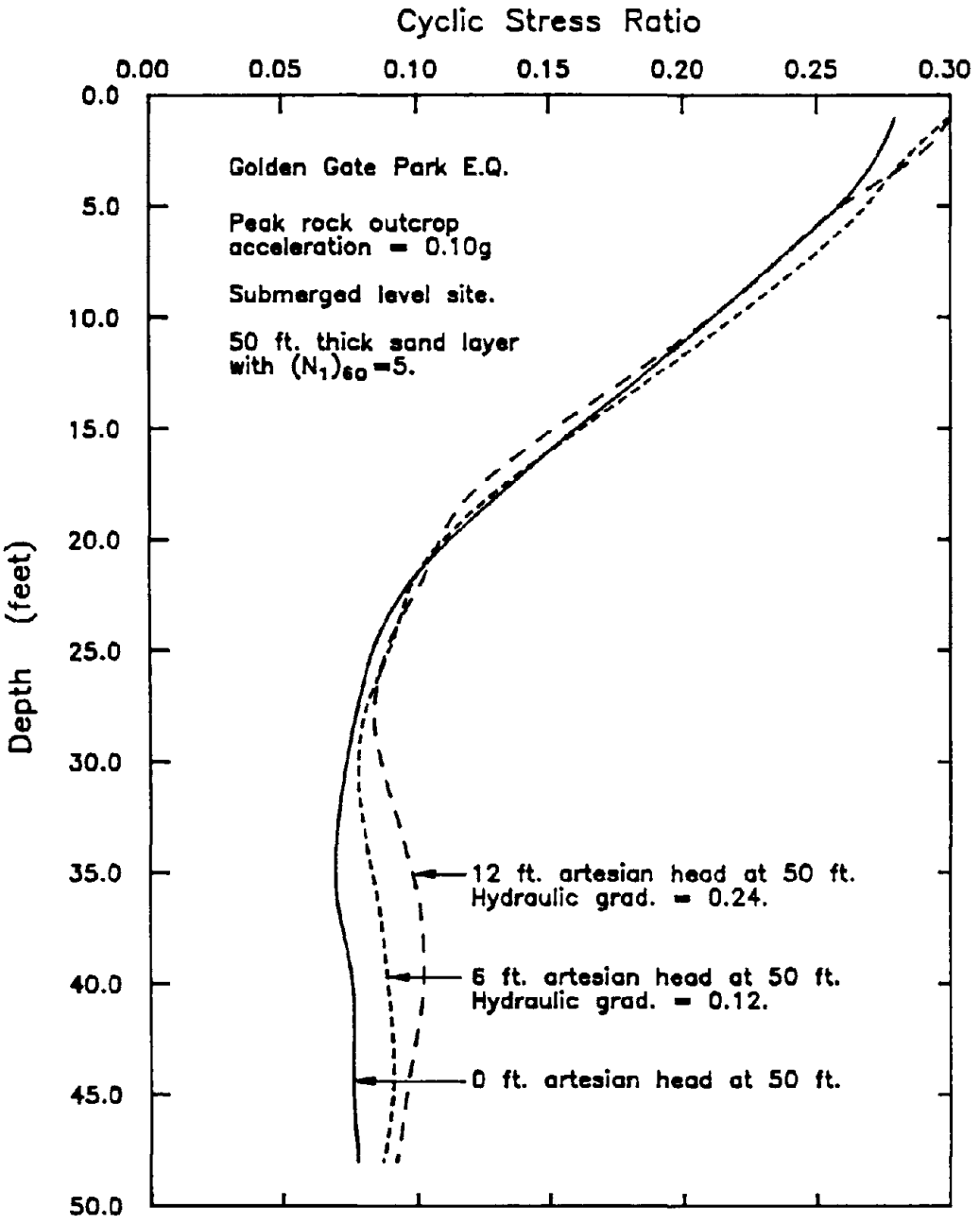

FIG 6.14 EFFECT OF ARTESIAN PRESSURE CONDITIONS ON THE MAGNITUDES OF THE INDUCED CYCLIC STRESS RATIOS - EARTHQUAKE MAG. = 5.25.

seems reasonable to conclude that the minimum level of earthquake shaking required to cause liquefaction for level loose sand deposits is also relatively independent of the artesian pressure conditions. While this result was found in the case of the 50 ft site considered in this study, it may not occur for all site conditions and all levels of ground shaking.

The minimum level of shaking predicted to liquefy such deposits is shown in Figure 6.15. This figure implies that magnitude 5.25 earthquakes may be capable of causing liquefaction at distances where the peak rock outcrop accelerations exceed a value of about 0.06g. At these distances the ground surface accelerations are found to be about 130% larger than the rock outcrop accelerations, thereby suggesting a minimum level of shaking for level sites of about 0.14g. This value is similar in magnitude to the minimum level of 0.15g associated with the upper bound curve shown in Figure 2.3.

Since liquefaction appears to be confined to the surface layers, unless the peak ground surface accelerations are significantly greater than 0.14g (Figure 6.14), the minimum level of shaking determined from field performance data may well represent a practical minimum level for level sites. However, while such a conclusion seems reasonable for level sites, the minimum levels for sloping sites are predicted to be significantly less than this value. For example, the analyses for sloping sites summarized in Figures 6.16, 6.17, and 6.18 imply that rock motions with peak outcropping accelerations as low as about 0.02g may be capable of liquefying loose sand deposits within 10 degree slopes. This value was computed for the following conditions: water

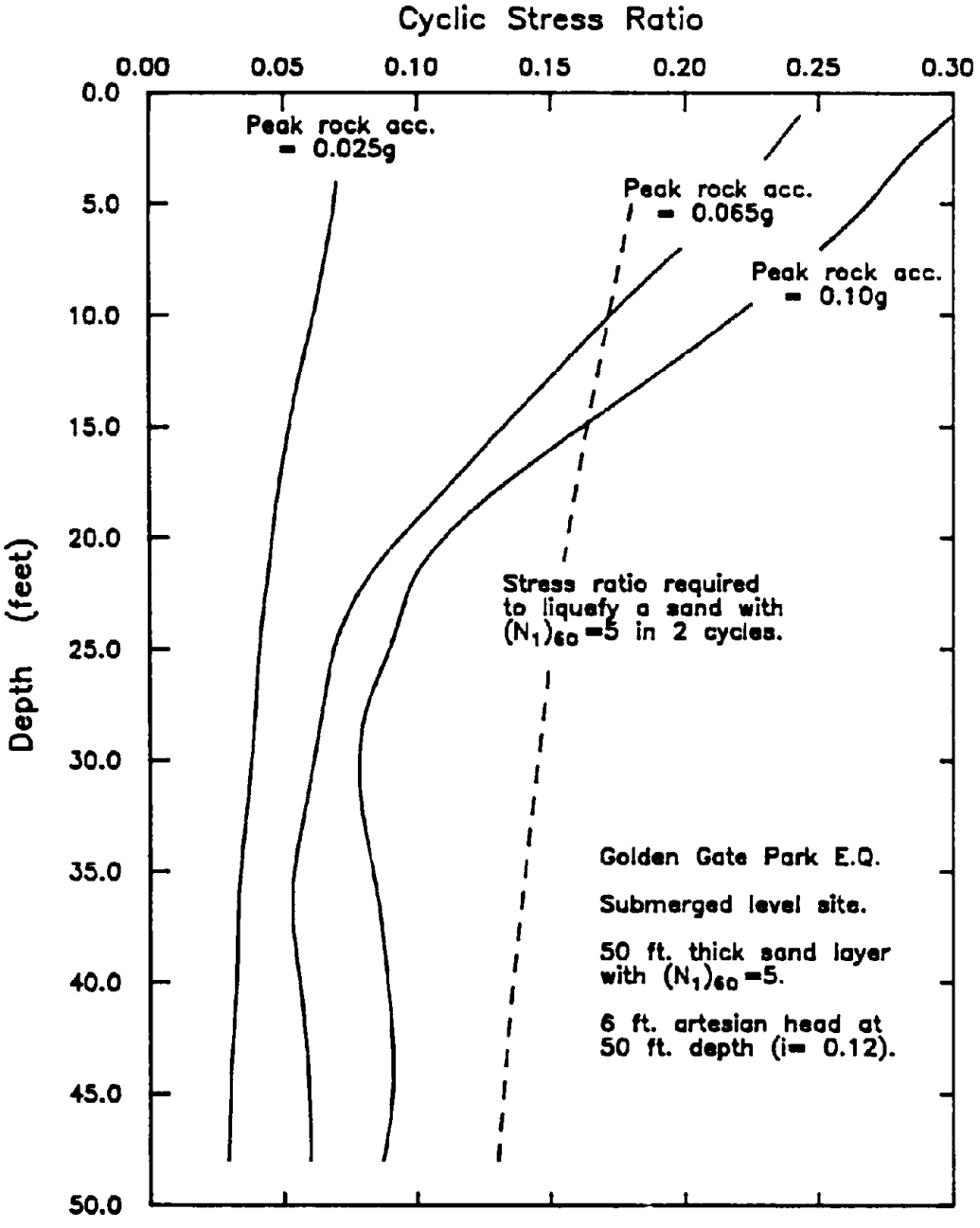

FIG 6.15 AVERAGE INDUCED CYCLIC STRESS RATIO AS A FUNCTION OF DEPTH FOR DIFFERENT LEVELS OF BEDROCK ACCELERATION - LEVEL SITE WITH ARTESIAN PRESSURE CONDITIONS - EARTHQUAKE MAG. = 5.25.

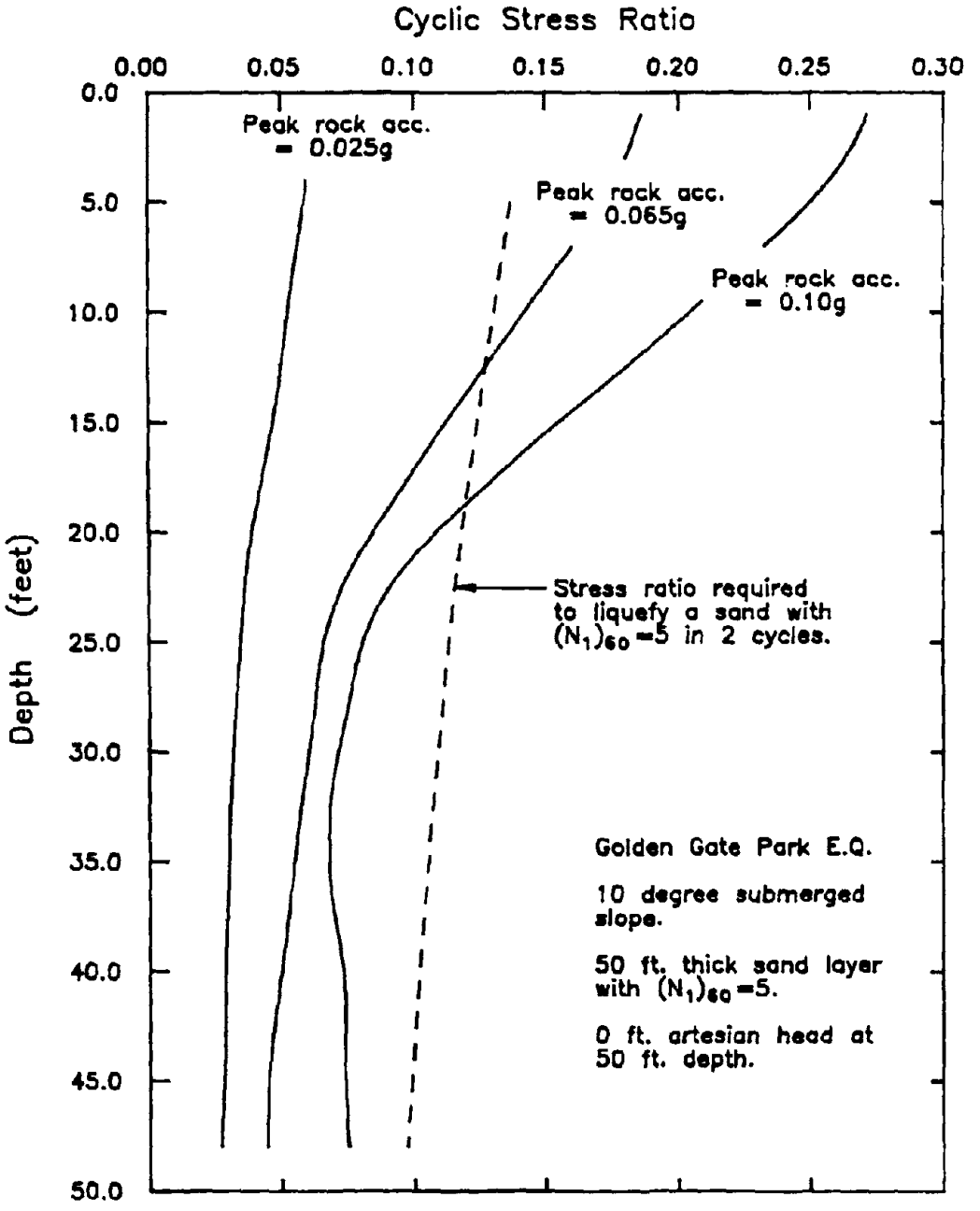

FIG 6.16 AVERAGE INDUCED CYCLIC STRESS RATIO AS A FUNCTION OF DEPTH FOR DIFFERENT LEVELS OF BEDROCK ACCELERATION - SLOPING SAND LAYER WITH NO ARTESIAN PRESSURES - EARTHQUAKE MAG. = 5.25.

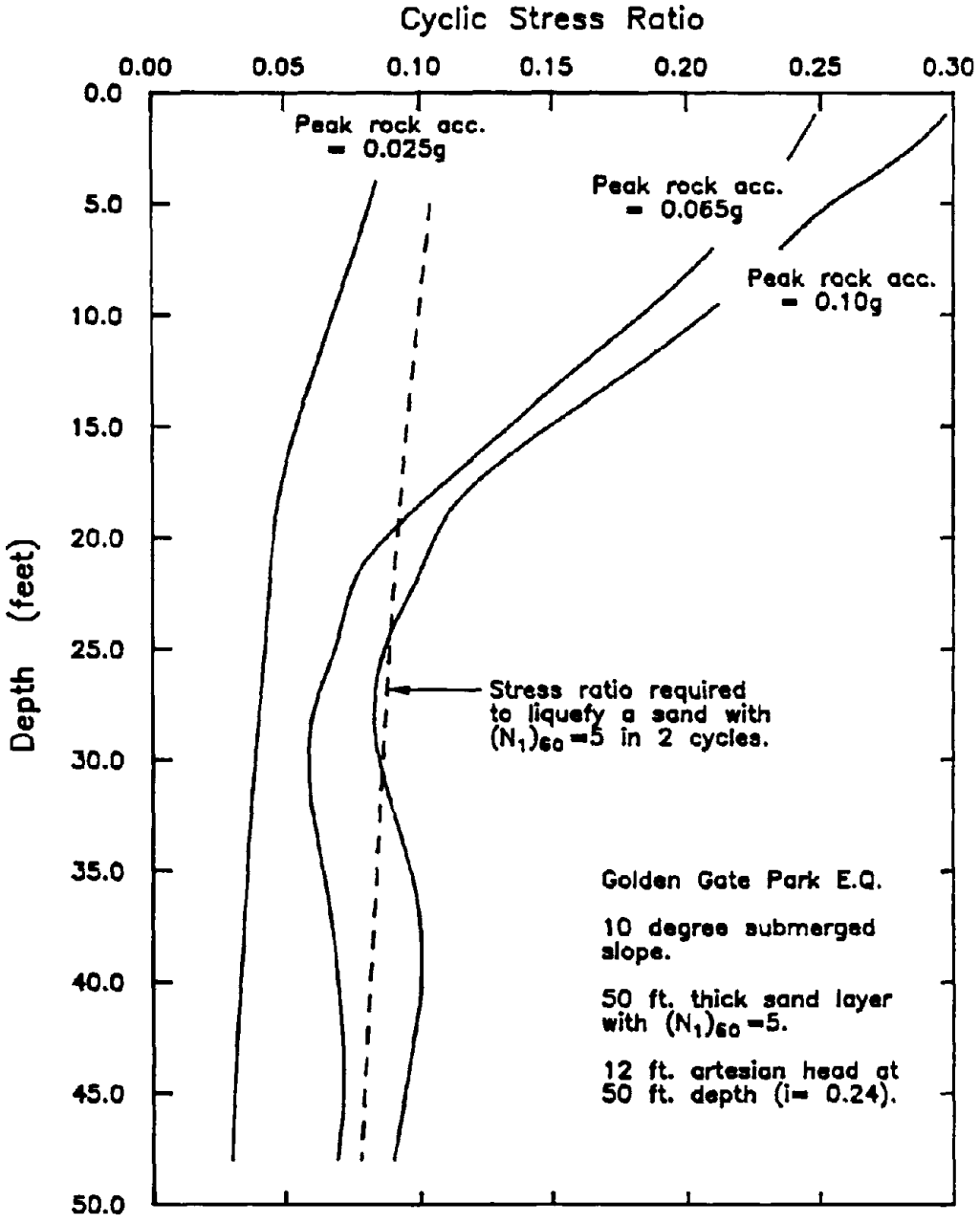

FIG 6.17 AVERAGE INDUCED CYCLIC STRESS RATIO AS A FUNCTION OF DEPTH FOR DIFFERENT LEVELS OF BEDROCK ACCELERATION - SLOPING SAND LAYER WITH ARTESIAN PRESSURE CONDITIONS - EARTHQUAKE MAG. = 5.25.

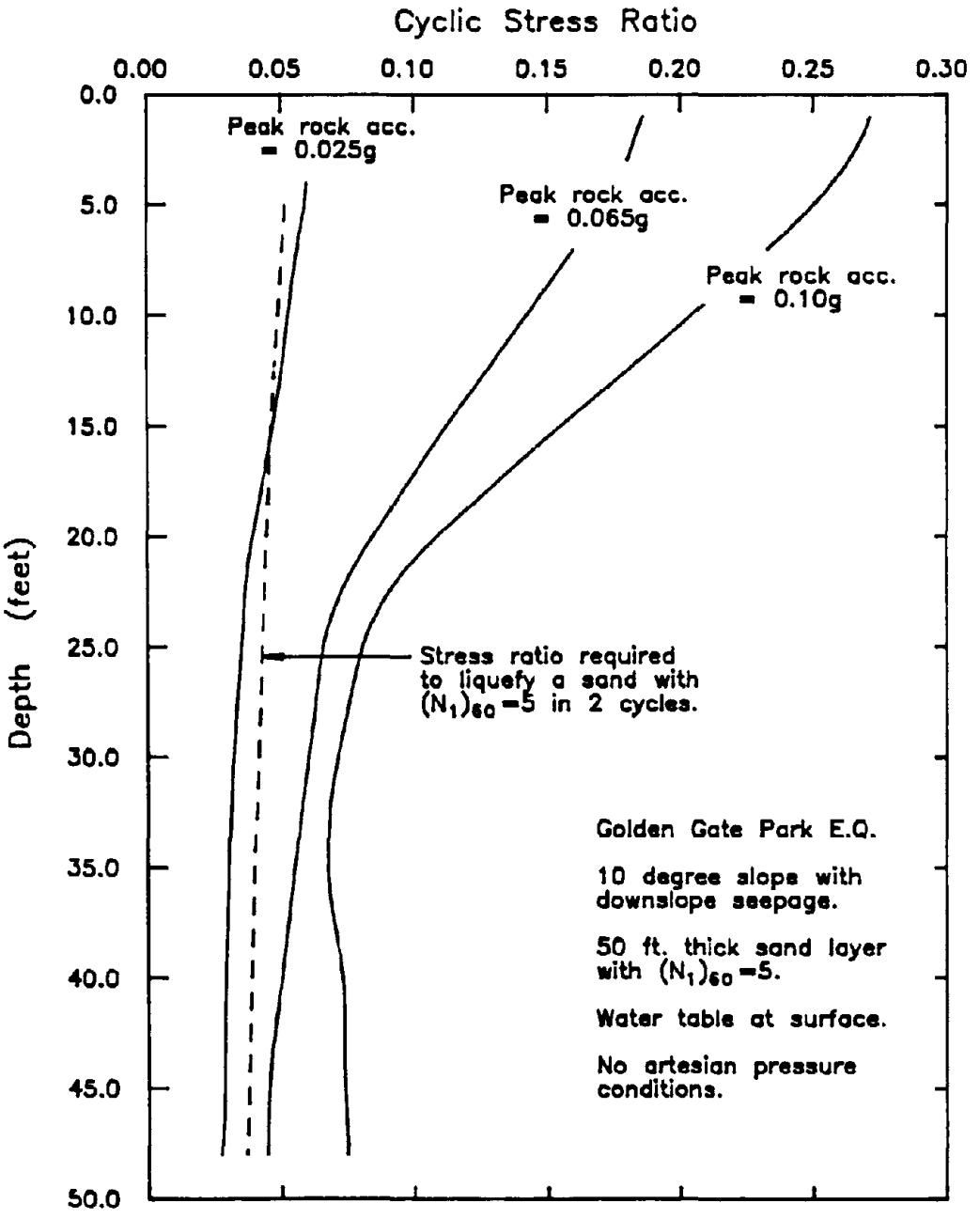

FIG 6.18 AVERAGE INDUCED CYCLIC STRESS RATIO AS A FUNCTION OF DEPTH FOR DIFFERENT LEVELS OF BEDROCK ACCELERATION - SLOPING SAND LAYER WITH DOWNSLOPE SEEPAGE - EARTHQUAKE MAG. = 5.25.

table at the ground surface, seepage occurring down the slope and parallel to the ground surface, and initial static shear stress ratios of about 0.37 (Equation 5.9) present on planes parallel to the ground surface. Assuming that the surface accelerations are about 130% larger than the corresponding bedrock motions, this result would indicate that loose sand deposits within 10 degree slopes may well liquefy under levels of shaking as low as 0.045g, a value approximately 3.5 times smaller than the value determined for level sites.

This predicted acceleration level for magnitude 5.25 earthquakes, is significantly less than 0.15g, the value indicated by the maximum distances at which liquefaction has been observed to occur in such earthquakes (see Figures 2.2 and 2.3). However, it is consistent with the maximum distances at which liquefaction has been observed to occur in larger magnitude earthquakes. For example, the upper bound curve shown in Figure 2.2 implies that magnitude 8 earthquakes may be capable of liquefying sand deposits at epicentral distances of about 400 kms. At such distances, these earthquakes are expected to generate peak ground surface accelerations of about 0.03g, and approximately 10 representative cycles of loading (at a cyclic stress level of 0.65 τ_{max}, Section 6.2). Thus, given that the cyclic stress ratio required to liquefy a sand in 2 to 3 cycles (for magnitude 5.25 earthquakes from Table 3.1) is only about 50 to 70% larger in magnitud. than the ratio required to liquefy the same sand in 10 cycles (Figure 3.3), it seems reasonable to conclude that the minimum level of shaking for magnitude 5.25 earthquakes should be about 0.05g. In fact, even if earthquakes of this magnitude are assumed to require cyclic stress ratios as much as 150% larger than those required for

higher magnitude earthquakes, the minimum level of shaking is still only predicted to be as high as about $0.03g \times 2.5 = 0.075g$. This level of acceleration is still significantly less than 0.15g. Thus it indeed seems possible that levels of shaking in Magnitude 5.25 earthquakes significantly less than the levels shown in figure 2.3 may be capable of causing liquefaction; this means that liquefaction may occur in these events at epicentral distances significantly greater than about 11 kms.

The fact that liquefaction does not appear to have been reported in Magnitude 5.25 earthquakes at epicentral distances greater than about 5 kms may well be due to some combination of the facts that : (1) earthquakes of this magnitude have caused liquefaction failures at greater distances, but they have not been reported in the technical literature because they are rarely significant events meriting major studies and (2) very few, if any, sufficiently susceptible sites are likely to exist, especially in areas prone to seismic shaking. This second factor is particularly appropriate when considering such low magnitude earthquakes because the region of significant shaking generated by such an earthquake, is small in comparison to the region shaken significantly by larger magnitude earthquakes. Therefore such critical sites, if they do exist, are less likely to be shaken by low magnitude earthquakes.

A rough estimate for the maximum distance at which critical sites may be liquefied, can possibly be obtained by using attenuation relationships to predict the levels of shaking induced at any given distance. Thus, the attenuation relationships listed in Section 2.2 were used to obtain approximate upper bound distances for the four sites analyzed in this section. It should be cautioned that these distances, which are

presented in Table 6.3, are at best very approximate values, as evidenced by the large scatter in the levels of shaking predicted for any given distance. In the near-field region (about 15 kms from the source) the scatter was as great as about ± 30%.

It may be seen from this table that the maximum distance at which liquefaction is predicted to occur is heavily dependent on the magnitudes of the initial shear stress/normal stress ratios. As these values are increased, the level of shaking required to induce liquefaction is significantly reduced, and hence the same deposit may be liquefied at even greater distances from the source than those indicated above. In reality, however, the distance determined for 10 degree slopes, with seepage occurring downslope, may well represent a practical upper bound distance since it seems reasonable to assume that very few natural deposits are likely to contain initial shear stress/normal stress ratios higher than about 0.4.

Table 6.3 : Approximate Upper Bound Distances for Liquefaction Occurring in Magnitude 5.25 Earthquake Shaking

Site	Static Shear Stress/ Normal Stress Ratio	Min. level of Shaking	Epicentral Dist. (kms)
Level ground Hydraulic grad. = 0.12	0.0	0.15g	12
10 degree slope Zero hydraulic grad.	0.18	0.10g	16
10 degree slope Hydraulic grad. = 0.24	0.24	0.07g	23
10 degree slope seepage down slope	0.37	0.05g	31

6.5. Summary and Conclusions

Many investigators currently believe that the minimum level of earthquake shaking required to liquefy a site is approximately equal to some value between about 0.05g and 0.10g. This level is supported by both field performance observations in the form of the modified Mercalli Intensity scale, and experimental data such as the concept of a threshold strain. However as discussed in Section 2.2 and reiterated in Section 6.2, it seems probable that levels of shaking significantly less than these values have already been known to cause liquefaction in, presumably, loose sand deposits. For example, the upper bound curve (fitted to the field performance data) shown in Figure 2.2, seems to imply that sites have been liquefied by earthquake shaking with peak ground surface accelerations as low as about 0.02g produced by earthquakes with Magnitudes ≈ 8.5 Figure 2.3).

It also seems probable that levels of shaking even less than those implied by Figure 2.3, may be capable of causing liquefaction. This prediction is based on the observation that as the magnitudes of the initial static shear stress/normal stress ratios imposed on a sand are increased, the liquefaction resistance of loose sands becomes very low (see Figure 3.5), indicating that liquefaction can be induced by extremely low levels of vibration. Obviously, such a prediction is contingent upon the fact that the site being shaken is in a sufficiently critical condition, i.e. that the sand within the deposit is both loose and subjected to very high initial shear stress ratios.

In reality, of course, few such sensitive sites are likely to exist, especially in areas that are prone to seismic shaking. Thus, it may well be that a practical minimum level

of shaking exists, not because of some characteristic property of sands such as threshold strain, but because of the maximum static shear stress/normal stress ratios that are likely to be present within a generally stable deposit, i.e. a deposit that would not have failed unless it was subjected to some critical level of seismic shaking.

The effects of artesian pressure conditions and initial static shear stresses on the minimum level of earthquake shaking required to cause liquefaction were evaluated by computing the responses of a variety of loose sand deposits. These deposits were situated within both level sites and 10 degree slopes and contained a range of artesian pore pressure conditions. It was found that for large (magnitude 8) earthquakes, the minimum level of shaking required to cause liquefaction for level sites appears to be reduced as the magnitudes of the excess pressures increase. Such pressures are predicted to have an even more substantial effect on the liquefaction potential of sloping sites since they also increase the initial shear stress/normal stress ratios present within the slope, and hence, further greatly reduce the liquefaction resistance of loose sand deposits.

The presence of initial static shear stresses has been shown by a number of investigators to have a significant effect on the cyclic loading resistance of loose ($D_R \approx 35\%$) sands (see Figure 3.5). Thus, the minimum levels of shaking required to liquefy sloping deposits is likely to be considerably less than the minimum level required for level sites. In consequence, the maximum distance at which sloping sites may liquefy is also predicted to be greater. An indication of the potential effects of site conditions on the maximum distance of liquefaction, is provided by the lines

depicting upper bound distances for the following four site conditions are shown in Figure 6.19: (1) level sites with 6 ft artesian head at a depth of 50 ft; (2) 10 degree slopes with 0 ft artesian head at a depth of 50 ft; (3) 10 degree slopes with 12 ft artesian head at a depth of 50 ft; and (4) 10 degree slopes with seepage down the slope. It is clear that such site conditions can have a significant influence on the distances to which liquefaction may be expected to occur in earthquakes of different magnitudes and that available data may not be indicative of these possibilities.

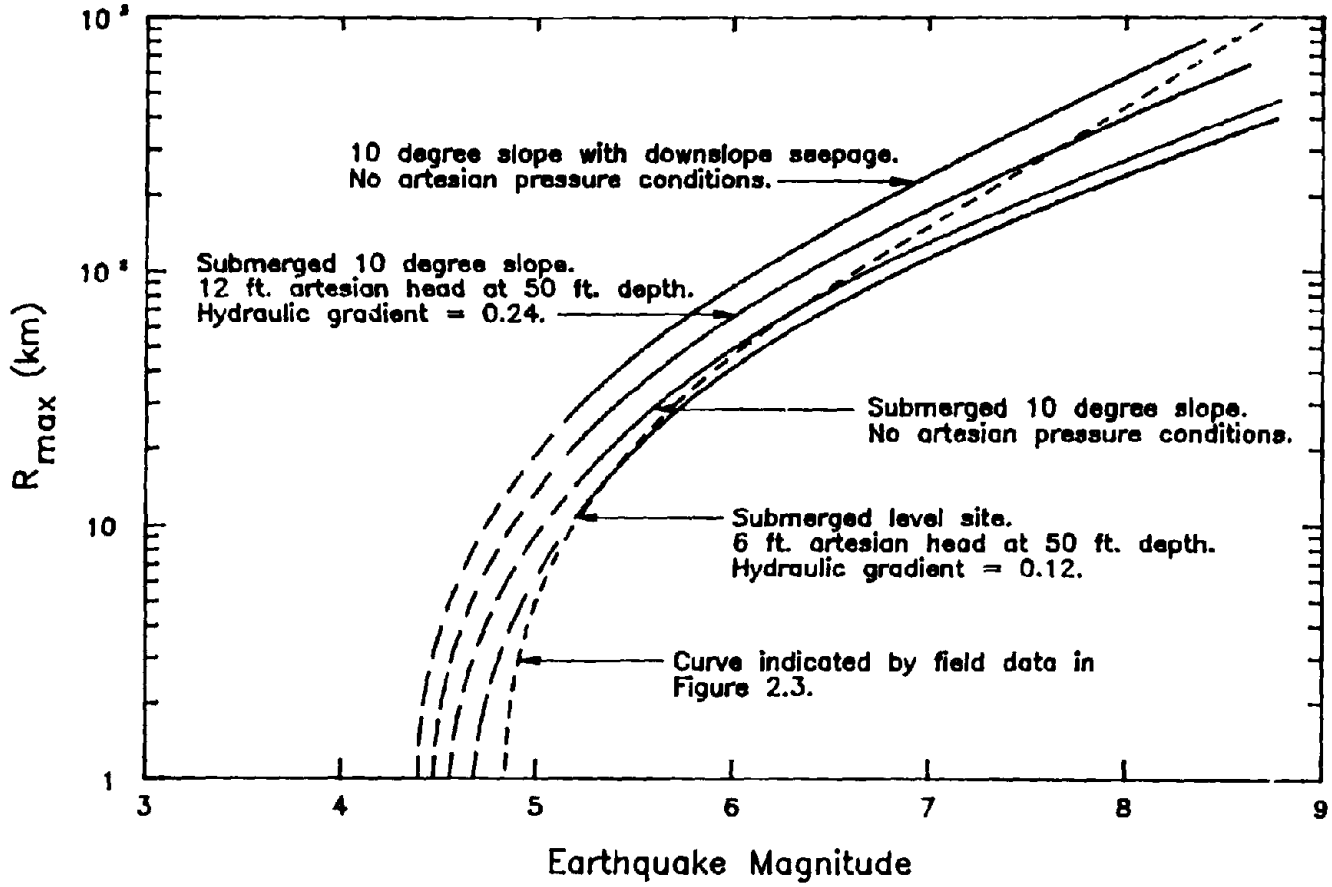

FIG 6.19 POTENTIAL EFFECTS OF SITE CONDITIONS ON THE MAXIMUM DISTANCE OF LIQUEFACTION FOR EARTHQUAKES OF DIFFERENT MAGNITUDES.

CHAPTER 7

Summary and Conclusions

7.1. Summary

The aim of this investigation was to determine the minimum levels of ground shaking that are capable of causing liquefaction both from seismic and non-seismic sources of vibration. As previously mentioned, many researchers currently believe that liquefaction will not occur unless the peak ground surface accelerations generated at a site exceed some value between about 0.05g and 0.10g. However, it now seems probable that levels of shaking significantly less than this value are not only capable of causing liquefaction, but have caused liquefaction in the past. This belief is based on the following:

1) the distances at which large (magnitude 8-9) earthquakes have induced liquefaction,

2) the fact that non-seismic sources of vibration appear to have caused a number of large-scale liquefaction failures, and such sources generate much lower levels of shaking than even small (magnitude 5) earthquakes, and

3) the liquefaction resistance of loose sands becomes very small as the magnitudes of the initial static shear stress/normal stress ratios imposed upon these sands are increased.

The ability of certain non-seismic sources to induce liquefaction has been noted for many years. In fact, engineers have used techniques such as blasting and dynamic compaction to deliberately liquefy the sands within loose sand deposits, as a means of densifying these deposits. Unfortunately, no information was found in the literature relating the levels of ground shaking generated by these two sources to observed field performance.

The non-seismic source that appears to generate the most liquefaction failures is pile driving. This source is particularly damaging for the following reasons: (1) a single pile driving operation may generate more than one million cycle of loading, (2) most of the energy transmitted from the pile to the soil is imparted at depth, rather than at the surface, as is the case with the majority of non-seismic sources, and (3) pore pressures are increased as a result of the volume of the soil displaced by the pile. Crockett (1979) reports that surface vibrations as low as about 0.3 mm/sec have been associated with significant ground settlements. However, for most cases, a higher level of 2.5 mm/sec may well be a more realistic minimum. A 36,000 ft-lb diesel pile driver is predicted to generate ground surface velocities in excess of this value at distances up to about 150 ft. from the pile (Figure 2.22).

Ground vibration attenuation relationships for most of the sources that were investigated are provided in Chapter 2. These relationships may be used to obtain approximate values for the levels of shaking likely to be induced at a site. At sites where it is necessary to determine these values with a reasonable degree of accuracy, a site-specific survey should be performed. In the absence of such a survey, it is

recommended that either upper bound, or 95 percentile curves, be used to predict ground vibration amplitudes because of the very large scatter in the ground vibration data on which these relationships are based.

Another non-seismic source which is capable of causing ground settlements is road traffic. For example, Terzaghi and Peck (1967) report that trucks had to banned from several streets in Munich because the settlements that they were causing were significant. However, given that the ground vibrations generated by even fully-loaded trucks (9 mm/sec from Figure 2.23), are only slightly larger in amplitude than the minimum levels determined for pile driving, and that these vibrations are confined to the surface layers (unlike pile driving), it seems reasonable to conclude that the ground shaking generated by road traffic is probably incapable of inducing large-scale liquefaction failures.

The train-induced ground vibration records that were obtained in this investigation confirm the common belief that trains are significant source of ground vibration. These records reveal that at distances closer than about 6 meters (20 ft.) from the tracks, trains are capable of generating peak ground surface accelerations in excess of 0.1g. In addition, the recorded motions were found to be considerably larger in amplitude than those reported in the literature. For example, Ames et al. (1976) report a peak particle velocity of about 4 mm/sec recorded at a distance of 2 meters from a diesel locomotive, while Figure 4.6 indicates that trains might be capable of generating velocities as large as about 20 mm/sec at the same distance.

The ability of trains to induce liquefaction was evaluated by following the shear stress approach, and the shear strain approach where applicable. The magnitudes of the stresses and strains induced within the various sites were computed on the assumption that such motions consist predominantly of Rayleigh waves, an assumption that is based on ideal elastic half-space theory, and supported by field attenuation measurements. It was found that for level sites, liquefaction is not predicted to occur at distances beyond about 3 meters (10 ft.) from the tracks. However, for sloping sites with seepage occurring down the slope and parallel to the ground surface, liquefaction might well occur as far as about 45 ft. from the tracks. It should be pointed out that even in this case, however, liquefaction is confined to the surface layers and is not predicted to occur at depths greater than about 15 ft at distances of about 10 ft. from the track.

Two failures that have been associated with trains (and are listed in Table 1.1) were analyzed during the course of this investigation. Since in both cases, the failure surfaces were located more than 35 ft below the ground surface, and train-induced ground vibrations appear to be confined to the surface layers, it seems reasonable to conclude that neither of these two failures were caused by trains. The Surte failure can most probably be attributed to ground shaking generated by pile driving. The second slide, which occurred at Guntorp, had started to fail prior to the passage of the train and while the train may have accelerated the failure, it seems likely that the slide may have occurred, anyway.

The effects of both artesian pore pressures, and initial static shear stresses, on the liquefaction potential of sand sites subjected to earthquake shaking, were evaluated by computing the responses of a variety of loose sand deposits. It was found that as the magnitudes of the initial shear stress/normal stress ratios imposed upon the deposits are increased, the levels of shaking required to cause liquefaction are significantly reduced. For example, level sites shaken by magnitude 8 earthquakes are not predicted to liquefy unless the peak ground surface accelerations exceed a value of about 0.07g. In contrast, saturated 10 degree slopes (with seepage down the slope) may liquefy under much lower levels of shaking of about 0.02g. Magnitude 8 earthquakes are predicted to generate accelerations of this magnitude at distances of about 570 kms (370 miles) from the epicenter of the earthquake.

In fact, analyses based on the shear stress approach imply that liquefaction can probably occur under extremely low levels of excitation. This prediction is based on the observation that as the magnitudes of the initial static shear stress/normal stress ratios imposed on loose sand deposits become large, the cyclic stress ratio required to cause liquefaction becomes very small. In reality of course, few natural deposits are likely to contain such high initial shear stress/normal stress ratios, especially in areas subject to ground shaking. Thus, levels of shaking of 0.02g to 0.03g may well represent a practical minimum for magnitude 8 earthquakes, not because lower levels are incapable of causing liquefaction, but because few, if any such critical sites, exist. The minimum levels of shaking for magnitude 5.25 earthquakes are believed to be considerably less than those implied by Figure 2.3.

The presence of artesian pore pressures is also predicted to have a significant effect on the minimum level of shaking required to liquefy a site. For example, submerged, level, loose sand deposits with artesian heads acting at depths of 50 ft., may liquefy under levels of shaking as low as 0.05g, while similar sites with zero artesian pore pressures are not predicted to liquefy unless the ground surface accelerations exceed a value of about 0.07g. Since the presence of such pressures increases the values of initial static shear stress/normal stress ratios within sloping sites, and hence lowers the liquefaction resistance of loose sand deposits, artesian pressures have an even more substantial effect on the liquefaction potential of sloping deposits.

REFERENCES

Ahlbeck, D.R. (1986), "A Review of Rail Behavior under Wheel/Rail Impact Loading", U.S. Dept. of Transportation, Federal Railroad Administration, Report No. DOT-FRA-ORD-86-01, April, 1986.

Ambraseys, N.R. and Hendron, A.R. Jr. (1968), "Dynamic Behaviour of Rock Masses", in Rock Mechanics in Engineering Practice, K.G. Stagg and O.C. Zienkiewicz, John Wiley and Sons, London, pp. 203-227.

Ames, W.H., Chow, W., Sequeira, A. and Johnson, R. (1976), "Survey of Earth-Borne Vibrations Due to Highway Traffic", Report No. CA-DOT-TL-1-76-20, prepared for California Dept. of Transportation, Sacramento, California 95807.

Atkins, K.P. and Dixon, D.E. (1979), "Concrete Structures and Construction Vibrations", Vibrations of Concrete Structures, SP-60, American Concrete Institute, 1979, pp. 213-247.

Attewell, P.D. and Farmer, I.W. (1973), "Attenuation of Ground Vibrations in Pile Driving", Ground Engineering, Vol. 6, No. 4, pp. 26-29.

Barkan, D.D. (1962), Dynamics of Bases and Foundations, McGraw-Hill Book Co., New York, 1962, 434 pp.

Barneich, J.A. (1985), "Vehicle Induced Ground Motion", in Vibration Problems in Geotechnical Engineering, A.S.C.E., Proceedings of a Symposium Sponsored by the Geotechnical Engineering Division, October 22, 1985, pp. 187-202.

Battis, J. (1981), "Regional Modification of Acceleration Functions", Bulletin of the Seismological Society of America, No. 71, pp. 1309-1321.

Bjurstrom, G. and Broms, B. (1982), "The Landslide at Froland, June 5, 1973", Proceedings of the Symposium on Slopes in Soft Clay, Linkoping, March 10, 1982, pp. 113-125.

Bollinger, G.A. (1970), "Blast Vibration Analysis", Manuscript of Sprengnether Instrument Company.

Brazee, R.J. (1979), "Reevaluation of Modified Mercalli Intensity Scale for Earthquakes Using Distance as Determinant", Bulletin of the Seismological Society of America, Vol. 69, No. 3, June, 1979, pp. 911-924.

Broms, B. (1978), "Translatory Slips in Soft Clays", Proc. of the International Conference on Evaluation and Prediction of Subsidence, Pensacola, Florida, USA, January, 1978, pp. 169-187.

Broms, B. and Bennermark, H. (1967), Free discussion, Proceedings of the Geotechnical Conference, Oslo, 1967, Vol. 2, pp. 118-120.

Brown, L.M. (1971), "Measurements of Vibrations Caused by Construction Equipment and Blasting", Dept. of Highways, Ontario, D.H.O. Report No. RR-172, April, 1971.

Castro, G., Poulos, S., France, J. and Eros, J. (1982), "Liquefaction Induced by Cyclic Loading", Geotechnical Engineers Inc., March, 1982.

Chae, Y.S. (1978), "Design of Excavation Blasts to Prevent Damage", Civil Engineering, A.S.C.E., Vol. 48, No. 4, April, 1978, pp. 77-79.

Charles, J.A., Burford, D. and Wattis, K.S. (1981), "Field Studies of the Effectiveness of Dynamic Consolidation", Proc. of the Tenth International Conference on Soil Mechanics and Foundation Engineering, Stockholm, 1981, Vol. 3, pp. 617-622.

Chilton, F., Friesz, T. and Chen, E. (1975), "Traffic Induced Vibration", in Effect of Roadway Geometrics on Traffic Operations, Transportation Research Record No. 541, pp. 40-49.

Clough, G.W. and Chameau, J.L. (1980), "Measured Effects of Vibratory Sheetpile Driving", Journal of the Geotechnical Engineering Division, A.S.C.E., Vol. 106, No. GT10, October, 1980, pp. 1081-1099.

Conlon, R. (1966), "Landslide at the Toulnustouc River, Quebec", Canadian Geotechnical Journal, Vol. 3, No. 3, August, 1966, pp. 113-144.

Cording, E.J., Hendron, A.J., Hansmire, W.H., MacPherson, H., Jones, R.A. and O'Rourke, T.D. (1975), "Method for Geotechnical Observations and Instrumentation in Tunneling", Vol. 2, National Science Foundation, Grant No. GZ-33644X.

Cornell, C.A., , H. and Shakal, A.F. (1979), "Seismic Motion and Response Prediction Alternatives", Journal of Earthquake Engineering and Structural Dynamics, No. 7, pp. 295-315.

Crandell, F.J. (1949), "Ground Vibrations due to Blasting and its Effects on Structures", Journal of the Boston Society of Civil Engineers, Vol. 3, pp. 222-245.

Crockett, J.H.A. (1966), "Some Practical Aspects of Vibrations in Civil Engineering", Proc. Symp. British National Society, International Soc. of Earthquake Engineering, Imperial College, London, 1965, pp. 253-271, Butterworths, London, 1966.

Crockett, J.H.A. (1979), "Piling Vibrations and Structural Fatigue", Recent Developments in the Design and Construction of Piles, I.C.E., London, pp. 305-317.

Dalmatov, B.I., Ershov, V.A. and Kovalevsky, E.D. (1968), "Some Cases of Foundation Settlement in Driving Sheeting and Piles", Proc. of the Symposium on Wave Propagation and Dynamic Properties of Earth Materials, University of New Mexico, Albuquerque, New Mexico, 1968, pp. 607-613.

Davis, R.O and Berrill, J.B. (1983), "Comparison of a Liquefaction Theory with Field Observations", Geotechnique, Vol. 33, No. 4, pp. 455-460.

Dawn, T.M. (1983), "Ground Vibrations from Heavy Freight Trains", Journal of Sound and Vibration, 1983, Vol. 85, pp. 177-255.

Dawn, T.M. and Stanworth, C.G. (1979), "Ground Vibrations from Passing Trains", Journal of Sound and Vibration, Vol. 66, No. 3, pp.355-362.

De Alba, P., Seed, H.B. and Chan, C.K. (1976), "Sand Liquefaction in Large-Scale Simple Shear Tests", Journal of the Geotechnical Engineering Division, A.S.C.E., Vol. 102, No. GT9, Proc. Paper 12403, September, 1976, pp. 909-927.

Devine, J. (1966), "Avoiding Damage to Residences from Blasting Vibrations", Highway Research Record No. 135, Highway Research Board, National Research Council, National Academy of Sciences, pp. 35-42.

Devine, J.F. and Duvall, W.I. (1963), "Effect of Charge Weight on Vibration Levels for Multi-Second Delayed Quarry Blasts", Earthquake Notes, Seismological Society of America, Eastern Section, Vol. 34, No. 2, p. 17.

Dobry, R. and Ladd, R.S. (1980), Discussion to "Soil Liquefaction and Cyclic Mobility Evaluation for Level Ground During Earthquakes" by H.B. Seed and "Liquefaction Potential: Science Versus Practice",by R.B. Peck, Journal of the Geotechnical Engineering Division, A.S.C.E., Vol. 106, No. GT6, June, 1980, pp. 720-724.

Dobry, R., Ladd, R.S., Yokel. F.Y., Chung, R.M. and Powell, D. (1982), "Prediction of Pore Water Pressure Buildup and Liquefaction of Sands During Earthquakes by the Cyclic Strain Method", NBS Building Science Series 138, July, 1982.

Dobry, R., Stokoe, K.H., Ladd, R.S. and Youd, T.L. (1981a), "In-Situ Shear Wave Velocity Measurements to Evaluate Liquefaction Susceptibility", A.S.C.E. National Convention, St. Louis, Missouri, October 27, 1981.

Dobry, R., Yokel, F.Y. and Ladd, R.S. (1981b), "Liquefaction Potential of Overconsolidated Sands in Areas with Moderate Seismicity", Proc. Conference on Earthquakes and Earthquake Engineering in the Eastern U.S., Knoxville, TN, September, 1981, Vol. 2, pp. 643-664.

Donovan, N.C. and Bornstein, A.E. (1978), "Uncertainties in Seismic Risk Procedures", Journal of the Geotechnical Engineering Division, A.S.C.E., Vol. 104, pp. 869-887.

Dowding, C.H. (1971), "Response of Buildings to Ground Vibrations Resulting from Construction Blasting", Ph.D. Thesis, University of Illinois, Urbana, Illinois, 1971.

Dowding, C.H. (1985), Blast Vibration Monitoring and Control, Prentice-Hall Inc..

Drnevich, V.P. and Richart, F.E. Jr. (1970), "Dynamic Prestraining of Dry Sands", Journal of the Soil Mechanics and Foundation Engineering Division, A.S.C.E., Vol. 96, No. SM2, March, pp. 453-469.

Duvall, W.I. and Fogelson, D.E. (1962), "Review of Criteria for Estimating Damage to Residences from Blasting Vibrations", Report of Investigations 5968, Bureau of Mines Report.

Dyvik, R., Dobry, R., Thomas, G.E. and Pierce, W.G. (1984), "Influence of Consolidation Shear Stresses and Relative Density on Threshold Strain and Pore Pressure During Cyclic Straining of Saturated Sands", U.S. Army Engineer Waterways Experiment Station, Report No. GL-84-15, June, 1984.

Edwards, A.J. and Northwood, T.D. (1960), "Experimental Studies of Blasting on Structures", in The Engineer, Vol. 210, pp. 538-546.

Fellenius, B. (1953), "The Landslide at Guntorp", Geotechnique, Vol. 5, No. 1, pp. 120-125.

Frederick, C.O. and Round, D.J. (1985), "Vertical Track Loading", Track Technology, Proc. of a Conference of the Institute of Civil Engineers, July 11-13, 1984., Thomas Telford Ltd, London, 1985.

Frydenlund, T.E. (no date), "Road Vibrations", Veglaboratoriet of Norges Geotekniske Instituut, Oslo, Norway.

Fuller, M.L. (1912), "The New Madrid Earthquake", Bulletin 494, U.S. Geologic Survey, Department of the Interior, Washington, D.C.

Gambin, M.P. (1984), "Ten Years of Consolidation", paper to be presented to the Eighth Regional Conference for Africa (I.S.S.M.F.E.), Harere, Zimbabwe, June 4-7, 1984.

Goldman, D.E.A. (1948), "A Review of Subjective Responses to Vibratory Motion of the Human Body in the Frequency Range 1 to 70 cps", Report NM-004-00, Naval Medical Research Institute, Washington D.C., 1948.

Goldman, D.E. and von Gierke, H.E. (1961), "Effects of Shock and Vibration on Man", in Shock and Vibration Handbook, New York, 1961.

Griffin, M.J. and Stanworth, C.G. (1985), "The Generation and Perception of Vibration from Rail Traffic", in Track Technology, Proc. of a Conference of the Institute of Civil Engineers, July 11-13, 1984., Thomas Telford Ltd, London, 1985.

Hansbo, S. (1977), "Dynamic Consolidation of Rockfill", Proc. of the Ninth International Conference on Soil Mechanics and Foundation Engineering, Vol. 2, Tokyo, Japan, 1977, pp. 241-246.

Hansbo, S. (1978), "Dynamic Consolidation of Soil by a Falling Weight", Ground Engineering, Vol. 11, No. 5, July, 1978, pp. 27-36.

Harder, L.F. (1988), "The Use of Penetration Tests to Determine the Liquefaction Potential of Soils During Earthquakes", Ph.D. Thesis, Dept. of Civil Engineering, University of California, Berkeley, 1988.

Hasegawa, H.S., Basham, P.W. and Berry, M.J. (1981), "Attenuation Relations for Strong Seismic Ground Motion", Bulletin of the Seismological Society of America, No. 71, pp. 2071-2095.

Heckman, W.S. and Hagerty, D.J. (1978), "Vibrations Associated with Pile Driving", Journal of the Construction Division, Vol. 104, No. CO4, pp. 385-395.

Hendron, A.J. Jr. (1977), "Engineering of Rock Blasting on Civil Projects", in Structural and Geotechnical Mechanics, edited by W.J. Hall, Prentice-Hall Inc.

Iwasaki, T., Katayama, T., Kawashima, K. and Saeki, M. (1978a), "Statistical Analysis of Strong Motion Acceleration Records Obtained in Japan", Proc. of the Second International Conference on Microzonation, San Francisco, Vol. 2, pp. 705-716.

Iwasaki, T., Tatsuoka, F., Tokida, K. and Yasuda, S. (1978b), "A Practical Method for Assessing Soil Liquefaction Potential Based on Case Studies at Various Sites in Japan, Proc. of the Second International Conference on Microzonation for Safer Construction-Research and Application, Vol. 2, pp. 885-896.

Jakobsen, B. (1952), "The Landslide at Surte on the Gota River, September 29, 1952", Royal Swedish Geotechnical Institute, Proceedings No. 5, Stockholm, 1952.

Jenkins, H.H., Stephenson, J.E., Clayton, G.A., Morland, G.W. and Lyon, D. (1974), "The Effect of Track and Vehicle Parameters on Wheel/Rail Vertical Dynamic Forces", Railway Engineering Journal, Vol. 3, No. 1., 1974

Koch, H.W. (1953), "Determining the Effects of Vibrations in Buildings", VDI Z, Vol. 95, No. 21, 1953, pp. 744-747.

Kovalevsky, E.D. (1965), "On the Problem of Determining Modulus of Total Sand Soil Deformation under Vibration. Some Problems of Mechanical Engineering and Structural Mechanics", Proc. of the Leningrad Institute of Economics, published 1957, Part 2, ed. Leningrad State University (L.G.U), Leningrad.

Krinitzsky, E.L. and Chang, F.K. (1987), "Parameters for Specifying Intensity-Related Earthquake Ground Motions", Dept. of the Army, Waterways Experiment Station, U.S. Army Corps of Engineers, Misc. Paper No. S-73-1, September, 1987, 43 pages.

Kuribayashi, E. and Tatsuoka, F. (1975), "Brief Review of Liquefaction during Earthquakes in Japan", Soils and Foundations, Vol. 15, No. 4, December, 1975, pp. 81-92.

Lacy, H.S. and Gould, J.P. (1985), "Settlement from Driving Piles in Sands", in Vibration Problems in Geotechnical Engineering, A.S.C.E., Proc. of a Symposium Sponsored by the Geotechnical Engineering Division, October 22, 1985, pp. 152-173.

LADWP (1981), Internal Report.

Lande, G. (1974), "Relation Between Traffic Generated Vibrations, their Frequency, Particle Motion, Displacement, Velocity and Speed of the Truck", Uppsala University, No. 47.

Langefors, U. and Kihlstrom, B. (1963), The Modern Technique of Rock Blasting, John Wiley and Sons Inc., New York.

Langefors, U., Kihlstrom, B. and Westerburg, H. (1958), "Ground Vibrations in Blasting", Water Power, February, 1958.

Leonards, G.A., Cutler, W.A. and Holtz, R.D. (1980), "Dynamic Compaction of Granular Soils", Journal of the Geotechnical Engineering Division, Vol. 106, No. GT1, January, 1980, pp. 35-44.

Lo, M.B. (1976), "Attenuation of Ground Vibrations Induced by Pile Driving", Proc. of the Ninth International Conference on Soil Mechanics and Foundation Engineering, Vol. 2, Paper No. 4/20, 1976, pp. 281-286.

Loos, W. (1936), "Comparative Study for Compacting Cohesionless Soils", Proc. of the First International Conference on Soil Mechanics and Foundation Engineering, Vol. 3, Harvard University, June, 1936, pp. 174-178.

Lukas, R.G. (1980), "Densification of Loose Deposits by Pounding", Journal of the Geotechnical Engineering Division, Vol. 106, No. GT4, April, 1980, pp. 435-446.

Lukas, R.G. (1984), "Dynamic Compaction Manual", STS Consultants Report to the Federal Highway Administration, Washington D.C., Contract No. DTFH-61-83-C-00095, March, 1984.

Luna, W.A. (1967), "Ground Vibrations due to Pile Driving", Foundation Facts, Vol. 3, No. 2, Raymond International, Houston, Texas, pp. 3-5.

Lynch, T.J. (1960), "Pile Driving Experiences at Port Everglades", Journal of the Soil Mechanics and Foundations Division, Vol. 86, No. SM2, Proc. Paper No. 2442, April, 1960, pp. 41-62.

Mallard, D.J. and Barstow, P. (1979), "Some Observations on the Vibration Caused by Pile Driving", Recent Developments in Design and Construction of Piles, I.C.E., London, pp. 261-284.

Martin, D.J. (1980), "Ground Vibrations from Impact Pile Driving During Road Construction", Transport and Road Research Laboratory Report No. 544, 1980, Crowthorne, England, 25 pages.

Mayne, P.W. (1985), "Ground Vibrations During Dynamic Compaction", in Vibration Problems in Geotechnical Engineering, Proc. of a Symposium Sponsored by the Geotechnical Engineering Division, October 22, 1985, pp. 247-265.

Mayne, P.W. and Jones, J.S. (1983), "Impact Stresses During Dynamic Compaction", Journal of the Geotechnical Engineering Division, Vol. 109, No. 10, October, 1983, pp. 1342-1346.

Mayne, P.W., Jones, J.S. and Boudra, L. (1983), "Field Testing Program of Dynamic Compaction for I-65, Jefferson County, Alabama", Law Engineering Report to Alabama Highway Department, Feb 11, 1983.

Mayne, P.W., Jones, J.S. and Dumas, J.C. (1984), "Ground Response to Dynamic Compaction", Journal of the Geotechnical Engineering Division, Vol. 110, No. 6, June, 1984, pp. 757-774.

Mayne, P.W., Jones, J.S. and Fedosick, R.P. (1982), "Predicting Subsurface Improvement due to Impact Densification", presented at the A.S.C.E. Geotechnical Conference, Session B2, April 28, 1982, Las Vegas, Nevada.

McGuire, R.K. (1977), "Seismic Design Spectra and Mapping Procedures using Hazard Analysis Based Directly on Oscillator Response, Journal of Earthquake Engineering and Structural Dynamics, No. 5, pp. 211-234.

McGuire, R.K. (1978), "Seismic Ground Motion Parameter Relations", Journal of the Geotechnical Engineering Division, A.S.C.E., Vol. 104, pp. 481-490.

Medearis, K. (1977), "The Development of Rational Damage Criteria for Low Rise Structures Subjected to Blasting Vibration", Proc. of the Eighteenth U.S. Symposium on Rock Mechanics, June, 1977, pp. 1A2-1 to 1A2-6.

Menard (no date), "The Dynamic Consolidation of Foundation Soils", Internal Publication, Techniques Louis Menard S.A..

Menard, L. and Broise, Y. (1975), "Theoretical and Practical Aspects of Dynamic Consolidation", Geotechnique, London, England, Vol. 25, No. 1, March 1975, pp. 3-18.

Miller, G.F. and Pursey, H. (1955), "On the Partition of Energy Between Elastic Waves in a Semi-Infinite Solid", Proc. of the Royal Society of London, Vol. 223, pp. 55-69.

Mitchell, J.K. (1981), "Soil Improvement: State-of-the-Art", Session 12, Tenth International Conference on Soil Mechanics and Foundation Engineering, Stockholm, Sweden, June 15-19, 1981.

Naik, T.R. (1979), "Predictions of Damage to Low-Rise Buildings Due to Ground Vibrations Created by Blastings", Vibrations of Concrete Structures, SP-60, American Concrete Institute, 1979, pp. 249-264.

Nicholls, H.R., Johnson, C.F. and Duvall, W.I. (1971), "Blasting Vibrations and their Effects on Structures", Bureau of Mines Report #656.

Northwood, T.D., Crawford, R. and Edwards, A.T. (1963), "Blasting Vibrations and Building Damage", The Engineer, Vol. 215, No. 5601, pp. 973-978.

O'Neill, D.B. (1971), "Vibration and Dynamic Settlement from Pile Driving", Proc. of the Conference on Behaviour of Piles, The Institute of Civil Engineers, London, pp. 135-140, 1971.

Oriard, L.L. (1971), "Blasting Effects and their Control in Open Pit Mining", Symposium and Speciality Seminar on Stability in Open Pit Mines, University of British Columbia, November, 1971.

Oriard, L.L. (1971), "Blasting Operations in the Urban Environment", Bulletin of the Association of Engineering Geologists, Winter 1971.

Orphal, D.L. and Lahoud, J.A. (1974), "Prediction of Peak Ground Motion from Earthquakes", Bulletin of the Seismological Society of America, No 64, pp. 1563-1574.

Park, T. and Silver, M.L. (1975), "Dynamic Soil Properties Required to Predict the Dynamic Behavior of Elevated Transportation Structures", U.S. Dept. of Transportation Report DOT-TST-75-44, May, 1975.

Peck, R.B., Hanson, W.E. and Thornburn, T.H. (1974), Foundation Engineering, 2nd Edition, John Wiley & Sons Inc., 1974.

Picornell, M. and del Monte, E. (1985), "Pile Driving Induced Settlements of a Pier Foundation", Vibration Problems in Geotechnical Engineering, A.S.C.E., Proc. of a Symposium Sponsored by the Geotechnical Engineering Division, October 22, 1985, pp. 174-186.

Pyke, R.M. (1973), "Settlement and Liquefaction of Sands under Multi-Directional Loading", Ph.D. Thesis, Dept. of Civil Engineering, University of California, Berkeley, 1973.

Rathbone, T.C. (1963), "Human Sensitivity to Product Vibration", Product Engineering.

Reiher, H., and Meister, F.J. (1931), "Human Sensitivity to Vibration", Forschung auf dem Gebiete Ingenieurwesens, 1931, Vol. 2, No. 11, pp 381-386.

Richart, F.E., Hall, J.R. and Woods, R.D. (1970), Vibrations of Soils and Foundations, Englewood Cliffs, Prentice-Hall Inc..

Rickley, E.J. and Rice, N.E. (1981), "Vibration Level Data, Brighton-New York City Transit Authority", Report No. UMTA-MA-06-0099-81-2, prepared for U.S. Dept. of Transportation, August, 1980.

Ross, Grant A. (1968) "Case Studies of Soil Stability Problems Resulting from Earthquakes", Ph.D. Thesis, Dept. of Civil Engineering, University of California, Berkeley, 1968.

Rudder, R.R. Jr. (1978), "Engineering Guidelines for the Analysis of Traffic Induced Vibration", Report No. FHWA-RD-78-166, February, 1978, prepared for U.S. Federal Highway Administration, Offices of Research and Development, Washington, D.C. 20590.

Scott, R.A. and Peirce, R.W. (1975), "Soil Compaction by Impact", Geotechnique, London, England, Vol. 25, No. 1, 1975, pp. 19-30.

Seed, H.B (1979), "Soil Liquefaction and Cyclic Mobility Evaluation for Level Ground During Earthquakes", Journal of the Geotechnical Engineering Division, A.S.C.E., Vol. 105, No. GT2, February, 1979, pp. 201-255.

Seed, H.B. and Idriss, I.M. (1970), "Soil Moduli and Damping Factors for Dynamic Response Analyses", University of California, Berkeley, EERC Report No. UCB/EERC 70-10, December, 1970.

Seed, H.B. and Idriss, I.M. (1971), "Simplified Procedure for Evaluating Soil Liquefaction Potential", Journal of the Soil Mechanics and Foundations Division, A.S.C.E., Vol. 97, No. SM9, September, p. 1249-1274.

Seed, H.B. and Idriss, I.M. (1982), "Ground Motions and Soil Liquefaction During Earthquakes", Engineering Monographs on Earthquake Criteria, Structural Design and Strong Motion Records, Earthquake Engineering Research Institute.

Seed, H.B., Idriss, I.M., and Arango, Ignacio (1983), "Evaluation of Liquefaction Potential Using Field Performance Data", Journal of the Geotechnical Engineering Division, Vol. 109, No. 3, March, 1983.

Seed, H.B., Idriss, I.M., Makdisi, F. and Banerjee, N. (1975), "Representation of Irregular Stress Time Histories by Equivalent Uniform Stress Series in Liquefaction Analyses", University of California, Berkeley, EERC Report No. UCB/EERC 75-29, October, 1975.

Seed, H.B., Romo, M.P., Sun, J.I., Jaime, A. and Lysmer, J. (1987), "Relationships Between Soil Conditions and Earthquake Motions in Mexico City in the Earthquake of Sept. 19, 1985", University of California, Berkeley, EERC Report No. UCB/EERC 87-15, October, 1987.

Seed, H.B., Singh, Sukhmander, Chan, C.K. and Vilela, F.F. (1982), "Considerations in Undisturbed Sampling of Sands", Journal of the Geotechnical Engineering Division, A.S.C.E., Vol 108, No. GT2, February, 1982, pp. 265-283.

Seed, H.B., Tokimatsu, K., Harder, L.F. and Chung, R.M. (1984), "The Influence of SPT Procedures in Soil Liquefaction Resistance Evaluations", University of California, Berkeley, EERC Report No. UCB/EERC 84-15, October, 1984.

Silver, M.L. and Seed, H.B. (1971), "Volume Changes in Sands during Cyclic Loading", Journal of the Soil Mechanics and Foundations Division, A.S.C.E., Vol. 97, No. SM9, September, 1971, pp. 1171-1182.

Siskind, D.E., Stagg, M.S., Kopp, J.W., and Dowding, C.H. (1980), "Structure Response and Damage Produced by Ground Vibrations from Surface Blasting", U.S. Bureau of Mines, Report of Investigations 8507.

Skipp, B.O. (1984), "Dynamic Ground Movements - Man-made Vibrations", in Ground Movements and their Effects on Structures, ed. by Attewell, P.B. and Taylor, R.K., Surrey University Press, London, 1984.

SN 640 312 "Effects of Vibration on Construction", Swiss Association of Standardization, Seefeldstrasse 9, CH 8008, Zurich, Switzerland.

Stagg, M.S. and Engler, A.J. (1980), "Measurement of Blast-Induced Ground Vibrations and Seismograph Calibrations", U.S. Bureau of Mines, Report of Investigations 8506.

Studer, J. and Suesstrunk, A. (1981), "Swiss Standard for Vibrational Damage to Buildings", Proc. of the Tenth International Conference on Soil Mechanics and Foundation Engineering, Vol. 3, Stockholm, 1981, pp. 307-312.

Szerdy, F.S. (1985), "Flow Slide Failures Associated with Low Level Vibrations", Ph. D. Thesis, Dept. of Civil Engineering, University of California, Berkeley, 1985.

Terzaghi, K. and Peck, R.B. (1967), Soil Mechanics in Engineering Practice, 2nd edition, John Wiley and Sons, New York, 1967.

Theissen, J.R. and Wood, W.C. (1982), "Vibrations in Structures Adjacent to Pile Driving", Engineering Bulletin 60, July, 1982, pp. 5-21.

Thoenen, S.R. and Windes, S.L. (1942), "Seismic Effects of Quarry Blasting", Bulletin 442, Bureau of Mines.

Thomas, G.E. and Dobry, R. (1984), "Cyclic Strain-Controlled Tests for Liquefaction Studies of Saturated Debris from Mount St. Helen Volcanic Explosion", sponsored by U.S. Geologic Survey, Rensselaer Polytechnic Institute, Report #CE-84-4, 1984.

Thompson, G.H. and Herbert, A. (1978), "Compaction of Clay Fills In-Situ by Dynamic Consolidation", Proc. of the Clay Fills Conference, I.C.E., London.

Tohno, I. and Yasuda, S. (1981), "Liquefaction of the Ground During the 1978 Miyagiken-oki Earthquake", Soils and Foundations, Vol. 21, No. 3, 1981, pp. 18-34.

Tohno, I., Yasuda, S. and Shamoto, Y. (1983), "Soil Liquefaction and Damage Caused by the Nihonkai-chubu Earthquakes", Kiso-ko, Vol. 11, No. 10, 1985, pp. 125-131 (in Japanese).

Tokimatsu, K. and Seed, H.B. (1984), Discussion on "Comparison of a Liquefaction Theory with Field Observations", Geotechnique, Vol. 34, No. 4, pp. 627-629.

Tokimatsu, K. and Yoshimi, Y. (1983), "Empirical Correlation of Soil Liquefaction Based on SPT N-value and Fines Content", Soils and Foundations, Vol. 23, No. 4, December, 1983.

Trifunac, M.D. and Brady, A.G. (1975), "On the Correlation of Seismic Intensity Scales with the Peaks of Recorded Strong Ground Motion", Bulletin of the Seismological Society of America, Vol. 65, pp. 139-162.

Tschebotarioff, G.P. (1973), Foundations, Retaining and Earth Structures, 2nd ed., McGraw-Hill Book Co., New York, 1973.

Tynan, A.E. (1973), "Ground Vibrations - Damaging Effects to Buildings", Special Report No. 11, Australian Road Research Board, 1973.

Vaid, Y. and Chem, J. (1983), "Effect of Static Shear on Resistance to Liquefaction", Soils and Foundations, Vol. 23, No 1, March, 1983, pp. 47-60.

Vucetic, M. and Dobry, R. (1987), "Cyclic Triaxial Strain-Controlled Testing of Liquefiable Soils", submitted for publication in the ASTM STP "Advanced Triaxial Testing of Soil and Rock", ASTM Conference, June 19-20, 1986, Louisville, Kentucky.

Waas, G. (1972), "Earth Vibration Effects and Abatement for Military Facilities - Analysis Method for Footing Vibrations Through Layered Media", Technical Report S-71-14, U.S. Army Engineer Waterways Experiment Station, Vicksburg, Mississippi, September, 1972.

Wallays, M. (1983), "Estimation of Required Energy Input for Dynamic Compaction of Various Soils", Discussion, Specialty Session 3, Topic 3, Proc. of the Eighth European Conference on Soil Mechanics and Foundation Engineering, Helsinki, May, 1983.

Whiffin, A.C. and Leonard, D.R. (1971), "A Survey of Traffic Induced Vibrations", Department of the Environment and the Dept. of Transportation, TRRL Report LR 418, Crowthorne, Berkshire, England.

Wiss, J.F. (1967), "Damage Effects of Pile Driving Vibration", Highway Research Record No. 155, Highway Research Board, Washington, D.C., 1967.

Wiss, J.F. (1974), "Vibrations during Construction Operations", Journal of the Construction Division, A.S.C.E., Vol. 100, No. C03, September, 1974, pp. 239-246.

Wiss, J.F. (1981), "Construction Vibrations, State-of-the-Art", Journal of the Geotechnical Engineering Division, A.S.C.E., Vol. 107, No. GT2, February, 1981, pp. 167-181.

Wiss, J.F. and Parmelee, R.A. (1974), "Human Perception of Transient Vibration", Journal of the Structural Division, A.S.C.E., Vol. 100, No. ST4, Proc. Paper 10495, April, 1974, pp. 773-787.

Wong, R.T. (1971), "Deformation Characteristics of Gravels and Gravelly Soils under Cyclic Loading Conditions", Ph. D. Thesis, Dept. of Civil Engineering, University of California, Berkeley, 1971.

Yoshimi, Y. and Oh-Oka, H. (1975), "Influence of Degree of Shear Stress Reversal on the Liquefaction Potential of Saturated Sand", Soils and Foundations, Vol. 15, No. 3, September, 1975, pp. 27-40.

Youd, T.L. (1972), "Compaction of Sands by Repeated Shear Straining", Journal of the Soil Mechanics and Foundations Division, A.S.C.E., Vol. 98, No. SM7, July, 1972, pp. 709-725.

Youd, T.L. (1977), Discussion on paper entitled "Brief Review of Liquefaction during Earthquakes in Japan", Soils and Foundations, Vol. 17, No. 1, pp. 82-85.

APPENDIX A

Derivations for Relevant Equations

A.1 Derivation of Equations to Compute Rayleigh Wave Cyclic Shear Strains

As discussed in Section 5.2, the ground motions that are associated with each Rayleigh wave mode of vibration may be described by the following equations:

$$u_x\ (x,z,t) = f(z) \cdot e^{i(\omega t - kx)} \qquad 5.1$$

$$u_z\ (x,z,t) = g(z) \cdot e^{i(\omega t - kx)} \qquad 5.2$$

where ω = frequency (rads/sec),
k = wave number,
z = depth,
x = horizontal distance, and
$f(z)$, $g(z)$ are complex functions

u_x is the horizontal displacement, u_z is the vertical displacement, and $f(z)$ and $g(z)$ are the horizontal and vertical mode shapes respectively. Once these modes shapes are known, the cyclic shear strains that are generated by each of the modes can be computed as described below.

The shear strains that exist on the horizontal and vertical planes within a soil are given by the equation:

$$\gamma_{90^\circ} = \gamma_{xz} = \gamma_{zx} = \frac{\partial u_x}{\partial z} + \frac{\partial u_z}{\partial x} \qquad \text{A.1}$$

Differentiating Equations 5.1 and 5.2 with respect to z and x, respectively, gives

$$\frac{\partial u_x}{\partial z} = f'(z) \cdot e^{i(\omega t - kx)} \qquad \text{A.2}$$

and

$$\frac{\partial u_z}{\partial x} = g(z) \cdot e^{i(\omega t - kx)} \cdot -i \cdot k \qquad \text{A.3}$$

At the fixed location, x = 0

$$\left[\frac{\partial u_x}{\partial z}\right]_{x=0} = f'(z) \cdot e^{i\omega t} \qquad \text{A.4}$$

and

$$\left[\frac{\partial u_z}{\partial x}\right]_{x=0} = -i \cdot k \cdot g(z) \cdot e^{i\omega t} \qquad \text{A.5}$$

and thus by Equation A.1,

$$\gamma_{90^\circ} = [f'(z) - i \cdot k \cdot g(z)] \cdot e^{i\omega t} \qquad \text{A.6}$$

The maximum shear strains on the horizontal and vertical planes are equal to the absolute value of the complex amplitude:

$$\max \gamma_{90^\circ} = \left| \gamma_{zx} \right| = \left| f'(z) - i \cdot k \cdot g(z) \right| \qquad 5.3$$

where $f'(z)$ is the derivative of $f(z)$ with respect to z

Since, for the "real" Rayleigh wave modes (which are of primary interest in this investigation), $f(z)$ is purely real, and $g(z)$ is purely imaginary, the expression within the absolute sign is real.

Similarly, the shear strains that exist on any 45^o plane within a soil are given by the equation,

$$\frac{\gamma_{45^o}}{2} = \frac{1}{2} \cdot (\varepsilon_x - \varepsilon_z) \qquad \text{A.7}$$

where ε_x and ε_z are the axial strains in the x and z directions, respectively. Differentiating Equation 5.1 with respect to x and Equation 5.2 with respect to z:

$$\varepsilon_x = \frac{\partial u_x}{\partial x} = -i \cdot k \cdot f(z) \cdot e^{i(\omega t - kx)} \qquad \text{A.8}$$

$$\varepsilon_z = \frac{\partial u_z}{\partial z} = g'(z) \cdot e^{i(\omega t - kx)} \qquad \text{A.9}$$

and considering the strains at x=0,

$$\varepsilon_x = \left[\frac{\partial u_x}{\partial x}\right]_{x=0} = -i \cdot k \cdot f(z) \cdot e^{i\omega t} \qquad \text{A.10}$$

and

$$\varepsilon_z = \left[\frac{\partial u_z}{\partial z}\right]_{x=0} = g'(z) \cdot e^{i\omega t} \qquad \text{A.11}$$

Thus, Equation A.9 leads to the following equation for Rayleigh waves,

$$\gamma_{45^\circ} = [-i \cdot k \cdot f(z) - g'(z)] \cdot e^{i\omega t} \qquad \text{A.12}$$

and the maximum shear strains on the 45 degree planes are equal to the absolute value of the complex amplitude, giving:

$$\max \gamma_{45^\circ} = \left| \gamma_{45^\circ} \right| = \left| k \cdot f(z) - i \cdot g'(z) \right| \qquad 5.4$$

where $g'(z)$ is the derivative of $g(z)$ with respect to z

Since, for the "real" Rayleigh wave modes, $f(z)$ is purely real, and $g(z)$ is purely imaginary, the expression within the absolute sign is once again real. This implies that the horizontal and vertical motions are 90 degrees out of phase with the motions on the 45 degree planes. It can also be shown that the maximum cyclic shear strains are the largest of either max γ_{90° or max γ_{45°.

A.2 Derivation of Equation 5.8

The buoyant weight, W, of a submerged block of soil (Figure A.1) of unit width, length, L, and vertical height, h_v, is given by the equation

$$W = \gamma' \cdot h_v \cdot \cos\alpha \cdot L \qquad \text{A.13}$$

where γ' = the buoyant soil density,
α = the slope angle, and
h_v = the vertical depth of the base of the block below the ground surface.

This force is resisted by a normal force, N, and a shear force, T, acting along the base of the block. The magnitude of the normal force,

$$N = W \cdot \cos\alpha \qquad \text{A.14}$$

Thus, the normal stress acting over the base of the block,

$$\sigma'_{n\alpha} = \frac{W \cdot \cos\alpha}{L} = \gamma' \cdot h_v \cdot \cos^2\alpha \qquad \text{A.15}$$

If an artesian pressure, u_e, acts at this depth within the slope then

$$\sigma'_{n\alpha} = (\gamma' \cdot h_v \cdot \cos^2\alpha) - u_e \qquad \text{A.16}$$

Summing forces parallel to the ground surface gives

$$T = W \cdot \sin\alpha \qquad \text{A.17}$$

and thus, the shear stress acting along the base of the block,

$$\tau_\alpha = \frac{W \cdot \sin\alpha}{L} = \gamma' \cdot h_v \cdot \cos\alpha \cdot \sin\alpha \qquad \text{A.18}$$

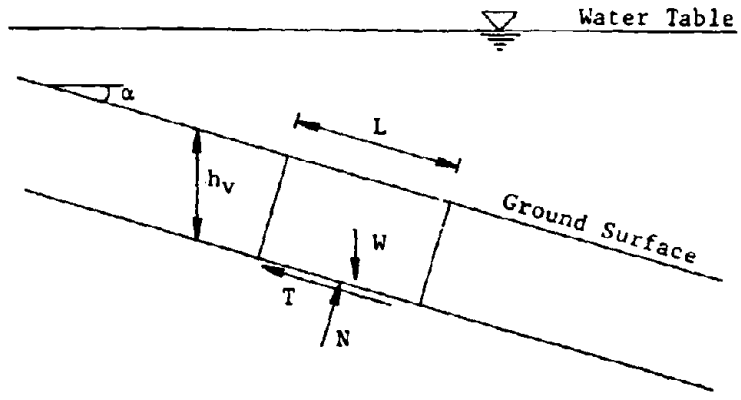

A.1 FORCES ACTING ON A BLOCK OF SOIL WITHIN A SUBMERGED INFINITE SLOPE.

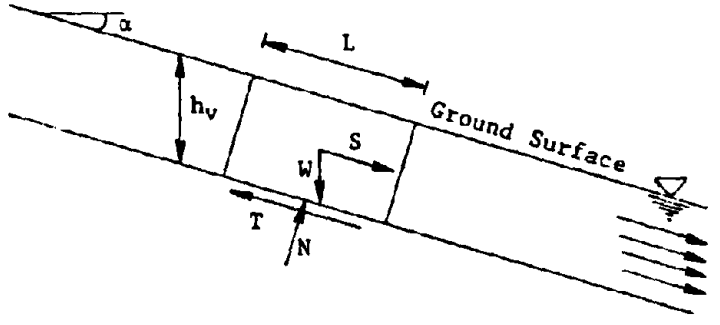

A.2 FORCES ACTING ON A BLOCK OF SOIL WITHIN AN INFINITE SLOPE WITH A WATER TABLE AT THE GROUND SURFACE AND SEEPAGE OCCURRING DOWN THE SLOPE.

The initial static shear stress/normal stress ratio acting on any plane parallel to the ground surface is therefore given by the equation

$$\frac{\tau_\alpha}{\sigma'_{n\alpha}} = \frac{\gamma' \cdot h_v \cdot \cos\alpha \cdot \sin\alpha}{(\gamma' \cdot h_v \cdot \cos^2\alpha) - u_e} \qquad 5.8$$

A.3 Derivation of Equation 5.9

The forces acting on a block of soil within an infinite slope with a water table at the ground surface and seepage occurring down the slope are shown in Figure A.2. As for the case of the submerged slope, the buoyant weight of this block,

$$W = \gamma' \cdot h_v \cdot \cos\alpha \cdot L \qquad A.13$$

where γ' = the buoyant soil density,
α = the slope angle, and
h_v = the vertical depth of the base of the block below the ground surface.

In addition to this force, a second driving force acts on the block due to the head loss experienced by the water flowing down the slope. This force,

$$S = \Delta h \cdot \gamma_w \cdot A = L \cdot \sin\alpha \cdot \gamma_w \cdot h_v \cdot \cos\alpha \qquad A.19$$

where Δh = head loss,
γ_w = density of water, and
A = area.

Summing forces normal to the base of the block,

$$N = W \cdot \cos\alpha \qquad \text{A.20}$$

Thus, once again the normal stress acting over the base of the block is given by

$$\sigma'_{n\alpha} = \frac{W \cdot \cos\alpha}{L} = \gamma' \cdot h_v \cdot cos^2\alpha \qquad \text{A.21}$$

and if an artesian pressure, u_e, acts at this depth within the slope then

$$\sigma'_{n\alpha} = (\gamma' \cdot h_v \cdot \cos^2\alpha) - u_e \qquad \text{A.22}$$

Summing forces parallel to the base of the block,

$$T = W \cdot \sin\alpha + S \qquad \text{A.23}$$

and dividing by the area of the base,

$$\tau_\alpha = (\gamma' + \gamma_w) \cdot h_v \cdot \cos\alpha \cdot \sin\alpha \qquad \text{A.24}$$

Thus, the static shear stress/normal stress ratio acting on any plane parallel to the ground surface at depth, h_v is given by the equation,

$$\frac{\tau_\alpha}{\sigma'_{n\alpha}} = \frac{\gamma_b \cdot h_v \cdot \cos\alpha \cdot \sin\alpha}{(\gamma' \cdot h_v \cdot \cos^2\alpha) - u_e} \qquad 5.9$$

where γ_b = the bulk density of the soil.

A.4 Derivation of Equation 6.7

The small strain shear modulus of a sand can be computed using the following equation,

$$G_{max} = 1000 \cdot (K_2)_{max} \cdot (\sigma'_m)^{\frac{1}{2}} \qquad 5.7$$

where G_{max} = shear modulus for sand (psf)
and σ'_m = mean effective stress (psf)

Assuming that,

$$\sigma'_m = 0.63 \cdot \sigma'_o \qquad A.25$$

where σ'_o = the effective overburden pressure.

then,

$$G_{max} = 1000 \cdot (K_2)_{max} \cdot (0.63 \cdot \sigma'_o)^{\frac{1}{2}} \qquad A.26$$

Since the presence of artesian pressure conditions reduces the shear modulus of a sand, and the computer program SHAKE does not account for the presence of such pressures, they may be taken into account by using a modified value of $(K_2)_{max}$ as input for the program. This modified value can be computed as follows,

$$1000 \cdot (K_2)_{new} \cdot (0.63 \cdot \sigma'_o)^{\frac{1}{2}} = 1000 \cdot (K_2)_{max} \cdot (0.63 \cdot \sigma'_o - u_e)^{\frac{1}{2}} \qquad A.27$$

which implies that

$$(K_2)_{new} = (K_2)_{\max} \cdot \frac{\sqrt{(0.63 \cdot \sigma'_o - u_e)}}{\sqrt{(0.63 \cdot \sigma'_o)}} \qquad \text{A.28}$$

Thus,

$$(K_2)_{new} = (K_2)_{\max} \cdot \frac{\sqrt{\sigma_o' - 1.5u_e}}{\sqrt{\sigma_o'}} \qquad 6.7$$

where σ_o' = effective overburden pressure
u_e = artesian pore pressure

APPENDIX B

Comparisons of Existing Damage Criteria (from Theissen and Wood, 1982).

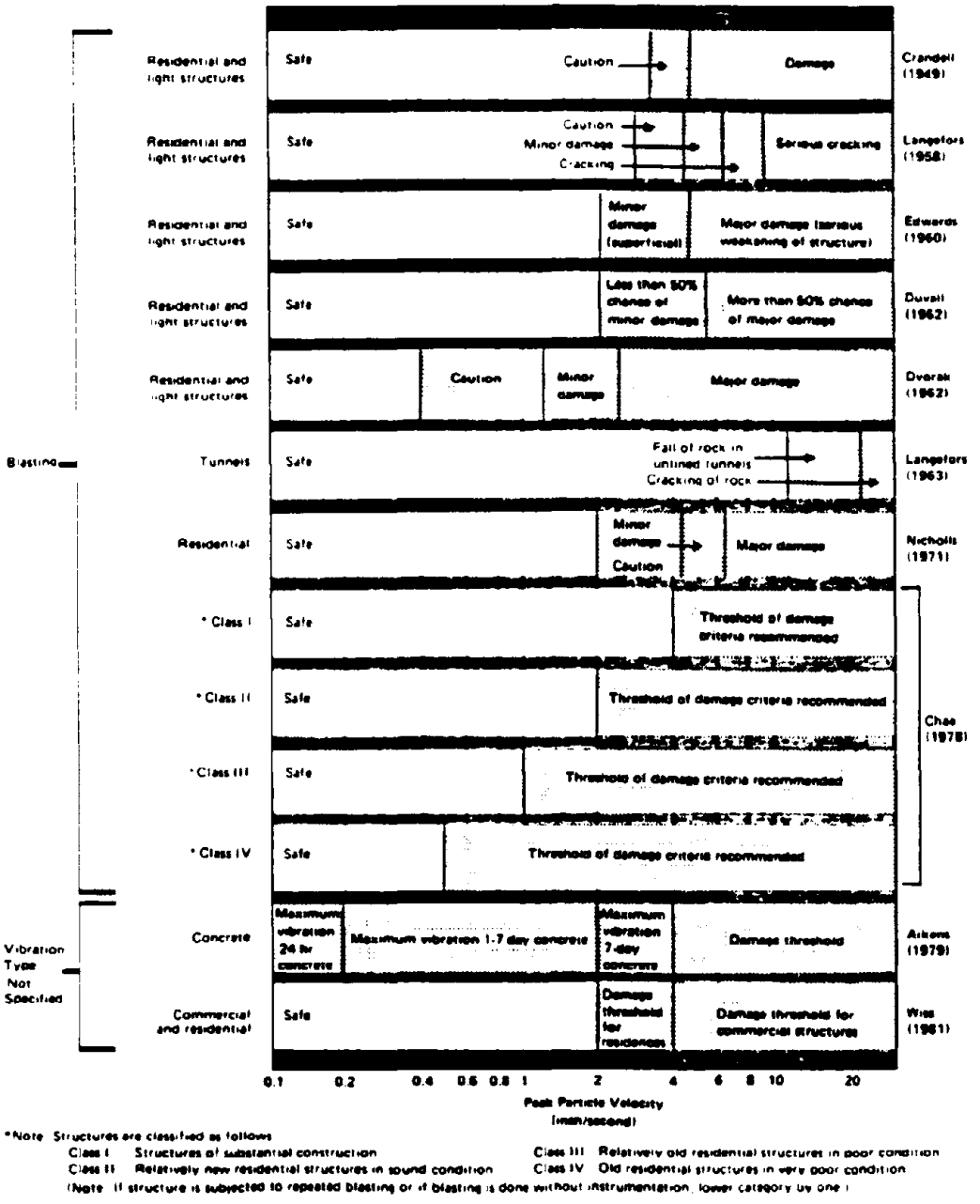

*Note Structures are classified as follows

Class I Structures of substantial construction

Class II Relatively new residential structures in sound condition

Class III Relatively old residential structures in poor condition

Class IV Old residential structures in very poor condition

(Note If structure is subjected to repeated blasting or if blasting is done without instrumentation, lower category by one.)

B.1 OBSERVED OR ANTICIPATED DAMAGE THRESHOLDS.

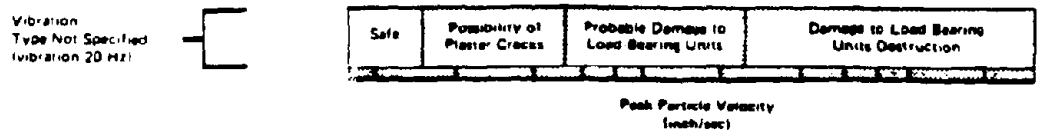

B.2a STANDARDIZED BRITISH DAMAGE CRITERIA.

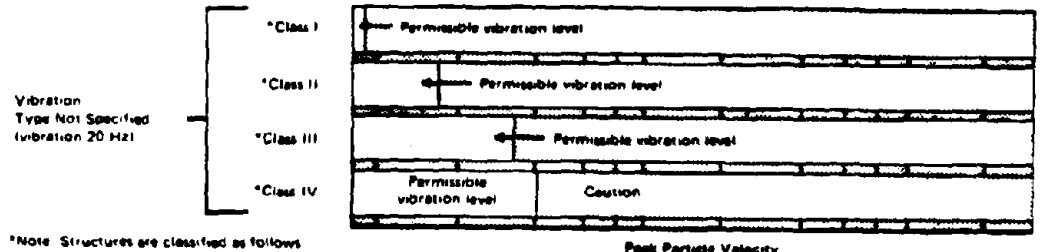

*Note Structures are classified as follows
I Ruins, historic monuments in poor state of repair
II Buildings with visible damage, cracks in walls
III Buildings without damage in good state of repair (may have plaster cracks)
IV Well-stiffened structures (for example, industrial buildings)
Source German Standard DIN 4150 (Proposed Revision) 1971 (Brenner and Chittikuladilok, 1975)

B.2b STANDARDIZED GERMAN DAMAGE CRITERIA.

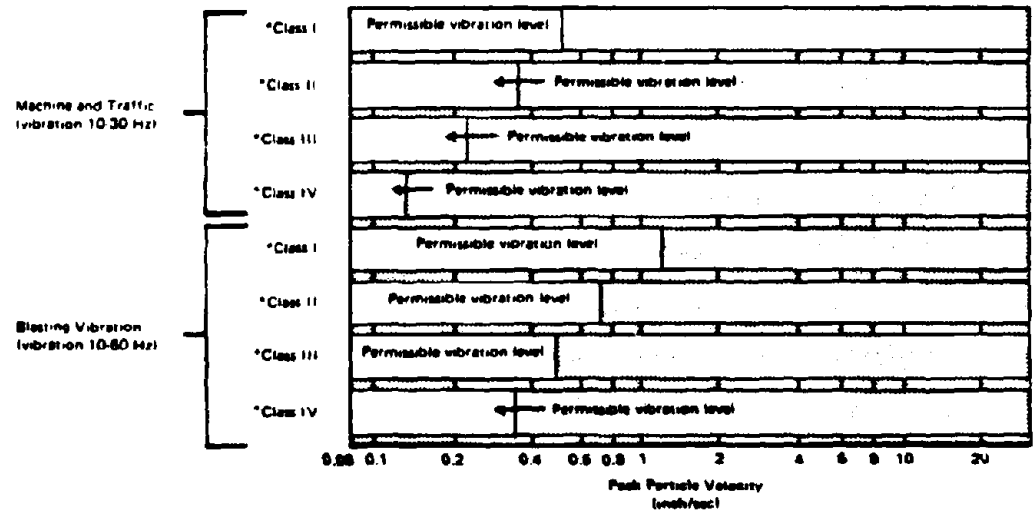

*Note Structures are classified as follows
I Buildings in steel or reinforced concrete, like factories, retaining walls, bridges, steel towers, open channels, underground chambers and tunnels with and without concrete alignment
II Buildings with foundation walls and floors in concrete, walls in concrete or masonry, stone masonry retaining walls, underground chambers and tunnels with masonry alignments, conduits in loose material
III Buildings as mentioned previously but with wooden ceilings and walls in masonry
IV Construction very sensitive to vibrations, objects of historic interest.
Source New Swiss Standard for Vibrations in Buildings (Wiss, 1981)

B.2c STANDARDIZED SWISS DAMAGE CRITERIA.

EARTHQUAKE ENGINEERING RESEARCH CENTER REPORT SERIES

EERC reports are available from the National Information Service for Earthquake Engineering(NISEE) and from the National Technical Information Service(NTIS). Numbers in parentheses are Accession Numbers assigned by the National Technical Information Service; these are followed by a price code. Contact NTIS, 5285 Port Royal Road, Springfield Virginia, 22161 for more information. Reports without Accession Numbers were not available from NTIS at the time of printing. For a current complete list of EERC reports (from EERC 67-1) and availability information, please contact University of California, EERC, NISEE, 1301 South 46th Street, Richmond, California 94804.

UCB/EERC-80/01 "Earthquake Response of Concrete Gravity Dams Including Hydrodynamic and Foundation Interaction Effects," by Chopra, A.K., Chakrabarti, P. and Gupta, S., January 1980, (AD-A087297)A10.

UCB/EERC-80/02 "Rocking Response of Rigid Blocks to Earthquakes," by Yim, C.S., Chopra, A.K. and Penzien, J., January 1980, (PB80 166 002)A04.

UCB/EERC-80/03 "Optimum Inelastic Design of Seismic-Resistant Reinforced Concrete Frame Structures," by Zagajeski, S.W. and Bertero, V.V., January 1980, (PB80 164 635)A06.

UCB/EERC-80/04 "Effects of Amount and Arrangement of Wall-Panel Reinforcement on Hysteretic Behavior of Reinforced Concrete Walls," by Iliya, R. and Bertero, V.V., February 1980, (PB81 122 525)A09.

UCB/EERC-80/05 "Shaking Table Research on Concrete Dam Models," by Niwa, A. and Clough, R.W., September 1980, (PB81 122 368)A06.

UCB/EERC-80/06 "The Design of Steel Energy-Absorbing Restrainers and their Incorporation into Nuclear Power Plants for Enhanced Safety (Vol 1a): Piping with Energy Absorbing Restrainers: Parameter Study on Small Systems," by Powell, G.H., Oughourlian, C. and Simons, J., June 1980.

UCB/EERC-80/07 "Inelastic Torsional Response of Structures Subjected to Earthquake Ground Motions," by Yamazaki, Y., April 1980, (PB81 122 327)A08.

UCB/EERC-80/08 "Study of X-Braced Steel Frame Structures under Earthquake Simulation," by Ghanaat, Y., April 1980, (PB81 122 335)A11.

UCB/EERC-80/09 "Hybrid Modelling of Soil-Structure Interaction," by Gupta, S., Lin, T.W. and Penzien, J., May 1980, (PB81 122 319)A07.

UCB/EERC-80/10 "General Applicability of a Nonlinear Model of a One Story Steel Frame," by Sveinsson, B.I. and McNiven, H.D., May 1980, (PB81 124 877)A06.

UCB/EERC-80/11 "A Green-Function Method for Wave Interaction with a Submerged Body," by Kioka, W., April 1980, (PB81 122 269)A07.

UCB/EERC-80/12 "Hydrodynamic Pressure and Added Mass for Axisymmetric Bodies," by Nilrat, F., May 1980, (PB81 122 343)A08.

UCB/EERC-80/13 "Treatment of Non-Linear Drag Forces Acting on Offshore Platforms," by Dao, B.V. and Penzien, J., May 1980, (PB81 153 413)A07.

UCB/EERC-80/14 "2D Plane/Axisymmetric Solid Element (Type 3-Elastic or Elastic-Perfectly Plastic)for the ANSR-II Program," by Mondkar, D.P. and Powell, G.H., July 1980, (PB81 122 350)A03.

UCB/EERC-80/15 "A Response Spectrum Method for Random Vibrations," by Der Kiureghian, A., June 1981, (PB81 122 301)A03.

UCB/EERC-80/16 "Cyclic Inelastic Buckling of Tubular Steel Braces," by Zayas, V.A., Popov, E.P. and Martin, S.A., June 1981, (PB81 124 885)A10.

UCB/EERC-80/17 "Dynamic Response of Simple Arch Dams Including Hydrodynamic Interaction," by Porter, C.S. and Chopra, A.K., July 1981, (PB81 124 000)A13.

UCB/EERC-80/18 "Experimental Testing of a Friction Damped Aseismic Base Isolation System with Fail-Safe Characteristics," by Kelly, J.M., Beucke, K.E. and Skinner, M.S., July 1980, (PB81 148 595)A04.

UCB/EERC-80/19 "The Design of Steel Energy-Absorbing Restrainers and their Incorporation into Nuclear Power Plants for Enhanced Safety (Vol 1B): Stochastic Seismic Analyses of Nuclear Power Plant Structures and Piping Systems Subjected to Multiple Supported Excitations," by Lee, M.C. and Penzien, J., June 1980, (PB82 201 872)A08.

UCB/EERC-80/20 "The Design of Steel Energy-Absorbing Restrainers and their Incorporation into Nuclear Power Plants for Enhanced Safety (Vol 1C): Numerical Method for Dynamic Substructure Analysis," by Dickens, J.M. and Wilson, E.L., June 1980.

UCB/EERC-80/21 "The Design of Steel Energy-Absorbing Restrainers and their Incorporation into Nuclear Power Plants for Enhanced Safety (Vol 2): Development and Testing of Restraints for Nuclear Piping Systems," by Kelly, J.M. and Skinner, M.S., June 1980.

UCB/EERC-80/22 "3D Solid Element (Type 4-Elastic or Elastic-Perfectly-Plastic) for the ANSR-II Program," by Mondkar, D.P. and Powell, G.H., July 1980, (PB81 123 242)A03.

UCB/EERC-80/23 "Gap-Friction Element (Type 5) for the Ansr-II Program," by Mondkar, D.P. and Powell, G.H., July 1980, (PB81 122 285)A03.

UCB/EERC-80/24 "U-Bar Restraint Element (Type 11) for the ANSR-II Program," by Oughourlian, C. and Powell, G.H., July 1980, (PB81 122 293)A03.

UCB/EERC-80/25 "Testing of a Natural Rubber Base Isolation System by an Explosively Simulated Earthquake," by Kelly, J.M., August 1980, (PB81 201 360)A04.

UCB/EERC-80/26 "Input Identification from Structural Vibrational Response," by Hu, Y., August 1980, (PB81 152 308)A05.

UCB/EERC-80/27 "Cyclic Inelastic Behavior of Steel Offshore Structures," by Zayas, V.A., Mahin, S.A. and Popov, E.P., August 1980, (PB81 196 180)A15.

UCB/EERC-80/28 "Shaking Table Testing of a Reinforced Concrete Frame with Biaxial Response," by Oliva, M.G., October 1980, (PB81 154 304)A10.

UCB/EERC-80/29 "Dynamic Properties of a Twelve-Story Prefabricated Panel Building," by Bouwkamp, J.G., Kollegger, J.P. and Stephen, R.M., October 1980, (PB82 138 777)A07.

UCB/EERC-80/30 "Dynamic Properties of an Eight-Story Prefabricated Panel Building," by Bouwkamp, J.G., Kollegger, J.P. and Stephen, R.M., October 1980, (PB81 200 313)A05.

UCB/EERC-80/31 "Predictive Dynamic Response of Panel Type Structures under Earthquakes," by Kollegger, J.P. and Bouwkamp, J.G., October 1980, (PB81 152 316)A04.

UCB/EERC-80/32 "The Design of Steel Energy-Absorbing Restrainers and their Incorporation into Nuclear Power Plants for Enhanced Safety (Vol 3): Testing of Commercial Steels in Low-Cycle Torsional Fatigue," by Spanner, P., Parker, E.R., Jongewaard, E. and Dory, M., 1980.

UCB/EERC-80/33 "The Design of Steel Energy-Absorbing Restrainers and their Incorporation into Nuclear Power Plants for Enhanced Safety (Vol 4): Shaking Table Tests of Piping Systems with Energy-Absorbing Restrainers," by Stiemer, S.F. and Godden, W.G., September 1980 (PB82 201 880)A05.

UCB/EERC-80/34 "The Design of Steel Energy-Absorbing Restrainers and their Incorporation into Nuclear Power Plants for Enhanced Safety (Vol 5): Summary Report," by Spencer, P., 1980.

UCB/EERC-80/35 "Experimental Testing of an Energy-Absorbing Base Isolation System," by Kelly, J.M., Skinner, M.S. and Beucke, K.E., October 1980 (PB81 154 072)A04.

UCB/EERC-80/36 "Simulating and Analyzing Artificial Non-Stationary Earth Ground Motions," by Nau, R.F., Oliver, R.M. and Pister, K.S., October 1980, (PB81 153 397)A04.

UCB/EERC-80/37 "Earthquake Engineering at Berkeley - 1980," by , September 1980, (PB81 205 674)A09.

UCB/EERC-80/38 "Inelastic Seismic Analysis of Large Panel Buildings," by Schricker, V. and Powell, G.H., September 1980, (PB81 154 338)A13.

UCB/EERC-80/39 "Dynamic Response of Embankment, Concrete-Gavity and Arch Dams Including Hydrodynamic Interation," by Hall, J.F. and Chopra, A.K., October 1980, (PB81 152 324)A11.

UCB/EERC-80/40 "Inelastic Buckling of Steel Struts under Cyclic Load Reversal," by Black, R.G., Wenger, W.A. and Popov, E.P., October 1980, (PB81 154 312)A08.

UCB/EERC-80/41 "Influence of Site Characteristics on Buildings Damage during the October 3,1974 Lima Earthquake," by Repetto, P., Arango, I. and Seed, H.B., September 1980, (PB81 161 739)A05.

UCB/EERC-80/42 "Evaluation of a Shaking Table Test Program on Response Behavior of a Two Story Reinforced Concrete Frame," by Blondet, J.M., Clough, R.W. and Mahin, S.A., December 1980, (PB82 196 544)A11.

UCB/EERC-80/43 "Modelling of Soil-Structure Interaction by Finite and Infinite Elements," by Medina, F., December 1980, (PB81 229 270)A04.

UCB/EERC-81/01 "Control of Seismic Response of Piping Systems and Other Structures by Base Isolation," by Kelly, J.M., January 1981, (PB81 200 735)A05.

UCB/EERC-81/02 "OPTNSR- An Interactive Software System for Optimal Design of Statically and Dynamically Loaded Structures with Nonlinear Response," by Bhatti, M.A., Ciampi, V. and Pister, K.S., January 1981, (PB81 218 851)A09.

UCB/EERC-81/03 "Analysis of Local Variations in Free Field Seismic Ground Motions," by Chen, J.-C., Lysmer, J. and Seed, H.B., January 1981, (AD-A099508)A13.

UCB/EERC-81/04 "Inelastic Structural Modeling of Braced Offshore Platforms for Seismic Loading," by Zayas, V.A., Shing, P.-S.B., Mahin, S.A. and Popov, E.P., January 1981, (PB82 138 777)A07.

UCB/EERC-81/05 "Dynamic Response of Light Equipment in Structures," by Der Kiureghian, A., Sackman, J.L. and Nour-Omid, B., April 1981, (PB81 218 497)A04.

UCB/EERC-81/06 "Preliminary Experimental Investigation of a Broad Base Liquid Storage Tank," by Bouwkamp, J.G., Kollegger, J.P. and Stephen, R.M., May 1981, (PB82 140 385)A03.

UCB/EERC-81/07 "The Seismic Resistant Design of Reinforced Concrete Coupled Structural Walls," by Aktan, A.E. and Bertero, V.V., June 1981, (PB82 113 358)A11.

UCB/EERC-81/08 "Unassigned," by Unassigned, 1981.

UCB/EERC-81/09 "Experimental Behavior of a Spatial Piping System with Steel Energy Absorbers Subjected to a Simulated Differential Seismic Input," by Stiemer, S.F., Godden, W.G. and Kelly, J.M., July 1981, (PB82 201 898)A04.

UCB/EERC-81/10 "Evaluation of Seismic Design Provisions for Masonry in the United States," by Sveinsson, B.I., Mayes, R.L. and McNiven, H.D., August 1981, (PB82 166 075)A08.

UCB/EERC-81/11 "Two-Dimensional Hybrid Modelling of Soil-Structure Interaction," by Tzong, T.-J., Gupta, S. and Penzien, J., August 1981, (PB82 142 118)A04.

UCB/EERC-81/12 "Studies on Effects of Infills in Seismic Resistant R/C Construction," by Brokken, S. and Bertero, V.V., October 1981, (PB82 166 190)A09.

UCB/EERC-81/13 "Linear Models to Predict the Nonlinear Seismic Behavior of a One-Story Steel Frame," by Valdimarsson, H., Shah, A.H. and McNiven, H.D., September 1981, (PB82 138 793)A07.

UCB/EERC-81/14 "TLUSH: A Computer Program for the Three-Dimensional Dynamic Analysis of Earth Dams," by Kagawa, T., Mejia, L.H., Seed, H.B. and Lysmer, J., September 1981, (PB82 139 940)A06.

UCB/EERC-81/15 "Three Dimensional Dynamic Response Analysis of Earth Dams," by Mejia, L.H. and Seed, H.B., September 1981, (PB82 137 274)A12.

UCB/EERC-81/16 "Experimental Study of Lead and Elastomeric Dampers for Base Isolation Systems," by Kelly, J.M. and Hodder, S.B., October 1981, (PB82 166 182)A05.

UCB/EERC-81/17 "The Influence of Base Isolation on the Seismic Response of Light Secondary Equipment," by Kelly, J.M., April 1981, (PB82 255 266)A04.

UCB/EERC-81/18 "Studies on Evaluation of Shaking Table Response Analysis Procedures," by Blondet, J. M., November 1981, (PB82 197 278)A10.

UCB/EERC-81/19 "DELIGHT.STRUCT: A Computer-Aided Design Environment for Structural Engineering," by Balling, R.J., Pister, K.S. and Polak, E., December 1981, (PB82 218 496)A07.

UCB/EERC-81/20 "Optimal Design of Seismic-Resistant Planar Steel Frames," by Balling, R.J., Ciampi, V. and Pister, K.S., December 1981, (PB82 220 179)A07.

UCB/EERC-82/01 "Dynamic Behavior of Ground for Seismic Analysis of Lifeline Systems," by Sato, T. and Der Kiureghian, A., January 1982, (PB82 218 926)A05.

UCB/EERC-82/02 "Shaking Table Tests of a Tubular Steel Frame Model," by Ghanaat, Y. and Clough, R.W., January 1982, (PB82 220 161)A07.

UCB/EERC-82/03 "Behavior of a Piping System under Seismic Excitation: Experimental Investigations of a Spatial Piping System supported by Mechanical Shock Arrestors," by Schneider, S., Lee, H.-M. and Godden, W. G., May 1982, (PB83 172 544)A09.

UCB/EERC-82/04 "New Approaches for the Dynamic Analysis of Large Structural Systems," by Wilson, E.L., June 1982, (PB83 148 080)A05.

UCB/EERC-82/05 "Model Study of Effects of Damage on the Vibration Properties of Steel Offshore Platforms," by Shahrivar, F. and Bouwkamp, J.G., June 1982, (PB83 148 742)A10.

UCB/EERC-82/06 "States of the Art and Pratice in the Optimum Seismic Design and Analytical Response Prediction of R/C Frame Wall Structures, by Aktan, A.E. and Bertero, V.V., July 1982, (PB83 147 736)A05.

UCB/EERC-82/07 "Further Study of the Earthquake Response of a Broad Cylindrical Liquid-Storage Tank Model," by Manos, G.C. and Clough, R.W., July 1982, (PB83 147 744)A11.

UCB/EERC-82/08 "An Evaluation of the Design and Analytical Seismic Response of a Seven Story Reinforced Concrete Frame," by Charney, F.A. and Bertero, V.V., July 1982, (PB83 157 628)A09.

UCB/EERC-82/09 "Fluid-Structure Interactions: Added Mass Computations for Incompressible Fluid," by Kuo, J.S.-H., August 1982, (PB83 156 281)A07.

UCB/EERC-82/10 "Joint-Opening Nonlinear Mechanism: Interface Smeared Crack Model," by Kuo, J.S.-H., August 1982, (PB83 149 195)A05.

UCB/EERC-82/11 "Dynamic Response Analysis of Techi Dam," by Clough, R.W., Stephen, R.M. and Kuo, J.S.-H., August 1982, (PB83 147 496)A06.

UCB/EERC-82/12 "Prediction of the Seismic Response of R/C Frame-Coupled Wall Structures," by Aktan, A.E., Bertero, V.V. and Piazzo, M., August 1982, (PB83 149 203)A09.

UCB/EERC-82/13 "Preliminary Report on the Smart 1 Strong Motion Array in Taiwan," by Bolt, B.A., Loh, C.H., Penzien, J. and Tsai, Y.B., August 1982, (PB83 159 400)A10.

UCB/EERC-82/14 "Shaking-Table Studies of an Eccentrically X-Braced Steel Structure," by Yang, M.S., September 1982, (PB83 260 778)A12.

UCB/EERC-82/15 "The Performance of Stairways in Earthquakes," by Roha, C., Axley, J.W. and Bertero, V.V., September 1982, (PB83 157 693)A07.

UCB/EERC-82/16 "The Behavior of Submerged Multiple Bodies in Earthquakes," by Liao, W.-G., September 1982, (PB83 158 709)A07.

UCB/EERC-82/17 "Effects of Concrete Types and Loading Conditions on Local Bond-Slip Relationships," by Cowell, A.D., Popov, E.P. and Bertero, V.V., September 1982, (PB83 153 577)A04.

UCB/EERC-82/18 "Mechanical Behavior of Shear Wall Vertical Boundary Members: An Experimental Investigation," by Wagner, M.T. and Bertero, V.V., October 1982, (PB83 159 764)A05.

UCB/EERC-82/19 "Experimental Studies of Multi-support Seismic Loading on Piping Systems," by Kelly, J.M. and Cowell, A.D., November 1982.

UCB/EERC-82/20 "Generalized Plastic Hinge Concepts for 3D Beam-Column Elements," by Chen, P. F.-S. and Powell, G.H., November 1982, (PB83 247 981)A13.

UCB/EERC-82/21 "ANSR-II: General Computer Program for Nonlinear Structural Analysis," by Oughourlian, C.V. and Powell, G.H., November 1982, (PB83 251 330)A12.

UCB/EERC-82/22 "Solution Strategies for Statically Loaded Nonlinear Structures," by Simons, J.W. and Powell, G.H., November 1982, (PB83 197 970)A06.

UCB/EERC-82/23 "Analytical Model of Deformed Bar Anchorages under Generalized Excitations," by Ciampi, V., Eligehausen, R., Bertero, V.V. and Popov, E.P., November 1982, (PB83 169 532)A06.

UCB/EERC-82/24 "A Mathematical Model for the Response of Masonry Walls to Dynamic Excitations," by Sucuoglu, H., Mengi, Y. and McNiven, H.D., November 1982, (PB83 169 011)A07.

UCB/EERC-82/25 "Earthquake Response Considerations of Broad Liquid Storage Tanks," by Cambra, F.J., November 1982, (PB83 251 215)A09.

UCB/EERC-82/26 "Computational Models for Cyclic Plasticity, Rate Dependence and Creep," by Mosaddad, B. and Powell, G.H., November 1982, (PB83 245 829)A08.

UCB/EERC-82/27 "Inelastic Analysis of Piping and Tubular Structures," by Mahasuverachai, M. and Powell, G.H., November 1982, (PB83 249 987)A07.

UCB/EERC-83/01 "The Economic Feasibility of Seismic Rehabilitation of Buildings by Base Isolation," by Kelly, J.M., January 1983, (PB83 197 988)A05.

UCB/EERC-83/02 "Seismic Moment Connections for Moment-Resisting Steel Frames," by Popov, E.P., January 1983, (PB83 195 412)A04.

UCB/EERC-83/03 "Design of Links and Beam-to-Column Connections for Eccentrically Braced Steel Frames," by Popov, E.P. and Malley, J.O., January 1983, (PB83 194 811)A04.

UCB/EERC-83/04 "Numerical Techniques for the Evaluation of Soil-Structure Interaction Effects in the Time Domain," by Bayo, E. and Wilson, E.L., February 1983, (PB83 245 605)A09.

UCB/EERC-83/05 "A Transducer for Measuring the Internal Forces in the Columns of a Frame-Wall Reinforced Concrete Structure," by Sause, R. and Bertero, V.V., May 1983, (PB84 119 494)A06.

UCB/EERC-83/06 "Dynamic Interactions Between Floating Ice and Offshore Structures," by Croteau, P., May 1983, (PB84 119 486)A16.

UCB/EERC-83/07 "Dynamic Analysis of Multiply Tuned and Arbitrarily Supported Secondary Systems," by Igusa, T. and Der Kiureghian, A., July 1983, (PB84 118 272)A11.

UCB/EERC-83/08 "A Laboratory Study of Submerged Multi-body Systems in Earthquakes," by Ansari, G.R., June 1983, (PB83 261 842)A17.

UCB/EERC-83/09 "Effects of Transient Foundation Uplift on Earthquake Response of Structures," by Yim, C.-S. and Chopra, A.K., June 1983, (PB83 261 396)A07.

UCB/EERC-83/10 "Optimal Design of Friction-Braced Frames under Seismic Loading," by Austin, M.A. and Pister, K.S., June 1983, (PB84 119 288)A06.

UCB/EERC-83/11 "Shaking Table Study of Single-Story Masonry Houses: Dynamic Performance under Three Component Seismic Input and Recommendations," by Manos, G.C., Clough, R.W. and Mayes, R.L., July 1983, (UCB/EERC-83/11)A08.

UCB/EERC-83/12 "Experimental Error Propagation in Pseudodynamic Testing," by Shiing, P.B. and Mahin, S.A., June 1983, (PB84 119 270)A09.

UCB/EERC-83/13 "Experimental and Analytical Predictions of the Mechanical Characteristics of a 1/5-scale Model of a 7-story R/C Frame-Wall Building Structure," by Aktan, A.E., Bertero, V.V., Chowdhury, A.A. and Nagashima, T., June 1983, (PB84 119 213)A07.

UCB/EERC-83/14 "Shaking Table Tests of Large-Panel Precast Concrete Building System Assemblages," by Oliva, M.G. and Clough, R.W., June 1983. (PB86 110 210/AS)A11.

UCB/EERC-83/15 "Seismic Behavior of Active Beam Links in Eccentrically Braced Frames," by Hjelmstad, K.D. and Popov, E.P., July 1983. (PB84 119 676)A09.

UCB/EERC-83/16 "System Identification of Structures with Joint Rotation," by Dimsdale, J.S., July 1983. (PB84 192 210)A06.

UCB/EERC-83/17 "Construction of Inelastic Response Spectra for Single-Degree-of-Freedom Systems," by Mahin, S. and Lin, J., June 1983. (PB84 208 834)A05.

UCB/EERC-83/18 "Interactive Computer Analysis Methods for Predicting the Inelastic Cyclic Behaviour of Structural Sections," by Kaba, S. and Mahin, S., July 1983. (PB84 192 012)A06.

UCB/EERC-83/19 "Effects of Bond Deterioration on Hysteretic Behavior of Reinforced Concrete Joints," by Filippou, F.C., Popov, E.P. and Bertero, V.V., August 1983. (PB84 192 020)A10.

UCB/EERC-83/20 "Analytical and Experimental Correlation of Large-Panel Precast Building System Performance," by Oliva, M.G., Clough, R.W., Velkov, M. and Gavrilovic, P., November 1983.

UCB/EERC-83/21 "Mechanical Characteristics of Materials Used in a 1/5 Scale Model of a 7-Story Reinforced Concrete Test Structure," by Bertero, V.V., Aktan, A.E., Harris, H.G. and Chowdhury, A.A., October 1983. (PB84 193 697)A05.

UCB/EERC-83/22 "Hybrid Modelling of Soil-Structure Interaction in Layered Media," by Tzong, T.-J. and Penzien, J., October 1983. (PB84 192 178)A08.

UCB/EERC-83/23 "Local Bond Stress-Slip Relationships of Deformed Bars under Generalized Excitations," by Eligehausen, R., Popov, E.P. and Bertero, V.V., October 1983. (PB84 192 848)A09.

UCB/EERC-83/24 "Design Considerations for Shear Links in Eccentrically Braced Frames," by Malley, J.O. and Popov, E.P., November 1983. (PB84 192 186)A07.

UCB/EERC-84/01 "Pseudodynamic Test Method for Seismic Performance Evaluation: Theory and Implementation," by Shing, P.-S.B. and Mahin, S.A., January 1984. (PB84 190 644)A08.

UCB/EERC-84/02 "Dynamic Response Behavior of Kiang Hong Dian Dam," by Clough, R.W., Chang, K.-T., Chen, H.-Q. and Stephen, R.M., April 1984. (PB84 209 402)A08.

UCB/EERC-84/03 "Refined Modelling of Reinforced Concrete Columns for Seismic Analysis," by Kaba, S.A. and Mahin, S.A., April 1984. (PB84 234 384)A06

UCB/EERC-84/04 "A New Floor Response Spectrum Method for Seismic Analysis of Multiply Supported Secondary Systems," by Asfura, A. and Der Kiureghian, A., June 1984. (PB84 239 417)A06.

UCB/EERC-84/05 "Earthquake Simulation Tests and Associated Studies of a 1/5th-scale Model of a 7-Story R/C Frame-Wall Test Structure," by Bertero, V.V., Aktan, A.E., Charney, F.A. and Sause, R., June 1984. (PB84 239 409)A09.

UCB/EERC-84/06 "R/C Structural Walls: Seismic Design for Shear," by Aktan, A.E. and Bertero, V.V., 1984.

UCB/EERC-84/07 "Behavior of Interior and Exterior Flat-Plate Connections subjected to Inelastic Load Reversals," by Zee, H.L. and Moehle, J.P., August 1984. (PB86 117 629/AS)A07.

UCB/EERC-84/08 "Experimental Study of the Seismic Behavior of a Two-Story Flat-Plate Structure," by Moehle, J.P. and Diebold, J.W., August 1984. (PB86 122 553/AS)A12.

UCB/EERC-84/09 "Phenomenological Modeling of Steel Braces under Cyclic Loading," by Ikeda, K., Mahin, S.A. and Dermitzakis, S.N., May 1984. (PB86 132 198/AS)A08.

UCB/EERC-84/10 "Earthquake Analysis and Response of Concrete Gravity Dams," by Fenves, G. and Chopra, A.K., August 1984. (PB85 193 902/AS)A11.

UCB/EERC-84/11 "EAGD-84: A Computer Program for Earthquake Analysis of Concrete Gravity Dams," by Fenves, G. and Chopra, A.K., August 1984. (PB85 193 613/AS)A05.

UCB/EERC-84/12 "A Refined Physical Theory Model for Predicting the Seismic Behavior of Braced Steel Frames," by Ikeda, K. and Mahin, S.A., July 1984. (PB85 191 450/AS)A09.

UCB/EERC-84/13 "Earthquake Engineering Research at Berkeley - 1984," by , August 1984. (PB85 197 341/AS)A10.

UCB/EERC-84/14 "Moduli and Damping Factors for Dynamic Analyses of Cohesionless Soils," by Seed, H.B., Wong, R.T., Idriss, I.M. and Tokimatsu, K., September 1984. (PB85 191 468/AS)A04.

UCB/EERC-84/15 "The Influence of SPT Procedures in Soil Liquefaction Resistance Evaluations," by Seed, H.B., Tokimatsu, K., Harder, L.F. and Chung, R.M., October 1984. (PB85 191 732/AS)A04.

UCB/EERC-84/16 "Simplified Procedures for the Evaluation of Settlements in Sands Due to Earthquake Shaking," by Tokimatsu, K. and Seed, H.B., October 1984. (PB85 197 887/AS)A03.

UCB/EERC-84/17 "Evaluation of Energy Absorption Characteristics of Bridges under Seismic Conditions," by Imbsen, R.A. and Penzien, J., November 1984.

UCB/EERC-84/18 "Structure-Foundation Interactions under Dynamic Loads," by Liu, W.D. and Penzien, J., November 1984. (PB87 124 889/AS)A11.

UCB/EERC-84/19 "Seismic Modelling of Deep Foundations," by Chen, C.-H. and Penzien, J., November 1984. (PB87 124 798/AS)A07.

UCB/EERC-84/20 "Dynamic Response Behavior of Quan Shui Dam," by Clough, R.W., Chang, K.-T., Chen, H.-Q., Stephen, R.M., Ghanaat, Y. and Qi, J.-H., November 1984. (PB86 115177/AS)A07.

UCB/EERC-85/01 "Simplified Methods of Analysis for Earthquake Resistant Design of Buildings," by Cruz, E.F. and Chopra, A.K., February 1985. (PB86 112299/AS)A12.

UCB/EERC-85/02 "Estimation of Seismic Wave Coherency and Rupture Velocity using the SMART 1 Strong-Motion Array Recordings," by Abrahamson, N.A., March 1985. (PB86 214 343)A07.

UCB/EERC-85/03 "Dynamic Properties of a Thirty Story Condominium Tower Building," by Stephen, R.M., Wilson, E.L. and Stander, N., April 1985. (PB86 118965/AS)A06.

UCB/EERC-85/04 "Development of Substructuring Techniques for On-Line Computer Controlled Seismic Performance Testing," by Dermitzakis, S. and Mahin, S., February 1985. (PB86 132941/AS)A08.

UCB/EERC-85/05 "A Simple Model for Reinforcing Bar Anchorages under Cyclic Excitations," by Filippou, F.C., March 1985. (PB86 112 919/AS)A05

UCB/EERC-85/06 "Racking Behavior of Wood-framed Gypsum Panels under Dynamic Load," by Oliva, M.G., June 1985.

UCB/EERC-85/07 "Earthquake Analysis and Response of Concrete Arch Dams," by Fok, K.-L. and Chopra, A.K., June 1985. (PB86 139672/AS)A10

UCB/EERC-85/08 "Effect of Inelastic Behavior on the Analysis and Design of Earthquake Resistant Structures," by Lin, J.P. and Mahin, S.A., June 1985. (PB86 135340/AS)A08.

UCB/EERC-85/09 "Earthquake Simulator Testing of a Base-Isolated Bridge Deck," by Kelly, J.M., Buckle, I.G. and Tsai, H.-C., January 1986. (PB87 124 152/AS)A06.

UCB/EERC-85/10 "Simplified Analysis for Earthquake Resistant Design of Concrete Gravity Dams," by Fenves, G. and Chopra, A.K., June 1986. (PB87 124 160/AS)A08.

UCB/EERC-85/11 "Dynamic Interaction Effects in Arch Dams," by Clough, R.W., Chang, K.-T., Chen, H.-Q. and Ghanaat, Y., October 1985. (PB86 135027/AS)A05.

UCB/EERC-85/12 "Dynamic Response of Long Valley Dam in the Mammoth Lake Earthquake Series of May 25-27, 1980," by Lai, S. and Seed, H.B., November 1985. (PB86 142304/AS)A05.

UCB/EERC-85/13 "A Methodology for Computer-Aided Design of Earthquake-Resistant Steel Structures," by Austin, M.A., Pister, K.S. and Mahin, S.A., December 1985. (PB86 159480/AS)A10.

UCB/EERC-85/14 "Response of Tension-Leg Platforms to Vertical Seismic Excitations," by Liou, G.-S., Penzien, J. and Yeung, R.W., December 1985. (PB87 124 871/AS)A08.

UCB/EERC-85/15 "Cyclic Loading Tests of Masonry Single Piers: Volume 4 - Additional Tests with Height to Width Ratio of 1," by Sveinsson, B., McNiven, H.D. and Sucuoglu, H., December 1985.

UCB/EERC-85/16 "An Experimental Program for Studying the Dynamic Response of a Steel Frame with a Variety of Infill Partitions," by Yanev, B. and McNiven, H.D., December 1985.

UCB/EERC-86/01 "A Study of Seismically Resistant Eccentrically Braced Steel Frame Systems," by Kasai, K. and Popov, E.P., January 1986. (PB87 124 178/AS)A14.

UCB/EERC-86/02 "Design Problems in Soil Liquefaction," by Seed, H.B., February 1986. (PB87 124 186/AS)A03

UCB/EERC-86/03 "Implications of Recent Earthquakes and Research on Earthquake-Resistant Design and Construction of Buildings," by Bertero, V.V., March 1986. (PB87 124 194/AS)A05.

UCB/EERC-86/04 "The Use of Load Dependent Vectors for Dynamic and Earthquake Analyses," by Leger, P., Wilson, E.L. and Clough, R.W., March 1986. (PB87 124 202/AS)A12.

UCB/EERC-86/05 "Two Beam-To-Column Web Connections," by Tsai, K.-C. and Popov, E.P., April 1986. (PB87 124 301/AS)A04.

UCB/EERC-86/06 "Determination of Penetration Resistance for Coarse-Grained Soils using the Becker Hammer Drill," by Harder, L.F. and Seed, H.B., May 1986. (PB87 124 210/AS)A07.

UCB/EERC-86/07 "A Mathematical Model for Predicting the Nonlinear Response of Unreinforced Masonry Walls to In-Plane Earthquake Excitations," by Mengi, Y. and McNiven, H.D., May 1986. (PB87 124 780/AS)A06.

UCB/EERC-86/08 "The 19 September 1985 Mexico Earthquake: Building Behavior," by Bertero, V.V., July 1986.

UCB/EERC-86/09 "EACD-3D: A Computer Program for Three-Dimensional Earthquake Analysis of Concrete Dams," by Fok, K.-L., Hall, J.F. and Chopra, A.K., July 1986. (PB87 124 228/AS)A08.

UCB/EERC-86/10 "Earthquake Simulation Tests and Associated Studies of a 0.3-Scale Model of a Six-Story Concentrically Braced Steel Structure," by Uang, C.-M. and Bertero, V.V., December 1986. (PB87 163 564/AS)A17.

UCB/EERC-86/11 "Mechanical Characteristics of Base Isolation Bearings for a Bridge Deck Model Test," by Kelly, J.M., Buckle, I.G. and Koh, C.-G., 1987.

UCB/EERC-86/12 "Effects of Axial Load on Elastomeric Isolation Bearings," by Koh, C.-G. and Kelly, J.M., November 1987.

UCB/EERC-87/01 "The FPS Earthquake Resisting System: Experimental Report," by Zayas, V.A., Low, S.S. and Mahin, S.A., June 1987.

UCB/EERC-87/02 "Earthquake Simulator Tests and Associated Studies of a 0.3-Scale Model of a Six-Story Eccentrically Braced Steel Structure," by Whittaker, A., Uang, C.-M. and Bertero, V.V., July 1987.

UCB/EERC-87/03 "A Displacement Control and Uplift Restraint Device for Base-Isolated Structures," by Kelly, J.M., Griffith, M.C. and Aiken, I.G., April 1987.

UCB/EERC-87/04 "Earthquake Simulator Testing of a Combined Sliding Bearing and Rubber Bearing Isolation System," by Kelly, J.M. and Chalhoub, M.S., 1987.

UCB/EERC-87/05 "Three-Dimensional Inelastic Analysis of Reinforced Concrete Frame-Wall Structures," by Moazzami, S. and Bertero, V.V., May 1987.

UCB/EERC-87/06 "Experiments on Eccentrically Braced Frames with Composite Floors," by Ricles, J. and Popov, E., June 1987.

UCB/EERC-87/07 "Dynamic Analysis of Seismically Resistant Eccentrically Braced Frames," by Ricles, J. and Popov, E., June 1987.

UCB/EERC-87/08 "Undrained Cyclic Triaxial Testing of Gravels-The Effect of Membrane Compliance," by Evans, M.D. and Seed, H.B., July 1987.

UCB/EERC-87/09 "Hybrid Solution Techniques for Generalized Pseudo-Dynamic Testing," by Thewalt, C. and Mahin, S.A., July 1987.

UCB/EERC-87/10 "Investigation of Ultimate Behavior of AISC Group 4 and 5 Heavy Steel Rolled-Section Splices with Full and Partial Penetration Butt Welds," by Bruneau, M. and Mahin, S.A., July 1987.

UCB/EERC-87/11 "Residual Strength of Sand from Dam Failures in the Chilean Earthquake of March 3, 1985," by De Alba, P., Seed, H.B., Retamal, E. and Seed, R.B., September 1987

UCB/EERC-87/12 "Inelastic Seismic Response of Structures with Mass or Stiffness Eccentricities in Plan," by Bruneau, M. and Mahin, S.A., September 1987.

UCB/EERC-87/13 "CSTRUCT: An Interactive Computer Environment for the Design and Analysis of Earthquake Resistant Steel Structures," by Austin, M.A., Mahin, S.A. and Pister, K.S., September 1987.

UCB/EERC-87/14 "Experimental Study of Reinforced Concrete Columns Subjected to Multi-Axial Loading," by Low, S.S. and Moehle, J.P., September 1987.

UCB/EERC-87/15 "Relationships between Soil Conditions and Earthquake Ground Motions in Mexico City in the Earthquake of Sept. 19, 1985," by Seed, H.B., Romo, M.P., Sun, J., Jaime, A. and Lysmer, J., October 1987.

UCB/EERC-87/16 "Experimental Study of Seismic Response of R. C. Setback Buildings," by Shahrooz, B.M. and Moehle, J.P., October 1987.

UCB/EERC-87/17 "Three Dimensional Aspects of the Behavior of R. C. Structures Subjected to Earthquakes," by Pantazopoulou, S.J. and Moehle, J.P., October 1987.

UCB/EERC-87/18 "Design Procedure for R-FBI Bearings," by Mostaghel, N. and Kelly, J.M., November 1987.

UCB/EERC-87/19 "Analytical Models for Predicting the Lateral Response of R C Shear Walls: Evaluation of their Reliability," by Vulcano, A. and Bertero, V.V., November 1987.

UCB/EERC-87/20 "Earthquake Response of Torsionally-Coupled Buildings," by Hejal, R. and Chopra, A.K., December 1987.

UCB/EERC-87/21 "Dynamic Reservoir Interaction with Monticello Dam," by Clough, R.W., Ghanaat, Y. and Qiu, X-F., December 1987.

UCB/EERC-87/22 "Strength Evaluation of Coarse-Grained Soils," by Siddiqi, F.H., Seed, R.B., Chan, C.K., Seed, H.B. and Pyke, R.M., December 1987.

UCB/EERC-88/01 "Seismic Behavior of Concentrically Braced Steel Frames," by Khatib, I., Mahin, S.A. and Pister, K.S., January 1988.

UCB/EERC-88/02 "Experimental Evaluation of Seismic Isolation of Medium-Rise Structures Subject to Uplift," by Griffith, M.C., Kelly, J.M., Coveney, V.A. and Koh, C.G., January 1988.

UCB/EERC-88/03 "Cyclic Behavior of Steel Double Angle Connections," by Astaneh-Asl, A. and Nader, M.N., January 1988.

UCB/EERC-88/04 "Re-evaluation of the Slide in the Lower San Fernando Dam in the Earthquake of Feb. 9, 1971," by Seed, H.B., Seed, R.B., Harder, L.F. and Jong, H.-L., April 1988.

UCB/EERC-88/05 "Experimental Evaluation of Seismic Isolation of a Nine-Story Braced Steel Frame Subject to Uplift," by Griffith, M.C., Kelly, J.M. and Aiken, I.D., May 1988.

UCB/EERC-88/06 "DRAIN-2DX User Guide," by Allahabadi, R. and Powell, G.H., March 1988.

UCB/EERC-88/07 "Cylindrical Fluid Containers in Base-Isolated Structures," by Chalhoub, M.S. and Kelly, J.M., April 1988.

UCB/EERC-88/08 "Analysis of Near-Source Waves: Separation of Wave Types using Strong Motion Array Recordings," by Darragh, R.B., June 1988.

UCB/EERC-88/09 "Alternatives to Standard Mode Superposition for Analysis of Non-Classically Damped Systems," by Kusainov, A.A. and Clough, R.W., June 1988.

UCB/EERC-88/10 "The Landslide at the Port of Nice on October 16, 1979," by Seed, H.B., Seed, R.B., Schlosser, F., Blondeau, F. and Juran, I., June 1988.

UCB/EERC-88/11 "Liquefaction Potential of Sand Deposits Under Low Levels of Excitation," by Carter, D.P. and Seed, H.B., August 1988.